Development of novel PROTAC Small-Molecule Degraders of MDM2 Protein and Peptidomimetic Inhibitors Targeting WDR5-MLL1 Protein-Protein Interaction

by

Yangbing Li

A dissertation submitted in partial fulfillment
of the requirements for the degree of
Doctor of Philosophy
(Medicinal Chemistry)
in The University of Michigan
2018

Doctoral Committee:

Professor Shaomeng Wang, Chair
Assistant Professor Amanda Garner
Assistant Professor Hui Jiang
Professor Nouri Neamati
Associate Professor Zaneta Nikolovska-Coleska

Yangbing Li

ybsli@umich.edu

ORCID iD: 0000-0002-2549-9528

ACKNOWLEDGENTS

First of all, I would like to express my sincere gratitude to my advisor Dr. Shaomeng Wang for his continuous support for my PhD study in the field of medicinal chemistry and my dual master's degree study in statistics. I would like to thank him for his great patience, encouragement and guidance on my research projects and life. I could not image a better advisor and mentor like him for my PhD study.

Besides my advisor, I would like to thank the rest of my thesis committee: Dr. Nouri Neamati, Dr. Zaneta Nikolovska-Coleska and Dr. Amanda Garner for their helpful advices, comments and encouragement on my projects, which helped me to widen my research from various perspectives. I would like to thank my committee member Dr. Hui Jiang for his great help and support for my dual master's degree study in statistics.

I would like to thank to Dr. Meihua Rose Feng for her great help and instructions in my population PK projects.

I would like to thank to all the friends and members in our lab for all your help on my projects and for all the fun we have had in the last five years. In particular, I am grateful to Jiuling Yang, Dr. Liu Liu, Dr. Liyue Huang, Dr. Jianfeng Lu, Donna McEachern, Sally Przybranowski and scientists at PK core for the all evaluations of my compounds; Dr. Angelo Aguilar, Dr. Xin Han and

Atsunori Kaneshige for the help of the synthetic intermediates and final compounds; Dr. Chao-Yie Yang for all the computation modeling.

Last but not the least, I would like to thank my family: my parents, my wife and my daughter for their great support through my PhD study and my life in general.

TABLE OF CONTENTS

LIST OF TABLES

LIST OF FIGURES

LIST OF SCHEMES

LIST OF ABBREVIATIONS

AcMPAG	MPA-acyl-glucuronide
ALL	acute lymphoid leukemia
AML	acute myeloid leukemia
AR	androgen receptor
ATRA	*all-trans* retinoic acid
AUC	area under the concentration-time curve
BET	Bromodomain and Extra-Terminal
CDK9	Cyclin-dependent kinase 9
cIAP-1	Cellular Inhibitor of Apoptosis Protein 1
CQS	chloroquinoxaline sulfonamide
CRABP	cellular retinoic acid-binding proteins
CRBN	cereblon
DHT	Dihydrotestosterone
EHR	enterohepatic recirculation
ER	estrogen receptor

ERRα	Estrogen related Receptor α
ERRα	estrogen-related receptor alpha
FKBP12	FK506 binding protein
FRAP	FKBP-rapamycin associated protein
FRS2α	fibroblast growth factor receptor substrate 2α
GIT	gastrointestinal tract
GTP	guanosine triphosphate
H3K4	Histone 3 Lysine 4
HIF1α	hypoxia inducible factor 1α
HMT	Histone methyltransferase
IIV	Inter-individual variability
IκBα	NF-κB inhibitor-α
IKZF1/3	Ikaros family zinc finger proteins 1 and 3
IMiDs	immunomodulatory drugs
IMPDH	inosine monophosphate dehydrogenase
ITS	iterative two-stage
MDM2	murine double minute 2
MeBS	methyl bestain
MEIS1	myeloid exotropic viral integration site 1

MetAP-2	methionine aminopeptidase-2
MLL1	Mixed Lineage Leukemia protein 1
MMF	Mycophenolate mofetil
MPA	Mycophenolic acid
MPAG	Glucuronide of MPA
MRP-2	multidrug-resistant protein-2
NONMEM	nonlinear mixed effects modeling
PD	Pharmacodynamic
PK	Pharmacokinetic
PROTAC	proteolysis targeting chimera
PTB	phosphotyrosine-binding
RARs	retinoic acid receptors
RbBP5	Retinoblastoma Binding Protein 5
RTK	receptor tyrosine kinase
SAEM	stochastic approximation expectation maximization
SARM	selective androgen receptor modulator
SH2	Src homology 2
SNIPER	specific and non-genetic inhibitors of apoptosis protein dependent protein erasers

UGT	UDP-glucuronosyl transferase
VHL	von Hippel-Lindau
WDR5	WD repeat domain 5
XIAP	X-linked inhibitor of apoptosis

ABSTRACT

The transcription factor p53 plays an important role in suppression of tumor development, as it is involved in several important regulation of cell process, such as activation of DNA repair, cell cycle arrest, apoptosis and senescence. About 50% of human cancers carry mutated or deleted *TP53*, the gene coding p53 protein, which renders p53 nonfunctional as a tumor suppressor. Even in cancer cells with wild-type *TP53*, the p53 functions are inhibited by several mechanisms. Human MDM2 protein is a primary, endogenous cellular inhibitor of the tumor suppressor p53 through a direct protein-protein interaction, which makes it an attractive target for cancer treatment. In the past 15 years, a number of potent, selective and efficacious MDM2 inhibitors have been developed and advanced into clinical trials for cancer treatment. Recently, targeting protein degradation using small molecules emerged as a novel strategy for drug development. Herein, we present our design, synthesis and evaluation of MDM2 degraders based on a proteolysis targeting chimera (PROTAC) strategy. One of our most promising compounds (**LE-102**) could effectively induce MDM2 degradation at a concentration as low as 1 nM within 0.5 hour in RS4;11 leukemia cells. **LE-102** achieves an IC_{50} value of 2.3 nM in cell growth inhibition of RS4;11 with wild-type p53. It can also induce complete and durable tumor regression *in vivo* against RS4;11 xenograft tumors in mice and can significantly extend the survival time in the RS4;11 survival model. Mechanism studies have shown that **LE-102** is a highly potent and

efficacious MDM2 degrader. The development of MDM2 degraders is a novel efficient strategy targeting MDM2 for cancer therapy.

Inducing MDM2 protein degradation by PROTACs has shown its promising potential in cancer treatment. While during our study, a class of compounds based on the core structure of our MDM2 inhibitor **MI-1061**, failed to induce degradation of their consensus target, they displayed pronounced cell proliferation inhibition effects in several cancer cell lines. The cell growth inhibition activity of **LD-277**, a compound in this class, is not related to MDM2 degradation and activation of p53 pathway but mediated through the cereblon-dependent ubiquitination and degradation of the translation termination factor GSPT1. These findings demonstrated that a small modification could convert a PROTAC to molecular glue with unexpected mechanisms and effects. Careful target validation and activity evaluation are required in the development of PROTACs and molecular glue.

MLL1 is a histone H3 Lysine 4 methyltransferase, an important regulator of transcription and mediator of normal development and disease. Translocation of MLL1 has been found widely in infant ALL and AML. Persistent activation of HoxA9 and MEIS1 caused by MLL1 fusions is important for sustaining the leukemic phenotype. Although MLL1 fusion proteins are oncogenic, they require the maintenance of a wild-type allele for leukemogenesis. WDR5 is important for the HMT activity of the wild-type MLL1 complex. Therefore, inhibition of WDR5-MLL1 protein-protein interaction could be a valid approach for the treatment of MLL-rearranged leukemias.

Herein, we report the design, synthesis and evaluation of macrocyclic peptidomimetics that bind to WDR5 and block the WDR5-MLL protein-protein interaction. **LC-337** binds to WDR5 with a K_i value << 1 nM, inhibits cell growth in MOLM13 with IC_{50} value of 33 nM and is >800 times better than the previously reported compound **MM-401**.

Chapter 1

Development of Small-Molecule PROTAC Degraders of the MDM2 Oncoprotein

Introduction

The tumor suppressor p53 plays a critical role in protection against tumor development.[1-3] Although p53 is inactivated by mutation or deletion in about 50% of human cancers, it retains its wild-type status in the remaining cases.[4] The function of wild-type p53 is impaired by other mechanisms. One important mechanism is the overproduction of MDM2 protein, which could disable p53 function by direct protein-protein interactions.[5] MDM2, as an E3 ubiquitin ligase, regulates p53 protein level through an autoregulatory feedback loop.[6-7] It has also been shown that MDM2 blocks the transactivation domain of p53 and transports p53 from nucleus to cytoplasm by direct binding.[8] Stabilization and activation of wild-type p53 by inhibition of the MDM2 p53 protein-protein interaction has been explored as a novel approach for cancer therapy with several small molecule inhibitors that have been developed and advanced to clinical trials.[9-14] Among them, Idasanutlin (**RG-7388**) is currently in a clinical phase III trial for the treatment of AML.

In addition to small-molecule inhibitors, a new approach has recently been developed for target protein degradation based upon the small molecular PROTAC concept.[15-17] In this strategy, a heterobifunctional molecule is designed to contain a target protein inhibitor, another small-molecule ligand, which binds to an E3 ubiquitin ligase complex, and a linker to tether these two

ligands together. Several target protein degraders have been developed based on this strategy, with targets including the Bromodomain and Extra-Terminal (BET) BRD4[18-20], Androgen Receptor[21], Bcr-Abl[22-23], Estrogen related Receptor α (ERRα)[24] and other proteins. The protein degraders are conjugated with the ligands of E3 ubiquitin ligases, and include cereblon, von Hippel-Lindau (VHL-1) ligase, and cellular inhibitors of apoptosis protein 1 (cIAP1) and MDM2. PROTACs have been shown to induce target protein degradation efficiently and to be more potent in inhibition of cancer cell growth.

Herein, we report the design, synthesis, and evaluation of a series of MDM2 degraders based on the PROTAC strategy. The MDM2 inhibitor **MI-1061**, with its high binding affinity to MDM2 (K_i = 0.16 nM) and good stability in solution[25] was used as a binding ligand to recruit MDM2 to the E3 ubiquitin ligase. Our studies have led to the discovery of **LE-102**, which significantly, can cause MDM2 degradation *in vitro* and *in vivo* and achieves complete and durable tumor regression in RS4;11 xenograft models in mice.

Literature Review

Development of Small Molecular MDM2 Inhibitors

The transcription factor p53 controls the expression of a number of genes, which play important roles in cell cycle progression, apoptosis, senescence, DNA repair and metabolism[1-2, 26-27] and it is also a well-known and powerful tumor suppressor. Previous research has shown that about 50% humor cancers carry mutated or deleted *TP53*, the gene encoding p53.[28] The level and activity of p53 is tightly controlled in cells because of its critical functions. Oncoprotein

MDM2 is a primary negative endogenous regulator of p53 and it can regulate the function of p53 through three major mechanisms: MDM2, as an E3 ubiquitin ligase can directly ubiquitinate p53 and induce its proteasomal degradation; MDM2 can also directly block functions of the p53 transcription factor by blocking the binding of p53 to its target DNA through protein-protein interactions between MDM2 and p53; it could make p53 inaccessible to its target genes by promoting the exporting of p53 out of the cell nucleus.[6, 8] Through these inhibitory mechanisms, MDM2 functions as an effective p53 antagonist in cancer cells with wild type p53. This makes MDM2 an oncoprotein target and a therapeutic target in human cancers with wild type p53. Overexpression of MDM2 protein has been found widely in human cancers. One of the critical mechanisms of MDM2 overexpression is the amplification of the *MDM2* gene. Based on an analysis of 4000 tumor samples in 28 different types of cancers,[29-30] the *MDM2 gene* has been found to be amplified in about 7% of human cancers

As MDM2 functions as a critical inhibitor of p53 tumor suppressor functions through direct binding to p53, inhibitors targeting the MDM2-p53 protein-protein interaction can reactivate p53 functions for cancer treatment. In the past 20 years, peptides and nonpeptide small molecule inhibitors have been designed to block the protein-protein interactions between MDM2 and p53. These MDM2 inhibitors can cause significant p53 accumulation and can activate p53 transcription functions, and this may have therapeutic potential for the treatment of human cancers with wild-type p53. [1, 31]

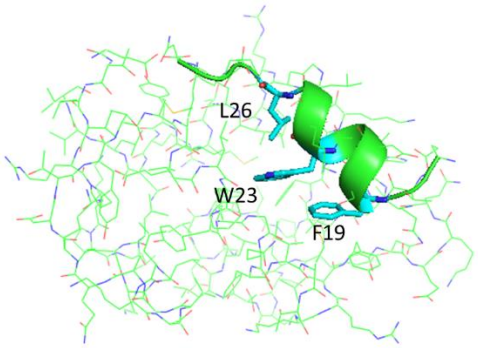

Figure 1-1. Co-crystal structure of MDM2 (Green) in complex with p53 peptide (Cyan) PDB ID:1YCR

From the early biochemical study, the first 120 amino-terminal amino acid residues of MDM2 and the first 30 N-terminal residues of p53 have been shown to be critical for the MDM2 p53 protein-protein interaction.[32] A high-resolution x-ray co-crystal structure of MDM2 in a complex with the p53 peptide (**Figure 1-1**) provided more details about their interaction.[33] It has been shown that three hydrophobic residues in p53 F19, W23, and L26 bind into a well-defined hydrophobic pocket in MDM2, which suggesting the feasibility of nonpeptide small-molecule inhibitors to block the MDM2-p53 interaction. This hydrophobic pocket in MDM2 can be used for the design of small molecule inhibitors.

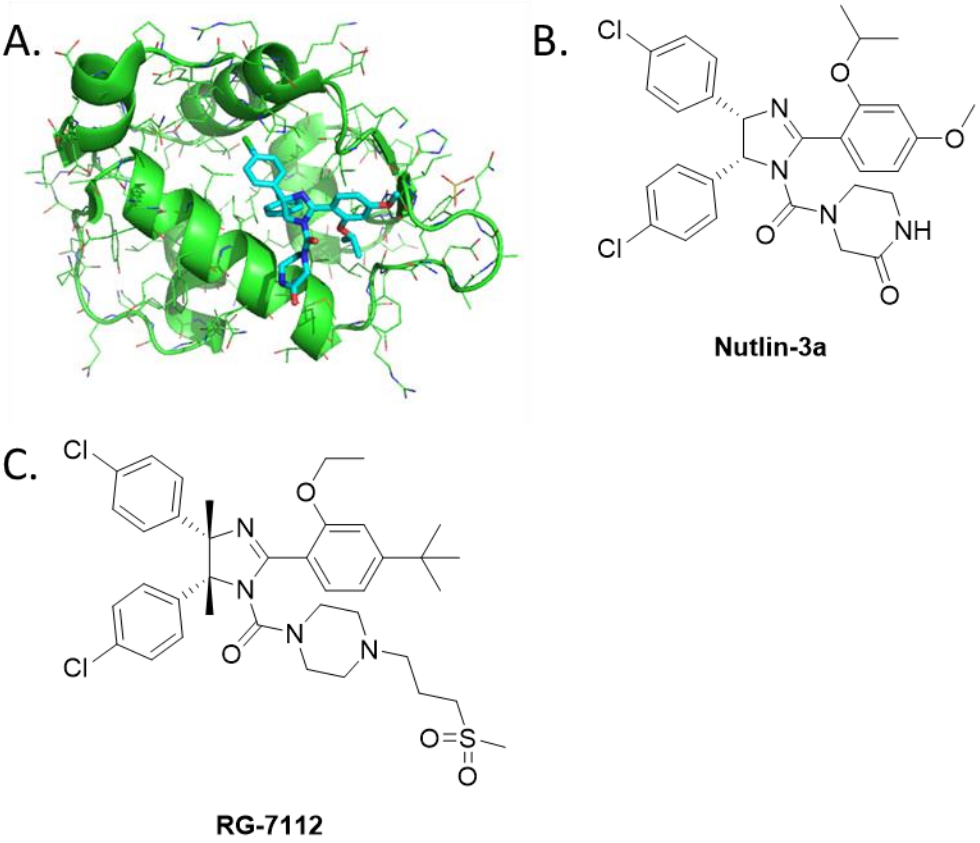

Figure 1-2. (A) Co-crystal structure of **Nutlin-3a** complexed with MDM2 (PDB ID:4HG7); (B) Structure of **Nutlin-3a** (C) Structure of **RG-7112**.

Nutlins, discovered by Hoffmann-La Roche were first published in 2004 as highly potent, specific, nonpeptide small-molecule inhibitors of the MDM2–p53 interaction.[34] **Nutlin-3a** can bind to MDM2 protein with an IC_{50} of 90 nM and effectively activate wild-type p53 in cancer cells, which is consistent with its targeting the MDM2–p53 interaction. It activates the p53 target genes *MDM2* and p21, which are critical for cell-cycle arrest. **Nutlin-3a** potently inhibits cancer cell growth with wild-type p53 in a dose-dependent manner and has more than 10-fold selectivity over cancer cell lines harboring p53 mutation or p53 deletion. It can also effectively inhibit tumor growth in the xenograft mice model of the human osteosarcoma SJSA-1 cell line with no signs of

toxicity to mice at oral doses up to 200 mg/kg. From co-crystal structure of **nutlin-3a** in a complex with MDM2, **nutlin-3a** mimics the three key binding residues (F19, W23, and L26) of p53 and occupies the important hydrophobic binding pocket of MDM2. (**Figure 1-2**) Preclinical studies of **nutlin-3a** have revealed its therapeutic potential for the treatment of human cancers retaining wild-type p53.

Following the pioneering study of **nutlin3a**, further studies were done by scientists at Hoffmann-La Roche to improve its binding affinity to MDM2, and its cellular potency and pharmacokinetics. Subsequently, **RG7112** (RO5045337), an analog of **nutlin3a**, was advanced into human clinical trials.[13] **RG7112** has a binding affinity to MDM2 (IC_{50} = 18 nM), and is 5-times more potent than **nutlin-3a**. It can effectively inhibit cell growth in cancer cell lines with wild-type p53 (IC_{50} = 0.18-2.2 μM) and exhibits good selectivity over cancer cell lines with a p53 mutation (IC_{50} = 5.7-20.3 μM). Pharmacodynamic studies have shown that **RG7112** can activate wild-type p53 dose-dependently in xenograft mice model of SJSA-1 and can achieve partial tumor regression upon oral administration, without any signs of toxicity in mice.

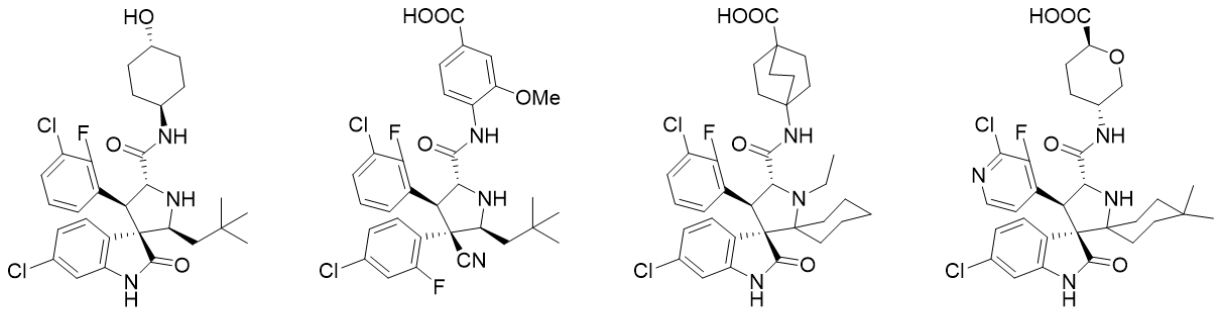

Figure 1-3. Structures of MDM2 inhibitors with a spiro-oxindole core structure.

Using the co-crystal structure of p53 peptide in a complex with MDM2, our laboratory completed a computational structure-based drug design for a new class of small-molecule inhibitors with a spiro-oxindole core structure.[35] **MI-77301** was the first compound in this series of compounds that was developed and ultimately advanced to clinical trials.[14] **MI-77301** binds to MDM2 with a K_i value of 0.88 nM and is 50 times more potent than **nutlin-3a** in the same binding assay. **MI-77301** can also selectively bind to MDM2 more than 10,000 times effectively than to MDMX, a protein homologous with MDM2. The co-crystal structure of **MI-77301** in a complex with the MDM2 protein has shown that **MI-77301** occupies the key hydrophobic pocket on MDM2, mimicking the three key p53-binding residues and has additional hydrophobic and hydrogen-bonding interactions. It was also shown that **MI-77301** has a π-π stacking interaction with the H96 residue of MDM2. It can also cause the refolding of the unstructured residues at the N-terminal region of MDM2, forming a new pocket with which to further enhance its binding affinity to MDM2.

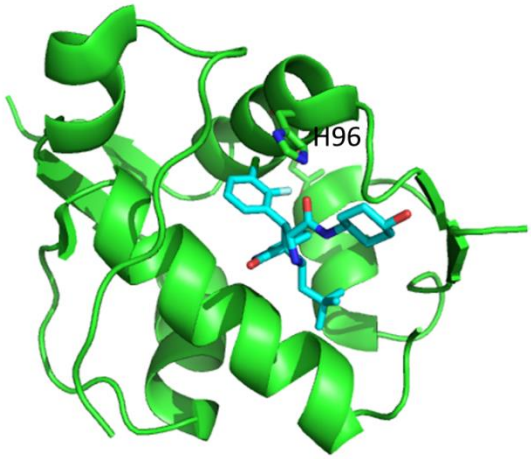

Figure 1-4. Co-crystal structure of **MI-77301** in a complex with MDM2. (PDB ID: 5TRF)

Another MDM2 inhibitor based on this spiro-oxindole core structure that has been advanced to clinical trials is **RG-7388** (RO5503781) from Hoffmann-La Roche, which was published in 2013.[9] **RG-7388** is currently in phase III clinical trials for acute myeloid leukemia and phase II clinical trials for polycythemia vera. **RG-7388** binds to MDM2 with an IC_{50} value of 6 nM, potently inhibits cell growth in cancer cell lines containing wild-type p53 at about 30 nM and is >100-fold more potent against cancer cell lines with mutated p53. Efficacy studies have shown that **RG-7388** can achieve complete tumor regression in the SJSA-1 xenograft model when orally administered to mice.

Based on the spiro-oxindole core structure for MDM2 inhibitors, our group discovered **APG-115** following an extensive structure–activity relationship study.[11] **APG-115** has a very high affinity to MDM2 with an IC_{50} value of 3.8 nM and a K_i < 1 nM. It has potent cellular activity on SJSA-1 with an IC_{50} value of 60 nM, and an excellent oral pharmacokinetic profile. **APG-115** can achieve complete and long-lasting tumor regression upon oral administration in tumor xenograft models and it is currently in phase I clinical trials for cancer treatment.

DS-3032 is another MDM2 inhibitor based on the spiro-oxindole core structure and currently in phase I clinical trials. DS-3032 was developed by scientists from Daiichi-Sankyo.[36] It can stabilize *TP53* and selectively induce CDKNA1, BAX and MDM2 expression in neuroblastoma cells with wild-type *TP53*. It can delay tumor growth and significantly improve the survival time in mice xenografted with wild-type *TP53* neuroblastoma cells.

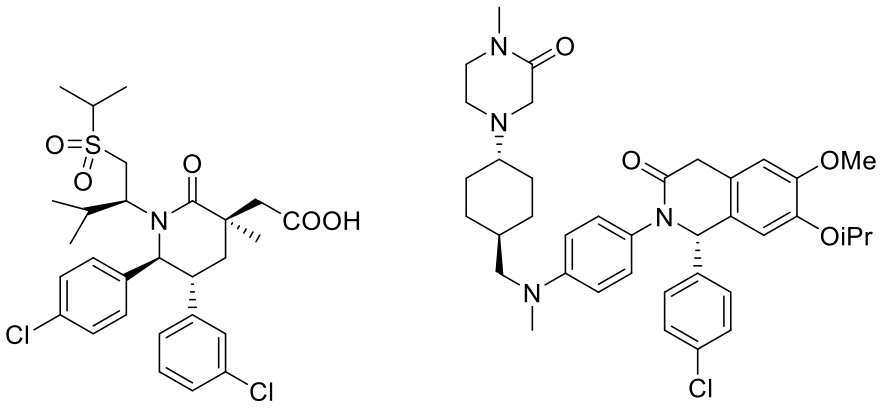

AMG-232 **NVP-CGM097**

Figure 1-5. Structures of **AMG-232** and **NVP-CGM097**

AMG-232 is a member of new class of potent MDM2 inhibitors which has been advanced to clinical trials.[12] It was discovered by scientists at Amgen through structure-based design and extensive optimization and its structure contains a 1,3,5,6-tetrasubstituted piperidinone scaffold. **AMG-232** has a K_d value of 0.045 nM in an MDM2 binding assay and a cell growth inhibition activity with IC_{50} values of 9.1 nM and 10 nM in SJSA-1 and HCT-116 cell lines with wild-type p53, respectively. An efficacy study has shown that **AMG-232** effectively inhibits tumor growth in the SJSA-1 osteosarcoma model and achieves complete tumor regression with a 60 mg/kg daily dose. **AMG-232** can also achieve complete tumor growth inhibition without tumor regression in the HCT-116 xenograft model. The co-crystal structures of **AMG-232** analogs complexed with MDM2 shows that it also targets all of the three key p53-binding residues in its interactions with MDM2. In addition, **AMG-232** also interacts with G58 of MDM2 through its sulfonyl isopropyl group and forms a salt bridge with H96 and the carboxylic acid group of **AMG-232**.

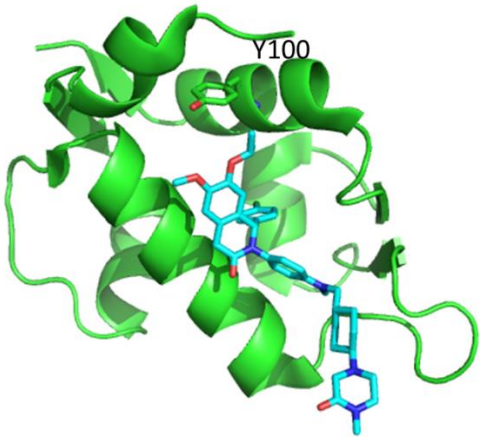

Figure 1-6 Co-crystal structure of **NVP-CGM097** in a complex with MDM2. (PDB ID:4ZYF)

NVP-CGM097 was reported as a new class of MDM2 inhibitor with a dihydroisoquinolinone scaffold and was advanced into clinical development.[10] The co-crystal structure of **NVP-CGM097** in a complex with MDM2 showed that the dihydroisoquinolinone scaffold can reach the critical binding pockets by interacting with the three key p53 residues in MDM2. Additional interactions were also achieved through water-mediated H-bond interactions of its isopropyl ether group with the hydroxyl group of Y100 and with the carbonyl oxygen of F55. **NVP-CGM097** binds to MDM2 with an IC_{50} value of 1.7 nM and has cell growth inhibition activity with a GI_{50} value of 350 nM in SJSA-1 cells. Pharmacodynamic studies have shown that **NVP-CGM097** can inhibit the interaction between p53 and MDM2 and reactivate the p53 pathway *in vivo* in a SJSA-1 human tumor model. Daily treatment for 3 weeks with **NVP-CGM097** can significantly induce >85% tumor regression in SJSA-1 tumor xenografts in rats with no negative histopathology findings.

MK-8242 (SCH 900242) was developed by the scientists from Merck as a potent MDM2 inhibitor and currently advanced into phase I clinical trials. The Structure of **MK-8242** and its characterization have not been disclosed.

In summary, several classes of highly potent and specific small-molecular MDM2 inhibitors designed to block the MDM2-p53 protein-protein interaction have been designed, synthesized and advanced into clinical trials for cancer treatment. These MDM2 inhibitors can efficient activate wild-type p53 *in vitro* and *in vivo*. It was also noted that they can also upregulate the MDM2 expression level through an autoregulatory feedback loop, as the *MDM2* gene is also the transcription target of p53.[6] Consequently, high concentrations of MDM2 inhibitors are needed to block the newly formed MDM2. Moreover, high expression levels of MDM2 may also lead to unknown side effects. Therefore, development of new strategies to activate wild-type p53 without upregulation of MDM2 can be more effective than the traditional method of inhibiting the MDM2-p53 protein-protein interaction.

Development of PROTACs Targeting Protein Degradation

In recent years, the PROTAC has become one of the most exciting strategies for therapeutic intervention.[17] PROTACs are heterobifunctional molecules containing an E3 binding ligand, a target protein binding ligand and a linker between them. Both the E3 binding ligand and target protein binding ligand can specifically and simultaneously bind to the E3 ubiquitin ligase and the target protein to form a ternary complex. By linking the target protein to the E3 ubiquitin ligase, PROTACs are capable of promoting the ubiquitination and subsequent proteasomal degradation of target proteins to achieve their therapeutic effect. There are two reasons why

this is a more efficient strategy than is offered by traditional protein inhibitors. If reversible binding ligands are involved in the PROTACs, they can function as catalysts to induce protein degradation. This suggests the use of lower drug concentrations of PROTACs than inhibitors with the same therapeutic efficacy. Lower drug concentrations can also help to lower the off-target side effects and toxicity.[15] A second reason is that PROTACs can be used with "undruggable" targets. Sometimes the nature of the functional domain or binding site makes it difficult to develop small molecule inhibitors. By targeting other druggable domains or binding sites on the same protein, PROTACs could induce the degradation of a whole protein to inhibit the protein functions which are "undruggable" for inhibitors.[37-38] In this thesis, we will assess the development of PROTACs during the past 20 years.

Peptide Based PROTACs

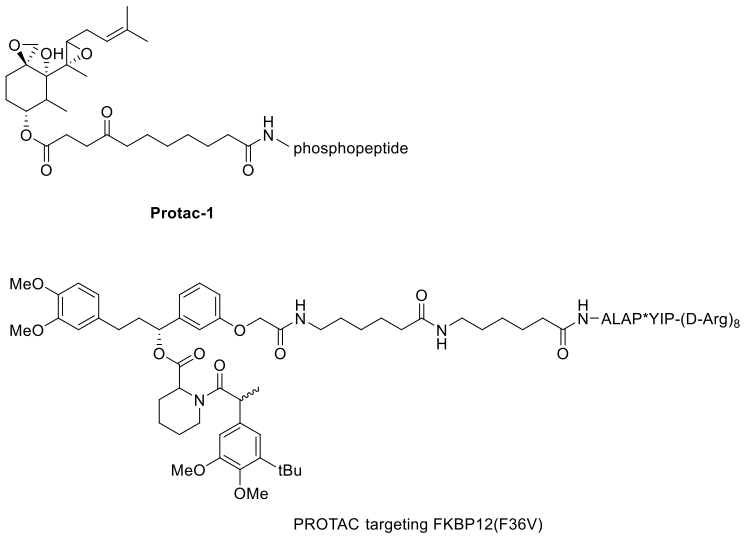

Figure 1-7. Structure of peptide-based PROTACs

In 2001, the Sakamoto group developed the first PROTACs targeting degradation of the methionine aminopeptidase-2 protein (MetAP-2).[39] **Ovalicin**, a covalent inhibitor was used as the target protein ligand and a phosphopeptide (DRHDpSGLDpSM) derived from the NF-κB inhibitor-α (IκBα) was used to recruit $SCF^{\beta\text{-}TrCP}$ E3 ubiquitin ligase. It was shown that MetAP-2 is recruited to the $SCF^{\beta\text{-}TrCP}$ E3 ubiquitin ligase by this chimeric molecule 1 (**Protac-1**) and is ubiquitinated and degraded in a **Protac-1**-dependent manner. As **Ovalicin** is a covalent inhibitor, only MetAP-2-PROTAC, but not the free MetAP-2 was degraded. Introduction of proteasome inhibitors **LLnL** or **epoxomicin** could block the degradation of MetAP-2.

In 2003, several new PROTACs targeting androgen receptor (AR) and estrogen receptor (ER) degradation were published by the Sakamoto group.[40] Both of these contained the phosphopeptide used in **Protac-1** to recruit $SCF^{\beta\text{-}TrCP}$ E3 ubiquitin ligase. Dihydrotestosterone (**DHT**) was used as the target protein ligand in AR PROTACs and estradiol in the ER PROTACs. It demonstrated that the ER PROTAC was capable of causing the ubiquitination and degradation of ERα in vitro, and AR PROTAC could promote the rapid disappearance of AR in a proteasome-dependent manner. Although all PROTACs designed with phosphopeptide can cause target protein degradation, these PROTACs are introduced to cells by microinjection. Development of cell permeable PROTACs is important for the application of the technique in drug development.

In 2004, the first cell permeable PROTAC was developed by the Crews group.[41] A 7-mer peptide (ALAPYIP) derived from hypoxia inducible factor 1α (HIF1α) was used to recruit VHL protein, which is the substrate acceptor of $CRL2^{VHL}$ E3 ubiquitin ligase. **AP21998** was used as target protein ligand to recruit FKBP12(F36V) protein and **DHT** was used to recruit the AR protein.

An eight-poly-D-arginine tag was attached to the PROTAC to improve its cell permeability and prevent nonspecific proteolysis. Protein degradation of FKBP12(F36V) and AR induced by the two PROTACs were clearly shown by western blot and fluorometric analyses.

PhosphoPROTACs

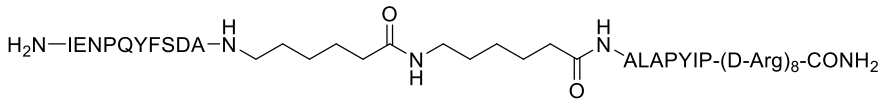

PROTAC target TrkA

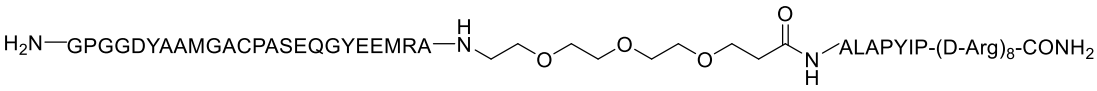

PROTAC targeting ErbB2

Figure 1-8. Structures of phosphoPROTACs

PhosphoPROTACs are composed of a receptor tyrosine kinase (RTK) phosphorylation sequence to recruit target protein, a VHL-binding sequence to recruit $CRL2^{VHL}$ E3 ubiquitin ligase, a poly-D-arginine tag to improve cell permeability and a linker. Phosphorylation of tyrosine in the RTK phosphorylation sequence can recruit target proteins with a phosphotyrosine-binding (PTB) or an Src homology 2 (SH2) domain.[42] In 2013, the Crews group published two phosphoPROTACs with tyrosine phosphorylation sequences derived from the nerve growth factor receptor, TrkA to recruit fibroblast growth factor receptor substrate 2α (FRS2α) or a sequence from neuregulin receptor ErbB3 to recruit p85 with an SH2 domain. It was demonstrated that these phosphoPROTACs could decrease target proteins both *in vitro* and *in vivo*. Treatment with p85

phosphoPROTAC significantly reduced tumor size in mouse xenograft tumor model, and this indicates the promising therapeutic effects of PROTACs.

Small-Molecule PROTACs

Both peptide-based PROTACs and phosphoPROTACs are not useful for drug development due to their poor cell permeability, high molecular weight and metabolic instability in cells. These disadvantages stem mainly from the peptide structure used in these PROTACs. Developing non-peptidic PROTACs with small molecules replacing the peptide ligands should achieve much better cell permeability and stability. Recent studies on PROTACs have shown the small molecule ligands known to bind to MDM2, cIAP1, CRBN and VHL could be used in the design of stable and cell permeable PROTACs.[43]

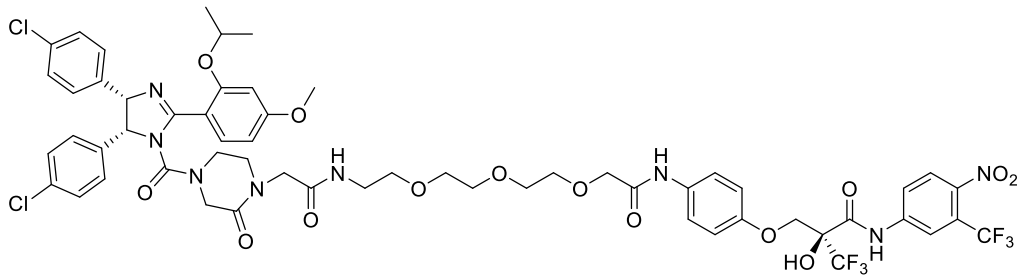

PROTAC targeting AR

Figure 1-9. Structure of an MDM2-based small molecule PROTAC.

In 2008, the Crews group reported the first non-peptide PROTACs targeting AR degradation.[44] They used **nutlin-3a** in the PROTACs to recruit the E3 ubiquitin ligase protein MDM2 and a non-steroidal, selective androgen receptor modulator ligand (**SARM)** was linked to the nutlin through a PEG linker. Nutlins were designed to bind to MDM2 at the pocket used for

binding of p53, which is the primary target protein for MDM2. A SARM-nutlin PROTAC could hijack MDM2 to the target protein and lead the ubiquitination and subsequent proteasomal degradation of AR by treatment of HeLa cells with 10 μM PROTAC for 7 h. Pretreatment of the proteasome inhibitor **epoxomicin** blocks the degradation of AR, which shows that the decrease of AR is through PROTAC induced proteasome degradation.

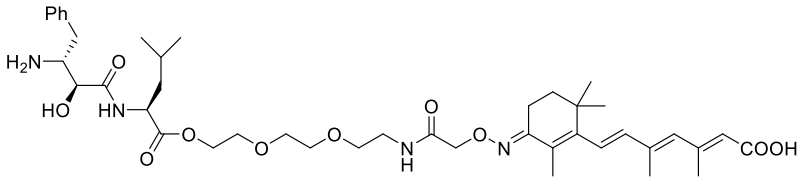

PROTAC targeting CRABP-I and CRABP-II

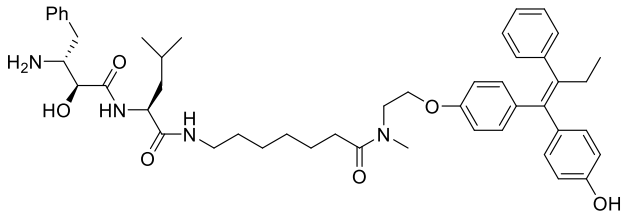

SNIPER(ER)-3

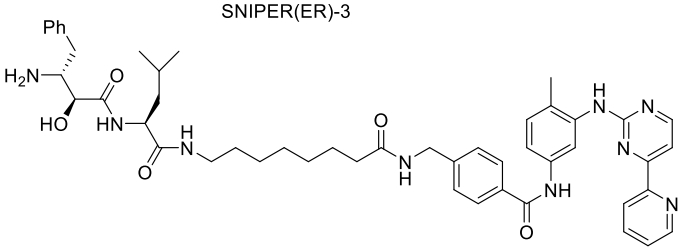

SNIPER(ABL)-3

Figure 1-10. Structures of cIAP-1 based small molecule PROTACs.

Another important E3 ubiquitin ligase is involved in the design of the PROTACs cIAP1. These PROTACs, which hijack cIAP-1 have also been called specific and non-genetic inhibitors of apoptosis protein dependent protein erasers (SNIPER).[45] In 2010, the Hashimoto group developed a PROTAC targeting cellular retinoic acid-binding proteins (CRABP-I and CRABP-II) for

degradation.[46] These PROTACs contain methyl bestain (**MeBS**), which can directly and selectively bind to the BIR3 domain of cIAP1, and to *all-trans* retinoic acid (**ATRA**), involving retinoic acid receptors (RARs). RARs could be used to further recruit CRABP-I and CRABP-II. The designed PROTACs induce proteasome protein degradation of CRABP-I and CRABP-II, and this could also inhibit the migration of neuroblastoma IMR-32 cells. Later, the Hashimoto group replaced **MeBS** with MV1, a pan-ligand for cIAP1, cIAP2 and the X-linked inhibitor of apoptosis (XIAP), as cIAP2 and XIAP also possess ubiquitin ligase activity.[47] These PROTACs can achieve double degradation of cIAP1 and CRABP-II and efficiently inhibit proliferation of IMR32 cells.

In 2013, cIAP-1-dependent PROTACs targeting ERα protein degradation by conjugating ERα ligand, 4-hydroxy tamoxifen (**4-OHT**), to **MeBS** were developed by the Naito group.[48] The PROTAC **SNIPER(ER)-3** can induce the proteasome degradation of ERα and inhibit estrogen-dependent expression of the pS2 gene in MCF-7 cells in 24 h with 10 μM treatment, causing necrotic cell death accompanied by a release of HMGB1, a marker of necrosis in MCF-7 cells.

In 2016, the Kurihara group developed a PROTAC, **SNIPER(ABL)-2** which targets BCR-ABL degradation. [23] An **imatinib** derivative that binds to BCL-ABL was linked to **MeBS** in the PROTAC to recruit BCR-ABL to cIAP1 thus inducing ubiquitination and subsequent proteasomal degradation. **SNIPER(ABL)-2** can cause BCR-ABL protein degradation and subsequent cell growth inhibition following treatment at 30-100 μM.

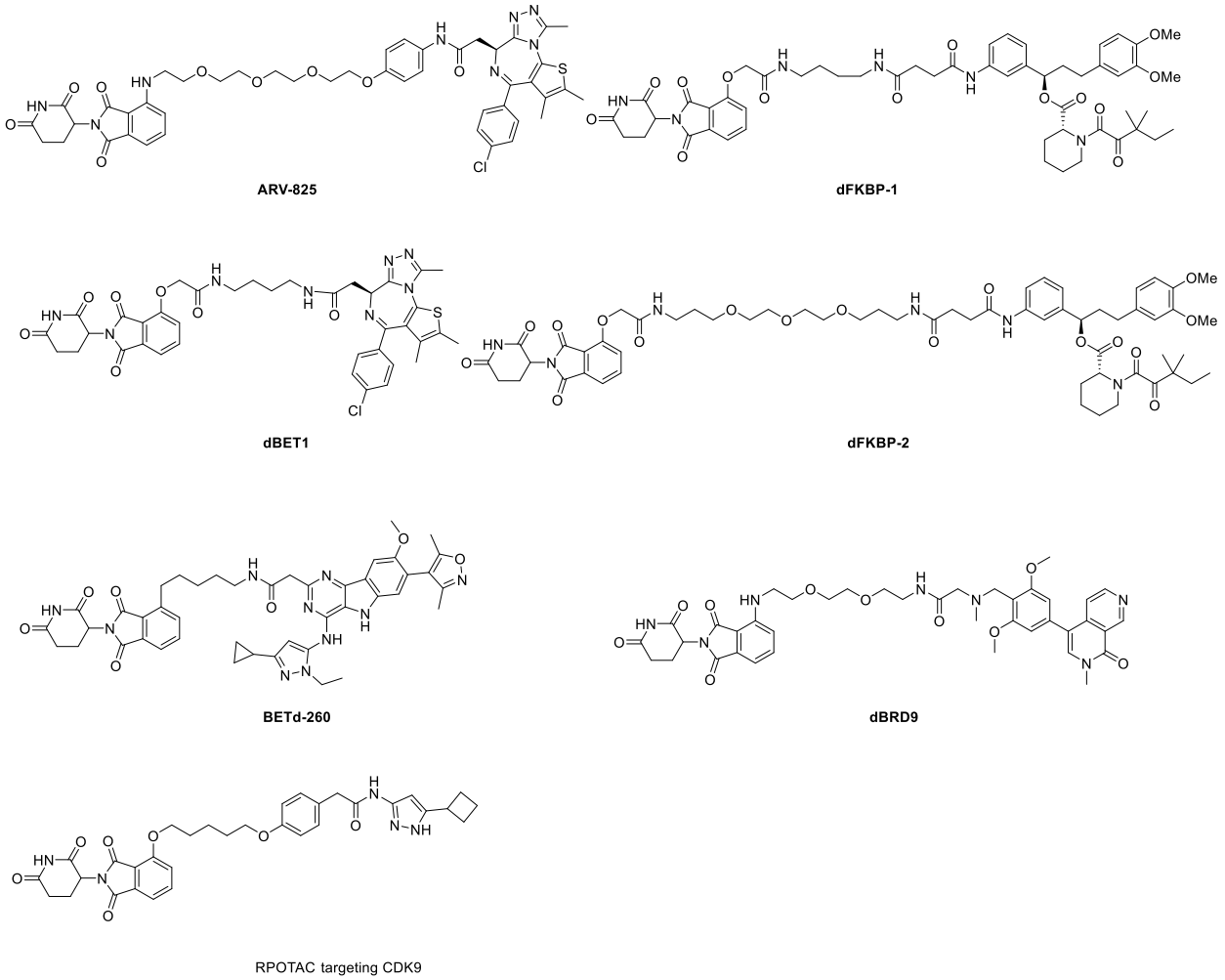

Figure 1-11. Structures of CRBN based PROTACs

In 2010, the Ito group showed that CRBN, which is the substrate acceptor of the $CRL4^{CRBN}$ E3 ubiquitin ligase, is the protein target for thalidomide.[49] This suggests that thalidomide and its derivatives could be used to hijack the ubiquitin ligase $CRL4^{CRBN}$ ligase in the design of PROTACs. Later in 2015, the Crews and Brander Groups both published new PROTACs designed to target the transcriptional co-activator BRD4 with thalidomide analogues.[18-19] **ARV-825,** published by the Arvinas and Crews group, recruits BRD4 using pomalidomide to recruit CRBN and **OTX015** to recruit a BRD4 bromodomain inhibitor. While **dBET1,** published by the Brander group, recruits

BRD4 and is composed of thalidomide to recruit CRBN and **JQ1**. Both **ARV-825** and **dBET1** can efficiently and rapidly cause proteasomal degradation of BRD4. **ARV-825** can completely degrade BRD4 in 6 h with a 10 nM treatment and efficiently inhibit cell proliferation and cause apoptosis. **dBET1** can cause complete BRD4 degradation in 2 h with a 100 nM treatment. It significantly inhibits tumor growth in mouse xenograft models and disseminated leukemia mouse models. To extend the application of this strategy, another two PROTACs causing degradation of cytosolic signaling protein FKBP12, were developed with FKBP12-directed ligand steel factor (SLF) and the same thalidomide moiety as was used in **dBET1**.[19] Both can cause complete FKBP12 degradation in 18 h with a 1 μM treatment. Later in 2017, **BETd-260**, developed by our group, was found to effectively degrade BRD4 protein at concentrations as low as 30 pM in the RS4;11 cell line and to induce rapid tumor regression *in vivo* against RS4;11 xenograft tumors.[50] With the previous success of PROTACs hijacking the target protein in CRBN, the Crews group developed BCR-ABL targeting PROTACs by linking **dasatinib** or **bosutinib** to CRBN. [22] Both PROTACs can cause the proteasomal degradation of ABL and BCR-ABL.

In 2017, PROTAC targeting of bromodomain-containing protein BRD9 degradation was developed by the Brander group.[51] BRD9 is a subunit of the SWI/SNF nucleosome remodeling complex. The BRD9 PROTAC (**dBRD9**) consists of **BI7273**, a potent BRD9 bromodomain inhibitor (K_d = 15.4 nM; IC_{50} = 19 nM)[52] which recruits BRD9 and pomalidomide to hijack CRBN. In this case, complete BRD9 degradation was achieved in 1 h with a 10 nM treatment of **dBRD9** in MOLM-13 cells.

In 2017 the Natarajan and Rana groups developed a PROTAC targeting cyclin-dependent kinase 9 (CDK9).[53] An aminopyrazole CDK9 inhibitor and thalidomide were linked with methylene linker in this PROTAC. In HCT116 cells, this CDK9 PROTAC can selectively cause CDK9 degradation without affecting other CDK family members, such as CDK2 or CDK5.

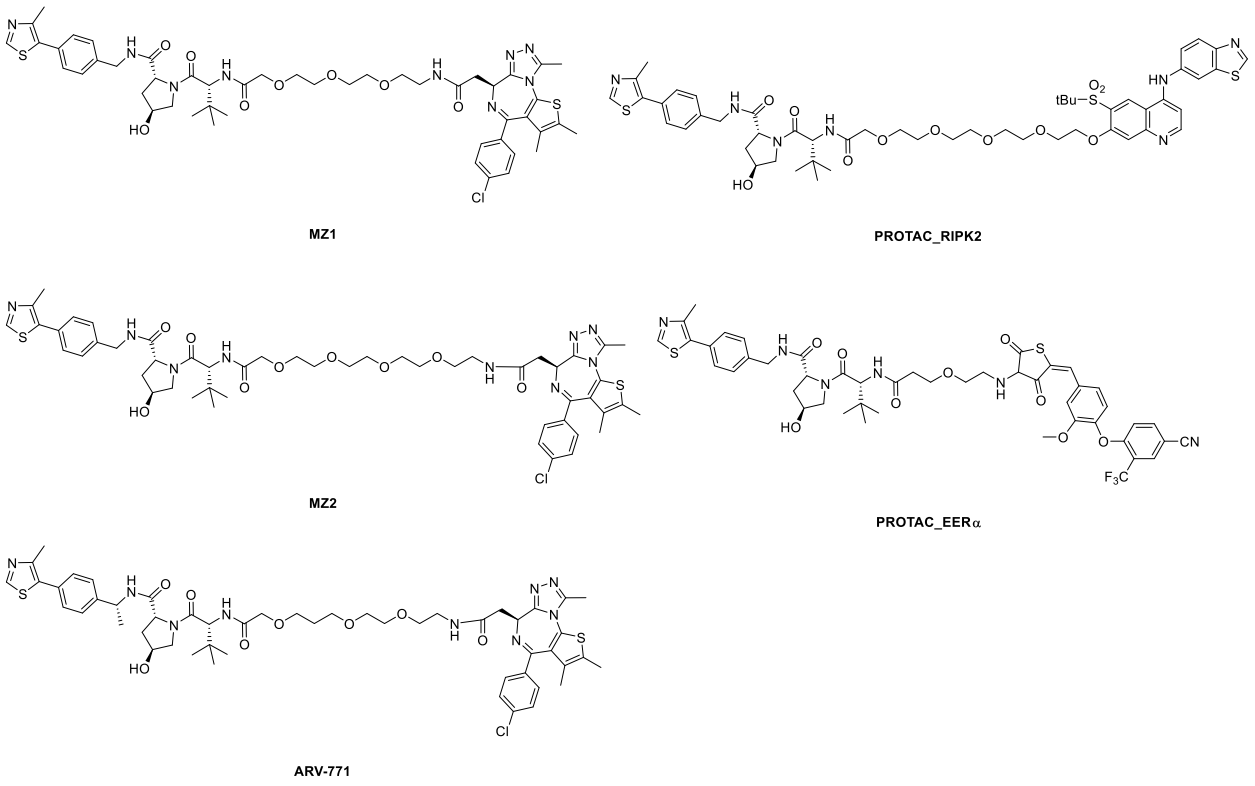

Figure 1-12. Structures of VHL-based BROTACs

Another important E3 ubiquitin ligase involved in small molecule PROTACs is $CRL2^{VHL}$. The strategy, which involves hijacking VHL to recruit $CRL2^{VHL}$ E3 ubiquitin ligase in PROTACs for protein degradation has been confirmed with a 7-mer peptide derived from HIF1α.[41] With the development of small molecule inhibitors targeting the HIF1α binding site of VHL, [54-56] development of small molecule PROTACs with a VHL binding ligand becomes attractive and

accessible. In 2015 and 2016, PROTACs with a VHL ligand targeting BRD4 degradation **MZ1**, **MZ2** and **ARV-771** with **JQ1** to recruit BRD4 were developed by the Cuilin group and Arvinas groups.[20, 57] **ARV-771** can cause almost complete degradation of BRD4 in 16 h with a 1 nM treatment in 22Rv1, VCap and LnCaP95 cells. It is much more potent than the BRD4 inhibitor **OTX015** for cell proliferation inhibition *in vitro* and tumor growth regression with a mouse xenograft model *in vivo*.

In 2015, two PROTACs, **PROTAC-ERRα**, targeting the estrogen-related receptor alpha (ERRα), and **PROTAC-RIPK2** targeting the serine/threonine kinase RIPK2, were published by the Crews group.[24] Both hijacked $CRL2^{VHL}$ E3 ubiquitin ligase, causing target protein degradation. **PROTAC_ERRα** causes almost complete degradation of ERRα in 8 h by the treatment with 1 μM in MCF7 cells and **PROTAC_RIPK2** can induce more than 90% degradation of RIPK2 in 16 h with a 10 nM treatment in THP-1 cells.

Another PROTAC (**ARV-330**) targeting AR degradation with a VHL binding ligand was developed by Arvinas et al.[21] The Structure of **ARV-330** has not been revealed, but data have shown that DC_{50} of **ARV-330** for AR degradation is lower than 1 nM, and it can cause cell proliferation and apoptosis in VCap cells following treatment with 20 nM. It can also robustly block tumor growth in the xenograft VCap mouse model.

In summary, PROTAC strategy shows great potential in field of drug discovery, especially the recently published small molecule PROTACs which have good cell permeability, stability, solubility and appropriate pharmacokinetic properties. PROTACs eliminate the target proteins by inducing ubiquitination and degradation, which is more efficient than traditional small molecule

inhibitors, which simply bind to the protein. This also provides a promising method with which to target undruggable disease-related proteins. To extend the application of PROTAC strategy, more druggable proteome and better binding ligands for E3 ubiquitin ligase should be explored. As most of PROTACs generally have larger molecular weights and more hydrogen bonding donors and acceptors than small molecule inhibitors, improvement of pharmacokinetic properties is also important for the application of this strategy in the future.

Results and Discussion

Judging from published reviews, the PROTAC strategy targeting MDM2 degradation can be more efficient than the traditional MDM2 inhibitors. **MI-1061,** a potent MDM2 inhibitor, which can bind to MDM2 with K_i value of 0.16 nM, was employed in our design of MDM2 PROTAC degraders.

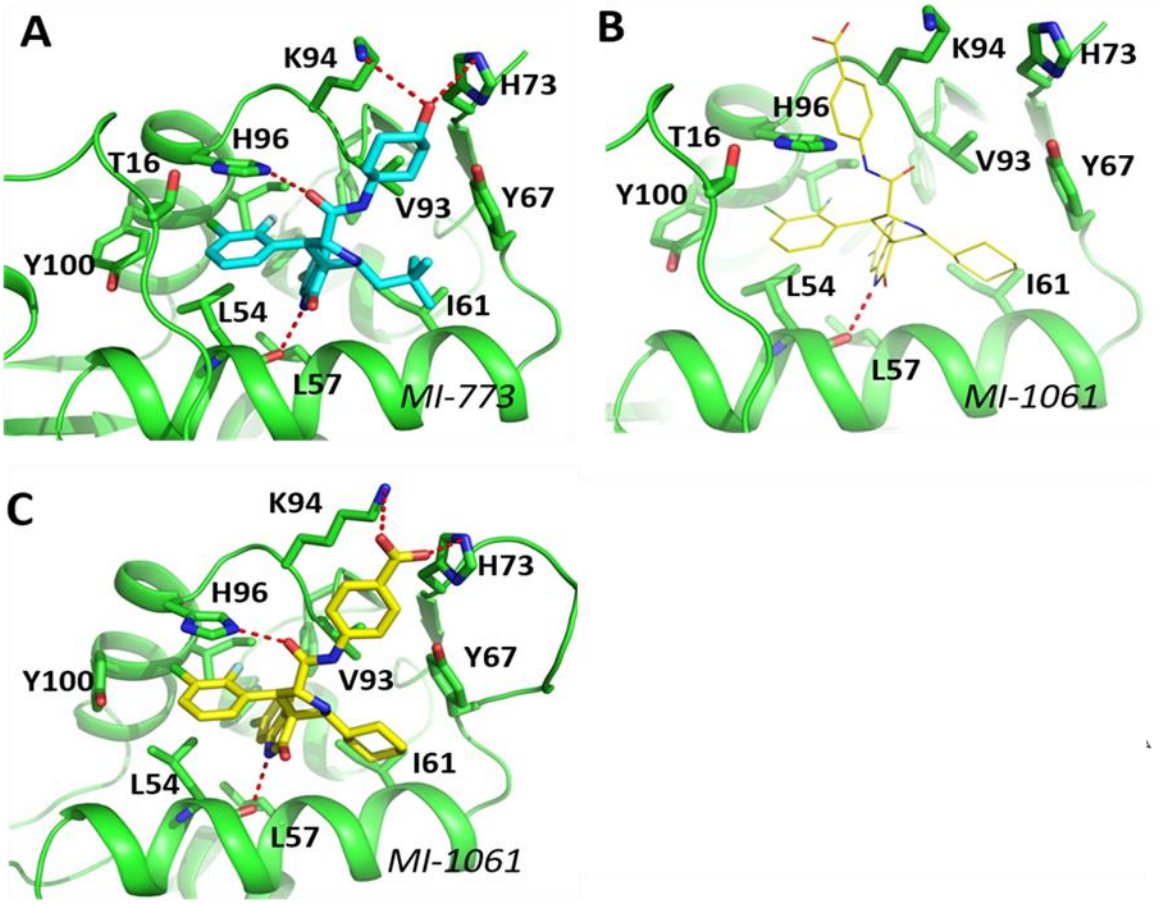

Figure 1-13. (A) Co-crystal structure of MDM2 complexed with **MI-77301** (Cyan, PDB ID: 5TRF); (B) Modeled structure of MDM2 complexed with **MI-1061** (Yellow, PDB ID: 5TRF); (C) Modeled structure of MDM2 complexed with **MI-1061** (Yellow, PDB ID: 4LWU).

Upon the basis of the co-crystal structure of MDM2 complexed with **MI-77301** (PDB ID: 5TRF)[14], we modeled the structure of MDM2 (PDB ID: 4LWU)[58] complexed with **MI-1061**. In the crystal structure of MDM2-**MI-77301**, the hydroxy-cyclohexyl group of **MI-77301** forms at least one hydrogen bond with K94. When the same MDM2 structure was used to model **MI-1061**, we failed to obtain a docking pose of **MI-1061** similar to **MI-77301** (**Figure 1-13B**.) possibly due to the restricted conformation of K94 that was observed in the MDM2-**MI-77307** crystal structure.

Another MDM2 crystal structure (PDB ID: 4LWU) in which K94 adopts a different conformation for docking simulation led to a pose of **MI-1061** similar to that of **MI-73301**. In this model, **MI-1061** is involved in a salt-bridge interaction with K94 (3.4 Å) and H73 (2.5 Å) The benzoic acid group in this model is exposed to solvent, making it a suitable site for tethering to E3 ubiquitin ligase ligand for the design of potential PROTAC degraders of MDM2 proteins.

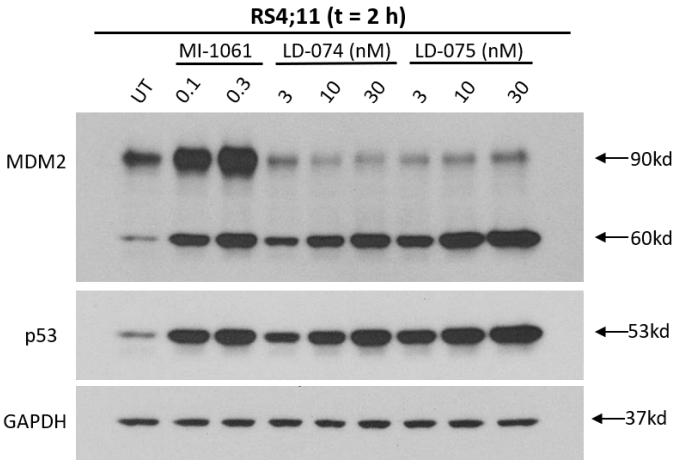

Figure 1-14. Western blotting analysis of MDM2 and p53 proteins in RS4;11 cells treated with MDM2 inhibitor **MI-1061** and MDM2 degraders **LD-074**, **LD-075**. RS4;11 cells were treated for 2 h with each individual compound at indicated concentrations, and proteins were probed by specific antibodies. GAPDH was used as the loading control.

Thalidomide analogues, which can recruit CRBN, the substrate accepter of the $CUL4A^{CRBN}$ E3 ubiquitin ligase, was used in the design of MDM2 degrader. We designed and synthesized **LD-074** and **LD-075** (**Table 1-1**) as potential MDM2 degraders using **MI-1061** for the MDM2 inhibitor portion, thalidomide as the cereblon ligand, and in the beginning, the hydrophobic carbon and hydrophilic PEG linker were used. WST-8 cell viability assay showed that **LD-074** and **LD-075** can

efficiently inhibit cell growth in the RS4;11 acute leukemia cell line with IC_{50} values of 10 nM or 7 nM respectively, and are 14-20 times more potent than **MI-1061**. Western blotting analysis showed that both **LD-074** and **LD-075**, at concentrations as low as 10 nM, are effective in decreasing the level of the MDM2 protein and increasing the level of p53 protein in the RS4;11 cells when compared with the MDM2 inhibitor **MI-1061** (**Figure 1-14**). It was concluded that **LD-074** and **LD-075** are promising MDM2 degraders for further optimization.

Table 1-1. MDM2 degraders designed with thalidomide and linkers with various lengths.

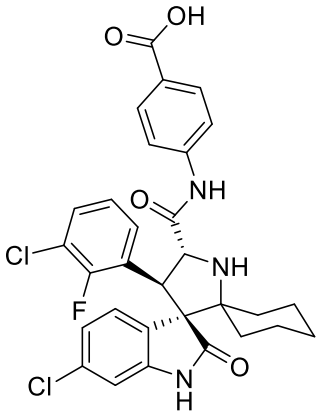

MI-1061

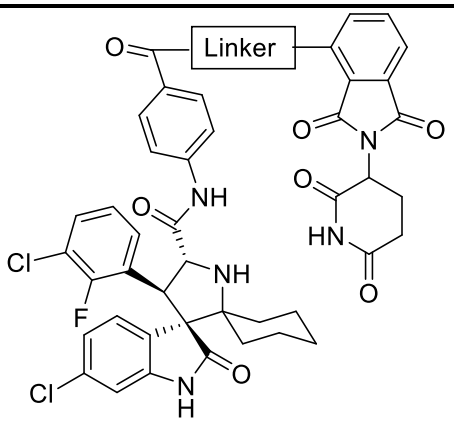

Compound No.	Linker	IC_{50}/μM RS4;11
MI-1061		0.141±0.012
LD-117	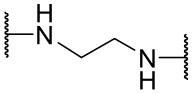	0.015±0.002
LD-270	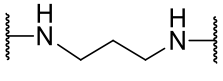	0.009±0.002

LD-074	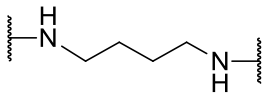	0.010±0.001
LD-252	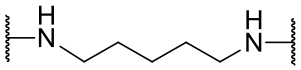	0.012±0.002
LD-091	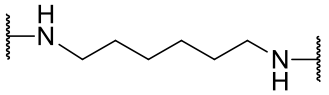	0.022±0.007
LD-251	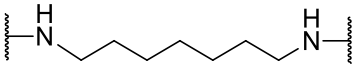	0.100±0.027
LD-111	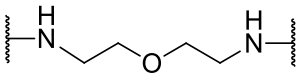	0.008±0.002
LD-075	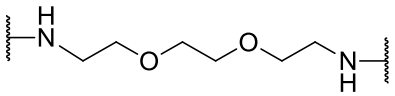	0.007±0.002
LD-112	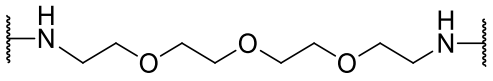	0.0045±0.0001
LD-086	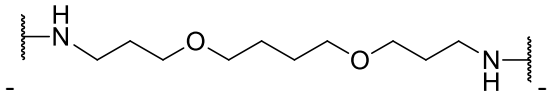	0.005±0.001
LD-085	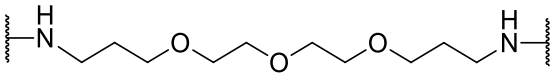	0.024±0.006
LD-076	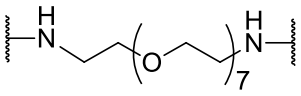	0.009±0.002

Then we next explored the linker length optimal for cellular potency for both hydrophobic and hydrophilic linkers in MDM2 degraders and results are shown in **Table 1-1**. For the hydrophobic carbon linker, the linker length was increased progressively by one methylene group.

Similar IC_{50} values from 9 nM to 12 nM in inhibition of RS4;11 cell growth were obtained with linkers composed of 3 to 5 methylene groups. But compound **LD-117** with one methylene group less than **LD-270** is about half as potent as **LD-270**. Further elongation of carbon linkers to 6 or 7 methylenes resulted in a 2-fold or 10-fold decrease in the cellular potency compared with **LD-074**. Hence the optimal length of a hydrophobic carbon linker is 3-5 methylene groups. With the hydrophilic PEG linkers, no significant change in cell growth inhibition activity was obtained from single ethylene glycol unit up to seven units. Among these, **LD-112**, with two such units shows best cell growth inhibitory activity with an IC_{50} value of 4.5 nM. Thus, modifications of the linker compositions identified compounds **LD-074** and **LD-112** as two potent MDM2 degraders with low nanomolar IC_{50} values in inhibition of RS4;11 cell growth. These two compounds were used for further modification.

Table 1-2. MDM2 degraders designed with different cereblon ligands.

	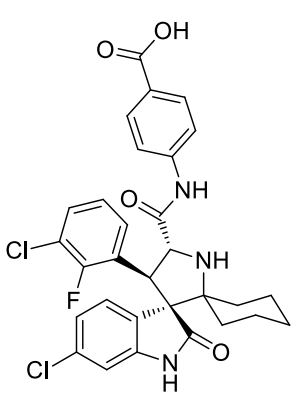 **MI-1061** 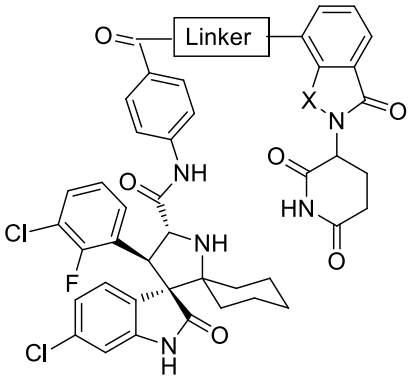		
Compound No.	Linker	X	IC_{50}/μM RS4;11

MI-1061			0.141±0.012
LD-110	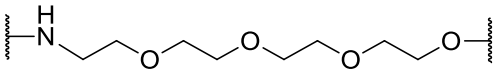	CO	0.026±0.011
LD-210	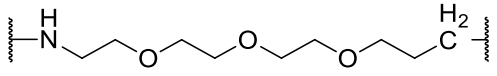	CO	0.053±0.015
LD-131	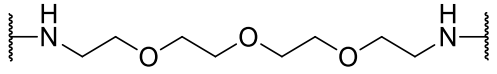	CH_2	0.006±0.001
LD-243	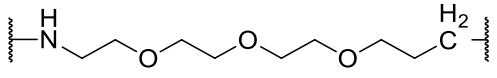	CH_2	0.0038±0.0006
LD-188	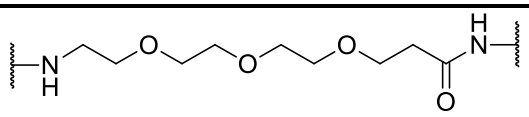	CH_2	0.022±0.005
LD-214	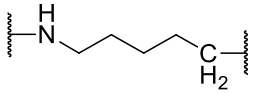	CO	0.029±0.008
LE-021	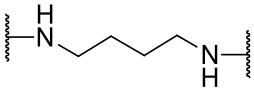	CH_2	0.005±0.005
LD-186	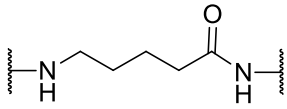	CH_2	0.012±0.001
LD-222	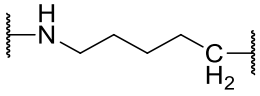	CH_2	0.0028±0.0011

Having determined the optimal linker length, we next sought to focus on the modifications of the linker composition and the cereblon ligand. Replacing NH in **LD-112** by oxygen or methylene resulted in **LD-110** and **LD-210**, which were 5 and 10 times less potent than **LD-112**, respectively. A similar result was obtained when **LD-214** was compared with **LD-074**, as

LD-214 is 3-fold less potent than **LD-074**. In all these synthetic compounds, we employed thalidomide as the ligand for cereblon. Lenalidomide, a second-generation thalidomide analogue used for the treatment of multiple myeloma and myelodysplastic syndromes, was also employed for the design of MDM2 degraders. Similar cellular potency was obtained by changing thalidomide in **LD-112**, to lenalidomide, which yielded **LD-131** with IC_{50} = 6 nM. **LD-243**, containing lenalidomide is 14 times more potent than **LD-210** which contains thalidomide. Introducing an amide attachment to lenalidomide in **LD-131** yielded **LD-188** and decreased the cellular potency. With a hydrophobic methylene linker, changing thalidomide to lenalidomide significantly improved the cellular potency in the RS4;11 cell line, **LD-222** being about 10 times more potent than **LD-074** and a similar loss of potency was obtained for **LD-186** with amide in the linker. The two most potent MDM2 degraders, **LD-222** and **LD-243** therefore were obtained by deleting one carbonyl group in thalidomide.

Table 1-3. MDM2 degraders designed with more rigid linkers.

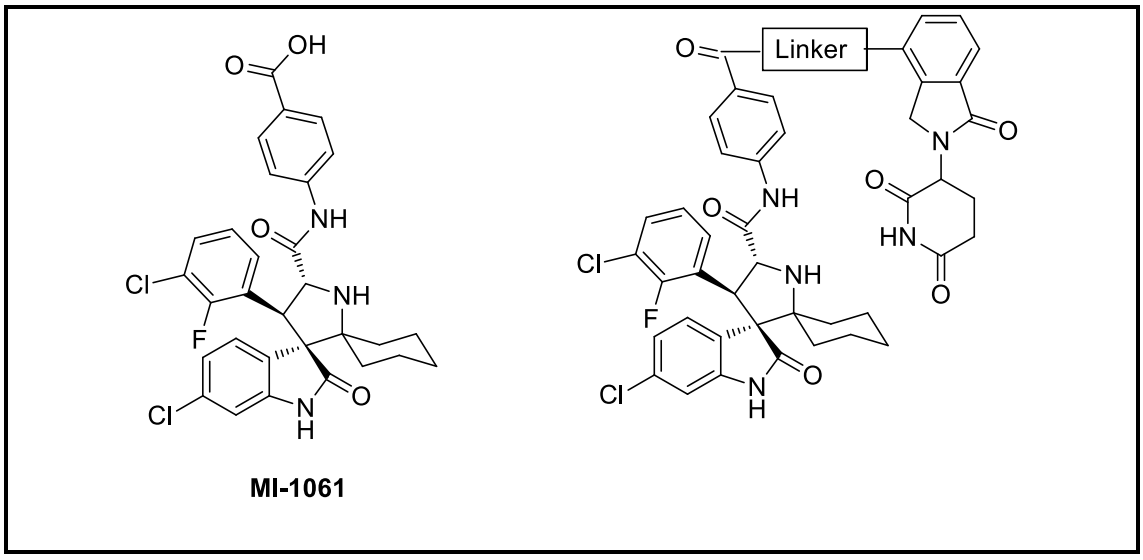

Compound No.	Linker	IC_{50}/μM RS4;11
MI-1061		0.141±0.012
LE-013	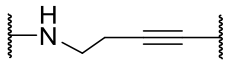	0.0039±0.0004
LE-004	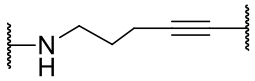	0.0015±0.0005
LE-081	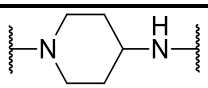	0.013±0.004
LE-082	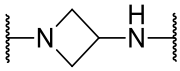	0.014±0.005
LE-083	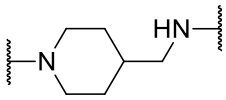	0.014±0.003
LE-084	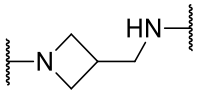	0.012±0.003
LE-254	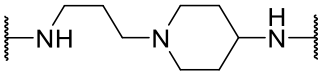	0.0012±0.0003
LE-093	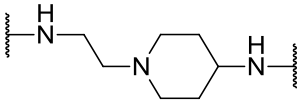	0.0041±0.0003
LE-094	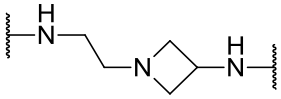	0.014±0.005
LE-095	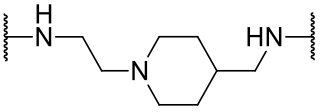	0.0039±0.0010

LE-096	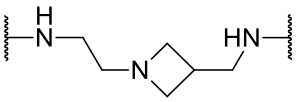	0.009±0.004
LE-102	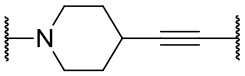	0.0023±0.0005
LE-103	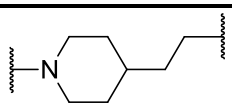	0.015±0.007
LE-194	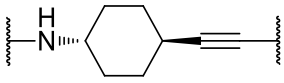	0.824±0.687
LE-200	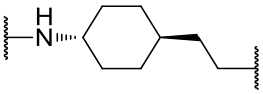	0.052±0.031
LD-254	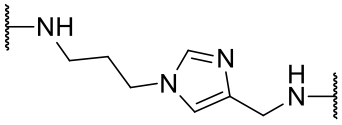	0.0029±0.0012
LE-243	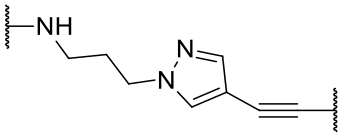	0.008±0.004
LE-244	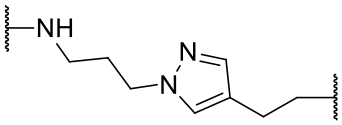	0.0047±0.0015
LE-224	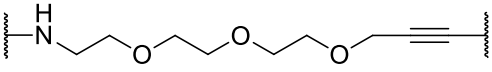	0.0030±0.0012

From the SAR study of linker length, composition and cereblon ligands, the two best compounds with hydrophobic linkers that were obtained were **LE-021** and **LD-222**. No co-crystal structures of MDM2 degraders in a complex with MDM2 and cereblon protein were obtained,

but several modifications to increase the linker rigidity were applied as increasing the rigidity of MDM2 degraders is thought to increase the potency, selectivity, stability and pharmacokinetic properties.[59] Several MDM2 degraders with rigid linkers were synthesized and tested and the results are summarized in **Table 1-3**. At first, based on the structure of **LE-**021, several piperidine or azetidine rings were introduced. Both **LE-081** and **LE-083** with piperidine or **LE-082** and **LE-084** with azetidine in the linker are about half as potent as **LE-021**, which indicates a poor conformation of the linkers. Introduction of a shorter flexible methylene linker to **LE-081** or **LE-083** yields **LE-254**, **LE-093** and **LE-095** all of which show better cell growth inhibitory activity. Among these, **LE-254** shows best cell growth inhibition activity with IC_{50}=1.2 nM in the RS4;11 cell line. Introduction of a triple bond into the hydrophobic methylene linkers, should decrease the flexibility of the linker and accordingly, **LE-013** and **LE-004** were synthesized. Both show good cellar potency with IC_{50} = 3.9 and 1.5 nM in the RS4;11 cell line. In a combination of these two strategies, a more rigid linker was used to yield **LE-102**, which shows good cell growth inhibitory activity with IC_{50} = 2.3 nM in the RS4;11 cell line, but increasing the flexibility by reducing the triple bond or using cyclohexylamine to replace piperidine in **LE-102** was found to decrease its inhibitory activity, indicating that **LE-102** reaches an appropriate confirmation to form the protein complex for MDM2 degradation. Imidazole and pyrazole rings were also introduced to the linker, and among these, **LD-254** shows good cellar potency with IC_{50} = 2.9 nM in the RS4;11 cell line. Introduction of a triple bond into the polyethylene glycol linker led to less potent compounds than introduction of the corresponding methylene linker. Thus, according to the study of MDM2 degrader with rigid linkers, **LE-102** was chosen for further preclinical evaluation.

Table 1-4. MDM2 degraders linked to different positions of the cereblon ligand.

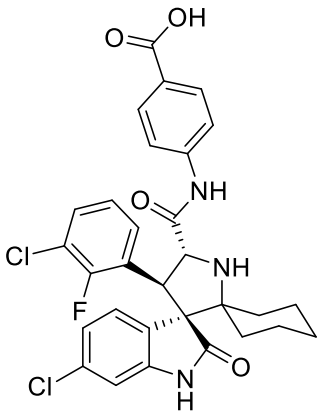

MI-1061

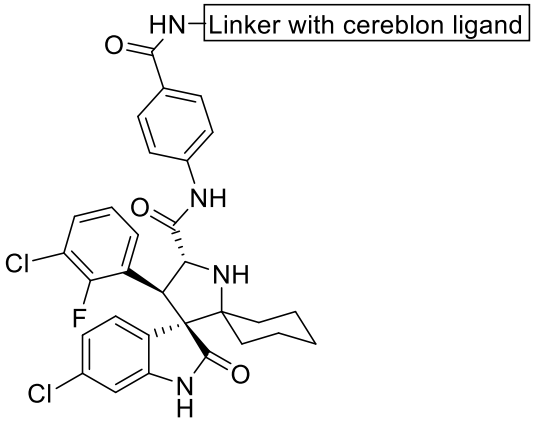

Compound No.	Linker with cereblon ligand	IC50/μM RS4;11
MI-1061		0.141±0.012
LE-178	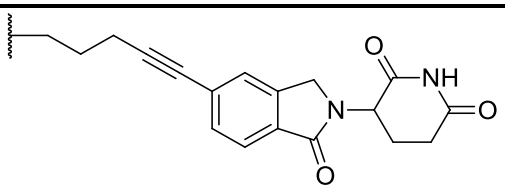	0.0048±0.0018
LE-179	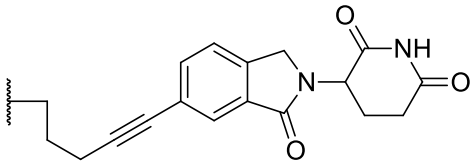	0..005±0.003
LE-180	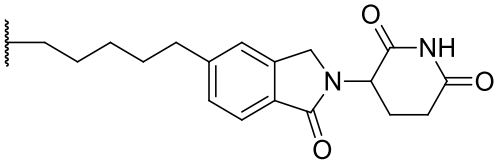	0.0030±0.0011
LE-181	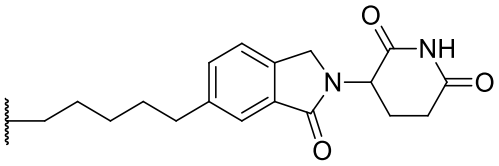	0.012±0.003

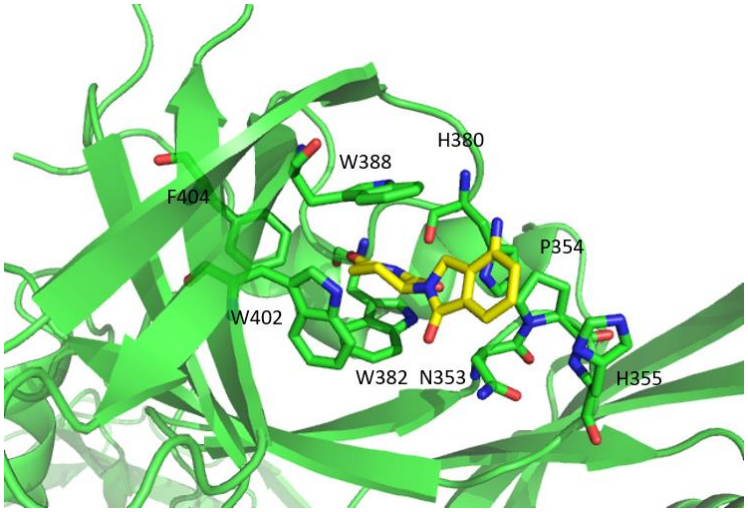

Figure 1-15. Co-crystal structure of DDB1-CRBN E3 ubiquitin ligase complexed with Lenalidomide (Yellow, PDB ID 4CI2).

Another important question is whether other parts of thalidomide analogues could be used to link to MDM2 inhibitors. To answer this question, different linking sites of lenalidomide analogues were explored with hydrophobic methylene linkers in **LD-222** and **LE-004**. Based on the co-crystal structures of lenalidomide with cereblon (PDB ID: 4CI2)[60], other positions on the phenyl ring facing outside the pocket could be useful for PROTAC design (**Figure 1-15**). Accordingly **LE-178, LE-179, LE-180** and **LE-181** were synthesized and tested (**Table 1-4**). These MDM2 degraders show good cellar potency in the RS4;11 cell line and the results indicate that 5- and 6-positions on the 1-oxoisoindolinyl group of lenalidomide ananlogue are promising linking sites for the design of PROTACs.

Further Evaluation of Two Potent PROTAC MDM2 Degraders LE-004 and LE-102

Next, extensive evaluations to investigate the mechanism of action and therapeutic potentials of **LE-004** and **LE-102**, were performed with **MI-1061** as the MDM2 inhibitor control.

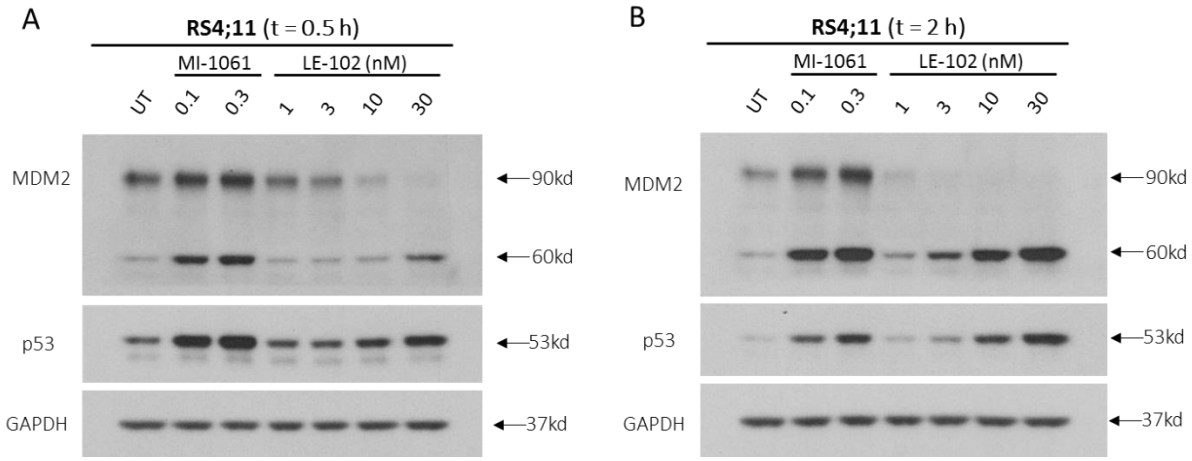

Figure 1-16. Western blotting analysis of MDM2 and p53 proteins in RS4;11 cells treated with MDM2 inhibitor **MI-1061** and MDM2 degraders **LE-102**. RS4;11 cells were treated for 0.5 and 2 h with each individual compound at indicated concentrations, and proteins were probed by specific antibodies. GAPDH was used as the loading control.

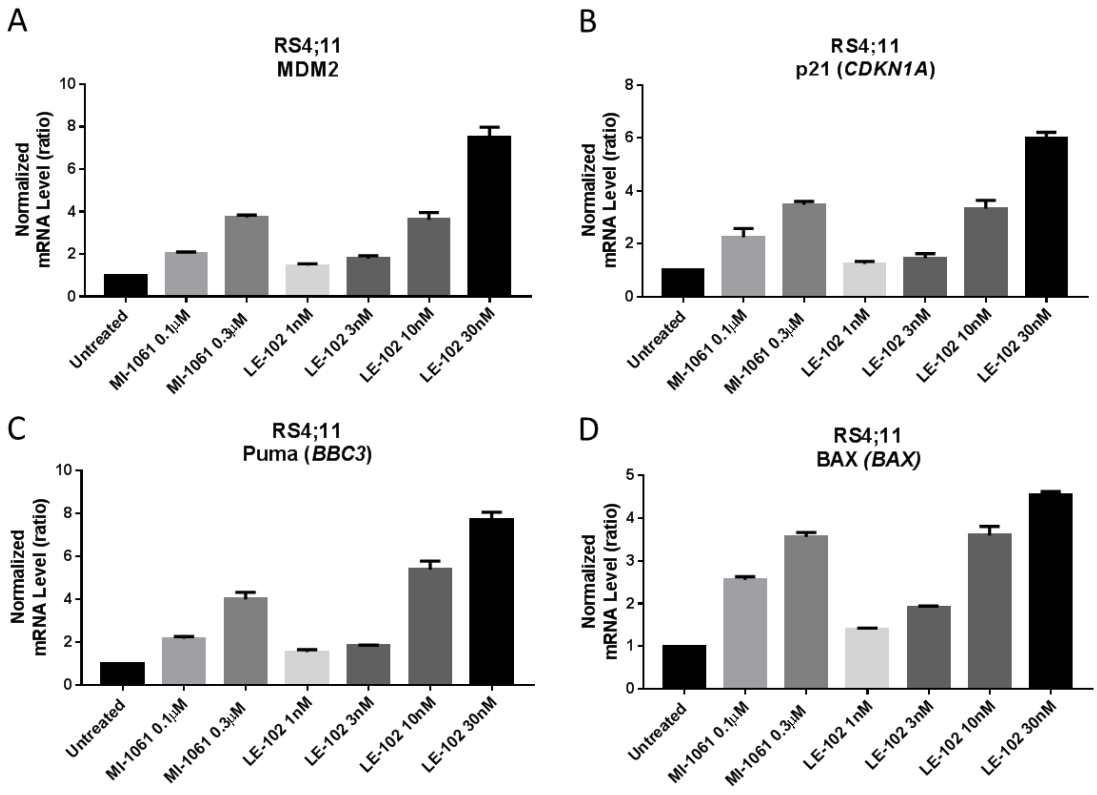

Figure 1-17. qPCR analysis of MDM2, p21, Puma and BAX mRNA levels in RS4;11 cells treated with **MI-1061** or **LE-102** degrader at the indicated concentrations for 6 h.

The results of the MDM2 degradation and p53 activation by **LE-102** were examined and compared with data from the MDM2 inhibitor **MI-1061** in the RS4;11 cell line giving the results shown in **Figure 1-16**. **LE-102** can effectively and potently induce degradation of MDM2 protein in a dose-dependent manner after 30 min treatment. Clear MDM2 degradation was observed at concentrations as low as 3 nM. After 2 h treatment, significant and more efficient p53 activation was obtained with **LE-102** than with **MI-1061**. No MDM2 protein accumulation was observed following MDM2 degrader treatment when compared with the MDM2 inhibitor treatment. qPCR

analysis also confirmed that **LE-102** is more effective than **MI-1061** in activation of p53 downstream genes (**Figure 1-17**).

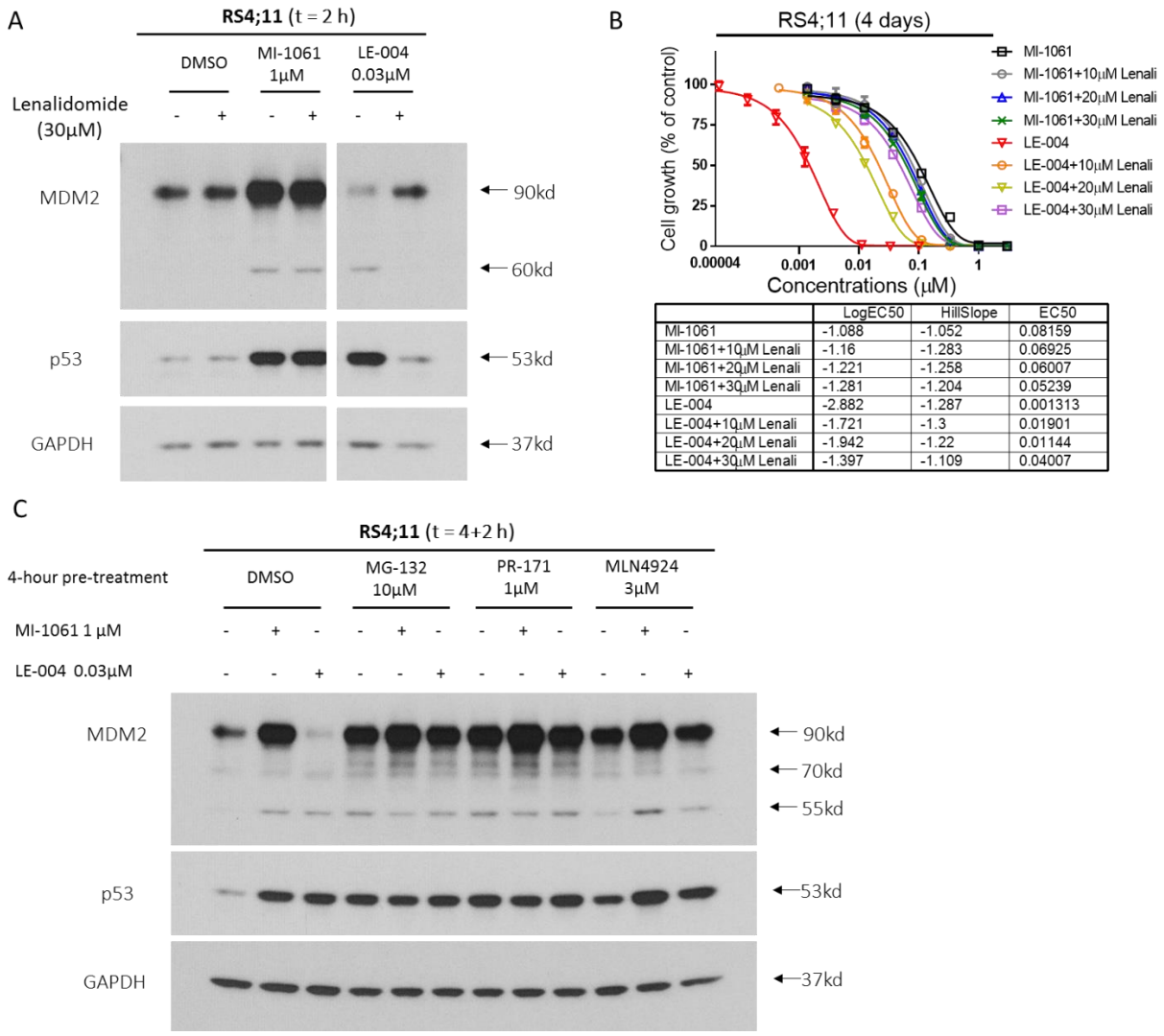

	LogEC50	HillSlope	EC50
MI-1061	-1.088	-1.052	0.08159
MI-1061+1μM Lenali	-1.16	-1.283	0.06925
MI-1061+2μM Lenali	-1.221	-1.258	0.06007
MI-1061+3μM Lenali	-1.281	-1.204	0.05239
LE-004	-2.882	-1.287	0.001313
LE-004+1μM Lenali	-1.721	-1.3	0.01901
LE-004+2μM Lenali	-1.942	-1.22	0.01144
LE-004+3μM Lenali	-1.397	-1.109	0.04007

Figure 1-18. (A) & (B) Excess lenalidomide reduces cell growth inhibition, MDM2 degradation and p53 activation activity of **LE-004**. (C) Proteasome inhibitors and neddylation inhibitors reduce MDM2 degradation and p53 activation activity of **LE-004**.

As the design of MDM2 PROTACs requires their binding to the $Cul4^{CRBN}$ 4 E3 ubiquitin ligase complex through CRBN for MDM2 degradation and p53 activation, we predicted that excess lenalidomide should effectively block the MDM2 degradation and p53 activation induced by **LE-004**. Lenalidomide should not affect the upregulation of MDM2 and p53 proteins induced by **MI-1061**. Western blotting analysis showed that lenalidomide indeed effectively blocks MDM2 degradation and accumulation of p53 protein by **LE-004** and has no effect on MDM2 and p53 accumulation induced by the MDM2 inhibitor **MI-1061** (**Figure 1-18A**). Co-treatment of **LE-004** with 30 μM of lenalidomide also greatly reduces its cell growth inhibitory activity and has essentially the same effect as the MDM2 inhibitor **MI-1061**, used alone. (**Figure 1-18B)** These data indicate that the binding of **LE-004** to cereblon is effectively blocked by lenalidomide, and the degradation of MDM2 induced by **LE-004** is dependent upon CRBN. We also found that proteasome inhibitors **MG-132** and **PR-171** and the neddylation inhibitor **MLN4924** can effectively block the MDM2 degradation caused by **LE-004** in RS4;11 cells. (**Figure 1-18c**)

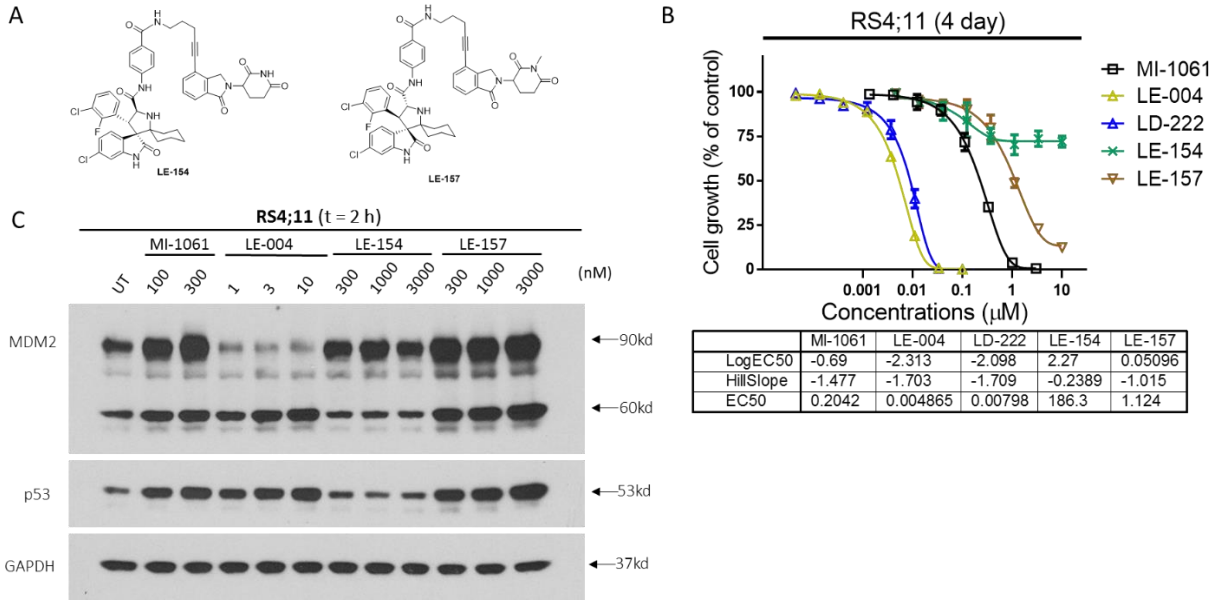

	MI-1061	LE-004	LD-222	LE-154	LE-157
LogEC50	-0.69	-2.313	-2.098	2.27	0.05096
HillSlope	-1.477	-1.703	-1.709	-0.2389	-1.015
EC50	0.2042	0.004865	0.00798	186.3	1.124

Figure 1-19. Activity of the negative control compounds **LE-154 and LE-157** with weaker binding affinity to MDM2 or CRBN compared with **LE-004**.

To further investigate the mechanism of MDM2 degradation induced by **LE-004**, two control compounds **LE-154** and **LE-157** were synthesized (**Figure 1-19A**). **LE-154**, an enantiomer of **LE-004** is more than 100-times less potent than **LE-004** in inducing MDM2 degradation in RS4;11 cells (**Figure 1-19B**). Consistently, it is more than 100-times less potent when compared to **LE-004** in growth inhibition assay in RS4;11 cells (**Figure 1-19C**). In the other negative control compound **LE-157**, the amino group of the piperidine-2,6-dione was methylated. The previous study showed that the amino group of the piperidine-2,6-dione in lenalidomide forms a strong hydrogen bond with CRBN[60-61] and methylation on this amino group can completely block its binding to CRBN[18, 60]. Indeed, **LE-157** was found to be completely inactive in inducing MDM2 degradation (**Figure 1-19B**) and is more than 100-times less potent than **LE-004** in inhibition of cell growth in RS4;11 cells (**Figure 1-19C**). These data confirm that the degradation of MDM2 induced by **LE-004** requires its strong binding to MDM2 and cereblon, which is consistent with our original PROTAC design.

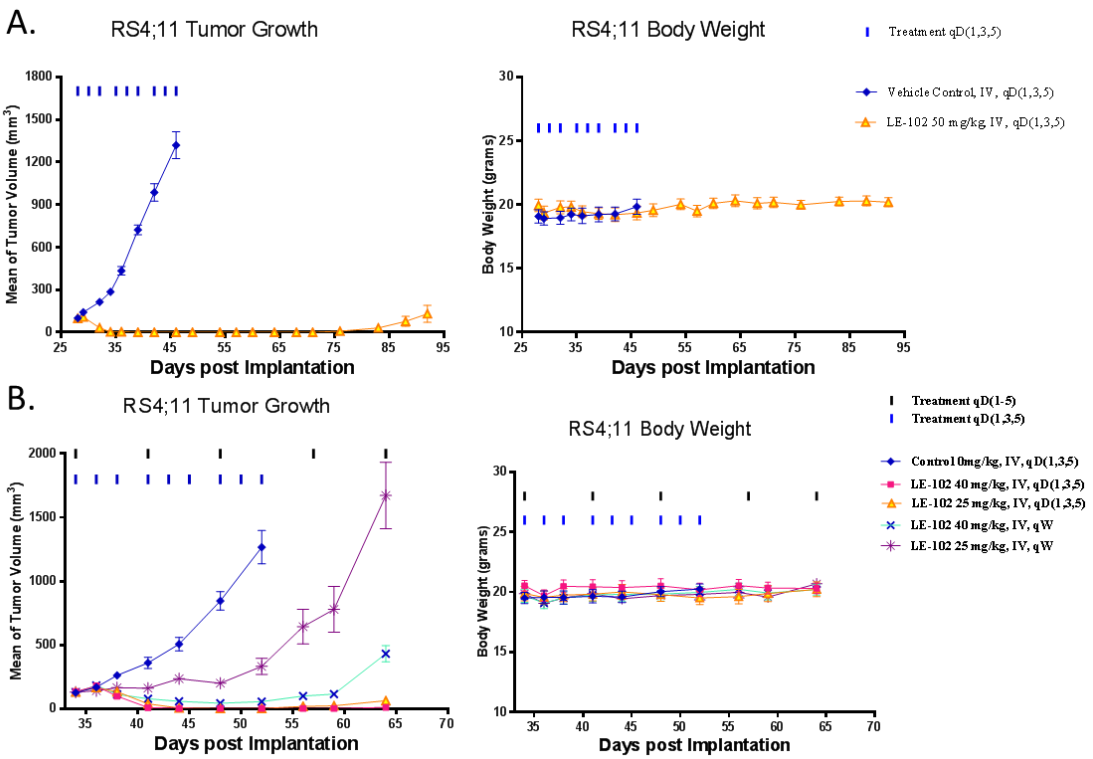

Figure 1-20. MDM2 degrader **LE-102** induces complete tumor regression in the xenograft model of human RS4;11 tumor cells with minimal body weight change with variety dose of **LE-102.**

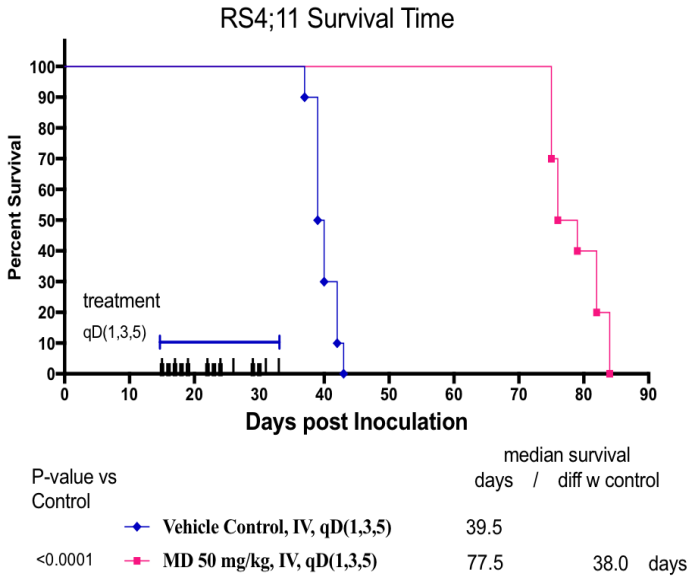

Figure 1-21. MDM2 degrader **LE-102** extended the survival time in RS4;11 disseminated model.

Based on this SAR study of MDM2 degraders, **LE-102** was chosen for further *in-vivo* study. The antitumor activity of **LE-102** was tested in the RS4;11 xenograft model in mice and the results are shown in **Figure 1-20**. Mice bearing RS4;11 xenograft tumors were administered 25, 40 and 50 mg/kg of **LE-102** intravenously every other day, three times a week for 3 weeks and achieved rapid and complete tumor regression. There was no weight loss or other signs of toxicity in mice treated with **LE-102**, and the animal weight gained in the vehicle control group of mice was attributed largely to rapid tumor growth. Although no complete tumor regression was obtained by doses of 25 or 40 mg/kg of **LE-102** once per week, such doses can significantly inhibit the tumor growth (**Figure 1-20)**. In the RS4;11 mice disseminated model, dosing of the mice with 50 mg/kg of **LE-102** intravenously every other day, three times a week for 3 weeks achieved significant extension of the survival time. No significant weight loss was observed in the treatment groups (**Figure 1-21**). Therefore, the *in vivo* data firmly establish that **LE-102** has highly efficacious antitumor activity at a well-tolerated dose-schedule in mice.

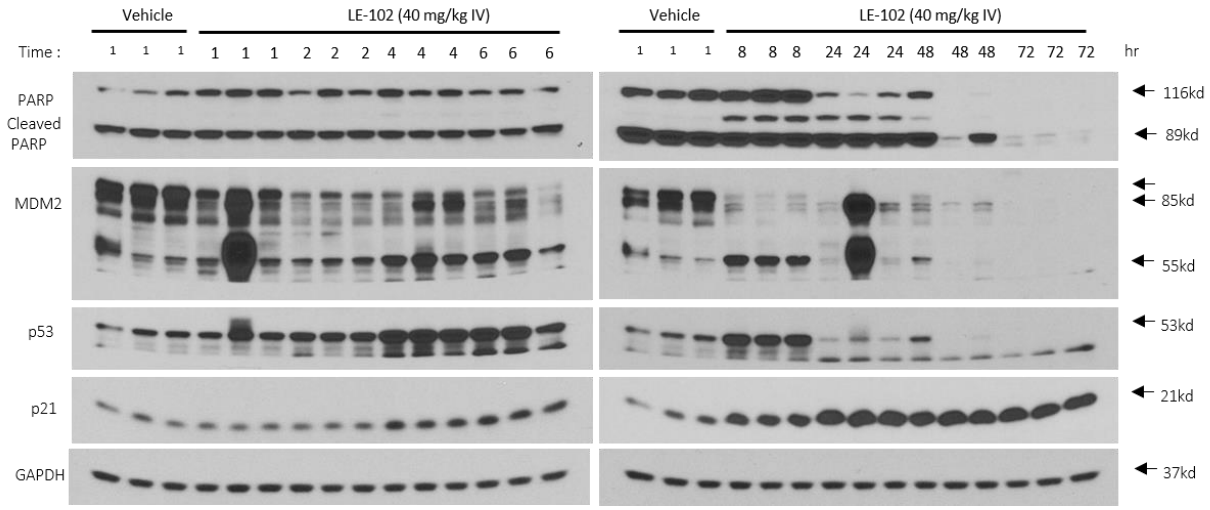

Figure 1-22. Pharmacodynamic analysis of **LE-102** in RS4;11 xenograft tumor tissue. SCID mice bearing RS4;11 tumors were treated with a single intravenous dose of **LE-102** of 40 mg/kg. Mice were sacrificed at 1, 2, 4, 6, 8, 24, 48 and 72 h time-points after administration of compound **LE-102** or at 6 h with vehicle control, and tumors were harvested from the mice for Western blotting analysis of MDM2, p53, p21, PARP and cleaved PARP (Cl PARP). GAPDH was used as the loading control and three mice were used for each time-point with each mouse bearing one tumor.

To gain a better understanding of the strong antitumor activity of **LE-102** and its mechanism of action *in vivo*, pharmacodynamics (PD) analysis in SCID mice bearing the RS4;11 xenograft tumors was performed. In this experiment, mice bearing RS4;11 xenograft tumor were administered a single dose of **LE-102** at 50 mg/kg intravenously and were sacrificed at 1, 2, 4, 6, 8, 24, 48 and 72 h time-points after the treatment. Mice treated with vehicle control were sacrificed at the 6 h time point. Western blotting analysis was performed to probe the level of MDM2 proteins, as well as p53, p21 and PARP proteins in the tumor tissue. The PD data in **Figure 1-22** clearly show that a single dose of **LE-102** is highly effective, dramatically reducing the level of MDM2 proteins with p53 protein accumulation in the RS4;11 tumor tissue. The effects persist longer than 24 h. The level of p21 is strongly up-regulated, with the effect persisting for as long as 72 h. PD analysis clearly demonstrates that a single dose of **LE-102** is sufficient to induce significant degradation of MDM2 protein with p53 accumulation for more than 24 h in mice.

Table 1-5. Analysis of concentration of **LE-102** in Plasma and RS4;11 Tumor Tissue.

Time (h)	Concn in plasma (ng/mL)					Concn in Tumor (ng/mL)				
	individual mice			mean	SD	individual mice			mean	SD
1	65453	106216	83165	84945	20440	1275	2041	3184	2167	961
2	47751	68303	72588	62881	13277	1868	1852	2472	2064	353
4	56811	48418	60267	55165	6094	2630	3547	2974	3050	463
6	43132	41466	37518	40705	2883	2736	6360	3576	4224	1897
8	24969	26867	35131	28989	5403	4336	5317	4257	4636	591
24	5085	5869	5796	5583	433	4253	5045	3241	4180	904
48	1776	2196	3301	2424	788	1937	2539	4297	2924	1226
72	2466	1657	3700	2608	1029	4576	3309	3422	3769	701

Pharmacokinetic (PK) analysis was performed to study the concentrations of **LE-102** in plasma and RS4;11 xenograft tumors in the same mice used in the PD experiment. PK data have shown that despite its relatively large size, **LE-102** can effectively penetrate the RS4;11 xenograft tumor tissue and stay in the tumor for a long time. It produces a concentration of **LE-102** of 2064 to 4636 ng/mL in the tumor from 1 h to 72 h, thus exceeding the drug concentrations shown in our *in vitro* experiments to be necessary for effective MDM2 degradation. Our PK data indicates that a single dose of **LE-102** at 40 mg/kg achieves sufficient exposure in the tumor tissue for effective induction of MDM2 protein degradation for over 72 h.

Table 1-6. MDM2 inhibitors conjugated with VHL-1 ligands.

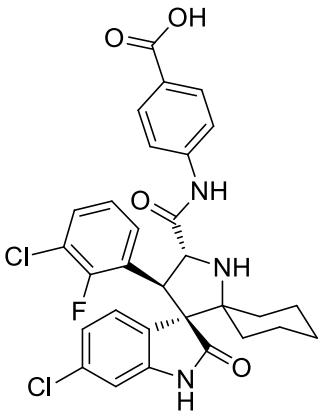

MI-1061

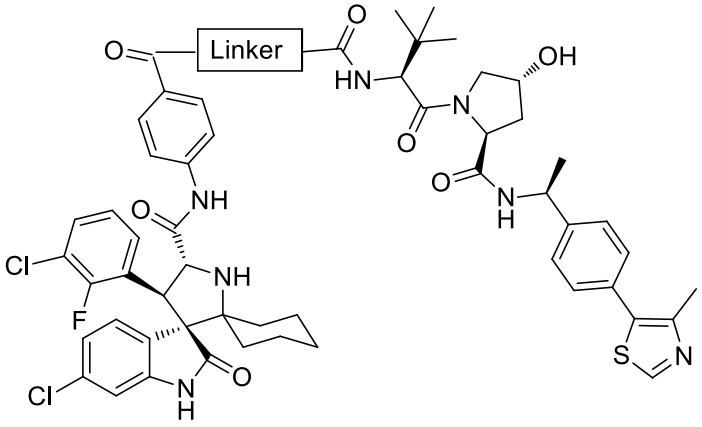

Compound No.	Linker	IC_{50}/µM RS4;11
MI-1061		0.141±0.012
LE-175	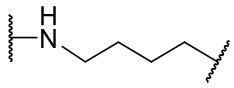	1.23±0.77
LE-176	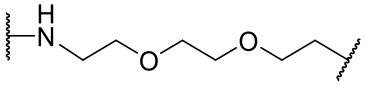	0.497±0.137
LE-177	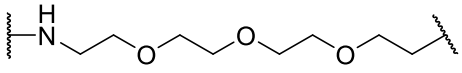	0.343±0.023

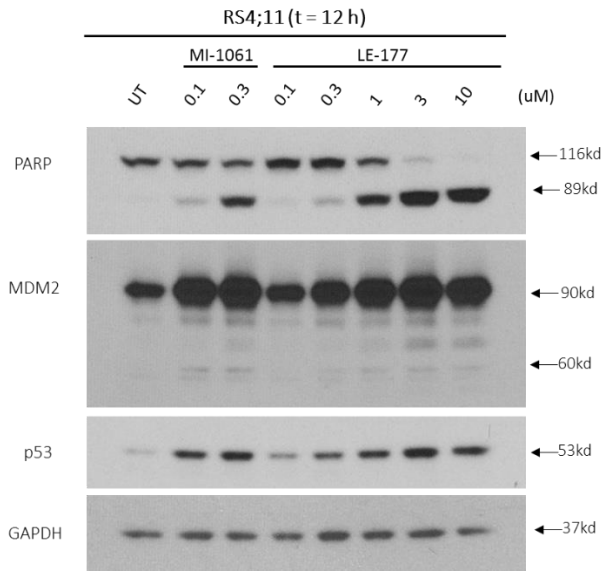

Figure 1-23. Western blotting analysis of MDM2 and p53 proteins in RS4;11 cells treated with MDM2 inhibitor **MI-1061** and MDM2 degraders **LE-177**. RS4;11 cells were treated for 12 h with each individual compound at indicated concentrations, and proteins were probed by specific antibodies. GAPDH was used as the loading control.

With the successful design of MDM2 PROTACs containing a cereblon binding ligand, we sought to explore other E3 ubiquitin ligases for MDM2 degradation. Specific small peptide mimetic VHL ligands were developed and successfully applied in the design of PROTACs targeting BET and AR protein degradation with $Cul2^{VHL}$ E3 ubiquitin ligase.[21, 57] Accordingly, **LE-175** with a hydrophobic linker and **LE-176** and **LE-177** with hydrophilic linkers were synthesized and tested. They were found to be 4-9 times weaker than **MI-1061** in a cell growth inhibition assay. No MDM2 degradation by treatment with these bivalent compounds was observed in a Western Blotting assay. The result indicates that PROTACs recruiting $Cul2^{VHL}$ E3 ubiquitin ligase could not induce

MDM2 degradation. (**Figure 1-23**) Similar results have been reported for the design of PROTACs targeting BCR-ABL protein.[22]

Table 1-7. MDM2 degraders and inhibitors with different binding affinity to MDM2.

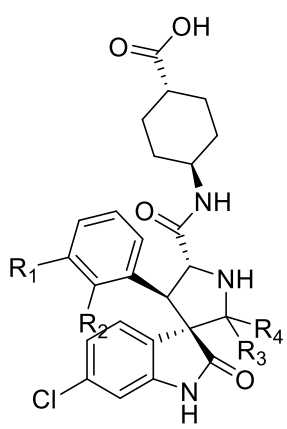

Inhibitor

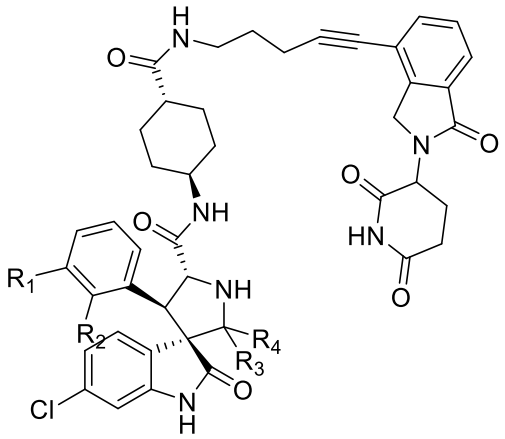

Degrader

Compound No.		R1	R2	R3, R4	K_d (nM)	RS4;11 IC_{50}/μM
HXA-110	Inhibitor	Cl	F	Cyclohexyl	11.2±0.9	0.025±0.006
AA-231	Degrader	Cl	F	Cyclohexyl		0.0008±0.0001
LE-211	Inhibitor	Cl	H	Cyclohexyl	18.3±4.1	0.058±0.015
LE-297	Degrader	Cl	H	Cyclohexyl		0.0007±0.0002
HXA-119	Inhibitor	H	F	Cyclohexyl	101±8	0.135±0.022
LE-295	Degrader	H	F	Cyclohexyl		0.203±0.106
LE-217	Inhibitor	F	H	Cyclohexyl	230±25	0.535±0.166

LE-298	Degrader	F	H	Cyclohexyl		2.71±0.57
HXA-120	Inhibitor	H	H	Dimethyl	5578±1670	1.75±0.09
LE-296	Degrader	H	H	Dimethyl		21.5±8.6

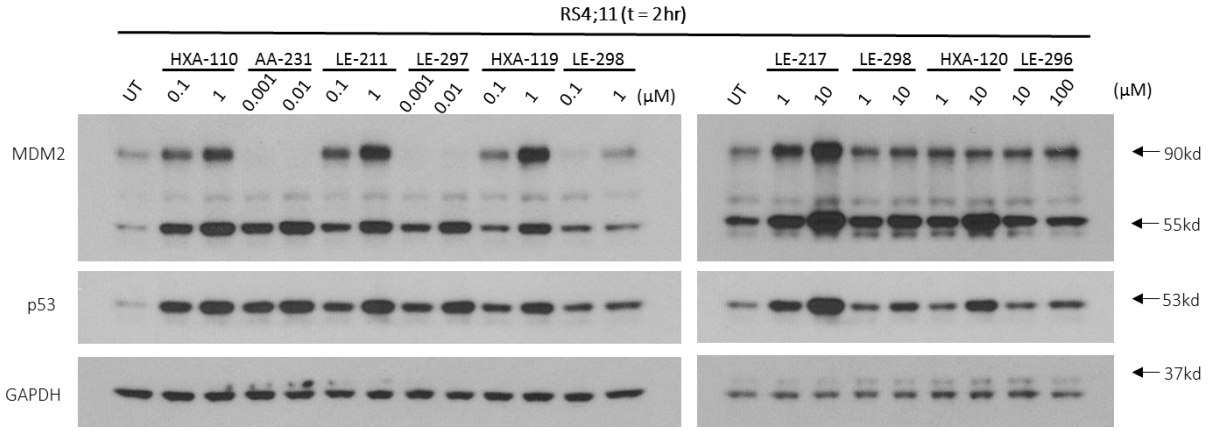

Figure 1-24. Western blotting analysis of MDM2 and p53 proteins in RS4;11 cells treated by MDM2 inhibitors and degraders with different binding affinities to MDM2. RS4;11 cells were treated for 2 h with each compound at indicated concentrations, and proteins were probed by specific antibodies. GAPDH was used as the loading control.

PROTAC strategy in which protein inhibitors are linked with an E3 ubiquitin ligase has become a promising method in drug discovery. The binding affinity requirement of the protein binding ligand has however not been clearly explored. To address this problem, several MDM2 inhibitors with different MDM2 binding affinities were synthesized. The linker and cereblon binding ligand used in **LE-004** were linked to these MDM2 inhibitors. The cell growth inhibition activities and MDM2 protein degradation effects of these MDM2 inhibitors and the

corresponding degraders have been tested and the results are summarized in **Table 1-7** and **Figure 1-24**. The binding affinity of MDM2 inhibitors was tested in an OctetRED assay. The most potent MDM2 degrader, **HXA-110** binds to MDM2 with K_d = 11 nM, and can efficiently inhibit the RS4;11 cell line with IC_{50} = 25 nM. The corresponding degrader, **AA-231** is 30 times more potent than **HXA-110** with IC_{50} = 0.8 nM in the RS4;11 cell line. Similar results were obtained with **LE-211** and **LE-297**. **HXA-119**, which binds to MDM2 with K_d= 101 nM has a cell growth inhibition activity similar to that of its corresponding degraders **LE-295**, with IC_{50} = 135 nM and 203 nM. The less potent inhibitor **LE-217** with K_d= 230 nM is 5 times more potent than the degrader **LE-298**. Similar results were obtained with the weakest inhibitor **HXA-120** with K_d = 5.6 μM and the degrader **LE-296**. Western Blotting has shown that **AA-231, LE-297** and **LE-295** could cause significant MDM2 degradation compared with their inhibitors, while little MDM2 degradation was observed in the treatment with **LE-298** and **LE-296**. This result indicates that MDM2 inhibitors with protein binding affinity < 200 nM can be applied with a cereblon ligand for MDM2 degradation only with difficulty. The weak binding affinity may fail to recruit the target proteins to the E3 ubiquitin ligases and subsequently induce protein degradation.

Synthesis

The synthesis of MDM2 inhibitors **HXA-110, LE-211, HXA-119, LE-217, HXA-120** and corresponding MDM2 degraders **AA-231, LE-297**, **LE-295**, **LE-298**, **LE-296** is shown in Scheme 1. Various substituted (E)-3-benzylidene-6-chloroindolin-2-one and ketones were used to synthesize compounds **108a-108e**. Then these intermediates were methylated with methanol and concentrated sulfuric acid and the chiral auxiliary group was removed with ammonium

cerium(IV) nitrate in acetonitrile/water to form **110a-110e**. Compounds **112a-112e** were obtained by hydrolysis with lithium hydroxide in water, MeOH and THF and subsequently, an amide condensation reaction with *trans*-methyl 4-aminocyclohexanecarboxylate. The esters were hydrolyzed and reacted with methylamine or with compound **105d** to form the MDM2 inhibitors and degraders.

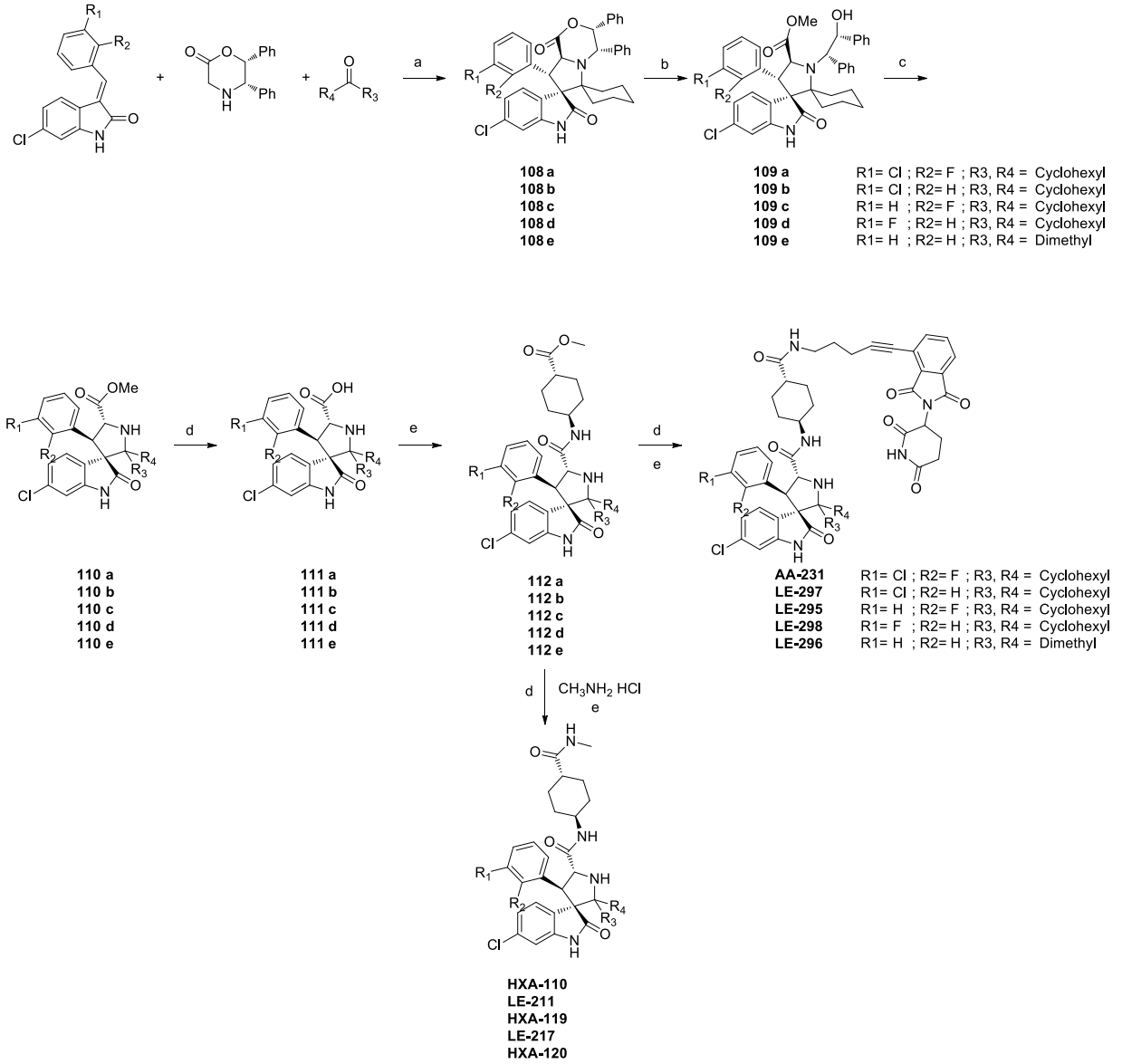

Scheme 1-1. Synthesis of **AA-231, LE-297, LE-295, LE-298, LE-296, HXA-110, LE-211, HXA-119, LE-217** and **HXA-120.** Reaction conditions: (a) toluene, reflux; (b) conc. H_2SO_4, MeOH rt; (c) ammonium cerium(IV) nitrate, acetonitrile, water; (d) LiOH, MeOH, H_2O, THF; (e) HATU, DIEA, DMF.

The synthesis of MDM2 degraders with thalidomide is shown in Scheme 2. The intermediates **101a-101j** were synthesized by a nucleophilic substitution reaction with 2-(2,6-dioxopiperidin-3-yl)-4-fluoroisoindoline-1,3-dione and the Boc protecting groups were removed under acidic conditions. MDM2 degraders **LD-117**, **LD-270**, **LD-074**, **LD-252**, **LD-091**, **LD-251**, **LD-111**, **LD-075**, **LD-112** and **LD-076** were then obtained by an amide condensation reaction with **MI-1061**. **LD-110** was synthesized from 2-(2,6-dioxopiperidin-3-yl)-4-hydroxyisoindoline-1,3-dione and 2,2-dimethyl-4-oxo-3,8,11,14-tetraoxa-5-azahexadecan-16-yl 4-methylbenzene- sulfonate under weak basic conditions. The Boc protecting group was removed with trifluoroacetic acid to yield **LD-114. LD-110** was obtained by an amide condensation reaction with **MI-1061**.

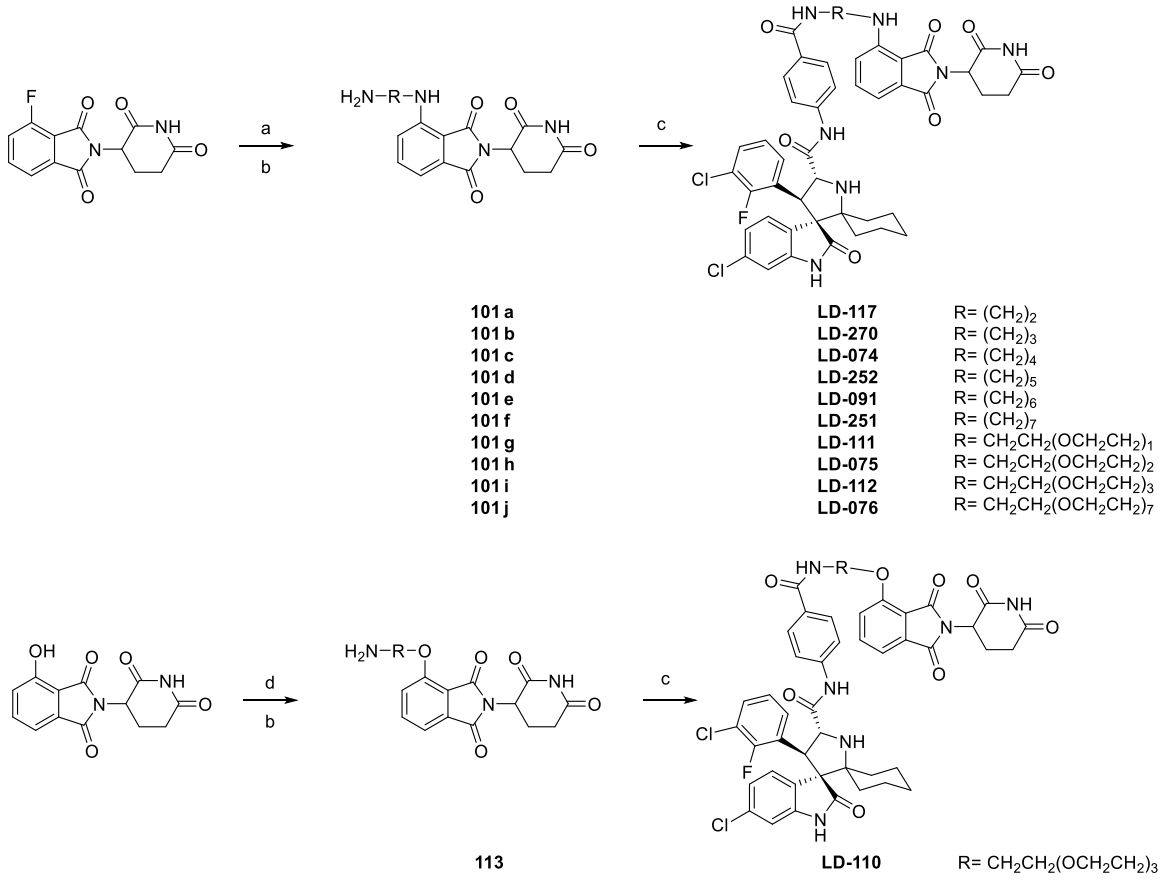

Scheme 1-2. Synthesis of **LD-117, LD-270, LD-074, LD-252, LD-091, LD-251, LD-111, LD-075, LD-112, LD-076** and **LD-110.** Reaction conditions: (a) DIPEA, DMF, 80 °C; (b) trifluoroacetic acid, DCM, rt; (c) HATU, DIPEA, DMF, rt; (d) $KHCO_3$, DMF, 50 ^oC.

The synthesis of MDM2 degraders containing lenalidomide is shown in Schemes 3 and 4. The intermediates **102a**-**102d** and **103a-103e** were synthesized by a reductive amination reaction with lenalidomide and the Boc groups were then removed under acidic conditions. Intermediates **104a-104e** were then synthesized by another reductive amination reaction with **103a-103d** and subsequent deprotection reactions. The MDM2 degraders **LD-131**, **LE-021, LD-188, LD-186, LE-**

081, LE-082, LE-083, LE-084, LD-254, LE-254, LE-093, LE-094, LE-095 and **LE-096** were then obtained by an amide condensation reaction with **MI-1061**.

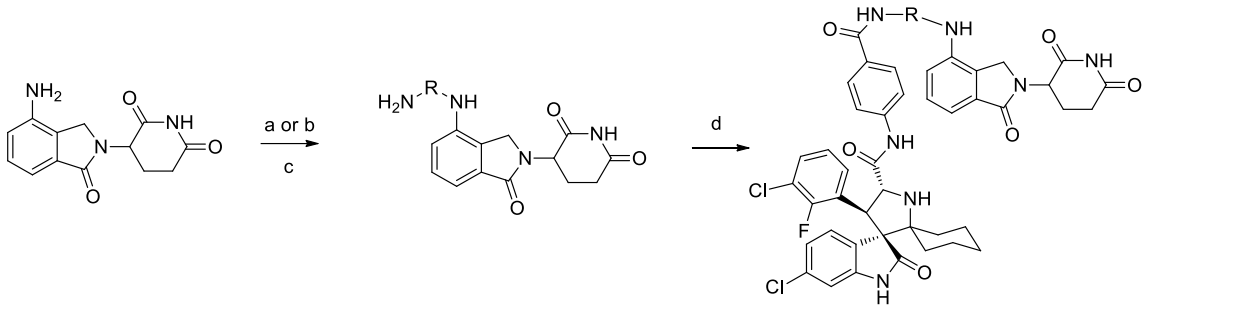

Scheme 1-3. Synthesis of **LD-131, LE-021, LD-188** and **LD-186.** Reaction conditions: (a) $NaBH(OAc)_3$, HOAc, DCE; (b) HATU, DIEA, DMF, rt; (c) trifluoroacetic acid, DCM, rt; (d) HATU, DIPEA, DMF, rt.

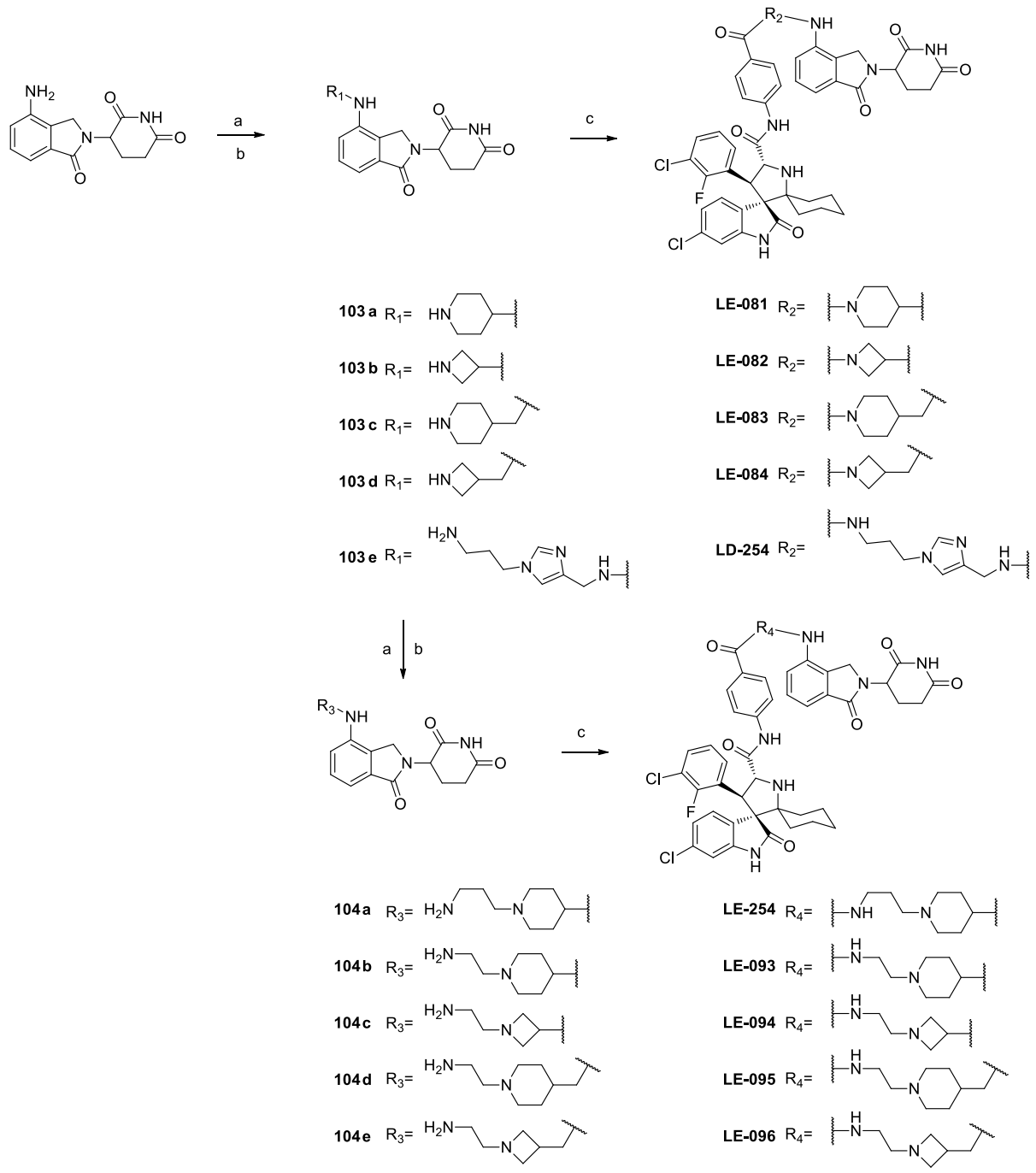

Scheme 1-4. Synthesis of **LE-081, LE-082, LE-083, LE-084, LD-254, LE-254, LE-093, LE-094, LE-095** and **LE-096.** Reaction conditions: $NaBH(OAc)_3$, HOAc, DCE; (b) trifluoroacetic acid, DCM, rt; (c) HATU, DIPEA, DMF, rt.

The synthesis of MDM2 degraders with direct C-C bond linking to 3-(1-oxoisoindolin-2-yl)piperidine-2,6-dione is shown in Schemes 5 and 6. Linkers with a Boc protected amino group and an ethynyl group were linked to the cereblon binding ligand by Sonogashira coupling reactions with corresponding bromo-substituted thalidomide or the bromo-substituted 3-(1-oxoisoindolin-2-yl)piperidine-2,6-dione. The Boc protecting groups were removed with trifluoroacetic acid to obtain intermediates **105a-105g** and **113a-113b**. The triple bonds were then reduced by H_2 with Pd/C to form intermediates **106a-106g** and **114a-114b**. MDM2 degraders **LE-224, LE-04, LE-102, LE-194, LE-243, LD-210, LD-214, LD-243, LD-222, LE-103, LE-200, LE-244, LE-178, LE-179, LE-180, LE-181** were then obtained by an amide condensation reaction with **MI-1061**.

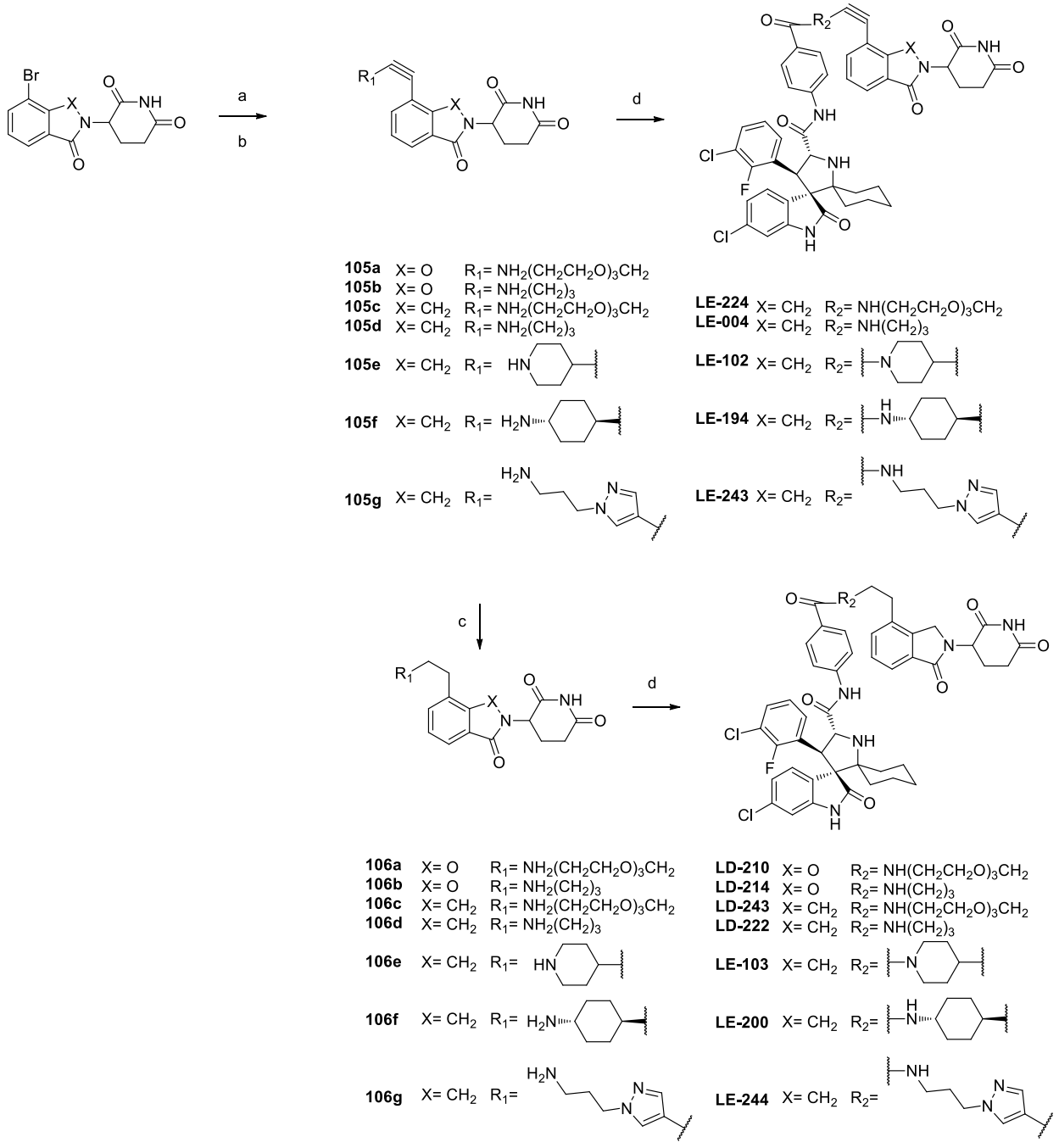

Scheme 1-5. Synthesis of **LE-224, LE-004, LE-102, LE-194, LE-243, LD-210, LD-214, LD-243, LD-222, LE-103, LE-200** and **LE-244.** Reaction conditions: (a) $Pd(PPh_3)_2Cl_2$, CuI, triethylamine, DMF, 80 °C; (b) trifluoroacetic acid, DCM, rt; (c) H_2 (1 atm), Pd/C, EtOH, rt; (d) HATU, DIPEA, DMF, rt.

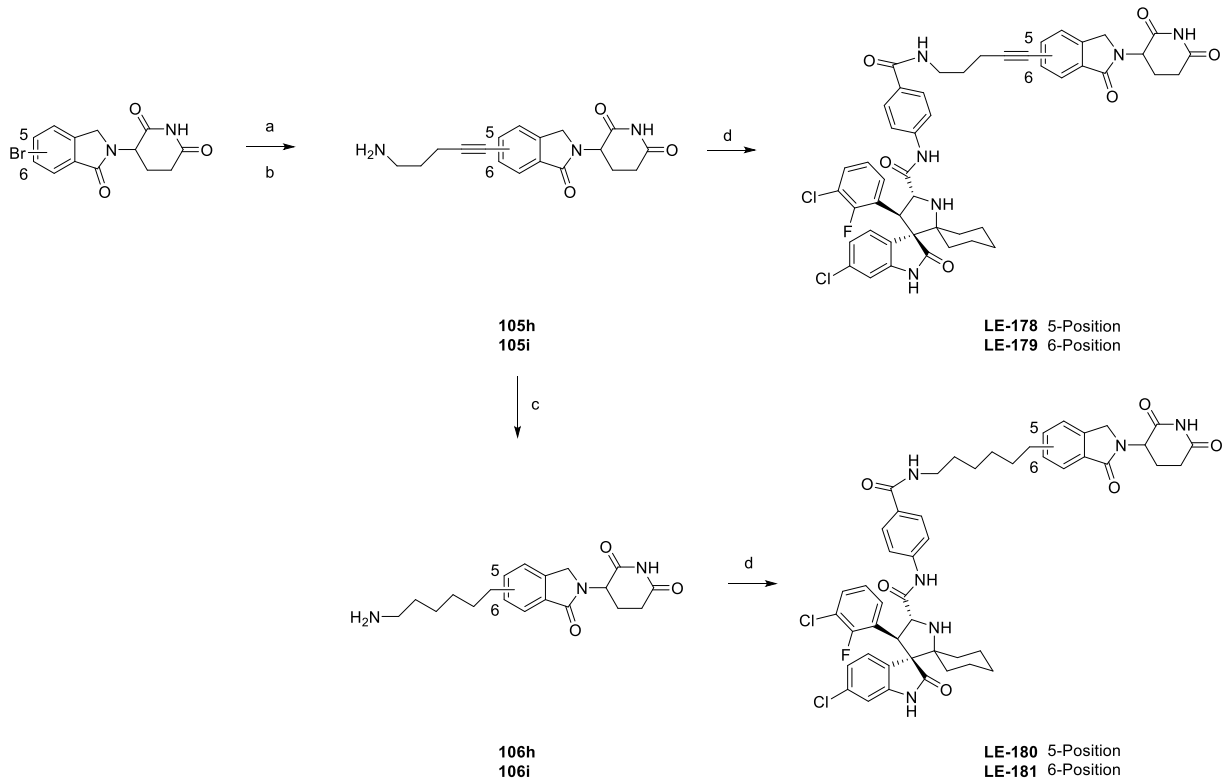

Scheme 1-6. Synthesis of **LE-178, LE-179, LE-180** and **LE-181.** Reaction conditions: (a) $Pd(PPh_3)_2Cl_2$, CuI, triethylamine, DMF, 80 °C; (b) trifluoroacetic acid, DCM, rt; (c) H_2 (1 atm), Pd/C, EtOH, rt; (d) HATU, DIPEA, DMF, rt.

The synthesis of MDM2 degraders with a VHL ligand are shown in Scheme 7. The VHL binding ligands **107a-107d** with different linkers were synthesized according to previous reports published by Crews et al.[18] The bivalent molecules **LE-175, LE-176, LE-177** and **LE-334** were then obtained by an amide condensation reaction with **MI-1061**.

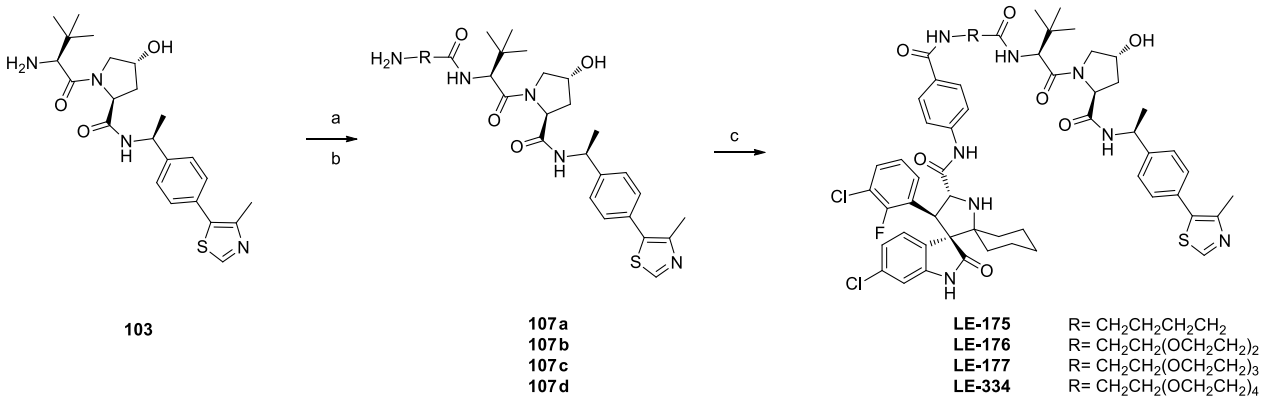

Scheme 1-7. Synthesis of **LE-175, LE-176, LE-177** and **LE-334.** Reaction conditions: (a) HATU, DIPEA, DMF, rt; (b) trifluoroacetic acid, DCM, rt; (c) HATU, DIPEA, DMF, rt.

Summary

A new class of PROTAC small-molecule degraders of MDM2 proteins has been developed based on our potent and selective MDM2 inhibitors and thalidomide derivatives. Several highly potent MDM2 protein degraders, exemplified by **LE-102**, were obtained by extensive optimization of the linker length and composition. **LE-102** effectively induces degradation of MDM2 protein and activates p53 pathway within 0.5 h at concentrations as low as 1 nM in the RS4;11 acute leukemia cell line. It achieves an IC_{50} value of 2.3 nM in cell growth inhibition in the RS4;11 cell line. Significantly, **LE-102** achieves complete tumor regression with an every second day dosing schedule and tumor growth inhibition with a weekly dosing schedule in RS4;11 xenograft model in mice. Collectively, our data demonstrate that **LE-102** is a highly potent, efficacious, and promising MDM2 degrader which warrants further evaluation as a potential new therapy for the treatment of human acute leukemia. Development of PROTACs targeting MDM2 protein degradation is a new strategy with which to target acute leukemia harboring wild-type

p53 and the designed PROTACs are much more potent and efficacious than simple MDM2 inhibitors.

Chapter 2

Development of Molecular Glues from PROTACs

Introduction

PROTAC as an emerging method targeting protein degradation has been widely used for target validation and development of novel therapeutics[15, 39, 62]. PROTACs are designed by linking the target protein ligand to an E3 ubiquitin ligase ligand. These bifunctional molecules can recruit a target protein into proximity with an E3 ubiquitin ligase to induce target protein ubiquitination and subsequent proteasomal degradation. Recent development of PROTACs with more 'drug-like' molecular properties has led to remarkable improvement of *in vitro* and *in vivo* activities compared with the traditional target protein inhibitors. CRBN has been identified as a substrate acceptor for $Cul4^{CRBN}$ E3 ubiquitin ligase. Its ligands, thalidomide and various corresponding derivatives have been widely used in PROTACs design, leading to BET, MDM2, and BCR-Abl proteins PROTAC degraders[23].

Thalidomide and its derivative molecules, which are named immunomodulatory drugs (IMiDs) are widely used in the treatment of multiple myeloma with excellent efficacy.[63-64] Recent research has shown that IMiDs can bind to cereblon, a critical substrate acceptor of $Cul4^{CRBN}$ E3 ubiquitin ligase and as "molecular glue" or molecular switches, promote recruitment and ubiquitination of substrate proteins.[49, 60, 65-66] Lenalidomide can induce proteasomal degradation of essential transcription factors of the Ikaros family zinc finger proteins 1 and 3 (IKZF1/3) in

multiple myeloma.[63, 67] **CC-885**, derived from lenalidomide, has been developed with potent antitumor activity through the cereblon-dependent ubiquitination and degradation of the translation termination factor GSPT1[68]. The cereblon modulators are molecular glue which can recruit GSPT1 to cereblon through interaction with the modulators and a 'hotspot' on the cereblon surface. Structural degradation underlying cereblon substrate selectivity could be redefined by cereblon modulation.

During our study of MDM2 PROTAC degraders, a new cereblon modulator, **LD-277** was discovered with potent antitumor activity. The original design of **LD-277** was based on the PROTACs strategy for MDM2 degradation, but its antitumor activity is mediated through molecular glue mechanism, which could modulate the cereblon substrate selectivity. GSPT1 was identified as the primary target protein of **LD-277** and GSPT1 degradation dominantly drives the effect of **LD-277** in cancer cell lines and these findings identify a new class of cereblon modulators targeting GSPT1 degradation. The study also suggested the importance of careful evaluation of function and mechanism in the development of PROTACs.

Literature Review

Development of Molecular Glue Inducing Protein-Protein Interactions

In the past 20 years, development of compounds that perturb protein-protein interactions has been become a popular field in drug discovery and compounds that can enhance the novel protein-protein interactions provide another opportunity for drug discovery. Compounds which can induce protein-protein interactions are known as molecular glues, and

they can promote the new protein-protein interactions through direct binding at the protein-protein interaction surface or allosteric modification of protein structures.[69]

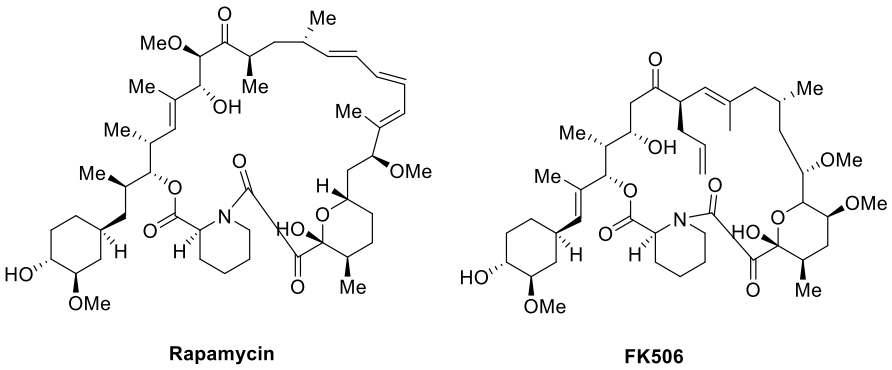

Figure 2-1. Structures of macrocyclic immunosuppressant molecular glues

Several macrocyclic immunosuppressants have been reported to function as molecular glues. Rapamycin[70] could attach to the FK506 binding protein (FKBP12) and the FKBP-rapamycin associated protein (FRAP) to inhibit IL-2 signaling. FK506[71] could also form a ternary complex with FKBP12 and calcineurin and so inhibit the phosphatase activity of calcineurin. With their large contact surfaces, these macrocyclic compounds could contribute more than 25% of the protein-protein interaction surface area.

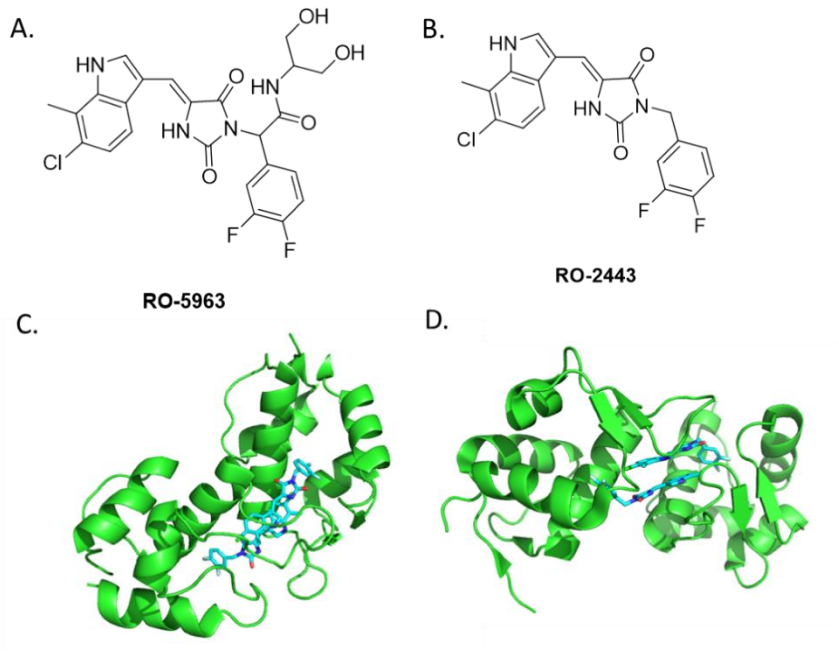

Figure 2-2. (A) Structures of **RO-5963**; (B) Structure of **RO-2443**; (C) Co-crystal structure of **RO-2443** in a complex with MDMX (PDB ID: 3U15); (D) Co-crystal structure of **RO-2443** in a complex with MDM2. (PDB ID: 3VBG)

In 2012, **RO-5963**[49] was discovered by scientists at Hoffmann-La Roche to activate the tumor suppressor gene p53. Unlike normal MDM2-p53 inhibitors or MDMX-p53 inhibitors, **RO-5963** can potently block p53 binding with both MDM2 and MDMX by inducing homo- and/or heterodimerization of MDM2 and MDMX proteins as molecular glue. Structural studies of an analogue compound, **RO-2443** have shown that these inhibitors might bind to and occupy the p53 pockets of MDM2 and MDMX by inducing the formation of dimeric protein complexes. The protein complexes were kept together by a dimeric small-molecule and then activated the tumor suppressor p53. Treatment with 10 μM of **RO-5963** could significantly inhibit the cell proliferation and promote apoptosis in cells with wild-type p53.

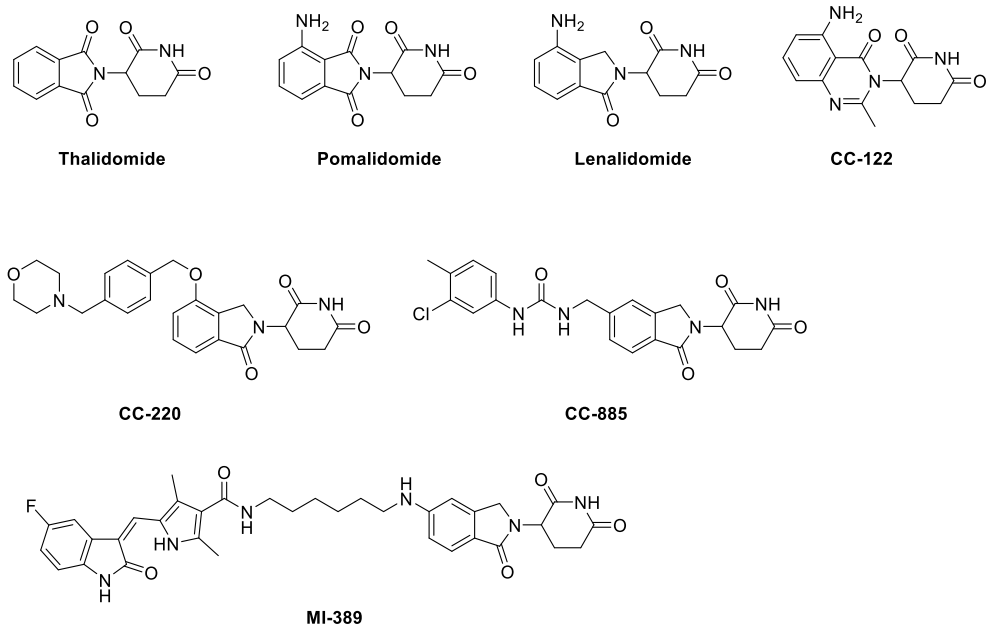

Figure 2-3. Structures of IMiDs

Immunomodulatory drugs (IMiD) and anticancer sulfonamides have also been reported as molecular glues. But distinct from the macrocyclic immunosuppressants and **RO-5963**, IMiDs and anticancer sulfonamides can cause target protein degradation. Recent studies have shown that the anticancer activity of IMiDs is related to their direct binding to cereblon, which is a substrate acceptor for $CRL4^{CRBN}$ E3 ubiquitin ligase, and blocking its autoubiquitination and native substrate ubiquitination.[49] By binding directly to cereblon, IMiDs can change the substrate specificity of the E3 ubiquitin ligase and cause abnormal target protein ubiquitination and degradation. As there is no interaction between cereblon and the target protein without IMiDs, this suggests that IMiDs function as molecular glues to fill in the binding surface between cereblon and target proteins.[68] It has been shown that **thalidomide**, **lenalidomide** and **pomalidomide** can all induce the cereblon-CK1α interaction, but only **lenalidomide** can promote the degradation of CK1α**.** This might be so because the extra carbonyl group in **thalidomide** and

pomalidomide could clash with the cereblon backbone. More recently developed IMiDs, **CC-122**[72] and **CC-220**[73], have been shown to promote the degradation of IKZF1/3. Another analogue, **CC-885** can cause cell growth proliferation in a large range of different cancer cells. Later studies have shown that **CC-885** can cause degradation of IKZF1/3 and GSPT1, which are cereblon-dependent.[74] Brander et al. and Winter et al. also reported a PROTAC, **MI-389 which** targets RTKs degradation can induce the degradation of GSPT-1 as a converging off-target.[75] **MI-389** can significantly cause GSPT-1 degradation with 100 nM treatment in 4 h in MOLT4 cells. **MI-389** might function as **CC-885**, as a knockout of CRBN can fully block the degradation of GSPT-1 in MOLT cells.

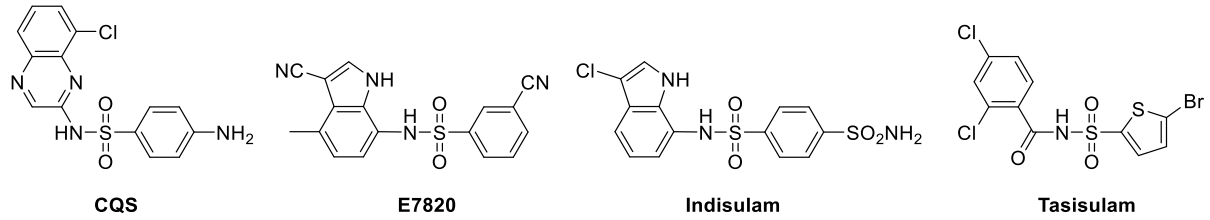

Figure 2-4. Structures of anti-cancer sulfonamide molecular glues.

Sulfonamides such as chloroquinoxaline sulfonamide (**CQS**), **E7820**, indisulam and tasisulam can inhibit the proliferation of certain human cancer cell lines. But the mechanism of action of these compounds has not been clear until recently. Two studies have shown that these anticancer sulfonamides are molecular glues which can induce the degradation of RNA splicing factor RBM39 (CAPERα), which is a coactivator for several transcription factors. Co-treatment with the neddylation inhibitor **MLN4924** or the proteasomal inhibitor bortezomib could block the

activity of **E7820** and indisulam.[76-77] The E3 ubiquitin ligase **DCAF15** was found in immunoprecipitation experiments to be responsible for the degradation of RBM39.

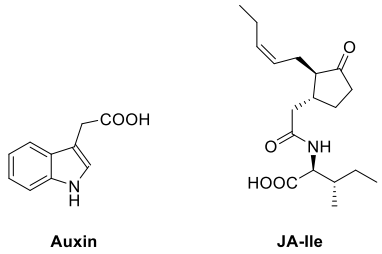

Auxin JA-Ile

Figure 2-5. Structures of plant hormone molecular glues

Plant hormones are well-known molecular glues which can cause protein degradation. The hormone **auxin** can bind to the Cullin-RING ubiquitin ligase TIR1 and activate the ubiquitination and degradation of transcriptional repressors AUX/IAAs.[78] The plant hormone **JA-Ile** can bind to the Cullin-RING ubiquitin ligase COI1 and catalyze the ubiquitination and degradation of transcriptional repressor JAZ proteins.[79]

In summary, molecular glues promote the association of proteins to form unnatural protein complexes, which could be widely used to alter cellular physiology for disease treatment. Although rational design of molecular glues is difficult because it involves multiprotein interactions, the recent structural studies on multiprotein and advanced technologies to identify protein interactions inside cells have encouraged the development of novel molecular glues for drug design in an effort to modulate the diverse processes implicated in diseases.[80]

Results and Discussion

In Chapter 1, we showed that MDM2 PROTACs formed by linking the MDM2 inhibitor **MI-1061** and a cereblon binding ligand such as **pomalidomide**, **lenalidomide** or **thalidomide** could successfully induce MDM2 degradation and activate the p53 pathway in p53 wild-type cancer cell lines. Based on our previous studies of the MDM2 inhibitor **MI-1061**[25], the core structure **LD-103** can also efficiently bind to MDM2 protein with K_d value of 80 nM and thus activate the p53 pathway. Linking **LD-103** to a cereblon binding ligand might yield a new class of MDM2 PROTACs with smaller molecular weights, which would be beneficial for the PK properties. **LD-222** is one of our best MDM2 degraders with a hydrophobic methylene linker. This linker and the cereblon binding ligand in **LD-222** was used in the design of our new bifunctional molecule **LD-277**, which was synthesized accordingly.

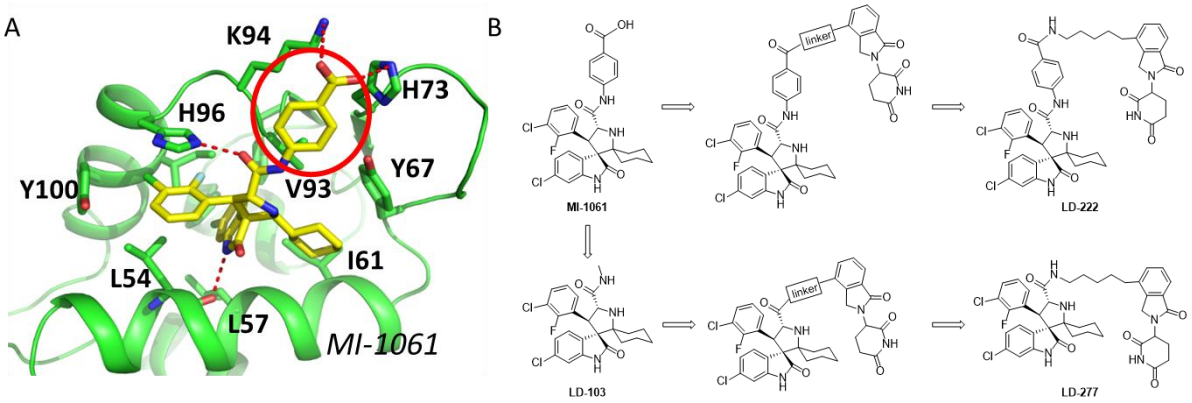

Figure 2-6. (A) Modeled structure of MDM2 complexed with **MI-1061** (yellow, PDB ID: 4LWU); (B) Design of **LD-277** based on **LD-103** and MDM2 degrader **LD-222**.

The anti-proliferative activities of **LD-277** were tested in RS4;11, MV-4-11, MOLM13 cells with wild-type p53 or RS4;11/IRMI-1 and RS4;11/IRMI-2, MDA-MB-231, and MDA-MB-468 cells

with mutated p53 and HL-60 cells without p53 to enable comparison with **LD-222** (**Table 2-1**). Both RS4;11/IRMI-1 and RS4;11/IRMI-2 cell lines were developed by our group. They all harbor mutated p53 and are resistant to the MDM2 inhibitor **MI-1061**. **LD-222** and **LD-277** can efficiently inhibit RS4;11 cell growth and are more potent than the corresponding MDM2 inhibitors **MI-1061** and **LD-103**. But **LD-277** also demonstrates good anti-proliferative activity in RS4;11/IRMI-1 and RS4;11/IRMI-2 cell lines with IC_{50} values of 1.5 nM and 1.4 nM, while no growth inhibition was observed upon treatment with the MDM2 degrader **LD-222** or the inhibitors **MI-1061** and **LD-103** at concentrations up to 3 μM. Similar results were obtained for MV-4-11, MOLM-13, MDA-MB-231, MDA-MB-468, HL-60 and RS4;11 with p53 knock-out cell lines (**Table 2-1**). **LD-277** potently inhibits cell proliferation in cancer cells with p53 wild-type, p53 mutation or p53 null, which indicates an inhibition mechanism for **LD-277** distinct from that of the *bona fide* MDM2 degrader **LD-222**. Protein expression levels of MDM2, p53 and p21 in RS4;11 and RS4;11/IRMI-1 cell lines treated with **LD-222** and **LD-277** were tested by Western Blotting and it was found that **LD-222** significantly causes MDM2 degradation in 2 h in both RS4;11 and RS4;11/IRMI-2 cell lines, which is consistent with our previous MDM2 PROTACs. Significant p53 accumulation was observed after 2 h treatment of **LD-222** in the RS4;11 cell line, while no significant upregulation of p53 was observed in the RS4;11/IRMI-2 cell line. The RS4;11/IRMI-2 cell line with p53 mutation is resistant to either MDM2 inhibitors or MDM2 degraders, as mutated p53 fails to activate its downstream gene and causes subsequent inhibition of cell proliferation. Comparing with **LD-222**, no clear MDM2 degradation was observed in a 2 h treatment with **LD-277** in RS4;11 and RS4;11/IRMI-2 cell lines. Results obtained with RT-qPCR results have shown that MDM2, p21, PUMA and BAX genes are all up-regulated by treatment with **LD-222** in the RS4;11 cell line. There

is no significant change of gene expression in RS4;11 of MDM2, p53, p21 and BAX following a 12 h treatment with **LD-277**, indicating that **LD-277** functions differently as a MDM2 degrader.

Table 2-1. Binding affinities of MDM2 and cell growth inhibitory activities of MDM2 inhibitors and corresponding degraders in RS4;11 parental cell lines and RS4;11/p53 mutated cell lines.

IC_{50}/ μM	p53	**MI-1061**	**LD-222**	**LD-103**	**LD-277**
RS4;11	Wild-type	0.12	0.005	0.9	0.001
MV-4-11	Wild-type	0.11	0.011	0.89	0.008
MOLM-13	Wild-type	0.10	0.015	1.2	0.025
HL60	Null	>3	>3	>3	0.0083
RS4;11/ IRMI-1	Mutation	>3	>3	>3	0.0015
RS4;11/ IRMI-2	Mutation	>3	>3	>3	0.0014
MDA-MB-231	Mutation	>3	>3	>3	0.039
MDA-MB-468	Mutation	>3	>3	>3	0.026
RS4;11 sh p53	Knock out	0.4	>3	>3	0.0028

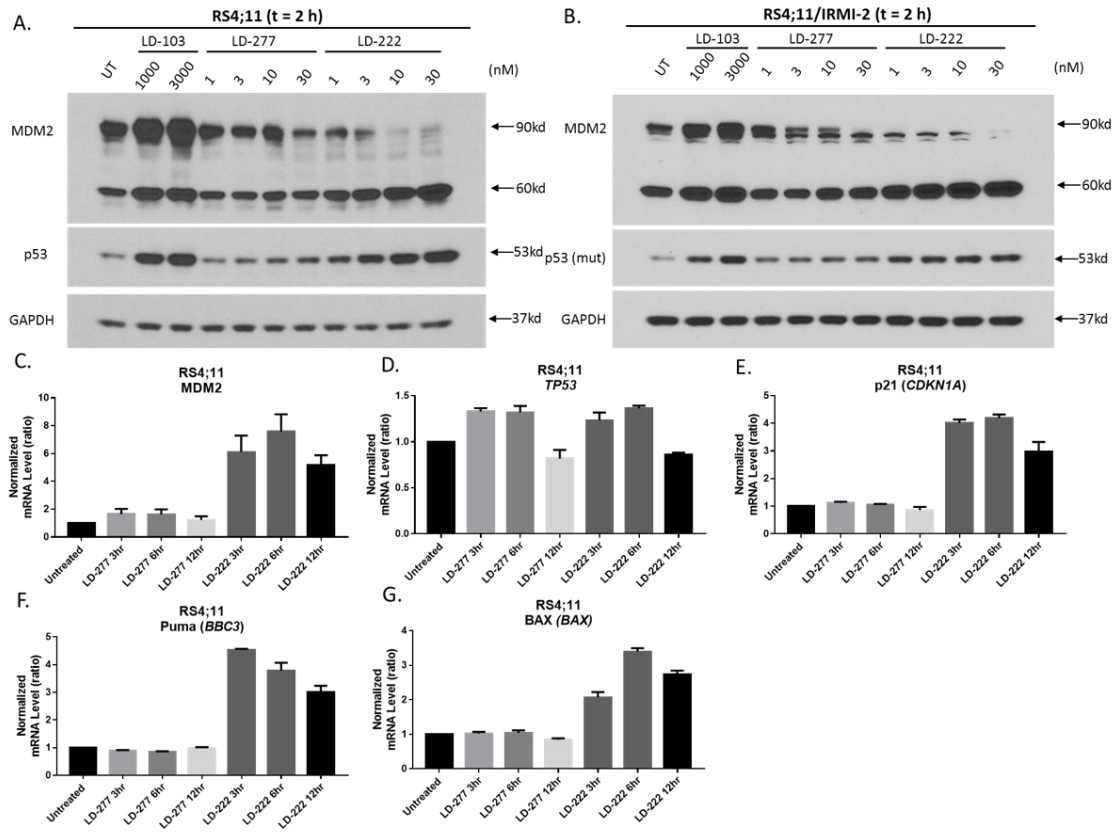

Figure 2-7. (A) MDM2, p53 and p21 protein expression levels in RS4;11 cell line after treatment for the indicated time with 10 nM **LD-222** or 3 nM **LD-277**; (B) MDM2, p53 and p21 protein expression levels in RS4;11/IRMI-1 cell line after treatment for the indicated time with 10 nM **LD-222** or 3 nM **LD-277**; (C)-(G) MDM2, p53, p21, PUMA, BAX mRNA levels in RS4;11 cell after treatment for the indicated time with 10 nM **LD-222** or 3 nM **LD-277**.

Linker-Activity relationship study of LD-277

To explore the linker-activity relationship of **LD-277**, a series of compounds with hydrophobic methylene linkers and hydrophilic polyethylene glycol linkers were synthesized and tested in RS4;11 cells. The observed cell growth inhibition activities are summarized in **Table 2-2**.

Compounds **LE-016** and **LD-277** with 4 and 5 methylene linkers had similar potencies. Further shortening the linker to 3 methylene groups gave compound **LE-010** which is 59 times less potent than **LE-016** and **LE-008** with no linker is 570 times less potent than **LE-006**, whose potency is similar to that of the MDM2 inhibitor **LD-103**. Compounds **LE-344**, **LD-257**, **LD-256** with 1-3 ethylene glycol units in the linkers were similarly potent , but all were slightly less potent than **LD-277** and **LE-016**. This result suggests that to retain the potent anti-proliferative activity, a linker at least 4-atoms long is needed between the inhibitor and cereblon ligand.

Table 2-2. Linker-activity relationship results for cell growth inhibitory activities of degraders with different linker in RS4;11 cell line.

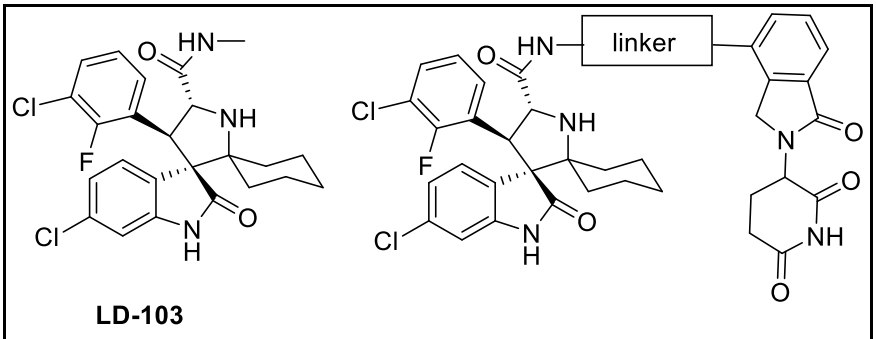

LD-103

	Linker	RS4;11 IC_{50}/ μM
LD-103		0.89
LE-008	No linker	0.56
LE-010	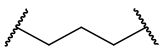	0.055

LE-016	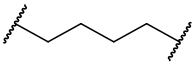	0.00083
LD-277	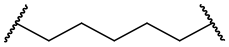	0.0012
LE-344	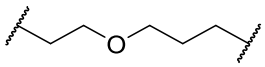	0.0011
LD-257	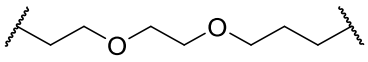	0.0033
LD-256	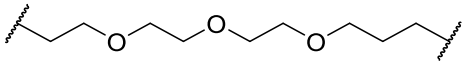	0.01

LD-277 is a cereblon-dependent and MDM2- or p53-independent antitumor agent

Although good activities were obtained by **LD-277** and its analogues, the mechanism was not fully understood. **LD-277** has two components, an MDM2 inhibitor and a cereblon binding ligand. The importance of both these moieties was further explored.

To check the importance of cereblon binding in the anti-proliferative activity, one methyl group was introduced to **LD-277** to block the lenalidomide site at which cereblon binds (**Figure 2-8**A). **LE-024** was synthesized accordingly and showed weak cell growth inhibition activity with IC_{50} = 1.5 μM in RS4;11 cell line and no inhibition in RS4;11-IRMI-1 at **LE-024** concentrations up to 3 μM (**Figure 2-8B**). The significant decrease in cell growth inhibition activity of **LE-024** compared with **LD-277** indicated that cereblon binding was critical for the anti-proliferative effect of **LD-277**. Further, the MDA-MB-231 cell line was treated with **LD-277** in presence of an excess of the cereblon ligand lenalidomide and as expected, the excess lenalidomide was able to block

cell growth inhibition by **LD-277**, confirming the existence of a cereblon-mediated mechanism. Lenalidomide treatment in the same experiment had little impact on cell growth (**Figure 2-8**C).

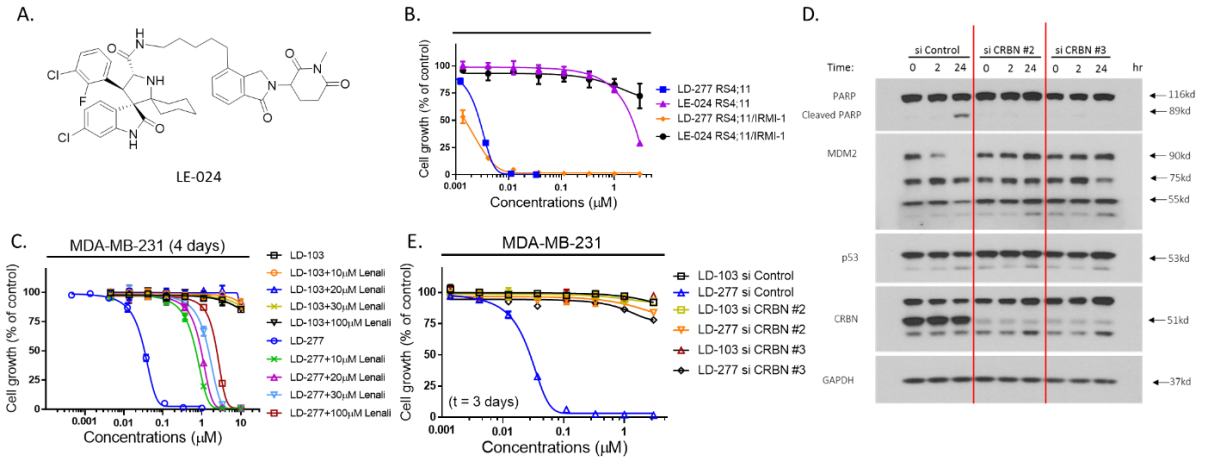

Figure 2-8. (A) Structure of LE-024; (B) Dose-dependent response of **LD-277** and **LE-024** in RS4;11 and RS4;11/IRMI-1 cell lines with indicated concentrations of **LD-277** or **LE-024**; (C) Dose-dependent response of **LD-103** or **LE-024** in the MDA-MB-231 cell line with excess **lenalidomide**; (D) cereblon, MDM2 and p53 and p21 protein expression levels in MDA-MB-231 cell lines pretreated with siControl, siCRBN #2 or siCRBN#3 after time treatment for the indicated time with 100 nM **LD-277**; (E) Dose-dependent response of **LD-277** and **LD-103** in RS4;11 cell line pretreated with siControl, siCRBN #2 or siCRBN#3, with the indicated concentrations of **LD-277** or **LD-103**.

To further confirm this result, two siRNAs targeting different cereblon sequences were used to genetically inhibit cereblon gene expression in the breast cancer cell line MDA-MB-231. The knockdown efficiency and cell growth inhibition results in **Figure 2-8**D show that **LD-277** could efficiently inhibit MDA-MB-231 cell line treated with control siRNA with IC_{50} = 50 nM, while

no cell growth inhibition activities were obtained in cereblon knockdown cell lines at concentrations up to 3 μM. Taken together, these data demonstrate that the anti-proliferation phenotype induced by **LD-277** is cereblon-mediated.

Another important component in **LD-277** is the MDM2 inhibitor **LD-103**. To further explore the relationship between the activity of **LD-103** and MDM2 binding, the core structures of two weaker MDM2 inhibitors **AA-211** and **AA-214** were linked to the cereblon binding ligand. Although **AA-211** and **AA-214** are more than 600 times less potent to **MI-1061**, the corresponding degraders, **AA-215** and **AA-216** are only 20 and 50 times less potent than **LD-277**. Knockdown of MDM2 in breast cancer cell lines MDA-MB-231 and MDA-MB-468 and knockdown of p53 in RS4;11 failed to affect the cell growth inhibition activities of **LD-277**. Similar results were also obtained in MEF p53 -/- and MEF p53 -/- MDM2 -/- cells, when compared with wild-type MEF cell lines (**Figure 2-9**). Taken together, the anti-proliferation effect of **LD-277** is independent of both MDM2 and p53.

Table 2-3. Results for binding affinities to MDM2 and cell growth inhibitory activities of degraders with weaker binding affinities to MDM2 in RS4;11 and RS4;11/IRMI-1 cell lines.

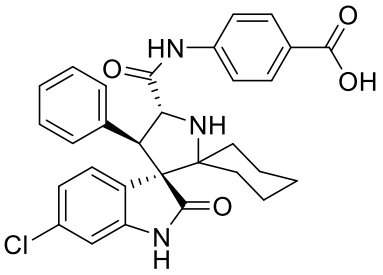

AA-MI-211

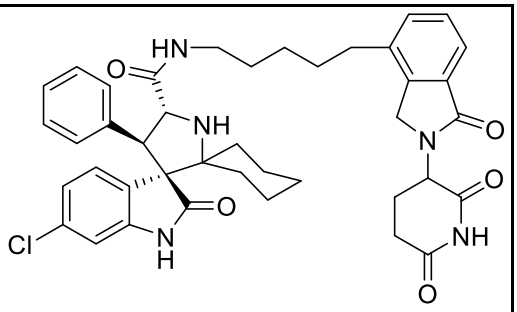

AA-MI-215

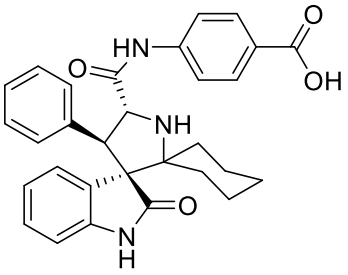

AA-MI-214

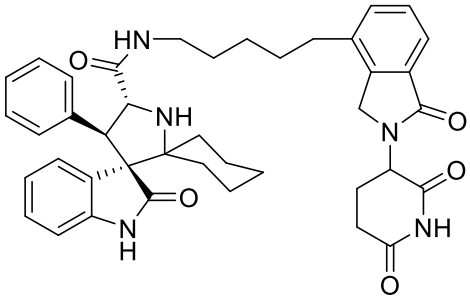

AA-MI-216

IC_{50}/μM	Binding Affinity to MDM2 K_d /μM	RS4;11	RS4;11/IRMI-1
AA-MI211	6.5	>3	>3
AA-MI-215		0.020	0.022
AA-MI-214	> 30	>3	>3
AA-MI-216		0.054	0.061

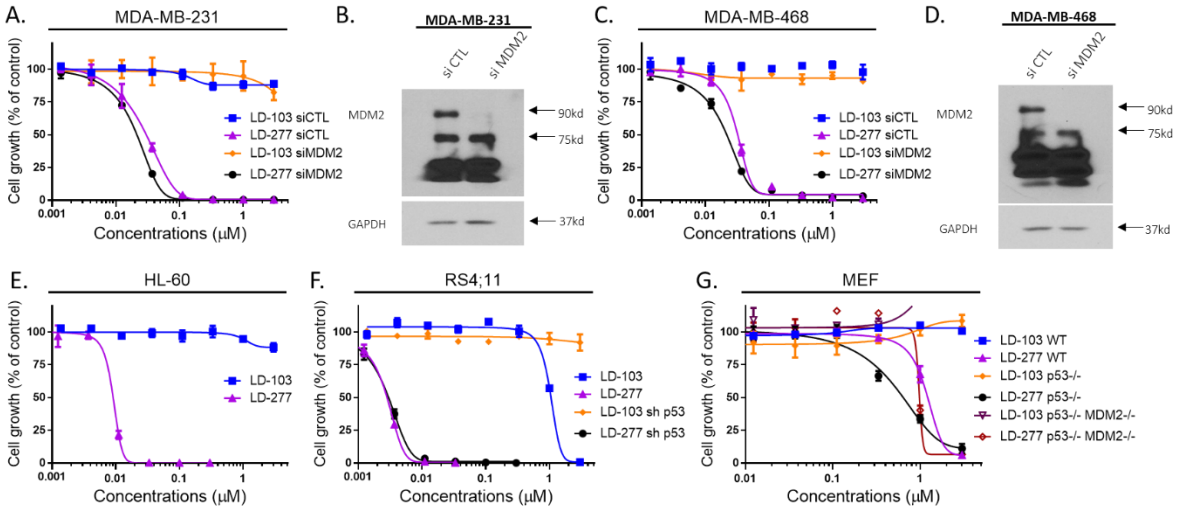

Figure 2-9. (A) Dose-dependent responses of **LD-277** and **LD-103** in the MDA-MB-231 cell line pretreated with siControl, siMDM2, with indicated concentrations of **LD-277** or **LD-103**. Data are mean ± s.d; n = 3 independent experiments; (B) MDM2 protein expression level in MDA-MB-231 cell lines treated with siControl and siMDM2; (C) Dose-dependent response of **LD-277** and **LD-103** in the MDA-MB-468 cell line pretreated with siControl, siMDM2, with indicated concentrations of **LD-277** or **LD-103**; (D) MDM2 protein expression level in MDA-MB-468 cell lines treated with siControl, siMDM2; (E) Dose-dependent response of **LD-277** and **LD-103** in HL-60 cell line with indicated concentrations of **LD-277** or **LD-103**; (F) Dose-dependent response of **LD-277** and **LD-103** in RS4;11 cell line pretreated with sh control or sh p53 , with indicated concentrations of **LD-277** or **LD-103**; (G) Dose-dependent response of **LD-277** and **LD-103** in MEF WT, MEF p53-/-, MEF p53-/- MDM2-/- cell lines, with indicated concentrations of **LD-277** or **LD-103**.

LD-277 promotes cereblon-dependent GSPT1 degradation

As the substrate acceptor of $CRL4^{CRBN}$(CUL4-DDB1-RBX1-cereblon) E3 ubiquitin ligase, CRBN is critical for the substrate protein recruitment. Previous experiments have demonstrated that the anti-proliferation effect of **LD-277** is cereblon- and proteasome-dependent. Upon treatment with **LD-277**, CRBN might recruit other proteins to the E3 ubiquitin ligase and promote their ubiquitination and degradation. To identify potential substrates of $CRL4^{CRBN}$ regulated by **LD-277**, quantitative proteomic profiling by tandem mass spectrometry was used to compare the protein expression level with treatment of **LD-277**. GSPT1(eRF3a) was identified as a key protein down-regulated by **LD-277**. The results are summarized in **Figures 2**-10, **A** and B. The statistical p-value was calculated by permutation-based statistical testing of peptide ratios[81-82]. The translation termination factor GSPT1 in RS4;11 was significantly down-regulated compared to other identified proteins after 3 h treatment with **LD-277**. Similar results were obtained in the RS4;11/IRMI-1 cell line (**Figure 2**-**10**, C **and D**). Western blotting assay of GSPT1 in RS4;11 cell treated by **LD-103** and **LD-277** analogues also confirmed the degradation of GSPT1 induced by these compounds (**Figure 2-10**, **E** and **F**). In presence of excess lenalidomide, GSPT1 degradation induced by **LD-277** was blocked due to competition from cereblon binding in the MDA-MB-231 cell line. (**Figure 2-10, G**) Consistently, the presence of excessive lenalidomide rescues the proliferation suppression effect of **LD-277** in previous experiments (**Figure 2-8E**).

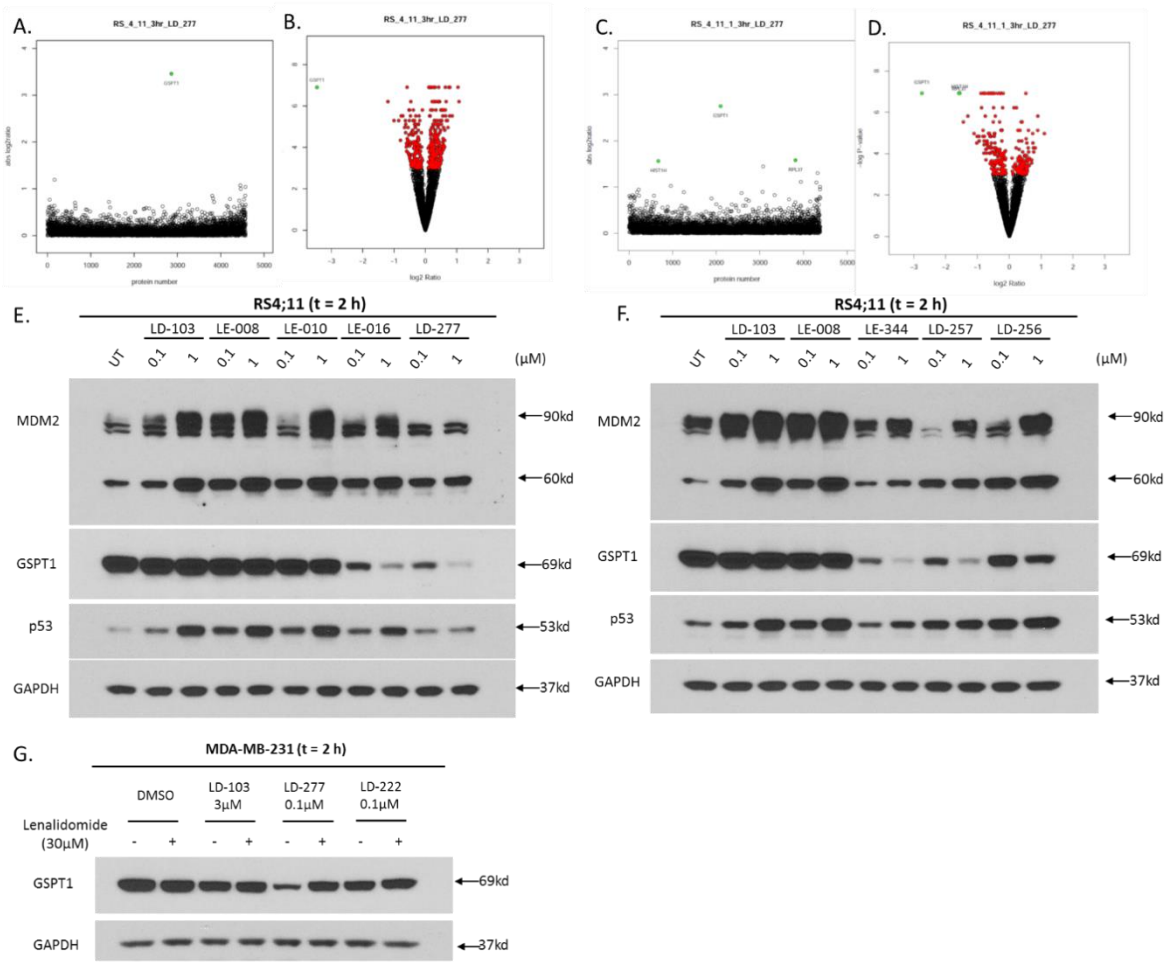

Figure 2-10. (A) & (C) Protein expression levels in RS4;11 cell line or RS4;11 IMRI-1 are ranked in a scatter plot according to absolute value of the relative abundance ratio (log2 fold change) between a 3 h **LD-277** treatment and untreated groups (y-axis). Green points represent proteins with absolute value of the relative abundance ratio (log2 fold change) higher than 2. (B) & (D) Volcano plot according to negative log P-value (y-axis) and relative abundance ratio (log2 fold change) of each protein between 3 h **LD-277** treatment and untreated groups (x-axis). Red points represent proteins with statistical P-value lower than 0.05. Green points with statistical P-value lower than 0.05 and absolute value of the relative abundance ratio (log2 fold change) higher than 2. (E) & (F) MDM2, p53 , GSPT-1 protein expression level in RS4;11 cell lines treated with **LD-103,**

LE-008, LE-016, LD-277, LE-344, LD-257, LD-256. (G) GSPT-1 protein expression level in RS4;11 cell lines treated with **LD-103, LD-277 and LD-222** with and without co-treatment with lenalidomide.

Synthesis

The synthesis of MDM2 inhibitors **AA-MI-211** and **AA-MI-214** and the corresponding molecular glues **AA-MI-215** and **AA-MI216** is shown in Scheme 1.[25] Various (E)-3-benzylidene-6-chloroindolin-2-ones and (E)-3-benzylideneindolin-2-ones were used as starting materials. Cyclohexanone and the chiral auxiliary (5S,6R)-5,6-diphenylmorpholin-2-one were used to synthesize **201a** and **201b**. These intermediates were methylated with methanol with concentrated sulfuric acid and the chiral auxiliary group was removed with ammonium cerium(IV) nitrate in acetonitrile/water to form **203a** and **203b**. **204a** and **204b** were obtained by hydrolysis with lithium hydroxide in water, MeOH and THF. **AA-MI-211** and **AA-MI-214** were obtained by an amide condensation reaction with methyl 4-aminobenzoate and subsequent hydrolysis with sodium hydroxide in water and methanol. **AA-MI-215** and **AA-MI-216** were synthesized from **204a** and **204b** by an amide condensation reaction with 3-(4-(5-aminopentyl)-1-oxoisoindolin-2-yl)piperidine-2,6-dione.

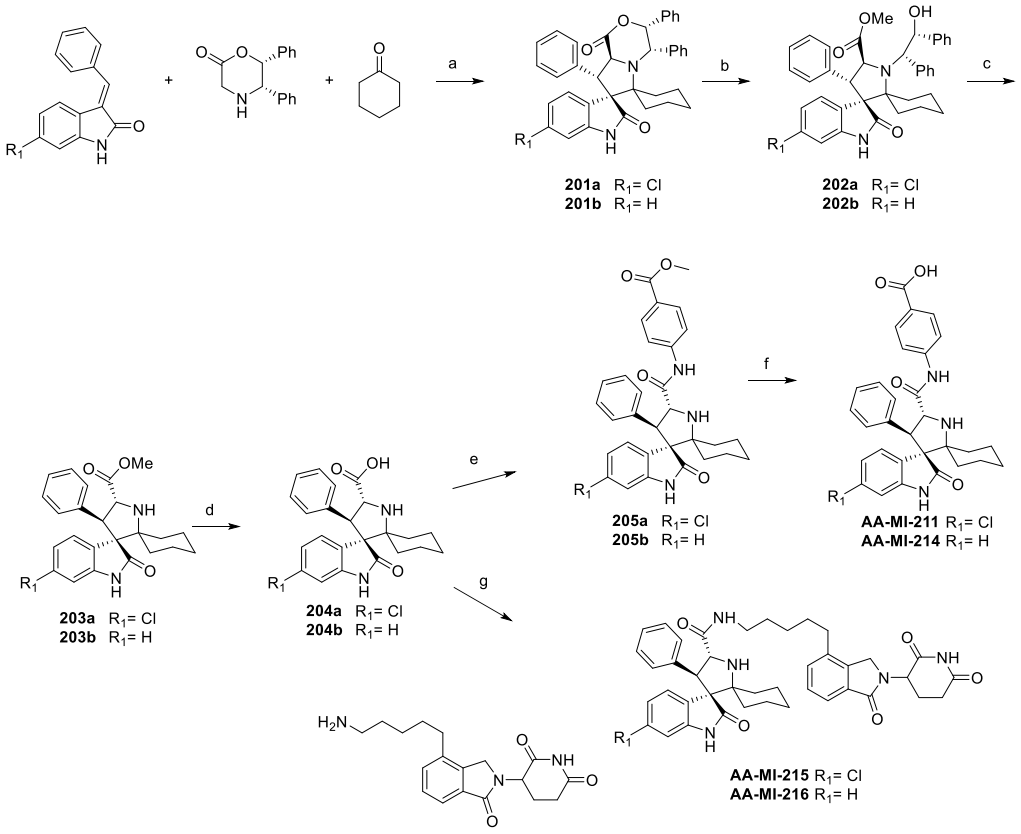

Scheme 2-1. Synthesis of **AA-MI-211, AA-MI-214, AA-MI-215** and **AA-MI-216.** Reaction conditions: (a) toluene, reflux; (b) conc. H_2SO_4, MeOH. rt; (c) ammonium cerium(IV) nitrate, acetonitrile, water; (d) LiOH, MeOH, water, THF; (e) diphenylphosphinic chloride, DIEA, DCM, methyl 4-aminobenzoate, DMAP; (f) Sodium hydroxide, MeOH, water (g) HATU, DIEA, DMF.

The synthesis of the molecular glues in Table 2-2 and **LE-024** is shown in **Scheme 2-2**. The intermediate **206a-206g** was synthesized by Sonogashira coupling reaction from 3-(4-bromo-1-oxoisoindolin-2-yl)piperidine-2,6-dione or 3-(4-bromo-1-oxoisoindolin-2-yl)-1-methyl-piperidine-2,6-dione and the Boc protecting groups were then removed under acidic conditions. The carbon-carbon triple bonds were reduced by palladium-catalyzed hydrogenation. Target molecules were then obtained by an amide condensation reaction with (3'R,4'S,5'R)-6''-chloro-

4'-(3-chloro-2-fluorophenyl)-2''-oxodispiro[cyclohexane-1,2'-pyrrolidine-3',3''-indoline]-5'-carboxylic acid.

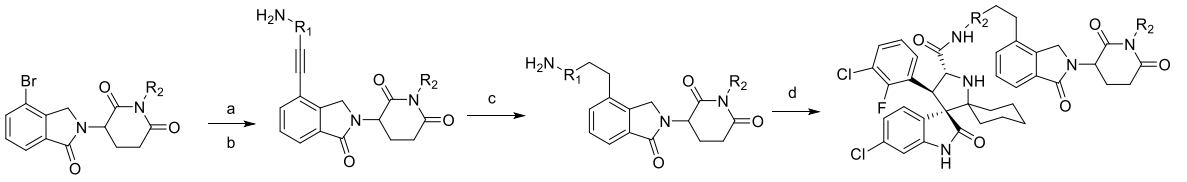

Scheme 2-2. Synthesis og **LE-010, LE-016, LD-277, LE-344, LD-257, LD-256** and **LE-024.** Reaction conditions: (a) $Pd(PPh_3)Cl_2$, CuCl, DIPEA, DMF, 80 °C; (b) trifluoroacetic acid, DCM, rt; (c) H_2, Pd/C, MeOH, rt. (d) HATU, DIPEA, DMF, rt.

LD-103 and **LE-008** were synthesized with the same method as was used for **LD-277**, and is shown in Scheme 2-3. **207c**, which was used for **LD-277** was replaced by methylamine and lenalidomide for the synthesis of **LD-103** and **LE-008**.

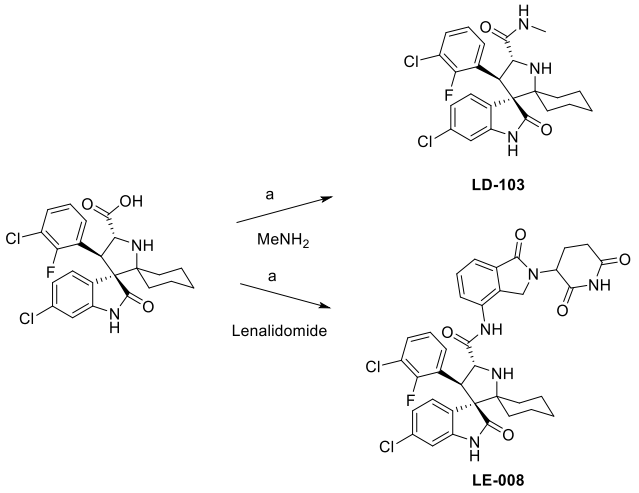

Scheme 2-3. Synthesis of **LD-103** and **LE-008.** Reaction conditions: (a) HATU, DIPEA, DMF, rt.

Summary

In this chapter, a new class of cereblon modulators with potent anti-proliferative activity in cancer cell lines based on the structures of MDM2 PROTACs was developed. Among them, **LD-277** was achieved by linking **LD-103**, the core structure of MDM2 inhibitor **MI-1061** with slightly weaker binding affinity to MDM2, to a cereblon binding ligand with a hydrophobic linker. Compared with the *bona fide* MDM2 degrader **LD-222**, which can cause MDM2 degradation and is activated in the p53 pathway, no significant MDM2 degradation or p53 activation was observed with **LD-277**. Further study has shown that the anti-proliferation activity of **LD-277** in cancer cell lines is independent of MDM2 and p53 but is related to the cereblon and proteasome activity. This result suggests that a new mechanism, distinct from the original MDM2-related p53 pathway is involved in the anti-proliferative activity of **LD-277**.

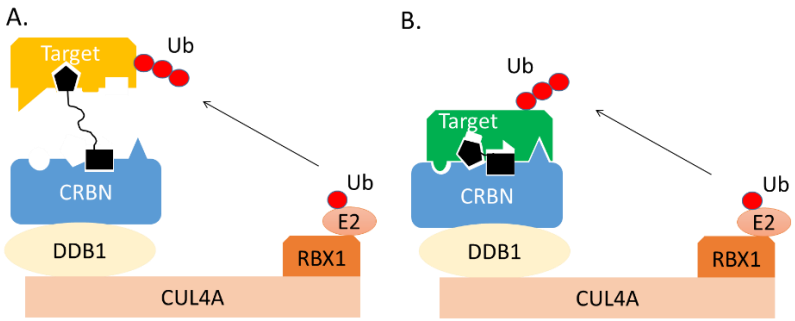

Figure 2-11. (A) Mechanisms for PROTACs; (B) Mechanisms for Molecular glue.

Further proteomics studies have shown that significant degradation of GSPT1 is induced by **LD-277**, which is similar to the behavior of the previously reported cereblon modulator **CC-**

885.[74] **CC-885** could direct cereblon to target GSPT1 by creating an interaction hotspot on the cereblon surface for direct protein–protein interactions with the substrate, which in this case works as molecular glue between cereblon and GSPT1. A similar mechanism for **LD-277** is proposed here.

PROTAC strategy has emerged as an efficient technology with which to target protein degradation, and it has attracted great interest in the pharmaceutical industry and drug discovery fields. It could efficiently induce protein degradation by dragging the target protein to a E3 ubiquitin ligase with a linker based on bifunctional molecules. Compared with PROTAC, molecular glue could modify the protein surface and create an interaction hotspot for direct protein–protein interactions with the substrate, underlying the gain-of-function 'chemo-neomorphic' activity (**Figure 2-11**). Discovery of **LD-277** has indicated that minor modification of PROTAC could convert it to molecular glue with unexpected functions. Even though these unexpected functions are still dependent on binding to E3 ubiquitin ligase and proteasome activity, they can be totally unrelated to the original targets. These functions could also dominate the phenotype of compounds *in vitro* and *in vivo*, which complicates their evaluation.[75] It may also be possible however to rationally design compounds with both PROTAC and molecular glue functions targeting degradation of various proteins in different signaling pathways, and this will be more efficient than targeting a single protein with either technology.

Chapter 3

Development of Macrocyclic Peptidomimetic Targeting WDR5-MLL1 Protein-Protein Interaction

Introduction

MLL1 is a Histone 3 Lysine 4 (H3K4) methyltransferase which plays an important role in hematopoiesis and neurogenesis in normal cells. It's also found to be mis-regulated in a number of human acute leukemia.[83-84] More than 70 MLL fusion proteins have found with chromosomal translocations at 11q23[85], which leads to aggressive leukemia with very poor prognosis and treatment.[83] MLL1 fusions occur in more than 70% of acute lymphoid leukemia (ALL), 35% of acute myeloid leukemia (AML) in infant and 5% ALL and 5-10% AML in adults. [86-88]

Interestingly, MLL translocations always occurs on only one MLL allele and result in the loss of the H3K4 methyltransferase activity. But the remaining wild-type MLL1 with H3K4 methyltransferase activity, is required by MLL-AF9 fusion protein to induce leukemogenesis and maintenance of MLL-AF9-transformed cells.[89-90] Therefore, inhibition of the wild-type MLL1 H3K4

methyltransferase activity could be developed as a novel therapeutic method for the treatment of aggressive leukemia harboring MLL fusion proteins[91-92].

Although the catalytic SET domain in MLL1 is responsible for its H3K4 methyltransferase (HMT) effect, the isolated MLL1 protein has very low enzymatic activity. While, the HMT activity of MLL1 is dramatically enhanced when it formed a protein complex with WDR5 (WD repeat domain 5 protein), ASH2L and RbBP5 (Retinoblastoma Binding Protein 5).[93] Research has shown that WDR5 is essential for MLL1 complex formation and its enzymatic activity.[93] Hence, targeting protein-protein interactions (PPIs) in the MLL core complex, especially WDR5-MLL1 protein-protein interaction could be an effective strategy to inhibit the H3K4 HMT activity of MLL1, and further for the treatment of leukemia with MLL1 fusion proteins.

Herein, we reported the design, modification and evaluation of macrocyclic peptidomimetics based on our previous inhibitors **MM-401.** These new WDR5 inhibitors have high binding affinities to WDR5 and achieve potent cell growth inhibitory activity in acute leukemia cells harboring MLL translocation. Of which, **LC-337** binds to WDR5 with an IC_{50} value of 1.9 nM (Ki value << 1 nM), and potently inhibits cell growth of MOLM13 cell line harboring MLL-AF9 fusion protein with IC_{50} value of 33 nM. **LC-337** is more than 800 times better than our previously reported compound **MM-401**. Further optimization of **LC-337** may ultimately yield a new therapy for acute leukemia.

Literature Review

MLL1 is a H3K4 methyltransferase, which has been shown to be associate with the process of leukemogenesis.[94-95] The methylated H3K4 markers regulated the expression of target clustered HOX genes, myeloid exotropic viral integration site 1 (MEIS1) gene[96]. Both are frequently overexpressed in leukemia with rearrangement of MLL1 and the overexpression of HOXA9 and MEIS1 were corelated with the inducement of leukemia.[97] Translocation and rearrangement of MLL1 genes, which caused abnormal MLL1 fusion proteins, are mostly found in ALL or AML, especially in more than 70% of infant ALL and 35%-50% infant AML.[98-99] Wild-type MLL1 is important for hematopoiesis and neurogenesis and regulation of stem cell functions.[84, 100] While MLL1 fusion proteins are responsible for the dysregulation of the hyperplasia, differentiation and death of hematopoietic cells.[101-102] In cancer cells with MLL1 fusion proteins, the transcription function of wild-type MLL1 is hijacked for cancer growth and angiogenesis.[103-104] Wild-type MLL1 is required by MLL1 fusion proteins for the full transformation activity, which it an attractive target for cancer therapy.

MLL1 has multiple domains including the catalytic C-terminal domain and the N-terminal domain.[102] The N-terminal domain interacts with Menin[105-106] and C-terminal domain interacts with WDR, ASH2L, RbBP5 and DPY30.[107] The SET domain, located in C-terminal domain process the catalytic activity when assembled in a core structure with WDR5, ASH2L, RbBP5 and DPY30.[107-108] Without WDR5, MLL1 shows very low histone methyltransferase activity.[107] It's because the SET domain has an open confirmation, and WDR5 could help to stabilize the whole complex to transfer the methyl group from S-adenosyl-L-methionine to H3K4. Developing antagonists targeting the protein-protein interactions between WDR5 and MLL1 is a promising therapeutic method for leukemia with MLL1 fusion proteins.

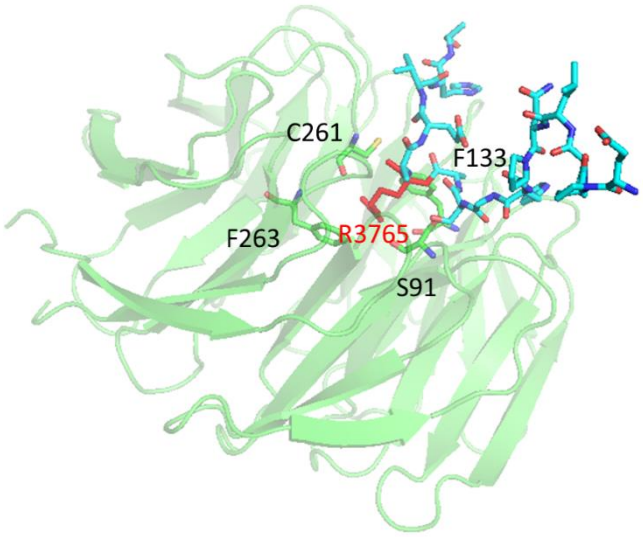

Figure 3-1. Co-crystal structure of WDR5-MLL1 Win motif peptide binary complex (PDB ID: 4ESG)

WDR5 is a highly conserved WD40 repeat protein, which is critical for the H3K4 methyltransferase activity of MLL1 and the following HOX genes expression in hematopoiesis.[108] It binds to the SET domain of MLL1, with RbBP5, ASH2L and DPY30 to form a core complex for methylation of H3K4. It has been shown that MLL1 binds to WDR5 with a conserved arginine motif (Win motif) and mutation on the Win motif on MLL1 could block the MLL1 H3K4 transferase activity.[109-110] The co-crystal structure of Win motif in complex with WDR5 was obtained to give much detailed information for the protein-protein interactions. The side chain of the R3765 was deeply anchored in the binding pocket. The guanidinium group forms strong π-π stacking interaction with WDR5 which is sandwiched between two phenyl rings from F133 and F263. It also forms hydrogen bonds with C261, F133, and S91 of WDR5.

Development of Peptidomimetic WDR5 Inhibitors

Based on the sequence of Win motif, our group did a detailed truncation study from 12mer peptide and found out the minimal element of 3mervpeptide ARA was critical for Win motif binding to WDR5. The 3mer Ac-ARA-NH_2 could bind to WDR5 with K_i value of 0.12 μM comparing with 12mer peptide K_i value of 0.16 μM. Changing one of the alanine to threonine yield another 3mer peptide Ac-ART-NH_2 could bind to MLL1 with K_i value of 0.02 μM.[111] Further detailed chemical modification of the side chains on the 3mer peptide was performed and a number of peptidomimetics with high binding affinity to WDR5, including **MM-101** and **MM-102** were obtained with K_i value lower than 1 nM. It has been shown that **MM-102** can suppress the expression of HOXA9 and MEIS1 genes in leukemia cells with MLL1-AF9 fusion.[92] The crystal structure (PDB ID: 4GM8) of **MM-102** in complex with WDR5 has shown that the side chain of unnatural amino acid on **MM-102** significantly enhanced hydrophobic interactions with WDR5 comparing with Win motif 12mer peptide. Study of the co-crystal structure also provided a further rational design and optimization to yield a cyclized peptidomimetic **MM-401**.[112] **MM-401** is also extremely potent binding to WDR5 with K_i value lower than 1 nM and IC_{50} value of 0.9 nM to disrupt WDR5 MLL1 interactions. The co-crystal structure (PDB ID: 4GM9) of **MM-401** in complex with WDR5 shows it has a similar binding mode comparing with previous linear peptide **MM-102**. Additionally, the phenyl group on Phg of **MM-401** stacks with the phenyl group on Y260 of WDR5 and the hydrophobic methylene linker interacts with the side chains of Y131 and F149 of WDR5.

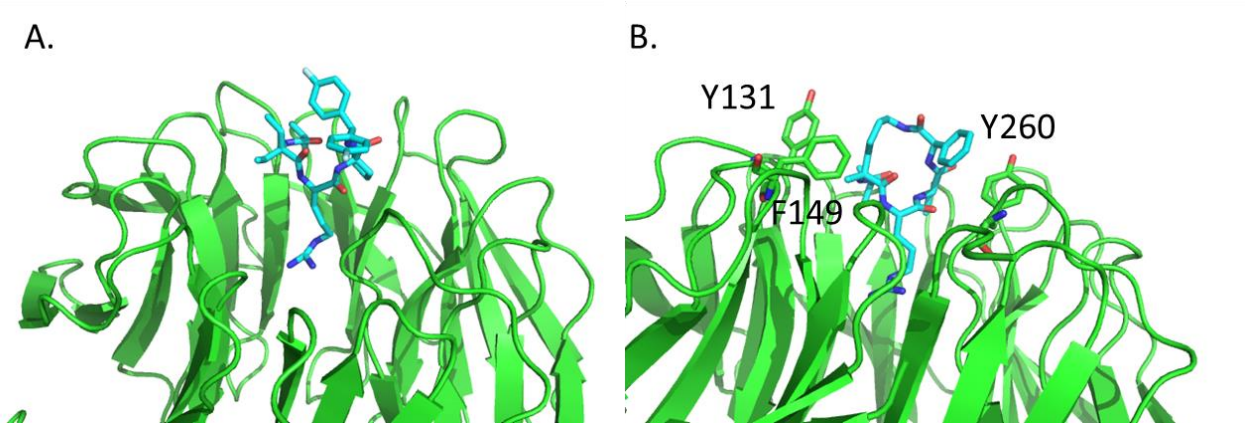

Figure 3-2. (A) Co-crystal structure of **MM-102** in complex with WDR5 (PDB ID: 4GM8); (B) Co-crystal structure of **MM-401** in complex with WDR5 (PDB ID: 4GM9).

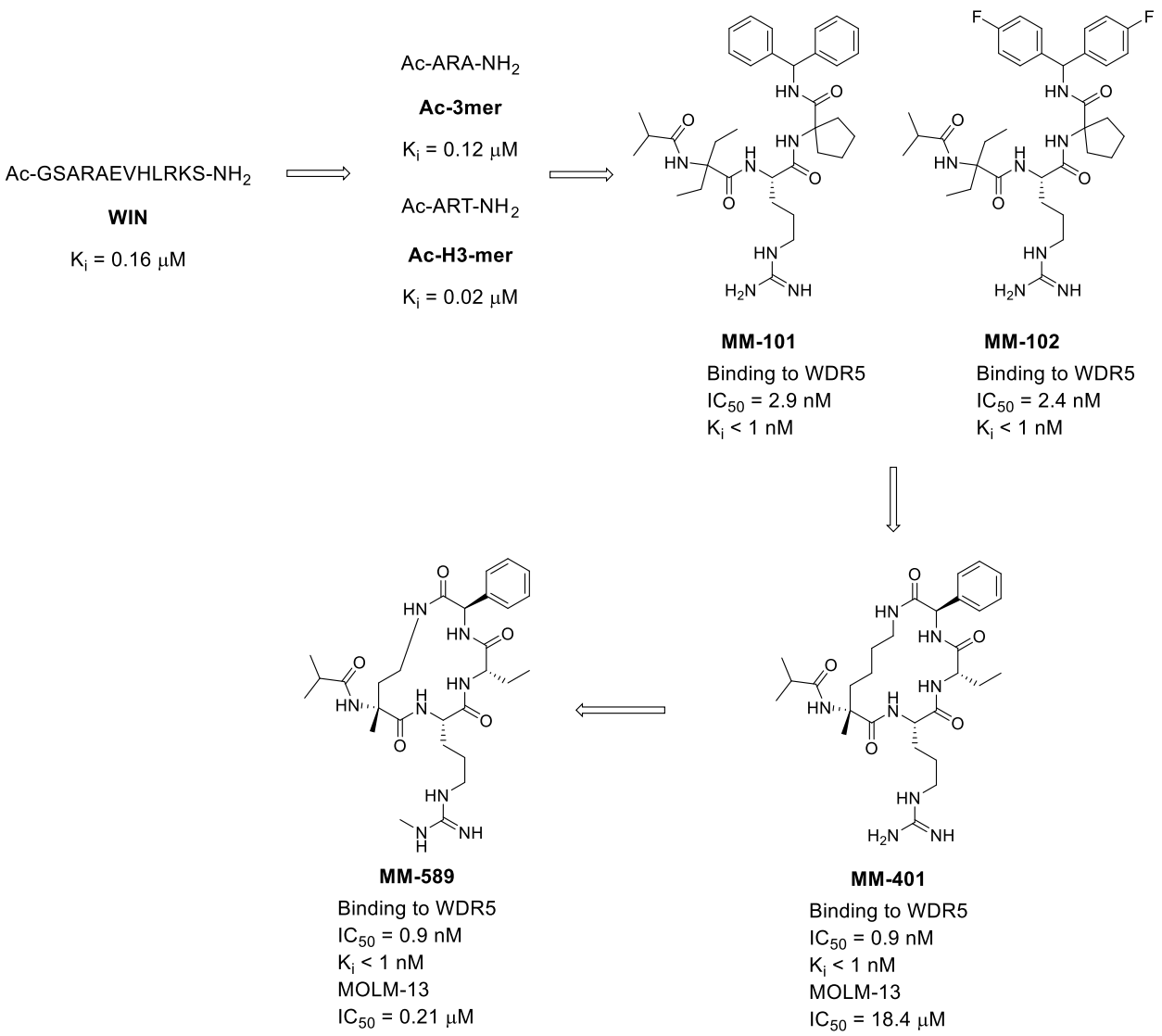

Figure 3-3. Structures of Peptidomimetic WDR5 Inhibitor

MM-401 specifically inhibit MLL1 without affecting other MLL or non-MLL family histone methyltransferases including MLL2, MLL3, MLL4, SET1, SET7/9 and EZH2. It has shown that **MM-401** can inhibit MLL1 methyltransferase activity and block proliferation of MLL cells by inducing cell-cycle arrest, apoptosis, and myeloid differentiation. No general toxicity was found to normal bone marrow cells or non-MLL cells by the treatment of **MM-401**.

Further optimization based on the structure of **MM-401** advanced **MM-589** which is 40-times more potent than **MM-401** in inhibition of the MLL HMT activity and growth of MV4;11 and MOLM-13 cell lines.[113] The smaller ring size of **MM-589** comparing with **MM-401** makes the confirmation more compact and stable with additional intra-molecular hydrogen bond. Methylation on guanidium group can also improve the cell permeability of these cyclic peptidomimetic inhibitors.

Development of Small Molecular WDR5 inhibitors

Besides the peptidomimetic WDR5 inhibitor, several small molecular inhibitors were also developed from Al-awar group and You group. In 2013, **WDR5-1010, WDR5-0102, WDR5-0103** was discovered from a high-throughput screening study with a K_d value of 0.45-5.5 μM. Crystal structure (PDB ID: 3SMR) of **WDR5-0102** in complex with WDR5 has shown that it occupies the Arginine binding pocket with a methyl piperidine group and formed two hydrogen bonds with S91 and C261. **WDR5-0103** occupies the binding pocket with a similar as **WDR5-0102**. The methoxy group on **WDR5-0103** induces a shift of benzamide ring and flip of S91. This also increases the hydrophobic interaction with F149 and Y191, which contributes the improvement of binding affinity.[114]

Further optimization of the benzamide moiety based on the structure of **WDR5-0102** yields compound **WDR5-47** with K_d value of 0.38 μM.[115] The co-crystal structure (PDB ID: 4IA9) of **WDR5-47** in complex with WDR5 has shown that the substituted benzamide group gains hydrophobic interactions with D107, A65, L321, A47 of WDR5.

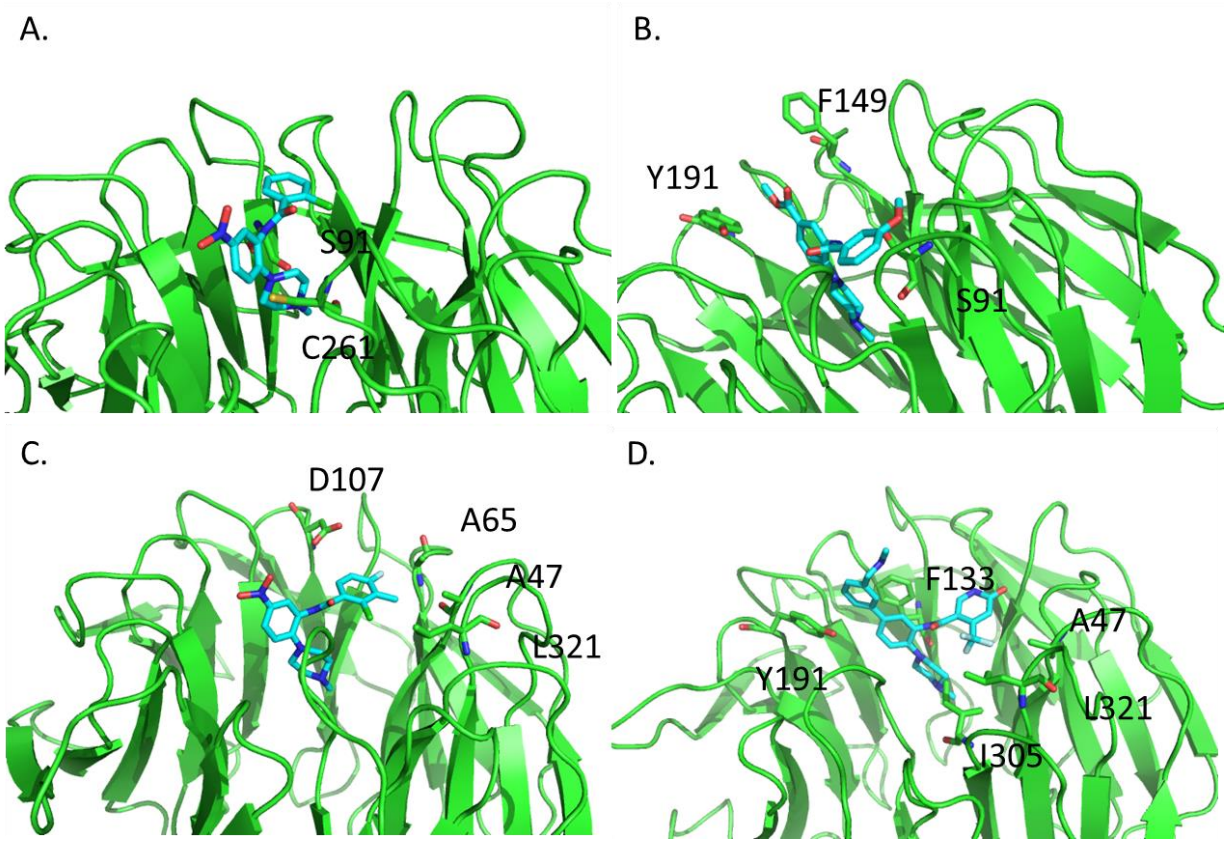

Figure 3-4. (A) Co-crystal structure of **WDR5-0102** complex with WDR5 (PDB ID: 3SMR); (B) Co-crystal structure of **WDR5-0103** complex with WDR5 (PDB ID: 3UR4); (C) Co-crystal structure of **WDR5-47** complex with WDR5 (PDB ID: 4IA9); (D) Co-crystal structure of **OICR-9429** complex with WDR5 (PDB ID: 4QL1).

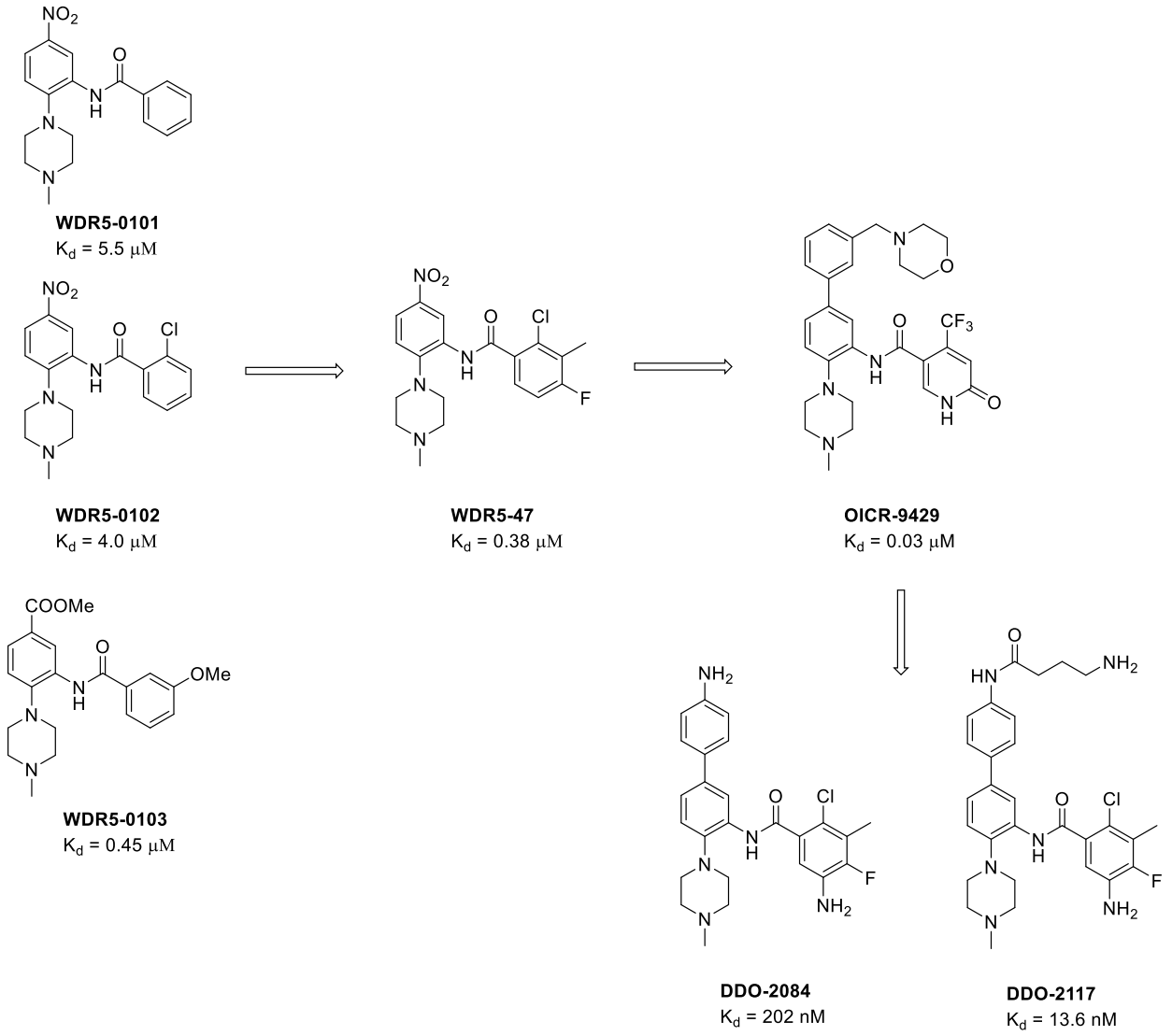

Figure 3-5. Structures of small molecular WDR5 inhibitors

Further SAR study based on **WDR5-47** led to the discovery of **OICR-9429**[91, 116], which could bind to WDR5 with K_d value of 0.03 μM. The co-crystal structure (PDB ID:4QL1) of **OICR-9429** has shown that the additional phenyl ring could form π-π stacking interactions with F133 and Y191. The trifluoromethyl group on the benzamide also forms hydrophobic interactions with A47, L321

and I305 of WDR5. Significantly **OICR-9429** selectively inhibited proliferation and induced differentiation in N-terminal C/EBPα-mutated p30-expressing human AML cells.[91]

In 2017**, DDO-2117** was developed based on the structure of **WDR5-47** with K_d value of 13.6 nM and IC_{50} value of 7.6 nM, which is currently published most potent small molecular inhibitor for WDR5.[117-119] Docking studies of **DDO-2117** with WDR5 has shown the additional phenyl group could occupy the hydrophobic pocket of F133, F149 and Y191.

In summary, both peptidomimetic and small molecular inhibitor targeting WDR5 MLL1 protein-protein interaction have been developed for the treatment of leukemia with MLL-FPs. Most of the published studies were done in vitro. Further evaluation of these compounds should focus on the efficacy and pharmacodynamic studies in vivo.

Results and Discussion

From **MM-102** to **MM-401,** great binding affinity improvement was achieved from the cyclization of the linear peptide to stabilize the bound confirmation of the peptidomimetics. Since the linker length or ring size of our peptidomimetics might play an important role for their confirmations, we did a model study on compounds with different linker lengths. Interestingly, modeling result suggested that cyclic peptidomimetics with a linker, as short as 2-carbon appear to be able to adopt low-energy conformations that closely resemble the bound conformation of compound **MM-401.**

As **MM-401** has a binding affinity exceeding the lower assay limit in the FP-based competitive binding assay, several less potent cyclic peptidomimetic with different linker length

were synthesized as template to better understand linker length effect on binding affinity to WDR5. From our previous study, the methyl group attached to the bridging carbon atom contributes significantly to their affinity to WDR5[92] Indeed, removal of this methyl group in **MM-401** yielded **LC-058**, which has a K_i value of 60.3 nM, > 50-times less potent than **MM-401**. Several compounds with variety linker length were synthesized based on the structure of **LC-058** and the results were summarized in **Table 3-1**. Compound **LC-043-1** with a 3-carbon linker has K_i value of 32.9 nM to WDR5 and is 2-times more potent than **LC-058**. Compound **LC-040** with a one-carbon linker, has K_i value of 242 nM to WDR5 and is thus 4-times less potent than **LC-058** with a 4-carbon linker. However, compound **LC-042-1** with a 2-carbon linker has K_i value of 0.8 nM to WDR5 and is > 70-times more potent than **LC-058**, which suggested 2-carbon linker achieves the best confirmation bound to WDR5.

MLL HMT functional assay developed by our group was used to test these compounds (**LC-058**-**LC-040**) for their inhibitory activity. The results showed that their potencies in inhibition of the MLL HMT activity correlate nicely with their binding affinities to WDR5. Accordingly, compound **LC-042-1** has the best potency to inhibit the MLL HMT activity (IC_{50}= 1.8 μM), while IC_{50} of the other compounds are higher than 10 μM (**Table 3-1**).

Table 3-1. Structures, binding affinities to WDR5 and MLL HMT inhibition activities of demethylated analogues of compound **MM-401** with different linker sizes.

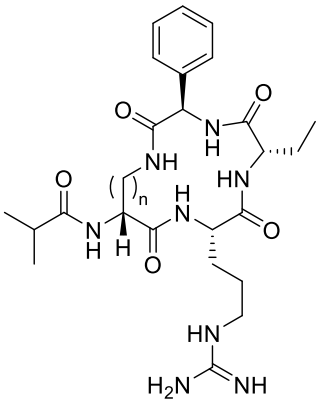

Compound	n	Binding Affinity to WDR5		Inhibition of MLL HMT Activity
		IC_{50} ± SD (nM)	K_i ± SD (nM)	IC_{50} ± SD (μM)
LC-058	4	298 ± 58	60.3 ± 11.9	> 10
LC-043-1	3	164 ± 26	32.9 ± 5.3	> 10
LC-042-1	2	6.2 ± 0.5	0.8 ± 0.1	1.8 ± 0.4
LC-040	1	1190 ± 160	242 ± 33	> 10

According to the promising data for **LC-042-1**, a series of analogues of compound **MM-401** with different ring sizes were synthesized and tested with the FP-binding assay and MLL HMT assay. The results were summarized in **Table 3-2**.

Table 3-2. Structures, binding affinities and MLL HMT inhibition activities of Compound **MM-401** analogues with different linker length.

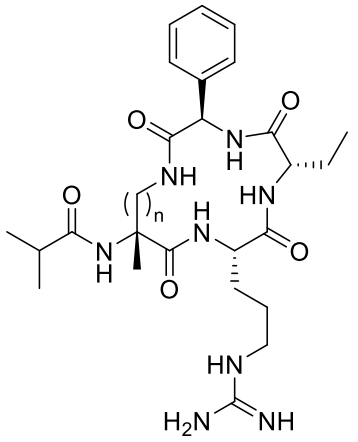

		Binding Affinity to WDR5		Inhibition of MLL HMT Activity
Compound	n	IC_{50} ± SD (nM)	K_i ± SD (nM)	IC_{50} ± SD (nM)
MM-401	4	0.9 ± 0.2	< 1	373 ± 44
LC-081 (MM-581)	2	1.08 ± 0.12	< 1	12.6 ± 1.2
LC-044	3	0.97 ± 0.13	< 1	84.8 ± 23.8
HK-06-223C	5	2.6 ± 0.2	< 1	1527 ± 218
HK-05-121C	6	1.0 ± 0.2	< 1	216 ± 88

HK-06-229C	8	1.3 ± 0.2	< 1	744 ± 79

Compounds **LC-081**, **LC-044**, **MM-401**, **HK-06-223C**, **HK-05-121C** and **HK-06-229C** with linker lengths of 2, 3, 4, 5, 6 and 8 carbons, respectively, all bind to WDR5 with very high affinities (IC_{50} = 0.9-2.6 nM, K_i < 1 nM), which exceed the lower assay limit. The potential differences in their binding affinities to WDR5 cannot be determined from the FP binding assay. While, our MLL HMT functional assay could help to compare these compounds. The results showed that all of them can effectively inhibit MLL HMT activity, but their potencies are not the same. Among these analogues, compound **LC-081** has the best inhibitory activity with IC_{50} value of 12.6 nM, which is about 30-times more potent than **MM-401**, similar to the difference between **LC-042-1** and **LC-058** in binding assay. Compound **LC-044** with a 3-carbon linker is the second most potent inhibitor of the MLL HMT activity with an IC_{50} value of 84.8 nM.

Then these compounds were evaluated for their cell growth inhibitory activity in MOLM-13, MV4;11 and HL-60 cell lines (**Table 3-3**). In the MV4;11 cell line harboring MLL-AF4 fusion protein and the MOLM-13 cell line harboring MLL-AF9 fusion protein, **MM-401** has IC_{50} values of 9.8 μM and 18.4 μM, similar to those values reported in the previous study.[112] **LC-042-1** displays modest cellular activities with IC_{50} values of 42.8 μM and 43.4 μM against MOLM-13 and MV4;11 cell lines, respectively, and **LC-058** and **LC-043-1** have minimal activity at 100 μM in both cell lines. Compound **LC-081** (**MM-581**) is the most potent compound in this series and has IC_{50} values of 0.28 μM and 0.46 μM, respectively, in inhibition of cell growth in the MOLM-13 and MV4;11 cell

lines. Significantly, compounds **LC-081** and **LC-044** have much weaker activity in the HL-60 cell line lacking MLL translocation and display more than 30-fold cellular selectivity.

Table 3-3. Inhibition of cell growth with representative cyclic peptidomimetics.

	IC_{50} (μM) in cell growth inhibition		
Compound	MOLM-13	MV-4-11	HL-60
MM-401	18.4 ± 6.6	9.8 ± 8.0	> 100
LC-042-1	42.8	43.4	> 100
LC-043-1	> 100	> 100	> 100
LC-058	> 100	> 100	> 100
LC-081	0.28 ± 0.02	0.46 ± 0.02	17.4
LC-044	1.28 ± 0.01	1.29	46.8
HK-06-223C	37.6 ± 12.1	15.1 ± 11.8	> 100
HK-05-121C	5.6 ± 0.7	3.2 ± 0.4	29.7 ± 11.5
HK-06-229C	21.6 ± 4.8	7.5 ± 3.0	> 100
LC-089	0.21 ± 0.02	0.25 ± 0.01	8.56 ± 1.14
LC-088	14.3 ± 0.9	35.0 ± 4.4	2.95

According to our previous study, mono-methylation of the guanidine group in **MM-401**, which yielded **MM-408**, improves cellular potency against MV4;11 and MOLM-13 cell lines.[113] **LC-**

089 was synthesized with mono-methylated the guanidine group in compound **LC-081** and tested. **LC-088**, with the chiral center in the phenylglycine residue changed from *D*- to *L*-configuration in **LC-089,** was used as a negative control compound (**Table 3-4**). Similar to compound **LC-081**, compound **LC-089** binds to WDR5 with high affinity (IC_{50}= 0.90 nM, K_i value of < 1 nM), which is also lower than assay limit and potently inhibits the MLL HMT activity with IC_{50} value of 12.7 nM.

Table 3-4. Structures, binding affinities to WDR5 and MLL HMT inhibition activities of compounds **LC-081**, **LC-089** and **LC-088**.

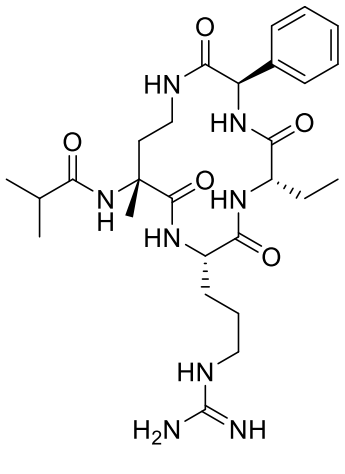

LC-081

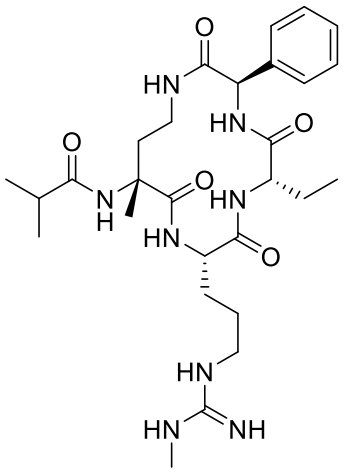

LC-088

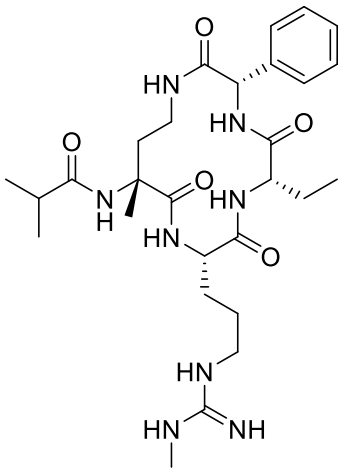

LC-089

	Binding Affinity to WDR5		Inhibition of MLL HMT Activity
Compound	IC_{50} ± SD (nM)	K_i ± SD (nM)	IC_{50} ± SD (nM)
LC-081	1.08 ± 0.12	< 1	12.6 ± 1.2

LC-089	0.90 ± 0.20	< 1	12.7 ± 1.5
LC-088	2.0 ± 0.1	< 1	477 ± 51

Compound **LC-089** was next evaluated for its cell growth inhibition activity on acute leukemia cancer cell lines (**Table 3-3.**). **LC-089** can well inhibit the cell proliferation of both the MV4;11 and MOLM-13 cell lines with IC_{50} values of 0.25 μM and 0.21 μM. It has much weaker activity in the inhibition of cell growth of the HL-60 cell line the IC_{50} value is 8.6 μM. **LC-089** displayed more than 30-times selectivity for the MV4;11 and MOLM-13 cell lines harboring MLL translocations over the HL-60 cell line without MLL translocation. Compound **LC-088** is 40-times less potent (IC_{50} = 477 nM) than **LC-089** (IC_{50} = 12.7 nM) in inhibition of the MLL HMT activity, although it can still bind to WDR5 with a high affinity (IC_{50} = 2.0 nM, K_i < 1 nM), **LC-088** shows 70-150 times weaker activity than **LC-089** in inhibition of cell growth of both MV4;11 and MOLM-13 cell lines (**Table 3-3**).

Several previous publications have reported that small molecule inhibitors targeting HMT activity, such as inhibitors of the EZH2 H3K27 activity[20] and the DOT1L H3K79 activity[21], had slow kinetics in inhibition of cell growth. Extra treatment time was needed for the cell growth inhibition assay. We therefore evaluated compound **LC-089** for its inhibitory activity of cell growth in MV4;11 and MOLM-13 leukemia cell lines with either 4- or 7-day treatment. Although 2-3 times IC_{50} value improvement from 4-day treatment to 7-day treatment in both cell lines were achieved, the maximum inhibition has changed from partial inhibition to essentially complete inhibition (**Figure 3-6**). With 4-day treatment. approximately 75% cell proliferation

inhibition was obtained with **LC-089** in MV4;11 and MOLM-13 cell lines. While with 7-day treatment, more than 95% inhibition was achieved in both cell lines.

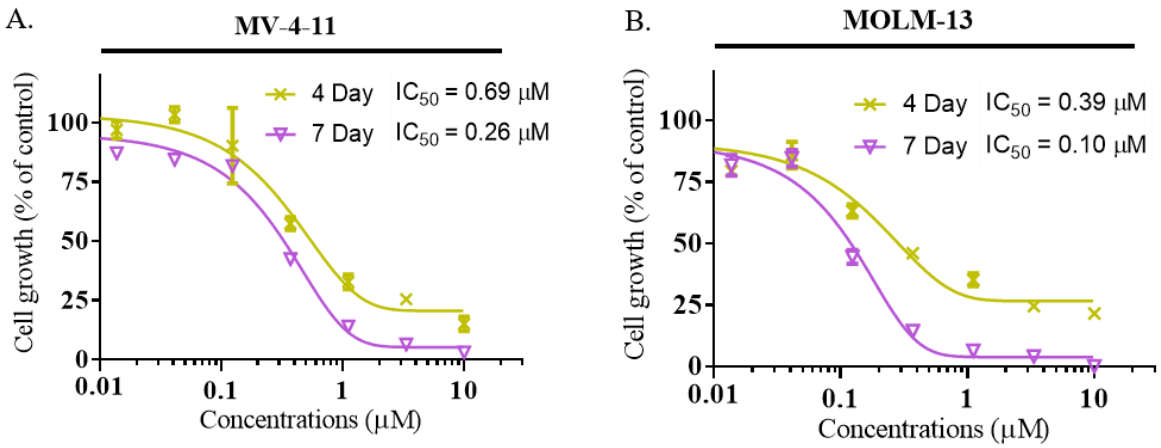

Figure 3-6. Cell growth inhibition of compound **LC-089** upon 4-day or 7-day treatment in MV4;11 and MOLM-13 acute leukemia cell lines.

To gain further structural insights into the high-affinity interactions of cyclic peptidomimetics with WDR5, we have successfully determined a co-crystal structure for **LC-089** in complex with WDR5 at a resolution of 1.64 Å (**Figure 3-7**, PDB code: 5VFC). In the co-crystal structures of **LC-089** in complex with WDR5, WDR5 adopts an almost identical β-propeller configuration as the apo-WDR5 structure (PDB ID: 2H14). The electron density map shows clear extra density in the central channel of the WD40 propeller where MLL peptide binds[120], enabling us to unambiguously dock **LC-089** into the structure (**Figure 3-7A**). **LC-089** adopts a compact bound conformation with three intramolecular hydrogen bonds, which is similar to that in **MM-401**.[112] **LC-089** binds to the central channel of WD40 propeller in WDR5 through the conserved interaction network as observed in WDR5/MLL and WDR5/**MM-401** complex structures.[112]

Comparing with **MM-401**, the methyl on the guanidinium moiety in **LC-089** gained hydrophobic interactions with C134 and F263, but lost a direct hydrogen bond with S175 (**Figure 3-7B**). The aliphatic carbon linker and side chains of **LC-089** gains strong hydrophobic interactions with the hydrophobic surfaces formed by the side chains of Y131, F149, F133, Y191, Y260, L321, I305, A47 and A65 from WDR5 (**Figure 3-7C**). The different linker length of **MM-401**, **HK-05-121C** and **LC-089** causes different orientations of the phenyl group on Phg. The phenyl groups in **LC-089** and **MM-401** stack almost parallel to the phenyl group of WDR5 Y260 (**Figure 3-7D**, magentas and yellow, respectively). In contrast, the phenyl group in **HK-05-121C** (cyan) is oriented near perpendicular to the phenyl group of WDR5 Y260, comprising an incomplete aromatic cage. But it can form cation-π interaction with K259, which is surrounded by the aromatic cage. Comparing with **MM-401** and **HK-05-121C**, **LC-089** with shorter linker length and small ring size can form a more compact structure, which forms several optimal intramolecular hydrogen bonds and reduces the conformational flexibility. This optimal confirmation helps to achieve a very high affinity to WDR5 and consequently strong MLL HMT inhibition activity.

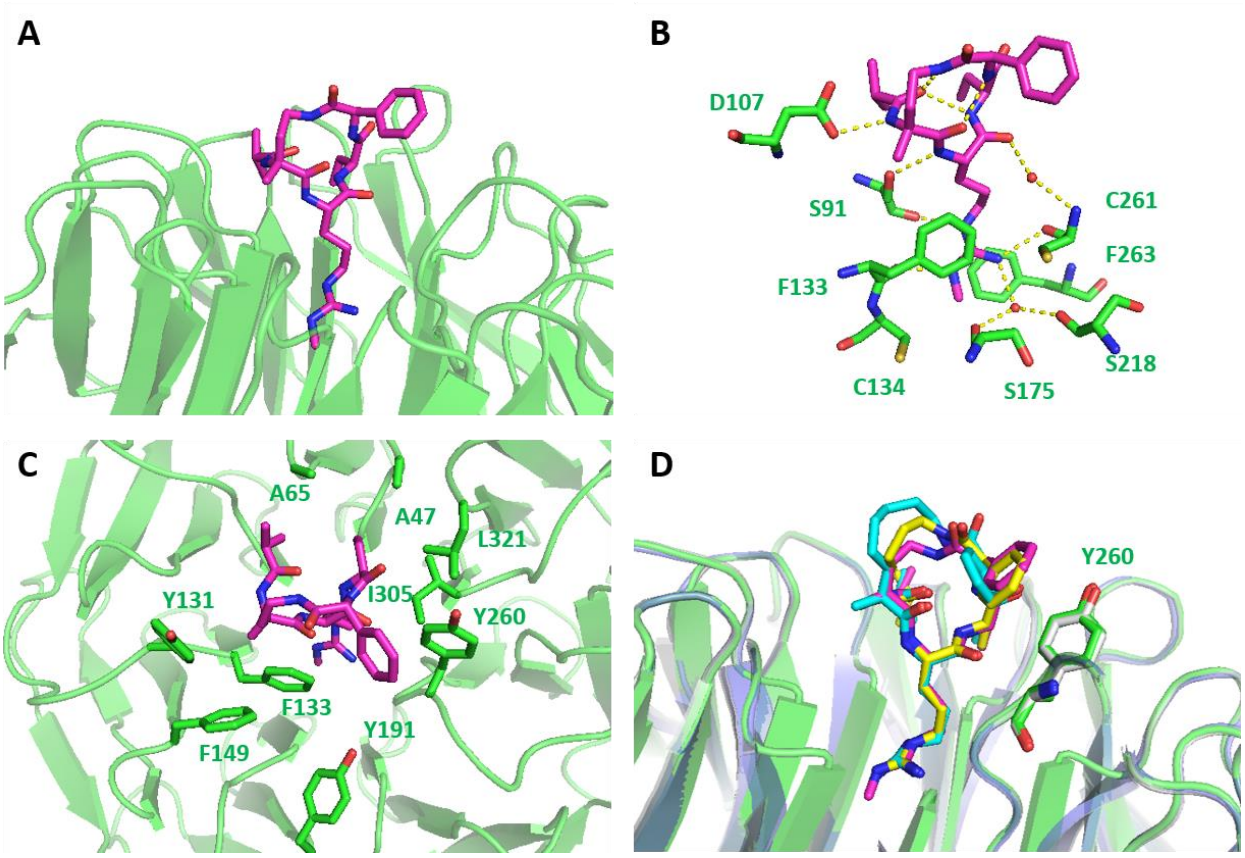

Figure 3-7. (A-C) Co-crystal structure of cyclic peptidomimetic **LC-089** in complex with WDR5 (PDB ID: 5VFC) and (D) in comparison with co-crystal structures of **MM-401** in complex with WDR5 (PDB ID: 4GM9) and **HK-05-121C** in complex with WDR5 (PDB ID: 4GMB). Carbon atoms for compound **LC-089, HK-05-121C** and compound **MM-401** are shown in magentas, cyan and yellow, respectively. Nitrogen atoms are shown in blue and oxygen atoms are shown in red.

From our study, the linear peptidomimetic **MM-101** has very poor stability in human microsomes ($T_{1/2}$ = 4 min) and moderate stability in mouse and rat microsomes ($T_{1/2}$ = 44 min and $T_{1/2}$ = 34 min, respectively). This limits its further application in drug discovery. While cyclized

peptidomimetics with more compact and stably confirmation can improve their stability. The microsomal stability result of the cyclized peptidomimetics **MM-401**, **LC-089** and others have shown excellent stability in human, mouse and rat microsomes with half-life greater than 60 minutes. (**Table 3-5**) This makes feel more confident about application of the cyclized peptidomimetics in drug discovery.

Table 3-5. Microsomal stabilities of linear peptidomimetic **MM-101** and selected cyclic peptidomimetics.

	$T_{1/2}$ (min)		
Compound	Human	Rat	Mouse
MM-101	4	34	44
MM-401	> 60	> 60	> 60
LC-081	> 60	> 60	> 60
LC-044	> 60	> 60	> 60
LC-089	> 60	> 60	> 60

Based on the promising data of the cyclized peptidomimetic inhibitors targeting WDR5, further modifications on the side chains of **LC-081** were performed. As the current cyclized peptidomimetic inhibitors have reached the assay limit of both FP binding assay and MLL1 HMT functional assay, cell growth inhibition assay was used to compare the different inhibitors.

Table 3-6. Modification on the side chain of Abu (L-2-aminobutyric acid)

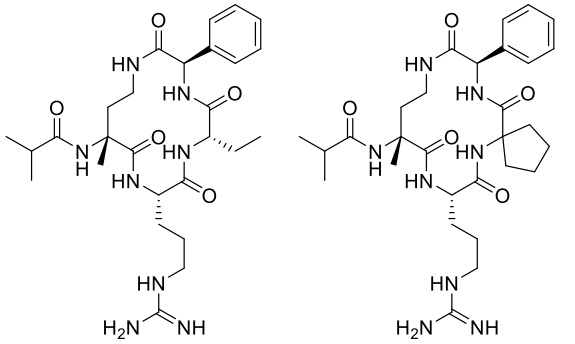

	R	MOLM-13 IC_{50} ± SD (μM)
LC-081		
LC-313		1.05
LC-300	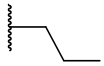	6.332
LC-314	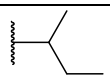	>10
LC-322		> 10

At first, modification on the side chain of L-2-aminobutyric acid was performed. From the co-crystal structure of **LC-081** in complex with WDR5, the ethyl group could form hydrophobic interaction with the hydrophobic surface formed with A47 and L321. And according to the previous study on the linear peptide[92], several modifications could be tolerated and cycloleucine

(CycLeu) was preferred at this position. Then several amino acids with variety hydrophobic side chains were tested and result is summarized in **Table 3-6**. To our surprise, all the modification could not be well tolerated. Changing ethyl group to isopropyl group reduced the cell growth inhibition activity by 3 folds, while with larger substitution groups such as n-propyl, sec-butyl group or using CylLeu instead of Abu cause more than 20-fold cell growth inhibition loss. So, ethyl group will be kept in this position and further modification can performed on other sites.

Table 3-7. Modification on the side chain of Phg (L-Phenyl glycine) with non-aromatic groups.

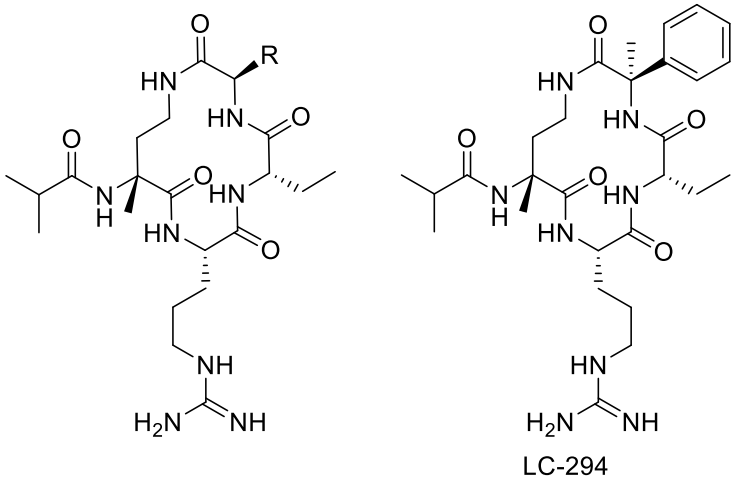

ID	R	MOLM-13 IC_{50} ± SD (μM)
LC-081	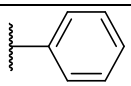	0.28
AK-012		1.72
AK-010	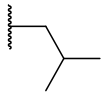	1.88

AK-020	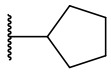	1.19
AK-011	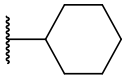	0.64
LC-261	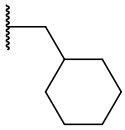	1.49
AK-005	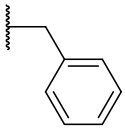	1.57
AK-021	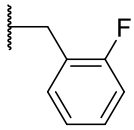	3.59
AK-022	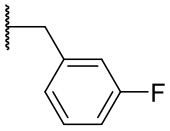	1.29
AK-036	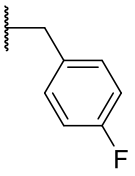	6.51
AK-033	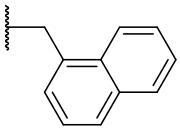	2.37
LC-294		1.01

Next, we focused on the modification of the phenyl group on Phg in **LC-081**. From the co-crystal structure of **LC-081** in complex with WDR5, the phenyl group in **LC-081** could form a π-π

stacking interaction. Well in the co-crystal structure of **HK-05-121C**, the orientation of phenyl ring could form hydrophobic interaction with K259. According to these different interactions between the inhibitors and WDR5, both aromatic and non-aromatic substitution groups were used to explore this binding site. In **Table 3-7**, different aromatic or non-aromatic substitution group were used to replace the phenyl group in **LC-081**. Replacing the phenyl group with methyl group yields **AK-012**, which is about 8 times less potent than **LC-081**, which means the π-π stacking interaction is important for the WDR5 binding and subsequent cell preliberation inhibition. While replacing the phenyl group with other non-aromatic aliphatic groups yields **AK-010-LC-261** are similar as **AK-012**, except for **AK-011**. Although **AK-011** is still less potent than **LC-081**, but results indicate that cyclohexyl group could form hydrophobic interaction with WDR5.

Next, some phenylaniline or substituted phenylaniline were used to replace the phenylglycine in the peptidomimetics. Using phenylaniline can help us to overcome the racemization problem of phenylglycine during the synthesis. And it might keep the π-π stacking interaction with WDR5. **AK-005** – **AK-033** were synthesized accordingly. But unfortunately, none of them is as potent as **LC-081** in cell growth inhibition assay. To overcome the racemization problem, a methyl group was introduced to the α-carbon of phenylglycine, which yields **LC-294.** But it's 3-fold less potent than **LC-081**, which indicates the methyl group can affect the orientation of the phenyl group and block the π-π stacking interaction.

Table 3-8. Modification on the side chain of Phg (L-Phenyl glycine) with aromatic groups.

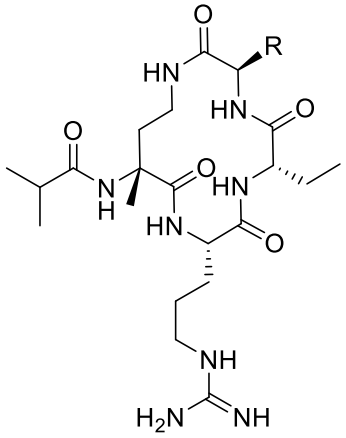

ID	R	MOLM-13 IC_{50} ± SD (μM)
LC-334	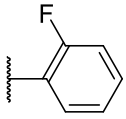	0.35
LC-321	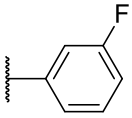	0.42
AK-035-2	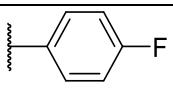	0.38
AK-057	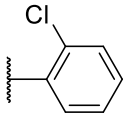	2.6
AK-058	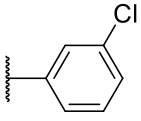	0.51
AK-059	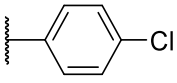	2.2

AK-042	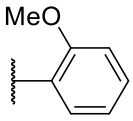	1.6
LC-345	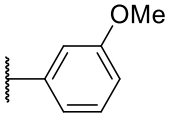	0.56
LC-339	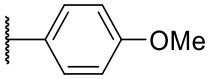	0.083
LC-324	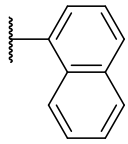	1.285
LC-326	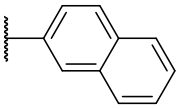	0.054

The results in **Table 3-7** indicate that the original phenylglycine structure is critical for the WDR5 binding and could not be replaced by non-aromatic substitution or substituted benzyl groups in the inhibitor design. So further modifications are directly on the structure of phenylglycine**.** Substitution at different positions on the phenyl ring with fluoro, chloro and methoxy groups were explored and the results are summarized in **table 3-8.** Fluoro substitutions on phenyl group can barely affect the cell growth inhibition activity, as IC_{50} of **LC-334 -AK-035-2** are 0.35-0.42 μM. While **AK-057** with 2-chloro and **AK-042** with 2-methoxyl substitutions are much less potent than **LC-081**, which suggests that the large substitution group at 2-position can affect the confirmation of the phenyl group. Similar results were obtained when Naphthalen-1-yl group was used to replace the phenyl group in **LC-081** to yield **LC-324**. Replacing the phenyl

group with naphthalen-2-yl group yields **LC-326,** which is 5-times more potent **LC-081**. It might be because the naphthalenyl group form stronger π-π stacking interaction with Y260 in WDR5. Similar result was found by introducing methoxy group at 4-position of the phenyl ring, which yields **LC-339** is about 3-fold more potent than **LC-081**.

Table 3-9. Modification on the side chain of Arg (L-Arginine)

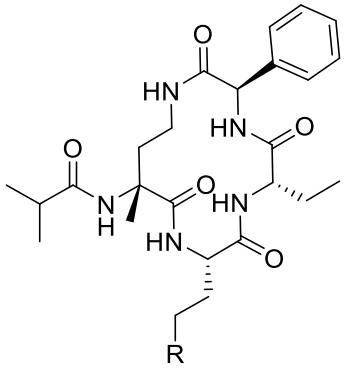

ID	R	MOLM-13 IC_{50} ± SD (μM)
LC-081	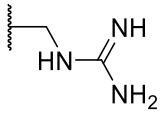	0.28
LC-186-2	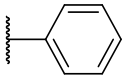	> 10
LC-183-2	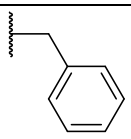	> 10
LC-187-2	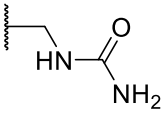	>10

LC-169	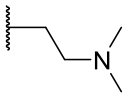	> 10
LC-174	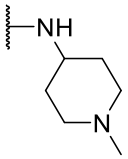	> 10
LC-164	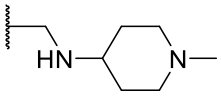	> 10
LC-210	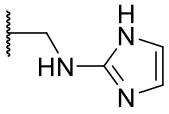	> 10
LC-182	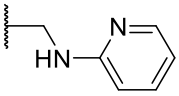	1.55
LC-227	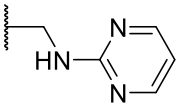	> 10
LC-202	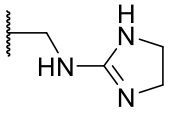	0.088
LC-337	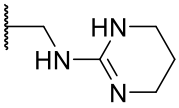	0.033
LC-315	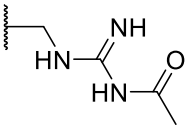	0.47

Comparing with the small molecule inhibitors, our peptidomimetic inhibitors have much better binding affinity to WDR5, but weaker or similar cell growth inhibition activities. This might

be because of low cell permeability caused by the polar guanidino group on arginine. The guanidino group is critical for the binding to WDR5 as it forms several important interactions with the protein. According to the co-crystal structures of **LC-089** and **MM-401** in complex with WDR5, guanidino group can form strong sandwiched π-π stacking interaction with F133 and F263, hydrogen bonds with C261, F133, S91, S218 and salt bridge with D92. Replacing the guanidino groups with variety groups targeting different interactions were explored and the results were summarized in **Table 3-9**. To keep the π-π stacking interaction, aromatic groups including phenyl, pyridinyl, pyrimidinyl, imidazolyl groups were used to replace the guanidino groups yields **LC-186-2, LC-183-2, LC-210, LC-182, LC-227**. Linkers with different length were used to offer variety orientation for these aromatic groups. But unfortunately, all these peptidomimetics are much weaker than **LC-081** in cell growth inhibition assay. (1-methylpiperidin-4-yl)amino group, which is used in **OICR-9429** and occupies the similar pocket as guanidino group in **MM-401**, was introduced to the peptidomimetic yields **LC-174** and **LC-164**, but no cell growth inhibition activities were obtained up to 10 μM treatment with such modification. So further modifications were done with the original guanidino group structure. Cyclization of the two nitrogen atoms with 5- and 6-member rings yields **LC-202** and **LC-337** with IC_{50} values of 88 nM and 33 nM in cell growth inhibition assay, which are 3-8 times more potent than **LC-081**. 4,5-dihydro-1H-imidazol-2-yl group in **LC-202** and 1-methylpiperidin-4-yl group in **LC-337** can interact with the hydrophobic surface composed with F219 and A176. It might also reduce the basicity of the guanidino group and improve the cell permeability of the peptidomimetics. Introducing electron withdrawing groups acetyl groups yields **LC-315**, which is 2 times less potent as **LC-081**.

Combining the SAR results above on different sites of **LC-081**, **LC-395** was synthesized accordingly. But the improvement of the different substitution groups could not be well combined. **LC-395** has similar cell growth inhibition activity as **LC-337**, with IC_{50} value of 38 nM.

Table 3-10. Binding affinity to WDR5 of selected peptidomimetic inhibitors.

	IC_{50}/ nM	K_i/ nM
AK-035-2	0.8783	< 1
AK-058	1.478	< 1
LC-089	2.129	< 1
LC-182	3.253	< 1
LC-202	2.397	< 1
LC-300	2.378	< 1
LC-313	1.833	< 1
LC-315	3.649	< 1
LC-321	2.874	< 1
LC-326	2.302	< 1
LC-334	0.3195	< 1
LC-337	1.865	< 1
LC-339	1.794	< 1
LC-345	3.997	< 1
LC-395	2.542	< 1

To further confirm our new cyclic peptidomimetic inhibitor could still bind to WDR5, the binding affinity to WDR5 of selected compounds were tested and the results were summarized in **Table 3-10**. All these potent WDR5 inhibitors can potently bind to WDR5 with IC_{50} values of 0.32-3.6 nM and K_i values << 1 nM, which are lower than the assay limit.

Synthesis

Intermediates **301** was prepared on the 2-chlorotrityl chloride resin using solid phase peptide synthesis with Fmoc chemistry and cleaved from the resin to yield carboxylic acids **302**, respectively (**Scheme 3-1**).

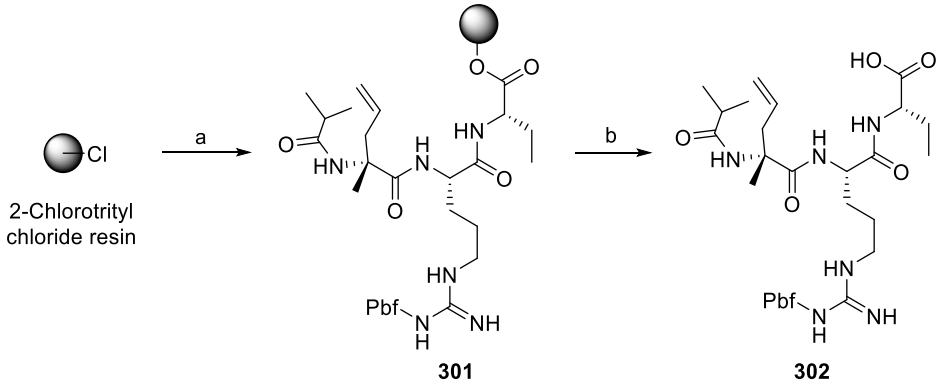

Scheme 3-1. Synthesis of **302.** Reaction conditions: (a) Solid phase peptide synthesis; (b) 1% CF_3COOH in CH_2Cl_2, rt, 30 min.

Synthesis of the designed cyclic peptidomimetics (**MM-401**, **HK-06-223C-HK-06-229C**) is shown in **Scheme 3-2**. Alkeneamines were first attached to an Fmoc-phenylglycine yielding **303a-303d**. Fmoc deprotection of **303a-303d** followed by amide coupling with intermediate **26** afforded **304a-304d**. RCM cyclization followed by catalytic hydrogenation and removal of the Pbf

protecting group from arginine side chain yielded the cyclic peptidomimetics **MM-401** and **HK-06-223C**-**HK-06-229C** as trifluoroacetic acid salt.

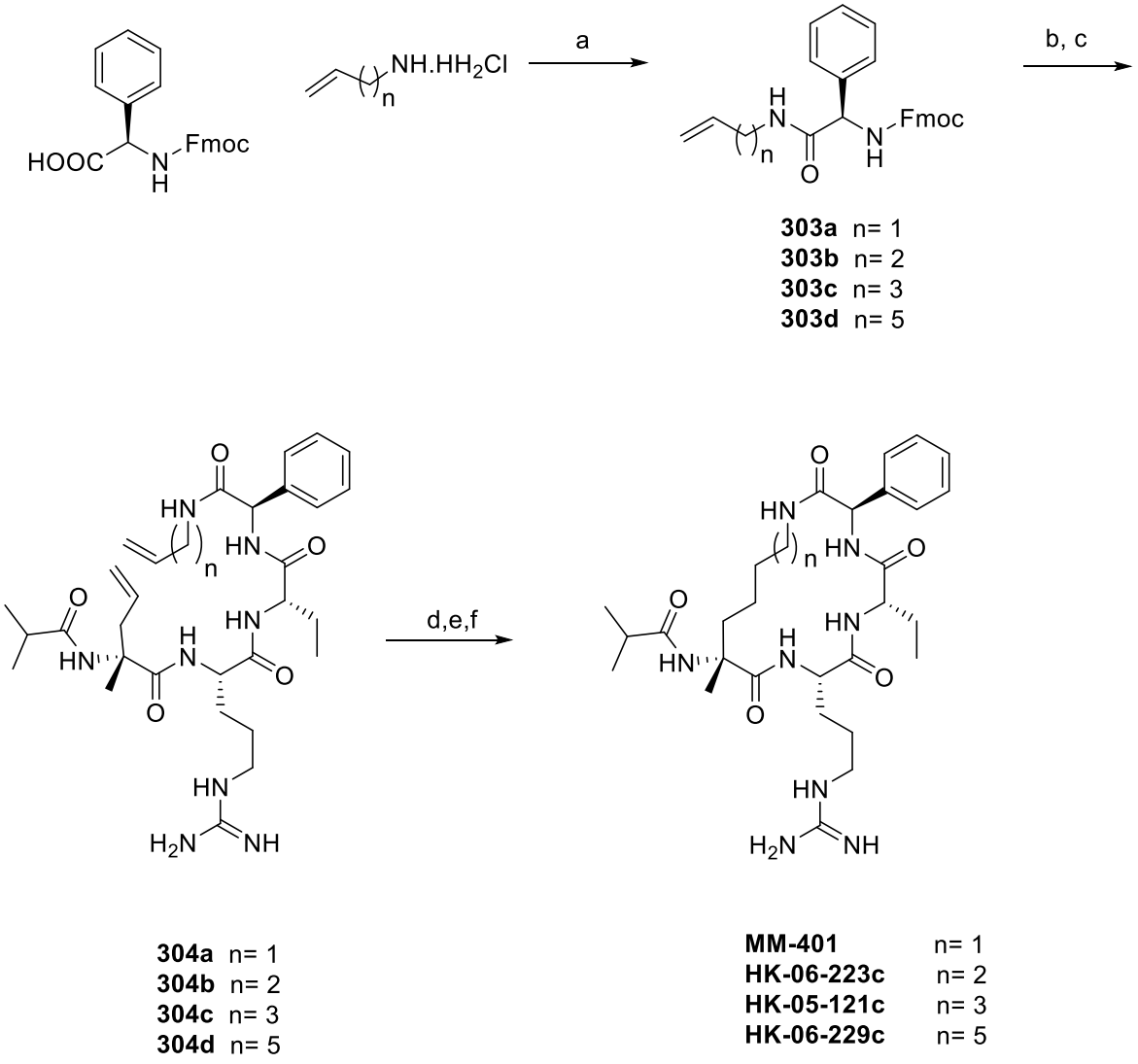

Scheme 3-2. Synthesis of **MM-401, HK-06-223c, HK-05-121c** and **HK-06-229c.** Reaction conditions: (a) EDCI, HOAt, DIPEA, CH_2Cl_2, rt, 2-3 h; (b) DEA, Acetonitrile, 2h; (c) **302**, EDCI, HOAt, DIPEA, CH_2Cl_2, rt, 4h; (d) Hoveyda-Grubb's 2nd generation catalyst, CH_2Cl_2, rt, overnight; (e) H_2/Pd.C, MeOH, rt, 2h; (f) CH_2Cl_2:CF_3COOH:H_2O (20:10:0.5), reflux, 2h;

Synthesis of cyclic peptidomimetics (**LC-040-LC-044**, **LC-089-LC-088**) is shown in **Scheme 3-3** and **Scheme 3-4**. Intermediates **305a-305e** and **309a-309b** were prepared on the 2 -chlorotrityl chloride resin using solid phase peptide synthesis with Fmoc chemistry. The intermediate peptides were cleaved from the resin followed by Boc or Benzyl protecting group removal with 10% trifluoroacetic acid in dichloromethane or hydrogenation with Pd/C in ethanol, respectively, to yield peptides **306a-306e (Scheme 3-3)** and **310a-310c (Scheme 3-4)**. Intramolecular amide coupling of **306a-306e**, **310a-310c** and followed by removal of Pbf protecting group from arginine side chain yielded cyclic peptidomimetics **LC-058-LC-044** and **LC-089-LC-088** as trifluoroacetic acid salt.

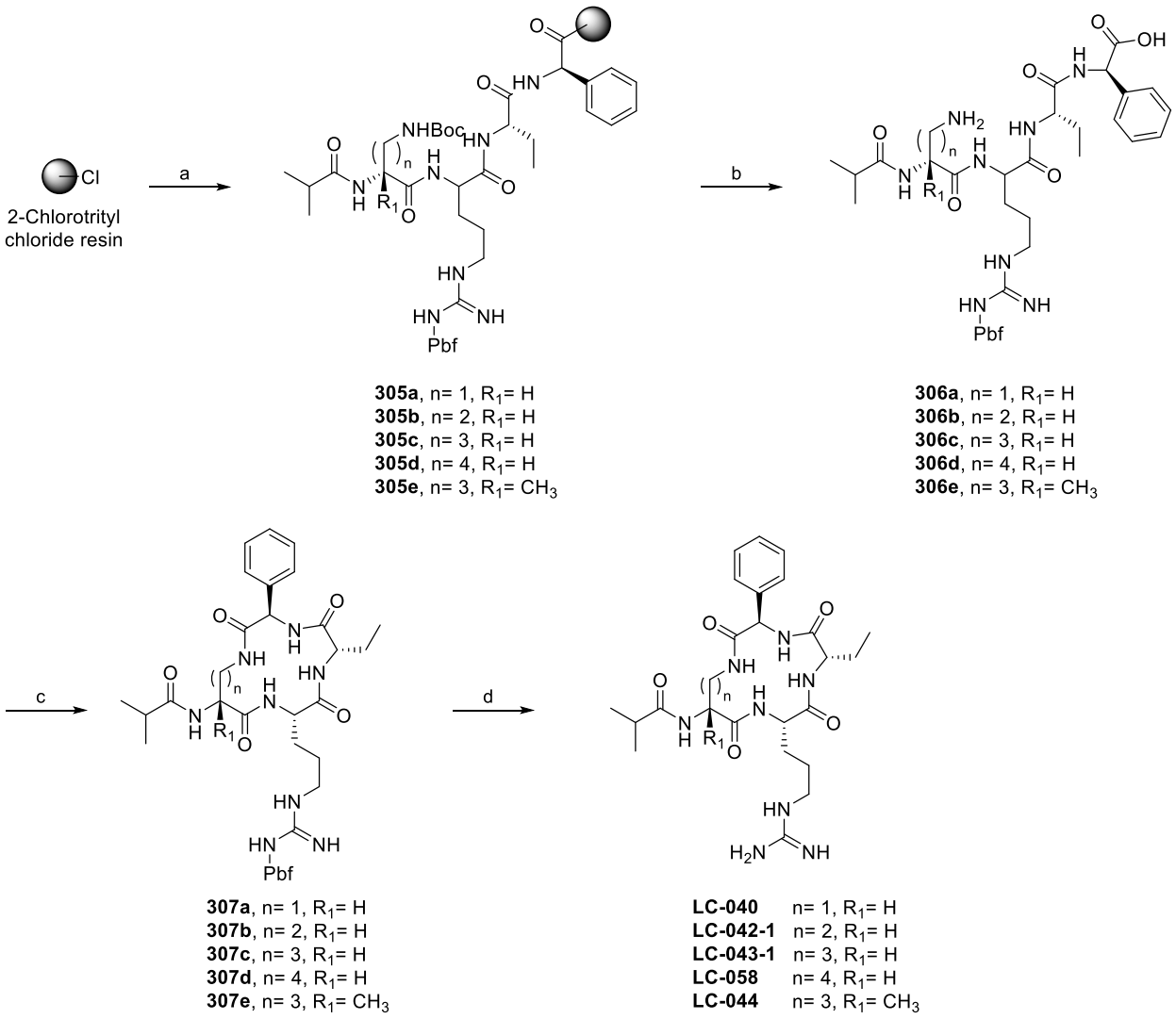

Scheme 3-3. Synthesis of **LC-040, LC-042-1, LC-043-1, LC-058** and **LC-044.** Reaction conditions: (a) Solid phase peptide synthesis; (b) 1% CF_3COOH in CH_2Cl_2, rt, 30 min then 10% CF_3COOH in CH_2Cl_2 1h; (c) HATU, DIPEA, DMF, rt, 1h; (d) 95% CF_3COOH in water, rt ,2h

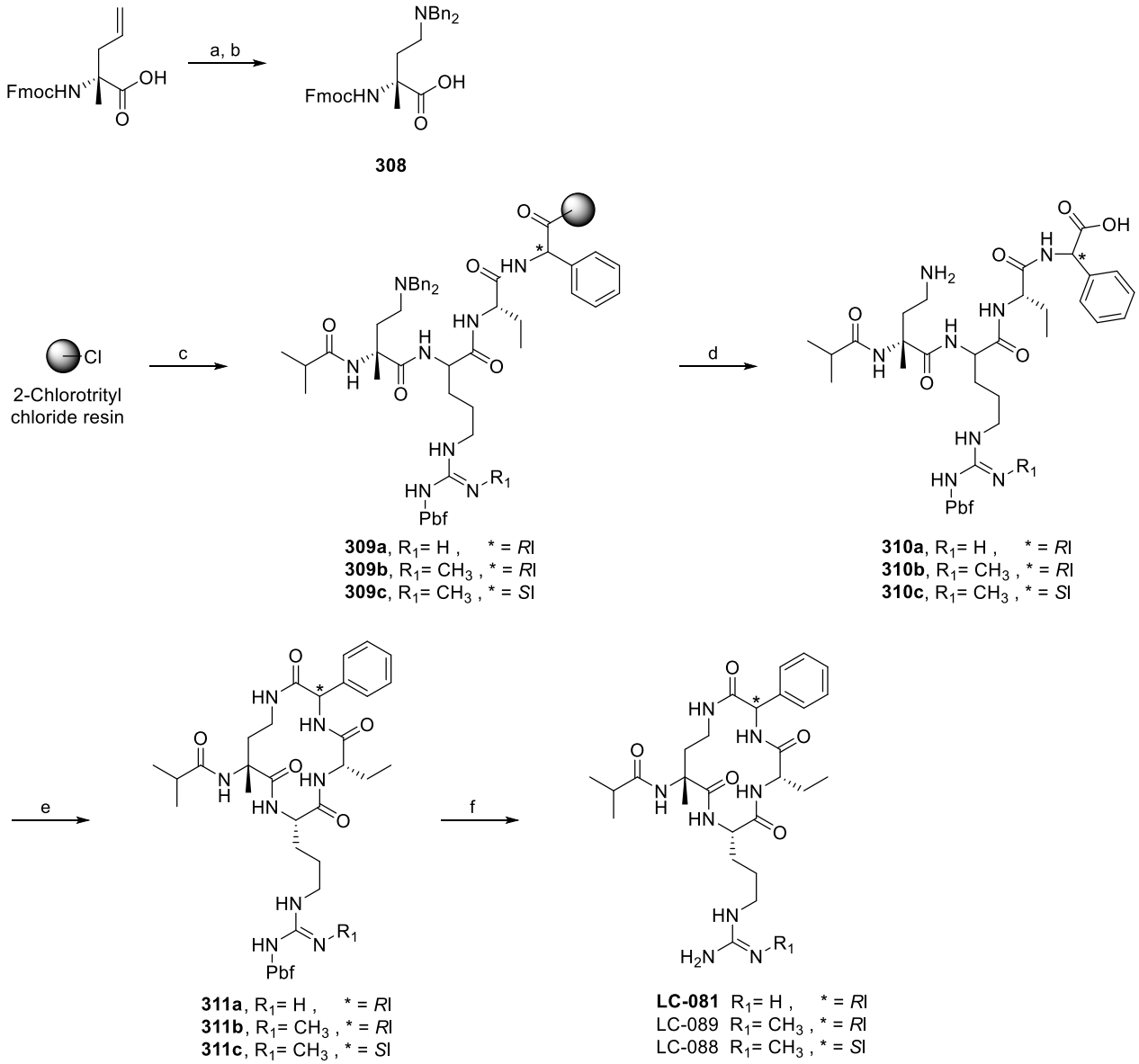

Scheme 3-4. Synthesis of **LC-081, LC-089** and **LC-088.** Reaction conditions: (a) OsO_4, $NaIO_4$, H_2O, THF, rt, 4h; (b) Dibenzylamine, $NaBH(OAc)_3$, $ClCH_2CH_2Cl$, rt, 10h; (c) Solid phase peptide synthesis; (d) 1% CF_3COOH in CH_2Cl_2, rt, 30 min then H_2, Pd/C, ethanol, 50 ^oC, 12h; (e) HATU, DIPEA, DMF, rt, 1h; (f) 95% CF_3COOH in water, rt, 2h

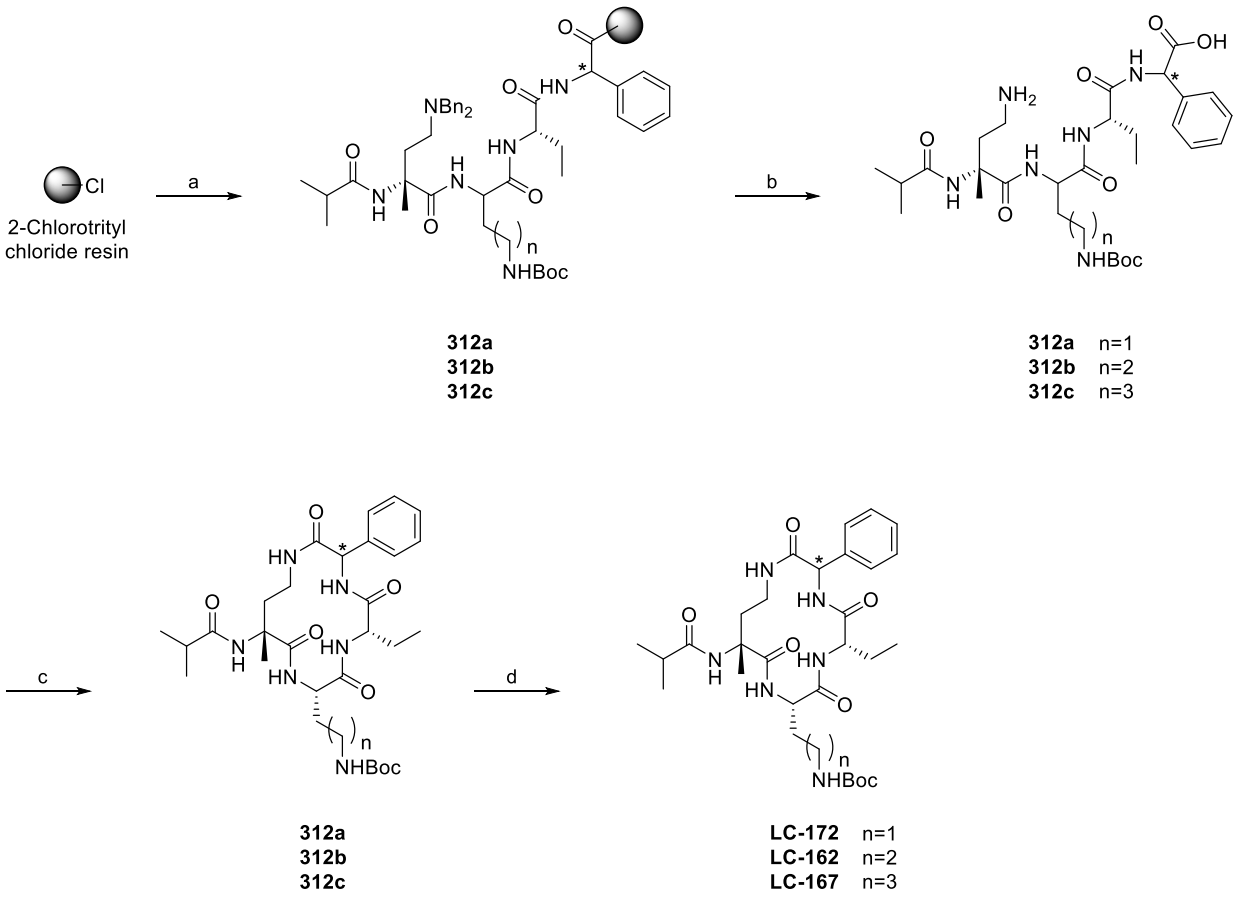

Scheme 3-5. Synthesis of **LC-172, LC-162** and **LC-167.** Reaction conditions: (a) Solid phase peptide synthesis; (b) 1% CF_3COOH in CH_2Cl_2, rt, 30 min then H_2, Pd/C, ethanol, 50 ^oC, 12h; (c) HATU, DIPEA, DMF, rt, 1h; (d) 20% CF_3COOH in in CH_2Cl_2, rt, 2h

Synthesis of the intermediates (**LC-172, LC-162, LC-167**) is shown in **Scheme 3-5**. Intermediates **312a-312d** were prepared on the 2 -chlorotrityl chloride resin using solid phase peptide synthesis with Fmoc chemistry. The intermediate peptides were cleaved from the resin followed by Benzyl protecting group removal with hydrogenation with Pd/C in ethanol, respectively, to yield peptides **313a-313d.** Intramolecular amide coupling and following removal

of Boc protecting group from L-ornithine side chain yielded cyclic peptide intermediates **LC-172, LC-162** and **LC-167**.

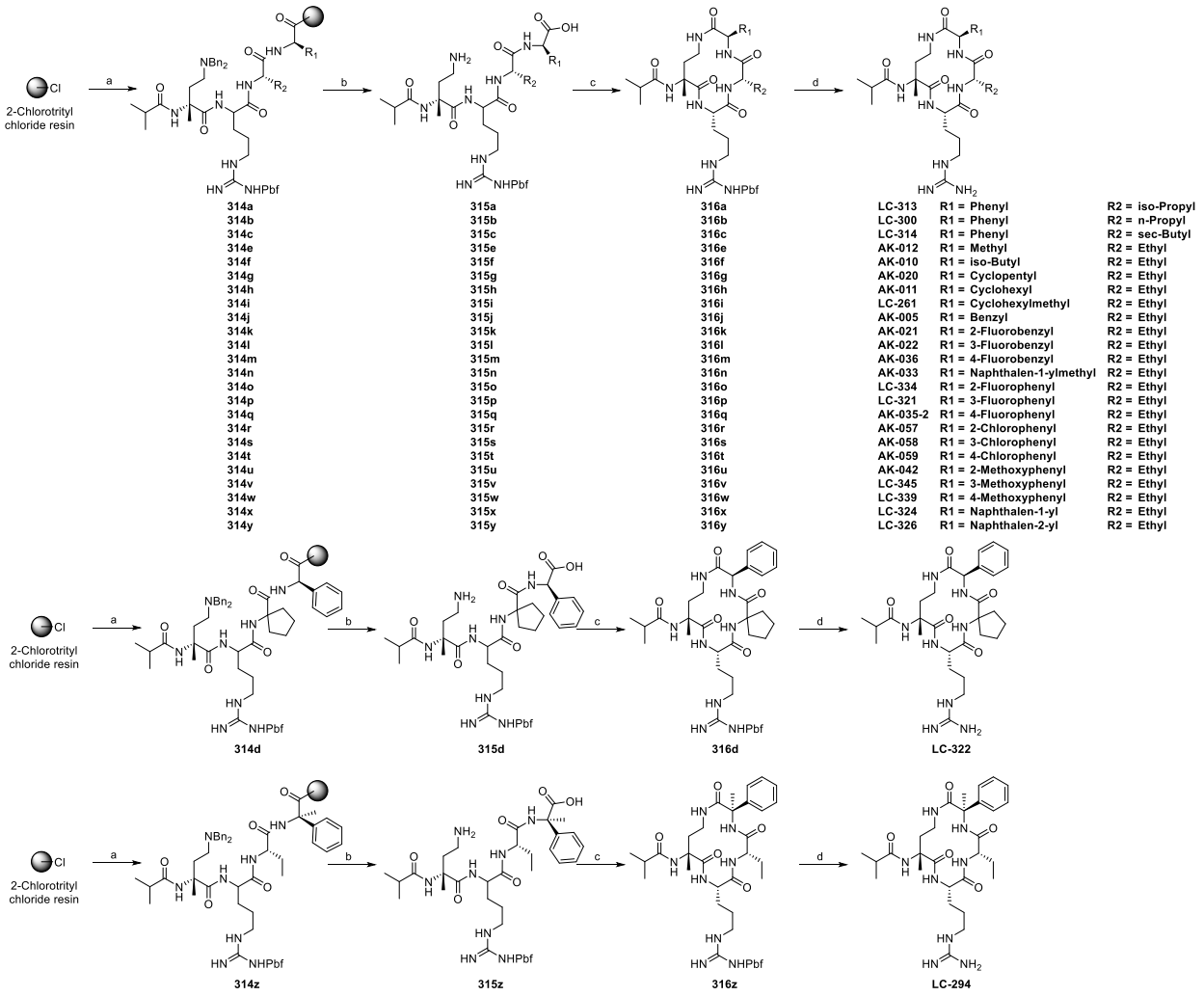

Scheme 3-6. Synthesis of **LC-313, LC-300, LC-314, AK-012, AK-010, AK-020, AK-011, LC-261, AK-005, AK-021, AK-022, AK-036, AK-033, LC-334, LC-321, AK-035-2, AK-057, AK-058, AK-059, AK-042, LC-345, LC-339, LC-324, LC-326, LC-322** and **LC-294**. Reaction conditions: (a) Solid phase peptide synthesis; (b) 1% CF_3COOH in CH_2Cl_2, rt, 30 min then H_2, Pd/C, ethanol, 50 ^oC, 12h; (c) HATU, DIPEA, DMF, rt, 1h; (d) 95% CF_3COOH in water, rt, 2h.

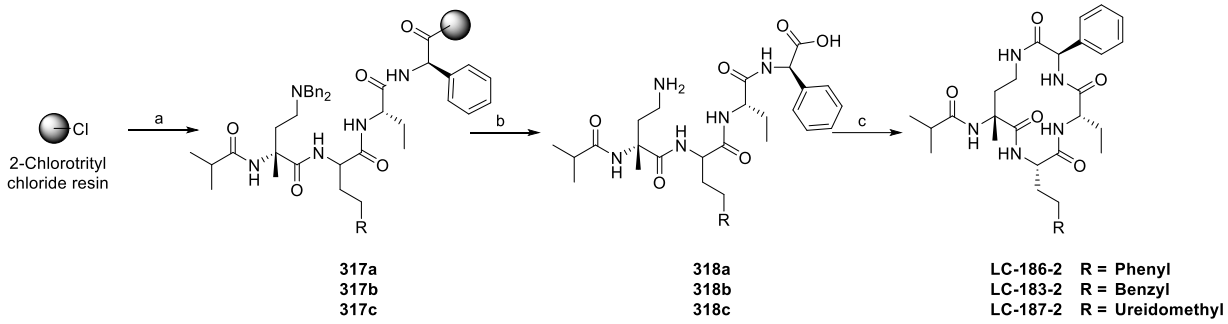

Scheme 3-7. Synthesis of **LC-186-2, LC-187-2** and **LC-183-2.** Reaction conditions: (a) Solid phase peptide synthesis; (b) 1% CF_3COOH in CH_2Cl_2, rt, 30 min then H_2, Pd/C, ethanol, 50 ^oC, 12h; (c) HATU, DIPEA, DMF, rt, 1h;

The synthesis of **AK-012 – LC-187-2** were shown in **Scheme 3-6** and **Scheme 3-7**. Different unnatural amino acids to replace Fmoc-D-Phg-OH, Fmoc-L-Abu-OH, Fmoc-L-Arg(Pbf)-OH in the original synthesis of **LC-081** were involved for the synthesis of intermediates **314a-314z** and **317a-317d,** which were prepared on the 2-chlorotrityl chloride resin using solid phase peptide synthesis with Fmoc chemistry. The intermediate peptides were cleaved from the resin followed by Benzyl protecting group removal with hydrogenation with Pd/C in ethanol, respectively, to yield peptides **315a-315z (Scheme 3-6)** and **318a-318d (Scheme 3-7)**. Intramolecular amide coupling of **315a-315z**, **318a-318d** and followed by removal of Pbf protecting group from arginine side chain yielded cyclic peptidomimetics **AK-012-LC-326** and **LC-186-2–LC-187-2**.

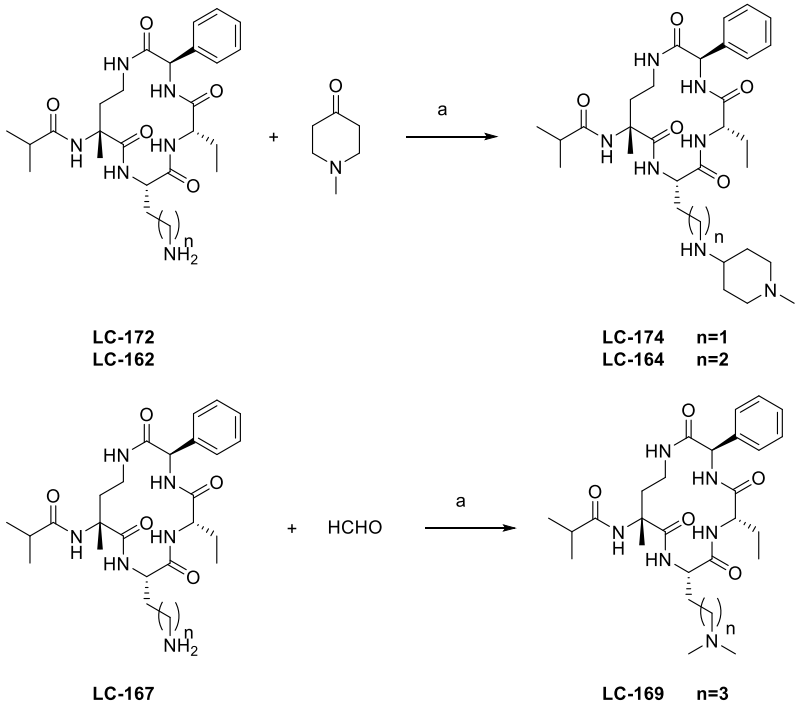

Scheme 3-8. Synthesis of **LC-174, LC-164** and **LC-169.** Reaction conditions: (a) Sodium triacetoxyborohydride, acetic acid, dichloroethane, overnight, rt.

The synthesis of **LC-169-LC-164** were shown in **Scheme 3-8** from **LC-172, LC-162** and **LC-167,** which were synthesized according to **Scheme 3-5**. **LC-169-LC-164** were synthesized with reduction amination reaction with Formaldehyde or 1-methylpiperidin-4-one.

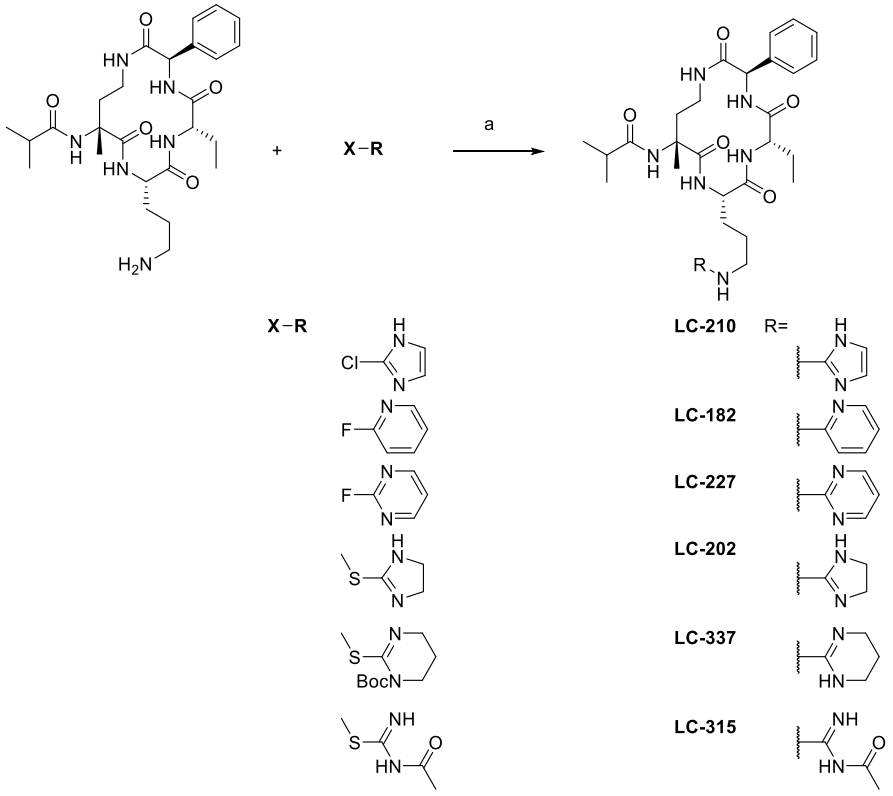

Scheme 3-9. Synthesis of **LC-210, LC-182, LC-227, LC-202, LC-337** and **LC-315.** Reaction conditions: (a) DIEA, Ethanol, 120 ^{o}C, microwave, 2h.

The synthesis of **LC-210 – LC-315** were shown in **Scheme 3-9.** The products were synthesized with a direct nucleophilic attack reaction with variety reagents under basic condition with microwave.

Summary

In this study, we describe the design, synthesis and evaluation of macrocyclic peptidomimetic inhibitors binding to WDR5 and blocking WDR5 MLL1 protein-protein interactions. Optimization of linker length and detailed SAR studies on the side chain of different amino acids were performed for these macrocyclic peptidomimetics. A number of potent and

promising macrocyclic peptidomimetics were discovered. **LC-089** potently binds to WDR5 with K_i value smaller than 1 nM and inhibits the MLL HMT activity with IC_{50} value of 12.7 nM. In cell growth inhibition assay in the MV4;11 and MOLM-13 human AML cell lines harboring MLL translocation, **LC-089** achieves IC_{50} values of 0.25 and 0.21 μM. It also displays more than 30-fold selectivity for the MV4;11 and MOLM-13 cell lines with MLL translocation over the HL-60 leukemia cell line without MLL translocation. **LC-089** also displays excellent metabolic stability in human, mouse and rat microsomes ($T_{1/2}$ > 60 min). With further SAR study, more potent compounds **LC-337** and **LC-395** were discovered with IC_{50} values of 33 nM and 38 nM in cell growth inhibition in MOLM13 cell line. In direct comparison, **LC-337** is more than 800-times more potent than **MM-401** in cell growth of MOLM-13 cell line. Collectively, our developed macrocyclic peptidomimetics are excellent agents to investigate the role of the MLL activity and the MLL-WDR5 protein-protein interaction in different biological and pathological processes. It may ultimately yield a new therapy for the treatment of human acute leukemia carrying MLL translocation. Future study on these cyclo peptidomimetic inhibitors will focus their in-vivo effects including PK/PD, efficacy and toxicity studies.

Chapter 4

Population Pharmacokinetics(PK) of Mycophenolic Acid(MPA) and its Metabolites in Liver Transplant Recipients

Introduction

Mycophenolate mofetil (MMF, CellCept, Hoffman-La Roche) is an immunosuppressant prodrug of mycophenolic acid (MPA), which is commonly used for the prophylaxis of acute allograft rejection in solid organ (kidney, liver, renal and lung) transplantation and autoimmune diseases.[121-124] MPA is a reversible inosine monophosphate dehydrogenase (IMPDH) inhibitor, which could selectively reduce guanine nucleotide synthesis. As T-cells and B-cells are more dependent on de novo synthesis of purines for their proliferation than regular cells. MPA could selectively inhibit the proliferation of lymphocytes resulting the immunosuppressing effect. MPA also could prevents antibody formation by B-lymphocytes and suppresses the glycosylation of lymphocyte and monocyte glycoproteins which is important for the intercellular adhesion to endothelial cell.[125-126]

MMF was first approval by the United States Food and Drug Administration (FDA) in 1995 for renal transplantation[127]. Currently, MMF is commonly used as maintenance

immunosuppressant for solid organ transplantation patients in combination with additional immunosuppressants, such as cyclosporine, sirolimus and tacrolimus.[124]

MMF could be rapidly and nearly completely absorbed following oral administration and hydrolyzed to the active metabolite MPA with undetectable MMF level in plasma after about 5 min. MPA is metabolized principally by UDP-glucuronosyl transferase (UGT) enzymes to form the phenolic glucuronide of MPA (MPAG) after oral dosing.[122] (**Figure 4-1**) MPAG is a stable metabolite and is not pharmacologically active. MPAG are excreted unchanged in the urine, but may undergo enterohepatic recirculation (EHR), and convert back to MPA via multidrug-resistant protein-2 (MRP-2). The EHR process of MPAG could contribute about 40% of MPA area under the concentration-time curve (AUC), which might result in multiple peaks in the plasma drug concentration-time curves of MPA.[123] MPA-acyl-glucuronide (AcMPAG) is a relative minor, but active metabolite. AcMPAG has been demonstrated that some independent mechanism from major MPA action, which is associated with inosine monophosphate dehydrogenase inhibition.[128] It has been speculated that AcMPAG could exert an antiproliferative effect and inhibit proliferation of human mononuclear leukocytes via a mechanism independent of guanosine triphosphate (GTP) depletion. Either MAPG or AcMPAG might be linked to side effects of MMF. In addition, unlike population PK models of MPA with renal transplantation patients, the population PK models with liver transplantation patients are quite limited, especially for the model with metabolites.[124, 129-130] And Therefore, a better understanding of the PK of MPA, MPAG and AcMPAG is needed considering its contributions to the systemic exposure and gastrointestinal toxicity of MPA.

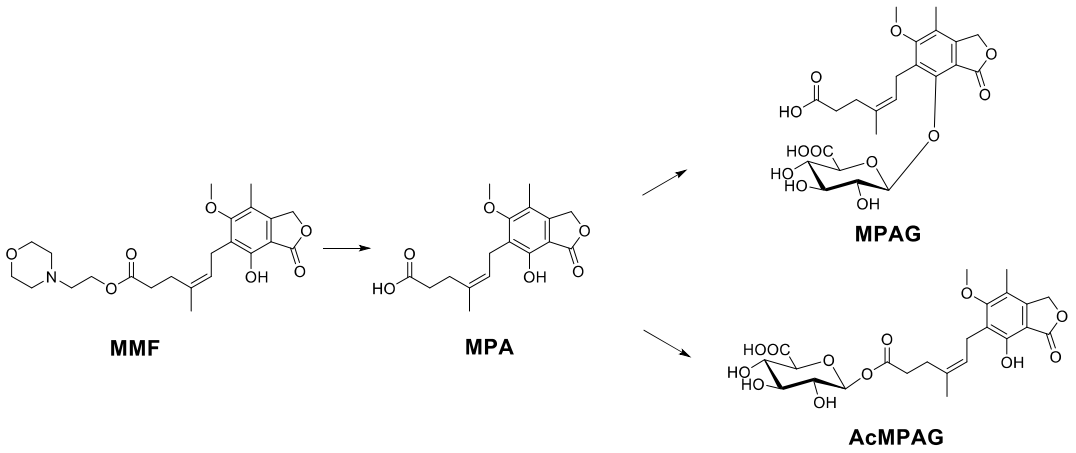

Figure 4-1. Hydrolyzation of MMF to MPA and metabolized to MAPG and AcMPAG.

The purpose of this work was to characterize the population PK of MPA and its metabolites MPAG and AcMPAG in adult Chinese liver transplant recipients following repeated oral administration of the prodrug MMF. And a good description of the metabolites of MPA may provide a useful tool future dose selection and in predicting some MPA-related side effects.

Method

Sixty-four adult patients (52 males, 12 females) received liver transplantation at Organ Transplantation Center in Ruijin Hospital were recruited. The study protocol was approved by the regional ethics committee (Ruijin Hospital, Shanghai Jiao Tong University School of Medicine) and performed in accordance with the Declaration of Helsinki and Chinese guidelines for good clinical practice. All the patients gave informed consent before inclusion. The demographic and pathophysiological data were collected retrospectively.

All patients received immunosuppressive therapy consisting of MMF, tacrolimus, and corticosteroids. 1g of MMF was given within 6h before liver transplantation. After transplantation, dosage of MMF was adjusted according to the occurrence of side effects. 1g Bid, 0.75g Bid and 0.5g Bid were given to 54, 8 and 2 patients, respectively. Tacrolimus was given as an oral dose of 0.1 mg/kg per day initially, and then adjusted to achieve a steady-state trough concentration of 10-15 ng/ml in the first week after the start of therapy and 5-10 ng/ml thereafter. Five hundred milligram of methylprednisolone was injected during a hepatic period and tapered after operation. After 7 days therapy, prednisone was used at a dosage of 20 mg daily, and then further tapered according to the protocol. All concomitant medications were recorded for each patient. Blood samples were collected at 0- 12 h after MMF administration after 7-30 days MMF oral administration. The plasma concentration of MPA and its metabolites was determined by HPLC assay we established.

Table 4-1. Clinical data summary of liver transplantation recipients

Characters (Unit)	Means ± SD (Range)
Age (yrs)	48.8±12.4 (14~76)
Gender	Male: 52; Famale: 12
weight (kg)	66.1±18.0 (37~87)
height (cm)	169.5±5.0 (158~182)
Time interval (days)	8.2±2.1 (7~15)
Total bilirubin (TBIL) (μmol/L)	72.7±62.7 (21.1~282.1)
Direct bilirubin (DBIL) (μmol/L)	38.8±38.4 (3.9~144.5)
Albumin (g/L)	35.1±5.2 (23~46)
Creatinine (μmol/L)	70.7±24.8 (37~181)
Creatinine clearance (ClCr) (ml/min)	108.4±43.4 (32.4~244.9)
White Blood Cells count (WBC) ($\times 10^9$/L)	7.98±3.71 (2.6~19.9)
Red Blood Cells count (RBC) ($\times 10^{12}$/L)	3.44±0.60 (2.4~5.0)
Platelet (PLT) ($\times 10^9$/L)	102.5±61.0 (10~249)

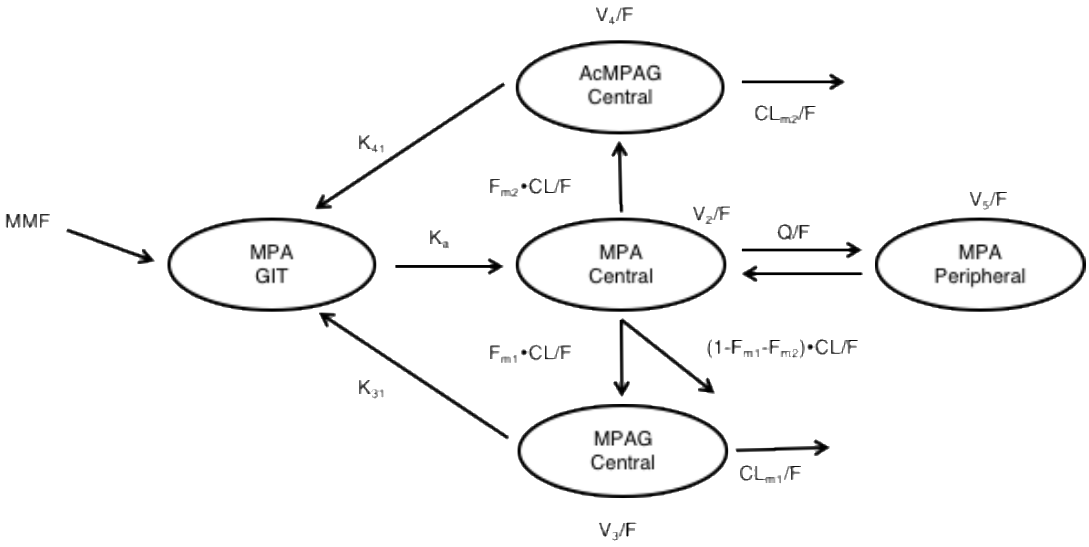

Figure 4-2. Population pharmacokinetic model of MPA, MPAG and AcMPAG. CL/F, CL_{m1}/F and CL_{m2}/F are the apparent clearance of MPA, MPAG and AcMPAG; V_2/F and V_5/F are apparent volume of distribution of MPA in central and peripheral compartments; V_3/F and V_4/F are the apparent volume of distribution of MPAG and AcMPAG; Q/F is apparent compartmental clearance between the MPA central and peripheral compartments; K_a is the absorption rate constant of MPA; F_{m1} and F_{m2} are the fraction of MPA metabolized to MPAG and AcMPAG; K_{31} and K_{41} are the rate constant for biliary excretion and enterohepatic recycling of MPAG and AcMPAG.

The population PK model with simultaneous modelling of MPA, MPAG and AcMPAG was developed with nonlinear mixed effects modeling (NONMEM) using the iterative two-stage (ITS) method, followed by the stochastic approximation expectation maximization (SAEM) method, followed by Monte Carlo importance sampling (IMP) method. Model development was guided by the likelihood ratio test using objective function values (OFV), graphical goodness-of-fit, and visual predictive check.

MPA, MPAG and AcMPAG plasma concentration-time data, after MMF oral administration, were adequately described by a 5-compartment model. The absorption of MPA from the gastrointestinal tract (GIT), central and peripheral compartments for MPA disposition, and the formation, EHR and elimination of MPA, MPAG and AcMPAG was assumed to follow first-order kinetic. The conversion from MMF to MPA was assumed to be rapid and complete prior to reaching the systemic circulation. The fractions of MPA metabolized to MPAG and AcMPAG were

assumed to be fixed 90% and 10% based on literature information[131-133], which indicates that clearance of MPA through MPAG and AcMPAG.

Inter-individual variability (IIV) of the PK parameters was assumed to follow a log-normal distribution and described by an exponential error model (1)with following equations

$$P_i = \theta * \exp(\eta_i) \quad (1)$$

where P_i is the parameter estimate for ith individual, θ is the typical individual and η_i is the IIV. Additive (2), proportional (3) and mixed (4) error models were evaluated for the residual unexplained variability using the following equations:

$$Y = IPRED + \varepsilon \quad (2)$$

$$Y = IPRED \times (1 + \varepsilon) \quad (3)$$

$$Y = IPRED \times (1 + \varepsilon_1) + \varepsilon_2 \quad (4)$$

where Y is the observed concentration, F is the individual prediction and ε is the residual variability. IIVs, residual errors were included in the model only if they were associated with a decrease in OFV by at least 3.84.

The final PK model was evaluated with visual predictive checks. Posterior prediction was obtained with 1000 simulation cooperating with the parameters' uncertainties from the final model. The 95% prediction intervals for the simulated median, 5th and 95th percentiles were calculated and compared with the observed data points of MPA, MPAG and AcMPAG, respectively.

Results and Discussion

Plasma MPA, MPAG and AcMPAG concentration-time profiles were described by the compartmental model shown in **Figure 4-2.** Proportional error model was selected as the final model for the residual unexplained variability.

The model estimated population means of the absorption rate constant K_a (0.93 h^{-1}), apparent clearance CL/F (18.1 L/hr), volumes of distribution (central compartment: V_2/F = 71.7 L, peripheral compartment: M_5/F = 2111 L), and intercompartmental clearance (Q = 28.4 L/hr) are shown in **Table 4-2**. Comparing with a previously published two compartment-model of MPA[129], the apparent clearance CL/F and intercompartmental clearance are higher than the two-compartment model (CL/F = 17.4 L/hr, Q= 21.7 L/hr). It could be explained by the following equation:

$$CL/F = \frac{Dose}{F*AUC} \quad (5)$$

With the same AUC value, EHR of MPAG is equivalent to add extra dose to the system which can increase CL/F and Q.

The apparent elimination clearance and volumes of distribution of the metabolites MPAG and AcMPAG are quantified (CL_{m1}/F = 1.2 L/hr, CL_{m2}/F = 4.8 L/hr, V_3/F = 19.9 L and V_4/F = 90.9 L respectively). The estimated rate constant describing the EHR of MPAG (K_{31}) and AcMPAG (K_{41}) are 2.3 * 10^{-5} and 0.024 h^{-1}. (**Table 4-2**.) The relative small K_{31} value probably is caused by the liver or renal functions in patients, which could not be evaluated in current model. The IIVs of

these parameter estimates are large which is consistent with literature.[134] The values of percentiles of RSE are acceptable except for CL_{m1}/F, which is close to 40%.

Table 4-2. Population PK parameter estimates for MPA, MPAG and AcMPAG.

Parameter	Estimate (%RSE)	IIV %CV (%RSE)
CL/F (L/hr)	18.1(2)	45.8(23)
CL_{m1}/F (L/hr)	1.2(37)	61.6(17)
CL_{m2}/F (L/hr)	4.8(10)	68(31)
V_2/F (L)	71.7(3)	88.7(40)
V_3/F (L)	19.1(7)	151.8(21)
V_4/F (L)	90.9(6)	187(34)
V_5/F (L)	2111(4)	94.8(27)
Q (L/hr)	28.4(5)	87.8(62)
K_a (1/hr)	0.93(8)	-
K_{31} (1/hr)	$2.3 * 10^{-5}$(0.02)	-
K_{41} (1/hr)	0.024(0.1)	-
Proportional residual error		
MPA	0.7(5)	
MPAG	0.42(4)	
AcMPAG	0.58(5)	

For model diagnosis, the population and individual predictions well follow the trend of the data, as it's shown in **Figure 4-3A.** No significant trend was observed in the conditional weighted residuals vs population predictions and time after last dose plots. (**Figure 4-3B**). As shown in the visual predicted check plots (**Figure 4-3C**), the trend is consistent to the observed data of MPA, MPAG and AcMPAG, but the coverage between 5^{th} and 95^{th} percentile of the 1000 simulated data suggests slightly over prediction of data variation, especially for the two metabolites MPAG and AcMPAG.

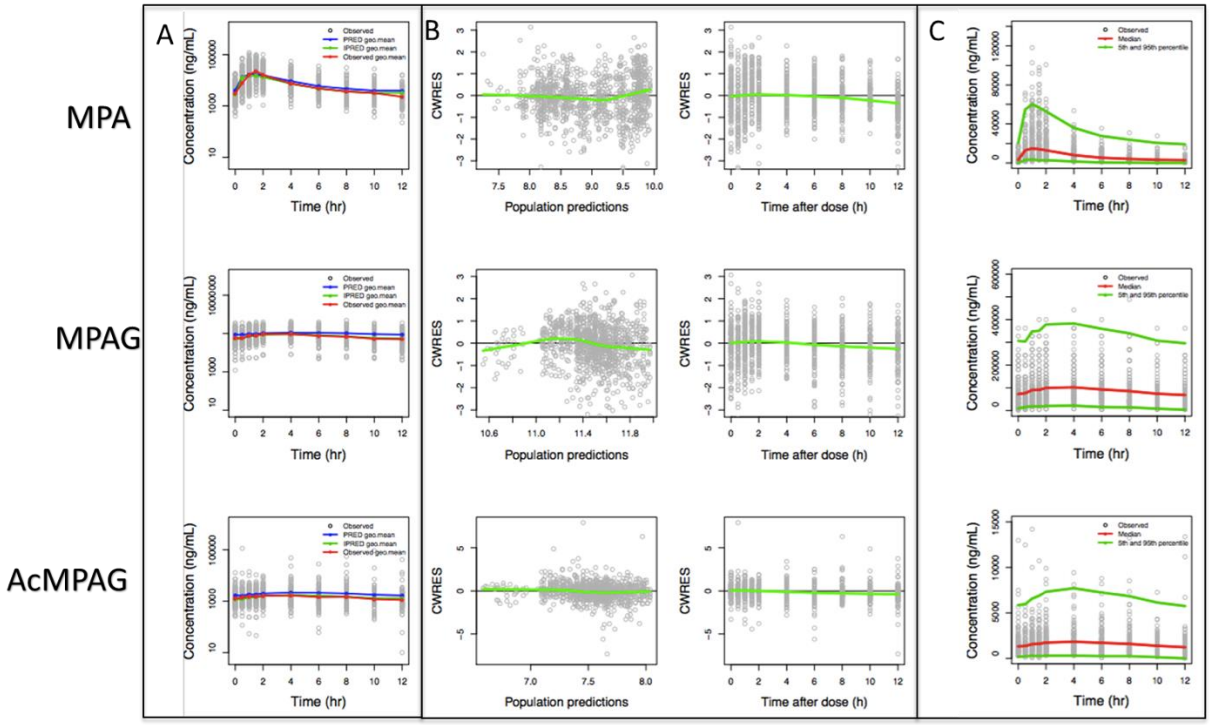

Figure 4-3. (A) & (B) Basic goodness-of-fit plots of population PK parameters. (C) Visual predictive check of final model.

Summary

The population PK model developed from our study successfully characterized the absorption, distribution, and elimination of MPA and its major metabolites in liver transplant recipients. A good description of the metabolites of MPA may provide a useful tool in predicting some MPA-related side effects. In the futures, covariate analysis with patient's gender, body weights, age, renal and liver functions could be done with current model.

Chapter 5

General Discussion

Design of PROTACs

A set of PROTACs were developed from the previously reports with different E3 ubiquitin ligase ligands. The PTORACs could simultaneously bind to the target proteins and E3 ubiquitin ligases causing target protein ubiquitination and degradation. The ubiquitination pathway includes three enzymes: an E1-activating enzyme, an E2-conjugating enzyme, and an E3 ligase, which needs to be activated sequentially.[135] E2-conjugating enzyme prepares ubiquitin for conjugation, while the E3 ligase recognizes the substrate protein and catalyzes the transfer of activated ubiquitin to it. Cullin E3 ubiquitin ligases are responsible for about 20% of the protein ubiquitination in cells. It contains a Cullin protein as a scaffold, a RING finger protein to recruit E2 enzyme with ubiquitin and a substrate receptor to recruit substrate protein. Substrate protein with ubiquitin tag is then recognized by the 26S proteasome, a very large multi-catalytic protease complex, then degraded to small peptides pieces.

Although PROTACs could successfully cause target protein degradation and some of them are much more efficient than the corresponding inhibitors, how to choose E3 ligase ligand is still

unclear for the design of efficient PROTACs. Currently the most efficient PROTACs were designed to recruit the Cul4A/B-DDB1-Cereblon E3 ubiquitin ligase complex and Cul2-Rbx1-EloBC-VHL ubiquitin ligase complex. In these PROTACs, the E3 ligase ligand could bind to cereblon or VHL-1 which are both the substrate receptors in the E3 ligase complex. Comparing them with PROTACs recruiting IAPs or MDM2, PROTACs recruiting Cullin E3 ligase can cause target protein degradation with much lower concentration treatment in cells. MDM2 PROTAC **LE-004** and BRD4 PROTAC **BETd-260** recruiting cereblon could cause MDM2 or BRD4 protein degradation with lower than 1 nM.[50] While AR PROTAC recruiting MDM2 could cause AR protein degradation with 10 μM treatments.[44] These results suggested that small molecule ligand targeting the substrate receptor of Cullin E3 ligase can be good choice for the design of successful PROTACs. Other important properties of PROTACs are the cell permeability, solubility, stability and PK properties. As both target protein and E3 ligase ligands are difficult to modify, more effort to improve these properties will focus on the modification of linkers. From our study, rigid and hydrophobic linker can improve the in-vivo PK properties. But these linkers may cause solubility problems. Development of novel hydrophilic rigid linker might further improve effects of PROTACs.

Evaluation of PROTACs

From our study of MDM2 PROTACs and the molecular glue causing GSPT-1 degradation, detailed evaluation of these bifunctional molecules is important for the development of PROTACs. The evaluation of PROTACs needs to two questions: confirmation of the biological effect; comparing the potencies for further modification. To solve these questions, the following assay is important for the evaluation of PROTACs.

1. Western Blot and qPCR for the target protein:

To confirm the biological effect of the designed PROTACs, western blot and qPCR assay are most important and direct evidence to confirm the degradation of target proteins. If the western blot indicates that target protein expression level is decreased and at the same time qPCR assay has confirmed the mRNA expression level of target protein does not change or increases, the PROTACs probably can cause the target protein degradation.

2. Proteomics Study

From our study of molecular glue LD-277 and the study from Bradner Group, bifunction molecules designed with lenalidomide and its derivatives can cause GSPT-1 degradation. It results un expected cell growth inhibition activities comparing with bona fide MDM2 degraders and inhibitors. Carefully evaluation of degradation events with proteomic study is important to figure out unpredictable effects. It is also significant to figure out off-target side effects for the future application.

3. Competition Study

Competition study is very useful to confirm the supposed mechanisms for the target protein degradation. If pretreatment of excess of target protein or E3 ligase ligands can block the protein degradation caused by the PROTACs, it indicates both interactions between target protein-PROTACs and E3 ligase-PROTACs are important for protein degradation. Besides the competition study with protein degradation, it could also be used for in-vitro efficiency assay, for

example, cell growth inhibition assay. Competition of excess target protein or E3 ligase ligands should also block the cell activities of PROTACs.

4. Cotreatment of Proteasome inhibitors

PROTACs can promote the ubiquitination of target proteins and increase its proteasome degradation. Cotreatment of proteasome inhibitors, such as MG-132 should significantly block the target protein degradation. But it might not be useful in certain cases. In p53 wildtype cell lines, MDM2 protein, as an E3 ligase, can ubiquitinate p53 protein and cause p53 protein degradation. Treatment of MDM2 PROTACs can cause MDM2 protein degradation and accumulation of p53. With feedback loop, activation of p53 can also increase the MDM2 protein expression level. While treatment of proteasome inhibitor MG-132 can efficiently block the degradation of p53, which can activate p53 and increase expression of MDM2. So cotreatment of proteasome inhibitor with MDM2 PROTACs could not give direct evidence about the blockage of protein degradation.

5. Cell growth inhibition evaluation

Currently, most of PROTACs developments are in the field of oncology. And then cell growth inhibition assay is an important method for the evaluation of PROTAC modification. Two important factors might affect the cell growth inhibition activities of PROTACs. The binding affinity to the target protein and E3 ligase of PROTACs is critical for the design of PROTACs. From our study of MDM2 PROTACs, the binding affinity of MDM2 inhibitor moiety is important for the cell anti-proliferation activity of PROTACs. PROTACs synthesized with MDM2 inhibitor with Kd

value higher than 200 nM to MDM2 failed to cause significant MDM2 degradation up to 3 □M. And the cell growth inhibition activity is also weaker than the corresponding MDM2 inhibitors. But PROTACs synthesized with MDM2 inhibitor with Kd value lower than 100 nM to MDM2 are much more potent their MDM2 inhibitors. So the binding affinity to target protein can significantly affect the cellular potency of PROTACs. Another important factor for cell growth inhibition activity is the cell permeability. Even currently most of the PROTACs are designed with small molecule ligands, the molecular weight is still around 1000 Da. Cell permeability might be poor for PROTACs with such high molecular weight. So cell permeability assay on PROTACs could bring us better understanding on the modification and mechanism of PROTACs.

6 In-vivo PK/PD, toxicity and efficacy studies

In-vitro assay on PROTACs can bring us clear mechanism of it in cell and also guide us for the chemical modification. But the significance of these results might be limited as the environment in body is quite different from in-vitro. In-vivo assay is important for the further application of PROTACs in drug development field. PK/PD and toxicity studies on our MDM2 PROTACs helped us to decide the efficient administration method and doses. Although PK data has shown the concentration of MDM2 PROTACs in tumor is lower than plasma, it's still much higher than the concentration required for MDM@ degradation in-vitro. Efficient MDM2 degradation was also obtained from the PD study. Efficacy studies then helped us to confirm the antitumor activities of our MDM2 PROTACs comparing with their MDM2 inhibitors. MDM2 PROTACs is much more potent than their inhibitors in xenograft tumor mice models.

Future Perspectives

Recently, PROTACs have become an important and popular area in drug discovery. While the development of PROTACs are still focused on preclinical stage. Further advanced evaluation in clinical studies are the main next stage for PROTACs. Another important future direction for PROTACs is to further explore its application for other protein targets. Although enormous effort has been spent in the field of drug discovery, only 2% of human proteins are the targets for current approved drugs. It's also estimated that only 1-2 % of disease modified proteins are likely to be druggable with inhibitors, which means most of the disease related protein could not be targeted by direct interaction with proteins.[136] While PROTACs offers the potential of reaching beyond the limitations of the current pharmaceutical and expand the druggable targets by inducing target protein degradation.

APPENDIX

Experimental Section

General

Unless otherwise noted, all purchased reagents were used as received without further purification. ^{1}H NMR and ^{13}C NMR spectra were recorded on a Bruker Advance 400 MHz spectrometer. ^{1}H NMR spectra were reported in parts per million (ppm) downfield from tetramethylsilane (TMS). All ^{13}C NMR spectra were reported in ppm and obtained with ^{1}H decoupling. In reported spectral data, the format (δ) chemical shift (multiplicity, *J* values in Hz, integration) was used with the following abbreviations: s = singlet, d = doublet, t = triplet, q = quartet, m = multiplet. MS analyses were carried out with a Waters UPLC–mass spectrometer. The final compounds were all purified by C18 reverse phase preparative HPLC column with solvent A (0.1% TFA in H_2O) and solvent B (0.1% TFA in MeCN) as eluents. The purity of all the final compounds was confirmed to be >95% purity by UPLC–MS or UPLC.

(3'R,4'S,5'R)-6''-chloro-4'-(3-chloro-2-fluorophenyl)-N-(4-((2-((2-(2,6-dioxopiperidin-3-yl)-1,3-dioxoisoindolin-4-yl)amino)ethyl)carbamoyl)phenyl)-2''-oxodispiro[cyclohexane-1,2'-pyrrolidine-3',3''-indoline]-5'-carboxamide (LD-117)

LD-117 (10.9 mg, Yield: 43% from **MI-1061**) was obtained as yellow powder using the same synthetic strategy described for **LD-074**.

LC-MS(ESI) m/z $(M+H)^+$: 880.21; calcd for $C_{45}H_{41}Cl_2FN_7O_7$ $(M+H)^+$: 880.24; >98% purity.

^{1}H NMR (400 MHz, Methanol-d_4) δ 7.85 – 7.75 (m, 2H), 7.74 – 7.61 (m, 3H), 7.53 (dd, *J* = 8.6, 7.1 Hz, 1H), 7.45 (dd, *J* = 8.2, 2.4 Hz, 1H), 7.25 (t, *J* = 7.4 Hz, 1H), 7.19 (d, *J* = 8.5 Hz, 1H), 7.13 – 6.98 (m, 3H), 6.74 (d, *J* = 2.0 Hz, 1H), 5.05 (dd, *J* = 12.4, 5.5 Hz, 1H), 4.83 – 4.63 (m, 2H), 3.69 – 3.52 (m, 4H), 2.93 – 2.59 (m, 4H), 2.25 – 1.90 (m, 5H), 1.79 – 1.71 (m, 2H), 1.62 – 1.59 (m, 1H), 1.15 – 0.99 (m, 2H).

(3'R,4'S,5'R)-6''-chloro-4'-(3-chloro-2-fluorophenyl)-N-(4-((3-((2-(2,6-dioxopiperidin-3-yl)-1,3-dioxoisoindolin-4-yl)amino)propyl)carbamoyl)phenyl)-2''-oxodispiro[cyclohexane-1,2'-pyrrolidine-3',3''-indoline]-5'-carboxamide (LD-270)

LD-270 (10.9 mg, Yield: 69% from **MI-1061**) was obtained as yellow powder using the same synthetic strategy described for **LD-074**.

LC-MS(ESI) m/z $(M+H)^+$: 894.24; calcd for $C_{46}H_{43}Cl_2FN_7O_7$ $(M+H)^+$: 894.26; >98% purity.

^{1}H NMR (400 MHz, Methanol-d_4) δ 7.87 – 7.74 (m, 2H), 7.72 (t, *J* = 7.4 Hz, 1H), 7.67 – 7.57 (m, 2H), 7.58 – 7.44 (m, 2H), 7.37 (t, *J* = 7.6 Hz, 1H), 7.18 (t, *J* = 8.0 Hz, 1H), 7.12 (dd, *J* = 8.2, 2.0 Hz, 1H), 7.08 – 6.94 (m, 2H), 6.79 (d, *J* = 2.0 Hz, 1H), 5.31 (d, *J* = 10.8 Hz, 2H), 5.07 – 4.93 (m, 2H), 3.55 – 3.37 (m, 5H), 2.93 – 2.77 (m, 3H), 2.78 – 2.60 (m, 1H), 2.24 – 2.13 (m, 1H), 2.12 – 2.01 (m, 1H), 2.03 – 1.90 (m, 5H), 1.84 – 1.71 (m, 3H), 1.54 (d, *J* = 14.0 Hz, 1H), 1.26 (d, *J* = 21.4 Hz, 2H).

(3'R,4'S,5'R)-6''-chloro-4'-(3-chloro-2-fluorophenyl)-N-(4-((4-((2-(2,6-dioxopiperidin-3-yl)-1,3-dioxoisoindolin-4-yl)amino)butyl)carbamoyl)phenyl)-2''-oxodispiro[cyclohexane-1,2'-pyrrolidine-3',3''-indoline]-5'-carboxamide (LD-074)

Reaction 1:

2-(2,6-dioxopiperidin-3-yl)-4-fluoroisoindoline-1,3-dione (200 mg, 0.73 mmol) was added to a solution of tert-butyl (4-aminobutyl)carbamate (207mg, 1.1 mmol) and DIEA (0.6 mL, 4 mmol) in DMF (2 mL). The reaction was heated to 90 ^{o}C for 12h. Then the mixture was cooled to room temperature and load on the celite. The crude residue was purified by reverse phase C18 column to afford tert-butyl (4-((2-(2,6-dioxopiperidin-3-yl)-1,3-dioxoisoindolin-4-yl)amino)butyl)carbamate without further purification. The product was then dissolved in 5 mL DCM and 1 mL trifluoroacetic acid was added to the reaction. The reaction was stirred for 2 h at room temperature until there is no starting material detected by HPLC. The solvent was removed to yield **101c** (107mg, Yield: 43%) as yellow solid.

Reaction 2:

HATU (13.3 mg, 1.2 eq.) and N,N-Diisopropylethylamine (0.026 mL, 0.15 mmol) were added to a solution of **MI-1061** (20 mg, 0.029 mmol) in 0.5 mL DMF and stirred. After 10 minutes, **101c** (0.35 mL, 0.1 M in DMSO) was added to the reaction. After 30 minutes, the solvent was removed and the crude was dissolved in 3:1 methanol/water, acidified with trifluoroacetic acid and purified by reverse-phase preparative HPLC. The purified fractions were combined, concentrated in vacuo, re-dissolved in H2O, frozen and lyophilized to give **LD-074** (18.5 mg, Yield: 71%) as a yellow powder.

LD-074 was obtained using the same synthetic strategy described for **LD-072**.

LC-MS(ESI) m/z $(M+H)^{+}$: 908.32; calcd for C47H45Cl2FN7O7 $(M+H)^{+}$: 908.27; >98% purity.

^{1}H NMR (400 MHz, MeOD) δ 7.79 – 7.68 (m, 3H), 7.63 – 7.58 (m, 2H), 7.53 (dd, *J* = 8.3, 2.4 Hz, 1H), 7.49 (ddd, *J* = 8.5, 7.1, 1.4 Hz, 1H), 7.39 – 7.32 (m, 1H), 7.17 (t, *J* = 8.1 Hz, 1H), 7.11 (dd, *J* = 8.2, 2.0 Hz, 1H), 7.02 (d, *J* = 8.6 Hz, 1H), 6.98 (dd, *J* = 6.8, 2.8 Hz, 1H), 6.79 (d, *J* = 1.9 Hz, 1H), 5.30 (d, *J* = 10.7 Hz, 1H), 5.03 (dd, *J* = 12.6, 5.5 Hz, 1H), 4.96 (d, *J* = 10.8 Hz, 1H), 3.44 – 3.34 (m, 4H), 2.92 – 2.79 (m, 2H), 2.78 – 2.65 (m, 2H), 2.17 (d, *J* = 14.1 Hz, 1H), 2.13 – 2.05 (m, 1H), 2.02 – 1.87 (m, 3H), 1.81 – 1.69 (m, 6H), 1.62 – 1.48 (m, 1H), 1.27 – 1.16 (m, 2H).

(3'R,4'S,5'R)-6''-chloro-4'-(3-chloro-2-fluorophenyl)-N-(4-((5-((2-(2,6-dioxopiperidin-3-yl)-1,3-dioxoisoindolin-4-yl)amino)pentyl)carbamoyl)phenyl)-2''-oxodispiro[cyclohexane-1,2'-pyrrolidine-3',3''-indoline]-5'-carboxamide (LD-252)

LD-252 (8.6 mg, Yield: 33% from **MI-1061**) was obtained as yellow powder using the same synthetic strategy described for **LD-074**.

LC-MS(ESI) m/z $(M+H)^+$: 922.30; calcd for $C_{48}H_{47}Cl_2FN_7O_7$ $(M+H)^+$: 922.29; >98% purity.

^{1}H NMR (400 MHz, MeOD) δ 7.79 – 7.67 (m, 3H), 7.63 – 7.57 (m, 2H), 7.57 – 7.46 (m, 2H), 7.37 – 7.30 (m, 1H), 7.16 (t, *J* = 7.9 Hz, 1H), 7.10 (dd, *J* = 8.2, 1.9 Hz, 1H), 7.02 (d, *J* = 8.6 Hz, 1H), 6.98 (dd, *J* = 6.7, 4.1 Hz, 1H), 6.78 (d, *J* = 1.9 Hz, 1H), 5.22 (d, *J* = 9.8 Hz, 1H), 5.04 – 4.98 (m, 1H), 4.95 (dd, *J* = 10.6, 2.9 Hz, 1H), 3.41 – 3.33 (m, 4H), 2.90 – 2.61 (m, 4H), 2.17 – 2.04 (m, 2H), 1.97 – 1.82 (m, 3H), 1.78 – 1.49 (m, 9H), 1.24 – 1.13 (m, 2H).

(3'R,4'S,5'R)-6''-chloro-4'-(3-chloro-2-fluorophenyl)-N-(4-((6-((2-(2,6-dioxopiperidin-3-yl)-1,3-dioxoisoindolin-4-yl)amino)hexyl)carbamoyl)phenyl)-2''-oxodispiro[cyclohexane-1,2'-pyrrolidine-3',3''-indoline]-5'-carboxamide (LD-091)

LD-091 (14.3 mg, Yield: 53% from **MI-1061**) was obtained as yellow powder using the same synthetic strategy described for **LD-074**.

LC-MS(ESI) m/z $(M+H)^+$: 936.27; calcd for $C_{49}H_{49}Cl_2FN_7O_7$ $(M+H)^+$: 936.31; >98% purity.

^{1}H NMR (400 MHz, MeOD) δ 7.76 (d, *J* = 8.7 Hz, 2H), 7.71 (t, *J* = 6.7 Hz, 1H), 7.60 (d, *J* = 8.7 Hz, 2H), 7.56 – 7.47 (m, 2H), 7.36 (t, *J* = 7.0 Hz, 1H), 7.18 (t, *J* = 8.0 Hz, 1H), 7.11 (dd, *J* = 8.2, 1.9 Hz, 1H), 7.02 – 6.97 (m, 2H), 6.79 (d, *J* = 1.9 Hz, 1H), 5.33 (d, *J* = 10.9 Hz, 1H), 5.03 (dd, *J* = 12.4, 5.3 Hz, 1H), 4.97 (d, *J* = 10.9 Hz, 1H), 3.40 – 3.27 (m, 4H), 2.93 – 2.65 (m, 4H), 2.19 (d, *J* = 11.6 Hz, 1H), 2.15 – 2.06 (m, 1H), 2.04 – 1.89 (m, 3H), 1.78 (d, *J* = 11.8 Hz, 2H), 1.71 – 1.59 (m, 4H), 1.55 – 1.38 (m, 5H), 1.27 – 1.18 (m, 2H).

(3'R,4'S,5'R)-6''-chloro-4'-(3-chloro-2-fluorophenyl)-N-(4-((7-((2-(2,6-dioxopiperidin-3-yl)-1,3-dioxoisoindolin-4-yl)amino)heptyl)carbamoyl)phenyl)-2''-oxodispiro[cyclohexane-1,2'-pyrrolidine-3',3''-indoline]-5'-carboxamide (LD-251)

LD-251 (16.3 mg, Yield: 60% from **MI-1061**) was obtained as yellow powder using the same synthetic strategy described for **LD-074**.

LC-MS(ESI) m/z $(M+H)^+$: 950.29; calcd for $C_{50}H_{51}Cl_2FN_7O_7$ $(M+H)^+$: 950.32; >98% purity.

^{1}H NMR (400 MHz, MeOD) δ 7.80 – 7.74 (m, 2H), 7.74 – 7.68 (m, 1H), 7.64 – 7.59 (m, 2H), 7.55 – 7.47 (m, 2H), 7.37 – 7.30 (m, 1H), 7.16 (t, *J* = 8.1 Hz, 1H), 7.10 (dd, *J* = 8.2, 1.9 Hz, 1H), 7.01 (s, 1H), 6.99 (d, *J* = 2.2 Hz, 1H), 6.79 (d, *J* = 1.9 Hz, 1H), 5.27 (d, *J* = 10.6 Hz, 1H), 5.03 (dd, *J* = 12.6, 5.4 Hz,

1H), 4.95 (d, *J* = 10.7 Hz, 1H), 3.38 – 3.27 (m, 4H), 2.90 – 2.64 (m, 4H), 2.20 – 2.05 (m, 2H), 2.00 – 1.84 (m, 3H), 1.83 – 1.71 (m, 2H), 1.67 – 1.53 (m, 5H), 1.46 – 1.35 (m, 6H), 1.25 – 1.13 (m, 2H).

(3'R,4'S,5'R)-6''-chloro-4'-(3-chloro-2-fluorophenyl)-N-(4-((2-(2-((2-(2,6-dioxopiperidin-3-yl)-1,3-dioxoisoindolin-4-yl)amino)ethoxy)ethyl)carbamoyl)phenyl)-2''-oxodispiro[cyclohexane-1,2'-pyrrolidine-3',3''-indoline]-5'-carboxamide (LD-111)

LD-111 (15.9 mg, Yield: 60% from **MI-1061**) was obtained as yellow powder using the same synthetic strategy described for **LD-074**.

LC-MS(ESI) m/z $(M+H)^+$: 924.20; calcd for $C_{47}H_{45}Cl_2FN_7O_8$ $(M+H)^+$: 924.27; >98% purity.

^{1}H NMR (400 MHz, MeOD) δ 7.76 – 7.68 (m, 3H), 7.61 – 7.51 (m, 3H), 7.47 – 7.39 (m, 1H), 7.35 (t, *J* = 7.6 Hz, 1H), 7.19 (t, *J* = 8.1 Hz, 1H), 7.11 (dd, *J* = 8.2, 0.9 Hz, 1H), 7.01 (d, *J* = 8.6 Hz, 1H), 6.91 (t, *J* = 7.2 Hz, 1H), 6.79 (d, *J* = 1.9 Hz, 1H), 5.39 (d, *J* = 10.9 Hz, 1H), 5.03 – 4.92 (m, 3H), 3.69 (dt, *J* = 10.5, 5.0 Hz, 4H), 3.58 – 3.50 (m, 2H), 3.45 (t, *J* = 4.9 Hz, 2H), 3.03 – 2.53 (m, 4H), 2.22 (d, *J* = 13.4 Hz, 1H), 2.09 – 1.86 (m, 4H), 1.78 (d, *J* = 12.1 Hz, 2H), 1.54 (dd, *J* = 27.2, 13.5 Hz, 1H), 1.29 – 1.12 (m, 2H).

(3'R,4'S,5'R)-6''-chloro-4'-(3-chloro-2-fluorophenyl)-N-(4-((2-(2-(2-((2-(2,6-dioxopiperidin-3-yl)-1,3-dioxoisoindolin-4-yl)amino)ethoxy)ethoxy)ethyl)carbamoyl)phenyl)-2''-oxodispiro[cyclohexane-1,2'-pyrrolidine-3',3''-indoline]-5'-carboxamide (LD-075)

LD-075 (20.8 mg, Yield: 75% from **MI-1061**) was obtained as yellow powder using the same synthetic strategy described for **LD-074**.

LC-MS(ESI) m/z $(M+H)^+$: 968.35; calcd for $C_{49}H_{49}Cl_2FN_7O_9$ $(M+H)^+$: 968.30; >98% purity.

^{1}H NMR (400 MHz, MeOD) δ 7.79 – 7.66 (m, 3H), 7.59 – 7.47 (m, 3H), 7.40 – 7.27 (m, 2H), 7.19 (t, *J* = 8.1 Hz, 1H), 7.10 (dd, *J* = 8.2, 1.8 Hz, 1H), 6.95 – 6.83 (m, 2H), 6.79 (d, *J* = 1.9 Hz, 1H), 5.40 (d, *J* = 10.9 Hz, 1H), 5.03 – 4.96 (m, 3H), 3.73 – 3.62 (m, 8H), 3.57 – 3.50 (m, 2H), 3.42 – 3.35 (m, 2H), 2.94 (d, *J* = 8.0 Hz, 1H), 2.85 – 2.57 (m, 3H), 2.21 (d, *J* = 13.6 Hz, 1H), 2.07 – 1.87 (m, 4H), 1.76 (d, *J* = 11.6 Hz, 2H), 1.53 (dd, *J* = 26.9, 13.3 Hz, 1H), 1.31 – 1.10 (m, 2H).

(3'R,4'S,5'R)-6''-chloro-4'-(3-chloro-2-fluorophenyl)-N-(4-((2-(2-(2-(2-((2-(2,6-dioxopiperidin-3-yl)-1,3-dioxoisoindolin-4-yl)amino)ethoxy)ethoxy)ethoxy)ethyl)carbamoyl)phenyl)-2''-oxodispiro[cyclohexane-1,2'-pyrrolidine-3',3''-indoline]-5'-carboxamide (LD-112)

LD-112 was (11.8 mg, Yield: 41% from **MI-1061**) obtained as yellow powder using the same synthetic strategy described for **LD-074**.

LC-MS(ESI) m/z $(M+H)^+$: 1012.30; calcd for $C_{51}H_{53}Cl_2FN_7O_{10}$ $(M+H)^+$: 1012.32; >98% purity.

^{1}H NMR (400 MHz, MeOD) δ 7.76 (d, *J* = 8.7 Hz, 2H), 7.72 (t, *J* = 6.6 Hz, 1H), 7.58 (d, *J* = 8.7 Hz, 2H), 7.53 (dd, *J* = 8.2, 2.3 Hz, 1H), 7.49 – 7.43 (m, 1H), 7.36 (t, *J* = 7.0 Hz, 1H), 7.19 (t, *J* = 8.1 Hz, 1H), 7.11 (dd, *J* = 8.2, 1.8 Hz, 1H), 6.99 (d, *J* = 8.0 Hz, 2H), 6.79 (d, *J* = 1.9 Hz, 1H), 5.37 (d, *J* = 10.9 Hz, 1H), 5.02 (ddd, *J* = 12.3, 5.4, 1.3 Hz, 1H), 4.97 (d, *J* = 11.0 Hz, 1H), 3.68 – 3.60 (m, 12H), 3.52 (t, *J* = 5.3 Hz, 2H), 3.42 (t, *J* = 5.2 Hz, 2H), 2.95 – 2.87 (m, 1H), 2.86 – 2.79 (m, 1H), 2.76 – 2.61 (m, 2H), 2.21 (d, *J* = 13.4 Hz, 1H), 2.13 – 2.05 (m, 1H), 2.00 – 1.88 (m, 3H), 1.77 (d, *J* = 11.7 Hz, 2H), 1.53 (dd, *J* = 27.1, 13.2 Hz, 1H), 1.29 – 1.19 (m, 2H).

(3'R,4'S,5'R)-6''-chloro-4'-(3-chloro-2-fluorophenyl)-N-(4-((3-(2-(2-(3-((2-(2,6-dioxopiperidin-3-yl)-1,3-dioxoisoindolin-4-yl)amino)propoxy)ethoxy)ethoxy)propyl)carbamoyl)phenyl)-2''-oxodispiro[cyclohexane-1,2'-pyrrolidine-3',3''-indoline]-5'-carboxamide (LD-076)

LD-076 (17.6 mg, Yield: 59% from **MI-1061**) was obtained as yellow powder using the same synthetic strategy described for **LD-074**.

LC-MS(ESI) m/z $(M+H)^+$: 1040.40; calcd for $C_{53}H_{57}Cl_2FN_7O_{10}$ $(M+H)^+$: 1040.35; >98% purity.

^{1}H NMR (400 MHz, MeOD) δ 7.80 – 7.74 (m, 2H), 7.70 (t, *J* = 7.1 Hz, 1H), 7.61 (d, *J* = 8.6 Hz, 2H), 7.55 – 7.46 (m, 2H), 7.39 – 7.31 (m, 1H), 7.17 (t, *J* = 8.1 Hz, 1H), 7.10 (dd, *J* = 8.2, 1.6 Hz, 1H), 7.04 – 6.96 (m, 2H), 6.79 (d, *J* = 1.9 Hz, 1H), 5.26 (d, *J* = 10.4 Hz, 1H), 5.03 (dd, *J* = 12.4, 5.5 Hz, 1H), 4.94 (d, *J* = 10.7 Hz, 1H), 3.68 – 3.62 (m, 4H), 3.62 – 3.54 (m, 8H), 3.45 (t, *J* = 6.6 Hz, 2H), 3.38 (t, *J* = 6.5 Hz, 2H), 2.90 – 2.67 (m, 4H), 2.20 – 2.05 (m, 2H), 1.96 – 1.73 (m, 9H), 1.55 (dd, *J* = 27.1, 13.6 Hz, 1H), 1.27 – 1.13 (m, 2H)

(3'R,4'S,5'R)-6''-chloro-4'-(3-chloro-2-fluorophenyl)-N-(4-((2-(2-(2-(2-((2-(2,6-dioxopiperidin-3-yl)-1,3-dioxoisoindolin-4-yl)oxy)ethoxy)ethoxy)ethoxy)ethyl)carbamoyl)phenyl)-2''-oxodispiro[cyclohexane-1,2'-pyrrolidine-3',3''-indoline]-5'-carboxamide (LD-110)

Reaction 1:

Potassium bicarbonate (150mg, 1.5 mmol) was added to a solution of 2-(2,6-dioxopiperidin-3-yl)-4-hydroxyisoindoline-1,3-dione (274 mg, 1.0 mmol) in DMF (5mL) and stirred for 30 min. Then 2,2-dimethyl-4-oxo-3,8,11,14-tetraoxa-5-azahexadecan-16-yl 4-methylbenzenesulfonate (492

mg, 1.1 mmol) was added to the reaction and stirred at 50°C overnight. Then the product was purified by reverse phase chromatography over C18 column to yield product. Then the product was dissolved in DCM (5 mL) and trifluoroacetic acid (1 mL) and stirred for 30 min until the reaction is complete. Solvent was removed under vacuum to yield **114**

Reaction 2:

HATU (13.3 mg, 0.035 mmol) and N,N-Diisopropylethylamine (0.026 mL, 0.15 mmol) were added to a solution of **MI-1061** (20 mg, 0.029 mmol) in 0.5 mL DMF and stirred. After 10 minutes, **114** (0.35 mL, 0.1 M in DMSO) was added to the reaction. After 30 minutes, the solvent was removed and the crude was dissolved in 3:1 methanol/water, acidified with trifluoroacetic acid and purified by reverse-phase preparative HPLC. The purified fractions were combined, concentrated in vacuo, re-dissolved in H2O, frozen and lyophilized to yield **LD-110 (**8.5 mg, Yield: 29%) as a white powder.

LC-MS(ESI) m/z $(M+H)^+$: 1013.33; calcd for C51H52Cl2FN6O11 $(M+H)^+$: 1013.31; >98% purity.

^{1}H NMR (400 MHz, MeOD) δ 7.77 (d, *J* = 8.8 Hz, 2H), 7.74 – 7.65 (m, 2H), 7.60 (d, *J* = 8.7 Hz, 2H), 7.52 (dd, *J* = 8.2, 2.4 Hz, 1H), 7.42 – 7.30 (m, 3H), 7.17 (t, *J* = 8.0 Hz, 1H), 7.10 (dd, *J* = 8.2, 1.5 Hz, 1H), 6.79 (d, *J* = 1.8 Hz, 1H), 5.29 (d, *J* = 10.7 Hz, 1H), 5.08 (dd, *J* = 12.4, 5.5 Hz, 1H), 4.95 (d, *J* = 10.8 Hz, 1H), 4.33 – 4.25 (m, 2H), 3.90 – 3.82 (m, 2H), 3.75 – 3.69 (m, 2H), 3.65 – 3.58 (m, 8H), 3.52 (t, *J* = 5.3 Hz, 2H), 2.89 – 2.66 (m, 4H), 2.19 – 2.05 (m, 2H), 1.98 – 1.84 (m, 3H), 1.77 (d, *J* = 10.9 Hz, 2H), 1.55 (dd, *J* = 27.2, 13.7 Hz, 1H), 1.26 – 1.14 (m, 2H).

(3'R,4'S,5'R)-6''-chloro-4'-(3-chloro-2-fluorophenyl)-N-(4-((2-(2-(2-(3-(2-(2,6-dioxopiperidin-3-yl)-1,3-dioxoisoindolin-4-yl)propoxy)ethoxy)ethoxy)ethyl)carbamoyl)phenyl)-2''-oxodispiro[cyclohexane-1,2'-pyrrolidine-3',3''-indoline]-5'-carboxamide (LD-210)

LD-210 (8.8 mg, Yield: 30% from **MI-1061**) was obtained as white powder using the same synthetic strategy described for **LD-222**.

LC-MS(ESI) m/z $(M+H)^+$:1011.31; calcd for $C_{52}H_{54}Cl_2FN_6O_{10}$ $(M+H)^+$: 1011.33; >98% purity.

^{1}H NMR (400 MHz, MeOD) δ 7.77 (d, *J* = 8.1 Hz, 2H), 7.74 – 7.64 (m, 3H), 7.64 – 7.56 (m, 3H), 7.53 (dd, *J* = 8.2, 2.4 Hz, 1H), 7.36 (t, *J* = 7.2 Hz, 1H), 7.19 (t, *J* = 8.1 Hz, 1H), 7.14 – 7.10 (m, 1H), 6.80 (d, *J* = 1.8 Hz, 1H), 5.37 (dd, *J* = 11.0, 1.6 Hz, 1H), 5.11 (dd, *J* = 12.9, 5.0 Hz, 1H), 4.97 (d, *J* = 10.9 Hz, 1H), 3.68 – 3.57 (m, 8H), 3.57 – 3.49 (m, 4H), 3.44 (t, *J* = 6.3 Hz, 2H), 3.17 – 3.06 (m, 2H), 2.98 – 2.91 (m, 1H), 2.89 – 2.79 (m, 1H), 2.79 – 2.65 (m, 2H), 2.22 (d, *J* = 15.2 Hz, 1H), 2.17 – 2.09 (m, 1H), 2.02 – 1.84 (m, 5H), 1.84 – 1.74 (m, 2H), 1.52 (dd, *J* = 27.2, 13.3 Hz, 1H), 1.30 – 1.19 (m, 2H).

(3'R,4'S,5'R)-6''-chloro-4'-(3-chloro-2-fluorophenyl)-N-(4-((2-(2-(2-(2-((2-(2,6-dioxopiperidin-3-yl)-1-oxoisoindolin-4-yl)amino)ethoxy)ethoxy)ethoxy)ethyl)carbamoyl)phenyl)-2''-oxodispiro[cyclohexane-1,2'-pyrrolidine-3',3''-indoline]-5'-carboxamide (LD-131)

Reaction 1:

Lenalidomide (73 mg, 0.28 mmol) was added to a solution of tert-butyl (2-(2-(2-(2-oxoethoxy)ethoxy)ethoxy)ethyl)carbamate (100 mg, 0.34 mmol) in 3 mL DCE and stirred for 30 min. Then sodium triacetoxyborohydride (120 mg, 0.56 mmol) was added to the mixture and

reaction was stirred at room temperature overnight. Then the reaction was quenched by adding saturated sodium bicarbonate solution (30 mL). The product was extracted out by DCM (30 mL*3) and the combined organic solution was washed by brine. Crude product was obtained by removing the solvent by vacuum. The crude product was then dissolved in 10 mL DCM and 2 mL trifluoroacetic acid. The reaction was stirred for 30 min and the solvent was removed by vacuo. The residue was purified by reverse phase chromatography over C18 column to yield **102a** as colorless oil.

Reaction 2:

HATU (13.3 mg, 1.2 eq.) and N,N-Diisopropylethylamine (0.026 mL, 0.15 mmol) were added to a solution of **MI-1061** (20 mg, 0.029 mmol) in 0.5 mL DMF and stirred. After 10 minutes, **102a** (0.35 mL, 0.1 M in DMSO) was added to the reaction. After 30 minutes, the solvent was removed and the crude was dissolved in 3:1 methanol/water, acidified with trifluoroacetic acid and purified by reverse-phase preparative HPLC. The purified fractions were combined, concentrated in vacuo, re-dissolved in H2O, frozen and lyophilized to yield **LD-186** 17.6 mg, Yield: 43%) as a white powder.

LC-MS(ESI) m/z $(M+H)^+$: 998.29; calcd for C51H55Cl2FN7O9 $(M+H)^+$: 998.34; >98% purity.

^{1}H NMR (400 MHz, MeOD) δ 7.76 (dd, *J* = 8.8, 2.8 Hz, 2H), 7.71 (t, *J* = 7.0 Hz, 1H), 7.57 (t, *J* = 8.3 Hz, 2H), 7.51 (dt, *J* = 8.2, 2.7 Hz, 1H), 7.36 (t, *J* = 7.6 Hz, 1H), 7.30 – 7.23 (m, 1H), 7.18 (t, *J* = 8.1 Hz, 1H), 7.11 (d, *J* = 8.2 Hz, 1H), 7.07 (dd, *J* = 7.3, 2.2 Hz, 1H), 6.84 – 6.77 (m, 2H), 5.32 (d, *J* = 10.9 Hz, 1H), 5.16 – 5.10 (m, 1H), 4.95 (dd, *J* = 10.8, 2.7 Hz, 1H), 4.32 – 4.19 (m, 2H), 3.68 – 3.60 (m, 12H), 3.52 (t, *J* = 5.3 Hz, 2H), 3.36 (t, *J* = 4.6 Hz, 2H), 2.97 – 2.86 (m, 2H), 2.80 – 2.71 (m, 1H), 2.50

– 2.37 (m, 1H), 2.22 – 2.12 (m, 2H), 1.94 (dd, *J* = 19.7, 10.4 Hz, 3H), 1.78 (d, *J* = 12.3 Hz, 2H), 1.54 (dd, *J* = 25.6, 13.6 Hz, 1H), 1.28 – 1.17 (m, 2H).

(3'R,4'S,5'R)-6''-chloro-4'-(3-chloro-2-fluorophenyl)-N-(4-((2-(2-(2-(3-(2-(2,6-dioxopiperidin-3-yl)-1-oxoisoindolin-4-yl)propoxy)ethoxy)ethoxy)ethyl)carbamoyl)phenyl)-2''-oxodispiro[cyclohexane-1,2'-pyrrolidine-3',3''-indoline]-5'-carboxamide (LD-243)

LD-243 (17.6 mg, Yield: 61% from **MI-1061**) was obtained as white powder using the same synthetic strategy described for **LD-222**.

LC-MS(ESI) m/z $(M+H)^+$:997.32; calcd for $C_{52}H_{56}Cl_2FN_6O_9$ $(M+H)^+$: 997.35; >98% purity.

^{1}H NMR (400 MHz, MeOD) δ 7.80 – 7.74 (m, 2H), 7.71 (t, *J* = 7.2 Hz, 1H), 7.63 – 7.54 (m, 3H), 7.54 – 7.48 (m, 1H), 7.47 – 7.29 (m, 3H), 7.18 (t, *J* = 8.1 Hz, 1H), 7.11 (ddd, *J* = 8.3, 1.9, 0.7 Hz, 1H), 6.79 (d, *J* = 1.9 Hz, 1H), 5.34 (d, *J* = 10.9 Hz, 1H), 5.16 (ddd, *J* = 13.4, 9.3, 5.2 Hz, 1H), 4.96 (dd, *J* = 10.9, 3.8 Hz, 1H), 4.43 (t, *J* = 4.9 Hz, 2H), 3.67 – 3.58 (m, 8H), 3.58 – 3.47 (m, 4H), 3.47 – 3.37 (m, 2H), 2.98 – 2.82 (m, 2H), 2.82 – 2.63 (m, 3H), 2.50 (qdd, *J* = 13.4, 8.8, 4.7 Hz, 1H), 2.27 – 2.10 (m, 2H), 2.03 – 1.81 (m, 5H), 1.77 (d, *J* = 11.9 Hz, 2H), 1.54 (dd, *J* = 26.4, 13.3 Hz, 1H), 1.34 – 1.12 (m, 2H).

(3'R,4'S,5'R)-6''-chloro-4'-(3-chloro-2-fluorophenyl)-N-(4-((2-(2-(2-(3-((2-(2,6-dioxopiperidin-3-yl)-1-oxoisoindolin-4-yl)amino)-3-oxopropoxy)ethoxy)ethoxy)ethyl)carbamoyl)phenyl)-2''-oxodispiro[cyclohexane-1,2'-pyrrolidine-3',3''-indoline]-5'-carboxamide (LD-188)

LD-188 (27.6 mg, Yield: 62% from **MI-1061**) was obtained as white powder using the same synthetic strategy described for **LD-186**.

LC-MS(ESI) m/z $(M+H)^+$:1026.30; calcd for $C_{52}H_{55}Cl_2FN_7O_{10}$ $(M+H)^+$: 1026.34; >98% purity.

^{1}H NMR (400 MHz, MeOD) δ 7.80 – 7.74 (m, 2H), 7.74 – 7.68 (m, 2H), 7.63 – 7.56 (m, 3H), 7.53 (dd, *J* = 8.2, 2.5 Hz, 1H), 7.46 (t, *J* = 7.8 Hz, 1H), 7.39 – 7.31 (m, 1H), 7.17 (t, *J* = 8.1 Hz, 1H), 7.13 – 7.03 (m, 1H), 6.79 (d, *J* = 1.9 Hz, 1H), 5.35 (d, *J* = 10.9 Hz, 1H), 5.15 (dt, *J* = 13.3, 5.4 Hz, 1H), 4.97 (d, *J* = 10.9 Hz, 1H), 4.45 (t, *J* = 2.6 Hz, 2H), 3.79 (t, *J* = 5.9 Hz, 2H), 3.64 – 3.51 (m, 10H), 3.48 (t, *J* = 5.2 Hz, 2H), 2.99 – 2.82 (m, 2H), 2.76 (ddd, *J* = 17.6, 4.5, 2.3 Hz, 1H), 2.65 (dd, *J* = 7.2, 4.7 Hz, 2H), 2.43 (qdd, *J* = 13.2, 4.6, 2.3 Hz, 1H), 2.25 – 2.10 (m, 2H), 2.04 – 1.85 (m, 3H), 1.76 (d, *J* = 11.7 Hz, 2H), 1.60 – 1.44 (m, 1H), 1.23 (td, *J* = 13.7, 3.8 Hz, 2H).

(3'R,4'S,5'R)-6''-chloro-4'-(3-chloro-2-fluorophenyl)-N-(4-((5-(2-(2,6-dioxopiperidin-3-yl)-1,3-dioxoisoindolin-4-yl)pentyl)carbamoyl)phenyl)-2''-oxodispiro[cyclohexane-1,2'-pyrrolidine-3',3''-indoline]-5'-carboxamide (LD-214)

LD-214 (18.2 mg, Yield: 58% from **MI-1061**) was obtained as white powder using the same synthetic strategy described for **LD-222**.

LC-MS(ESI) m/z $(M+H)^+$: 907.27; calcd for $C_{48}H_{46}Cl_2FN_6O_7$ $(M+H)^+$: 907.28; >98% purity.

^{1}H NMR (400 MHz, MeOD) δ 7.75 – 7.68 (m, 3H), 7.66 – 7.63 (m, 2H), 7.63 – 7.57 (m, 3H), 7.54 (dd, *J* = 8.2, 2.2 Hz, 1H), 7.37 (t, *J* = 7.4 Hz, 1H), 7.19 (t, *J* = 8.0 Hz, 1H), 7.11 (dd, *J* = 8.2, 1.4 Hz, 1H), 6.80 (d, *J* = 1.5 Hz, 1H), 5.38 (d, *J* = 10.9 Hz, 1H), 5.09 (dd, *J* = 12.6, 5.4 Hz, 1H), 4.99 (d, *J* = 11.0 Hz, 1H), 3.34 (t, *J* = 7.0 Hz, 2H), 3.11 (dd, *J* = 17.7, 10.1 Hz, 2H), 2.98 – 2.79 (m, 2H), 2.79 – 2.62 (m, 2H), 2.22 (d, *J* = 13.9 Hz, 1H), 2.10 (dd, *J* = 8.6, 3.5 Hz, 1H), 2.04 – 1.91 (m, 3H), 1.80 – 1.51 (m, 7H), 1.44 (dd, *J* = 15.0, 8.0 Hz, 2H), 1.31 – 1.19 (m, 2H).

(3'R,4'S,5'R)-6''-chloro-4'-(3-chloro-2-fluorophenyl)-N-(4-((5-((2-(2,6-dioxopiperidin-3-yl)-1-oxoisoindolin-4-yl)amino)-5-oxopentyl)carbamoyl)phenyl)-2''-oxodispiro[cyclohexane-1,2'-pyrrolidine-3',3''-indoline]-5'-carboxamide (LD-186)

Reaction 1:

HATU (380 mg, 1 mmol) and N,N-Diisopropylethylamine (0.44 mL, 2.5 mmol) were added to a solution of Boc-5-aminopentanoic acid (110 mg, 0.5 mmol) in 3 mL DMF and stirred. After 10 minutes, lenalidomide (200 mg, 0.75 mmol) was added to the reaction. After 30 minutes, the solvent was removed and the crude was dissolved in 10 mL DCM and 2 mL trifluoroacetic acid. The reaction was stirred for 30min and then the solvent was removed by vacuo. The residue was purified by reverse phase chromatography over C18 column to yield **102d** as colorless oil.

Reaction 2:

HATU (13.3 mg, 1.2 eq.) and N,N-Diisopropylethylamine (0.026 mL, 0.15 mmol) were added to a solution of **MI-1061** (20 mg, 0.029 mmol) in 0.5 mL DMF and stirred. After 10 minutes, **102d** (0.35 mL, 0.1 M in DMSO) was added to the reaction. After 30 minutes, the solvent was removed and the crude was dissolved in 3:1 methanol/water, acidified with trifluoroacetic acid and purified by reverse-phase preparative HPLC. The purified fractions were combined, concentrated in vacuo, re-dissolved in H2O, frozen and lyophilized to yield **LD-186** (24.2 mg, Yield: 91%) as a white powder.

LC-MS(ESI) m/z $(M+H)^+$:922.26; calcd for C48H47Cl2FN7O7 $(M+H)^+$: 922.29; >98% purity.

^{1}H NMR (400 MHz, MeOD) δ 7.77 (d, *J* = 8.2 Hz, 2H), 7.74 – 7.67 (m, 2H), 7.63 – 7.57 (m, 3H), 7.54 (dd, *J* = 8.2, 2.4 Hz, 1H), 7.47 (t, *J* = 7.7 Hz, 1H), 7.39 – 7.31 (m, 1H), 7.17 (t, *J* = 8.1 Hz, 1H), 7.11 (dd, *J* = 8.2, 1.9 Hz, 1H), 6.79 (d, *J* = 1.9 Hz, 1H), 5.38 (d, *J* = 10.9 Hz, 1H), 5.12 (dd, *J* = 13.3, 5.1 Hz, 1H), 4.98 (d, *J* = 10.9 Hz, 1H), 4.45 (d, *J* = 2.1 Hz, 2H), 3.40 (t, *J* = 6.7 Hz, 2H), 3.02 – 2.79 (m, 2H), 2.78 – 2.66 (m, 1H), 2.57 – 2.30 (m, 3H), 2.21 (d, *J* = 14.0 Hz, 1H), 2.17 – 2.07 (m, 1H), 2.06 – 1.88 (m, 3H), 1.81 – 1.63 (m, 6H), 1.60 – 1.46 (m, 1H), 1.24 (td, *J* = 13.8, 3.9 Hz, 2H).

(3'R,4'S,5'R)-6''-chloro-4'-(3-chloro-2-fluorophenyl)-N-(4-((5-(2-(2,6-dioxopiperidin-3-yl)-1-oxoisoindolin-4-yl)pentyl)carbamoyl)phenyl)-2''-oxodispiro[cyclohexane-1,2'-pyrrolidine-3',3''-indoline]-5'-carboxamide (LD-222)

Reaction 1:

To a solution of tert-butyl pent-4-yn-1-ylcarbamate (236 mg, 1.29 mmol) and 3-(4-bromo-1-oxoisoindolin-2-yl)piperidine-2,6-dione (400mg, 1.29 mmol) in Triethylamine (3mL) and DMF (3 mL), CuI (50mg, 0.25 mmol) and the $Pd(Ph_3P)_2Cl_2$ (90 mg, 0.13 mmol) were added. The mixture was stirred at 80^{o}C under N_2-atmosphere overnight. The reaction mixture was poured into a saturated aqueous solution of NH4Cl and after separation of the organic layer the aqueous layer was extracted with Ethyl Acetate. The combined organic layers were washed with brine, dried over Na2SO4 and concentrated in vacuo. The crude product was purified by flash chromatography to afford **105d** as white solid.

Reaction 2:

To a solution of **105d** (210 mg, 0.5 mmol) in EtOH (5 mL) was added Pd/C (20mg). The reaction was stirred under H2-atmosphere for 2 hr. Then the mixture was filtered by celite and the solvent was removed by vacuo. The residue was dissolved in 10 mL DCM and 2 mL trifluoroacetic acid. The reaction was stirred for 30min and then the solvent was removed by vacuo. The residue was purified by reverse phase chromatography over C18 column to **106d** as colorless oil.

Reaction 3:

HATU (13.3 mg, 1.2 eq.) and N,N-Diisopropylethylamine (0.026 mL, 0.15 mmol) were added to a solution of **MI-1061** (20 mg, 0.029 mmol) in 0.5 mL DMF and stirred. After 10 minutes, **106d** (0.35 mL, 0.1 M in DMSO) was added to the reaction. After 30 minutes, the solvent was removed and the crude was dissolved in 3:1 methanol/water, acidified with trifluoroacetic acid and purified by reverse-phase preparative HPLC. The purified fractions were combined, concentrated in vacuo, re-dissolved in H2O, frozen and lyophilized to give **LD-222** (17.5 mg, Yield: 68%) as a white powder.

LC-MS(ESI) m/z $(M+H)^+$: 893.19; calcd for C48H48Cl2FN6O6 $(M+H)^+$: 893.30; >98% purity.

^{1}H NMR (400 MHz, MeOD) δ 7.78 – 7.66 (m, 3H), 7.66 – 7.56 (m, 3H), 7.53 (dd, *J* = 8.2, 2.5 Hz, 1H), 7.47 – 7.38 (m, 2H), 7.38 – 7.32 (m, 1H), 7.17 (t, *J* = 8.1 Hz, 1H), 7.11 (dd, *J* = 8.2, 2.0 Hz, 1H), 6.79 (d, *J* = 1.9 Hz, 1H), 5.29 (d, *J* = 10.7 Hz, 1H), 5.14 (dd, *J* = 13.3, 5.2 Hz, 1H), 4.97 (d, *J* = 10.8 Hz, 1H), 4.46 (dd, *J* = 5.7, 2.5 Hz, 2H), 3.41 – 3.33 (m, 2H), 2.96 – 2.64 (m, 5H), 2.50 (qdd, *J* = 13.3, 4.6, 2.5 Hz, 1H), 2.22 – 2.09 (m, 2H), 2.02 – 1.84 (m, 3H), 1.79 – 1.48 (m, 7H), 1.48 – 1.35 (m, 2H), 1.22 (td, *J* = 13.7, 4.0 Hz, 2H).

(3'R,4'S,5'R)-6''-chloro-4'-(3-chloro-2-fluorophenyl)-N-(4-((5-(2-(2,6-dioxopiperidin-3-yl)-1,3-dioxoisoindolin-4-yl)pent-4-yn-1-yl)carbamoyl)phenyl)-2''-oxodispiro[cyclohexane-1,2'-pyrrolidine-3',3''-indoline]-5'-carboxamide (LE-004)

HATU (13.3 mg, 1.2 eq.) and N,N-Diisopropylethylamine (0.026 mL, 0.15 mmol) were added to a solution of **MI-1061** (20 mg, 0.029 mmol) in 0.5 mL DMF and stirred. After 10 minutes, **105d** (0.35 mL, 0.1 M in DMSO) was added to the reaction. After 30 minutes, the solvent was removed and the crude was dissolved in 3:1 methanol/water, acidified with trifluoroacetic acid and purified by reverse-phase preparative HPLC. The purified fractions were combined, concentrated in vacuo, re-dissolved in H2O, frozen and lyophilized to give **LE-004** (8.7 mg, Yield: 34%) as a white powder.

LC-MS(ESI) m/z $(M+2H)^{2+}$: 445.30; calcd for C48H45Cl2FN6O6 $(M+2H)^{2+}$: 445.14; >98% purity.

^{1}H NMR (400 MHz, Methanol-d_4) δ 7.83 – 7.62 (m, 4H), 7.56 (dd, *J* = 8.3, 2.5 Hz, 1H), 7.54 – 7.47 (m, 2H), 7.47 – 7.32 (m, 3H), 7.19 (ddd, *J* = 8.9, 7.6, 3.3 Hz, 1H), 7.12 (dd, *J* = 8.2, 2.0 Hz, 1H), 6.80 (d, *J* = 1.9 Hz, 1H), 5.30 (d, *J* = 10.8 Hz, 1H), 5.13 (ddd, *J* = 13.0, 7.4, 5.2 Hz, 1H), 4.98 (d, *J* = 10.9 Hz, 1H), 4.49 – 4.25 (m, 2H), 3.57 (t, *J* = 6.6 Hz, 2H), 2.97 – 2.83 (m, 2H), 2.83 – 2.73 (m, 1H), 2.68 – 2.42 (m, 3H), 2.28 – 2.13 (m, 2H), 2.13 – 1.84 (m, 5H), 1.84 – 1.68 (m, 2H), 1.57 (ddd, *J* = 16.3, 6.2, 3.0 Hz, 1H), 1.34 – 1.19 (m, 3H).

(3'R,4'S,5'R)-6''-chloro-4'-(3-chloro-2-fluorophenyl)-N-(4-(4-((2-(2,6-dioxopiperidin-3-yl)-1,3-dioxoisoindolin-4-yl)amino)piperidine-1-carbonyl)phenyl)-2''-oxodispiro[cyclohexane-1,2'-pyrrolidine-3',3''-indoline]-5'-carboxamide (LE-081)

LE-081 (24.2 mg, Yield: 93% from **MI-1061**) was obtained as white powder using the same synthetic strategy described for **LD-131**.

LC-MS(ESI) m/z $(M+H)^+$: 906.48; calcd for CC48H47Cl2FN7O6 $(M+H)^+$: 906.29; >98% purity.

^{1}H NMR (400 MHz, MeOD/ DMSO) δ 7.78 (t, *J* = 7.2 Hz, 1H), 7.71 (d, *J* = 8.6 Hz, 2H), 7.63 (dd, *J* = 8.2, 2.3 Hz, 1H), 7.51 – 7.43 (m, 3H), 7.39 (t, *J* = 7.8 Hz, 1H), 7.29 (t, *J* = 8.1 Hz, 1H), 7.19 (dd, *J* = 8.2, 1.9 Hz, 1H), 7.12 (d, *J* = 7.5 Hz, 1H), 6.99 (d, *J* = 8.2 Hz, 1H), 6.89 (d, *J* = 1.9 Hz, 1H), 5.44 (d, *J* = 10.9 Hz, 1H), 5.21 (dd, *J* = 13.3, 5.1 Hz, 1H), 5.01 (d, *J* = 11.0 Hz, 1H), 4.32 (q, *J* = 17.1 Hz, 2H), 3.93 – 3.59 (m, 2H), 3.20 – 2.86 (m, 4H), 2.84 – 2.74 (m, 1H), 2.49 (qd, *J* = 13.2, 4.5 Hz, 1H), 2.24 – 1.91 (m, 7H), 1.78 (d, *J* = 11.6 Hz, 2H), 1.56 (m,, 4H), 1.31 – 1.12 (m, 2H).

(3'R,4'S,5'R)-6''-chloro-4'-(3-chloro-2-fluorophenyl)-N-(4-(3-((2-(2,6-dioxopiperidin-3-yl)-1,3-dioxoisoindolin-4-yl)amino)azetidine-1-carbonyl)phenyl)-2''-oxodispiro[cyclohexane-1,2'-pyrrolidine-3',3''-indoline]-5'-carboxamide (LE-082)

LE-082 (24.4 mg, Yield: 97% from **MI-1061**) was obtained as white powder using the same synthetic strategy described for **LD-131**.

LC-MS(ESI) m/z $(M+H)^+$: 878.42; calcd for C46H43Cl2FN7O6 $(M+H)^+$: 878.26; >98% purity.

^{1}H NMR (400 MHz, MeOD) δ 7.71 (t, *J* = 6.6 Hz, 1H), 7.63 (s, 4H), 7.53 (dd, *J* = 8.3, 2.4 Hz, 1H), 7.41 – 7.26 (m, 2H), 7.23 – 7.13 (m, 2H), 7.11 (dd, *J* = 8.2, 1.9 Hz, 1H), 6.79 (d, *J* = 1.9 Hz, 1H), 6.64 (d, *J* = 8.0 Hz, 1H), 5.37 (d, *J* = 10.9 Hz, 1H), 5.15 (dd, *J* = 12.8, 5.7 Hz, 1H), 4.96 (d, *J* = 11.0 Hz, 1H), 4.73 (t, *J* = 8.0 Hz, 1H), 4.63 – 4.48 (m, 1H), 4.44 (dt, *J* = 12.0, 5.9 Hz, 1H), 4.38 – 4.25 (m, 2H), 4.20

(dd, *J* = 8.8, 4.5 Hz, 1H), 4.12 – 3.94 (m, 1H), 2.95 – 2.81 (m, 2H), 2.81 – 2.70 (m, 1H), 2.43 (dd, *J* = 26.0, 13.0 Hz, 1H), 2.26 – 2.10 (m, 2H), 2.03 – 1.87 (m, 3H), 1.77 (d, *J* = 11.9 Hz, 2H), 1.61 – 1.43 (m, 1H), 1.30 – 1.15 (m, 2H).

(3'R,4'S,5'R)-6''-chloro-4'-(3-chloro-2-fluorophenyl)-N-(4-(4-(((2-(2,6-dioxopiperidin-3-yl)-1,3-dioxoisoindolin-4-yl)amino)methyl)piperidine-1-carbonyl)phenyl)-2''-oxodispiro[cyclohexane-1,2'-pyrrolidine-3',3''-indoline]-5'-carboxamide (LE-083)

LE-083 (15.9 mg, Yield: 54% from **MI-1061**) was obtained as white powder using the same synthetic strategy described for **LD-131**.

LC-MS(ESI) m/z $(M+H)^+$: 920.29 calcd for $C_{49}H_{49}Cl_2FN_7O_6$ $(M+H)^+$: 920.31; >98% purity.

^{1}H NMR (400 MHz, MeOD) δ 7.72 (dd, *J* = 10.5, 3.9 Hz, 1H), 7.62 (d, *J* = 8.7 Hz, 2H), 7.53 (dd, *J* = 8.3, 2.4 Hz, 1H), 7.42 – 7.34 (m, 3H), 7.31 (t, *J* = 7.8 Hz, 1H), 7.19 (t, *J* = 8.0 Hz, 1H), 7.11 (dd, *J* = 8.2, 1.9 Hz, 1H), 7.06 (d, *J* = 7.5 Hz, 1H), 6.83 (d, *J* = 8.0 Hz, 1H), 6.80 (d, *J* = 1.9 Hz, 1H), 5.37 (d, *J* = 11.0 Hz, 1H), 5.14 (dd, *J* = 13.2, 5.0 Hz, 1H), 4.97 (d, *J* = 11.0 Hz, 1H), 4.69 – 4.48 (m, 1H), 4.27 (dd, *J* = 16.0, 8.0 Hz, 2H), 3.82 – 3.62 (m, 1H), 3.18 – 2.67 (m, 7H), 2.45 (qd, *J* = 13.1, 4.6 Hz, 1H), 2.25 – 2.10 (m, 2H), 2.04 – 1.84 (m, 5H), 1.78 (d, *J* = 11.6 Hz, 3H), 1.52 (dd, *J* = 27.0, 13.3 Hz, 1H), 1.31 – 1.09 (m, 4H).

(3'R,4'S,5'R)-6''-chloro-4'-(3-chloro-2-fluorophenyl)-N-(4-(3-(((2-(2,6-dioxopiperidin-3-yl)-1,3-dioxoisoindolin-4-yl)amino)methyl)azetidine-1-carbonyl)phenyl)-2''-oxodispiro[cyclohexane-1,2'-pyrrolidine-3',3''-indoline]-5'-carboxamide (LE-084)

LE-084 (13.5 mg, Yield: 53% from **MI-1061**) was obtained as white powder using the same synthetic strategy described for **LD-131**.

LC-MS(ESI) m/z $(M+H)^+$: 892.45; calcd for $C_{47}H_{45}Cl_2FN_7O_6$ $(M+H)^+$: 892.28; >98% purity.

^{1}H NMR (400 MHz, MeOD) δ 7.72 (t, *J* = 6.9 Hz, 1H), 7.61 (s, 4H), 7.54 (d, *J* = 7.6 Hz, 1H), 7.37 (t, *J* = 7.2 Hz, 1H), 7.31 (t, *J* = 7.2 Hz, 1H), 7.19 (t, *J* = 7.9 Hz, 1H), 7.16 – 7.02 (m, 2H), 6.87 (d, *J* = 8.0 Hz, 1H), 6.80 (s, 1H), 5.36 (d, *J* = 11.0 Hz, 1H), 5.15 (dd, *J* = 13.2, 5.1 Hz, 1H), 4.96 (d, *J* = 11.1 Hz, 1H), 4.45 (t, *J* = 8.3 Hz, 1H), 4.37 – 4.17 (m, 3H), 4.16 – 4.02 (m, 1H), 3.93 (dd, *J* = 9.6, 5.0 Hz, 1H), 3.48 (d, *J* = 6.6 Hz, 2H), 3.09 – 2.72 (m, 4H), 2.43 (dt, *J* = 13.3, 8.9 Hz, 1H), 2.31 – 2.11 (m, 2H), 2.05 – 1.85 (m, 3H), 1.78 (d, *J* = 11.5 Hz, 2H), 1.52 (d, *J* = 13.7 Hz, 1H), 1.31 – 1.16 (m, 2H).

(3'R,4'S,5'R)-6''-chloro-4'-(3-chloro-2-fluorophenyl)-N-(4-((3-(4-((2-(2,6-dioxopiperidin-3-yl)-1-oxoisoindolin-4-yl)amino)piperidin-1-yl)propyl)carbamoyl)phenyl)-2''-oxodispiro[cyclohexane-1,2'-pyrrolidine-3',3''-indoline]-5'-carboxamide (LE-254)

103a (50 mg, 0.15 mmol) was added to a solution of tert-butyl (2-oxoethyl)carbamate (60 mg, 0.3 mmol) in 3 mL DCE and stirred for 30 min. Then sodium triacetoxyborohydride (127 mg, 0.6 mmol) was added to the mixture and reaction was stirred at room temperature overnight. Then the reaction was quenched by adding saturated sodium bicarbonate solution (30 mL). The product was extracted out by DCM (30 mL*3) and the combined organic solution was washed by brine. Crude product was obtained by removing the solvent by vacuum. The crude product was then dissolved in 10 mL DCM and 2 mL trifluoroacetic acid. The reaction was stirred for 30 min

and the solvent was removed by vacuo. The residue was purified by reverse phase chromatography over C18 column to yield **104a** as colorless oil.

Reaction 2:

HATU (13.3 mg, 1.2 eq.) and N,N-Diisopropylethylamine (0.026 mL, 0.15 mmol) were added to a solution of **MI-1061** (20 mg, 0.029 mmol) in 0.5 mL DMF and stirred. After 10 minutes, **104a** (0.35 mL, 0.1 M in DMSO) was added to the reaction. After 30 minutes, the solvent was removed and the crude was dissolved in 3:1 methanol/water, acidified with trifluoroacetic acid and purified by reverse-phase preparative HPLC. The purified fractions were combined, concentrated in vacuo, re-dissolved in H2O, frozen and lyophilized to yield **LE-254** (7.8 mg, Yield: 25%) as a white powder.

LC-MS(ESI) m/z $(M+H)^+$: 963.62; calcd for $C_{51}H_{54}Cl_2FN_8O_6$ $(M+H)^+$ 963.35; >98% purity.

^{1}H NMR (400 MHz, MeOD) δ 7.86 (d, *J* = 8.7 Hz, 2H), 7.74 (t, *J* = 6.7 Hz, 1H), 7.68 (d, *J* = 8.7 Hz, 2H), 7.56 (dd, *J* = 8.2, 2.2 Hz, 1H), 7.44 – 7.32 (m, 2H), 7.25 – 7.09 (m, 3H), 7.01 – 6.89 (m, 1H), 6.82 (d, *J* = 1.8 Hz, 1H), 5.41 (d, *J* = 10.9 Hz, 1H), 5.17 (dd, *J* = 13.2, 5.2 Hz, 1H), 5.00 (d, *J* = 11.0 Hz, 1H), 4.43 – 4.22 (m, 2H), 3.78 – 3.64 (m, 2H), 3.57 – 3.36 (m, 3H), 3.30 – 3.01 (m, 4H), 3.01 – 2.85 (m, 2H), 2.85 – 2.74 (m, 1H), 2.47 (qd, *J* = 13.1, 4.5 Hz, 1H), 2.38 – 1.91 (m, 10H), 1.80 (d, *J* = 11.0 Hz, 3H), 1.55 (dd, *J* = 26.9, 13.6 Hz, 1H), 1.37 – 1.17 (m, 2H).

(3'R,4'S,5'R)-6''-chloro-4'-(3-chloro-2-fluorophenyl)-N-(4-((2-(4-((2-(2,6-dioxopiperidin-3-yl)-1-oxoisoindolin-4-yl)amino)piperidin-1-yl)ethyl)carbamoyl)phenyl)-2''-oxodispiro[cyclohexane-1,2'-pyrrolidine-3',3''-indoline]-5'-carboxamide (LE-093)

LE-093 (24.4 mg, Yield: 89% from **MI-1061**) was obtained as white powder using the same synthetic strategy described for **LE-254**.

LC-MS(ESI) m/z $(M+H)^+$: 949.44; calcd for C50H52Cl2FN8O6 $(M+H)^+$ 949.34; >98% purity.

^{1}H NMR (400 MHz, Methanol-d_4) δ 7.92 – 7.79 (m, 2H), 7.72 (ddd, *J* = 8.0, 6.3, 1.6 Hz, 1H), 7.69 – 7.62 (m, 2H), 7.53 (dd, *J* = 8.3, 2.5 Hz, 1H), 7.40 – 7.28 (m, 2H), 7.18 (td, *J* = 8.1, 1.2 Hz, 1H), 7.15 – 7.05 (m, 2H), 6.93 (d, *J* = 8.0 Hz, 1H), 6.80 (d, *J* = 2.0 Hz, 1H), 5.38 (d, *J* = 11.0 Hz, 1H), 5.14 (dd, *J* = 13.2, 5.2 Hz, 1H), 4.97 (d, *J* = 11.0 Hz, 1H), 4.46 – 4.15 (m, 2H), 3.93 – 3.34 (m, 8H), 3.19 (t, *J* = 12.8 Hz, 1H), 2.98 – 2.71 (m, 3H), 2.45 (qd, *J* = 13.2, 4.7 Hz, 1H), 2.38 – 2.02 (m, 5H), 2.02 – 1.87 (m, 3H), 1.85 – 1.75 (m, 3H), 1.63 – 1.45 (m, 1H), 1.32 – 1.16 (m, 2H).

(3'R,4'S,5'R)-6''-chloro-4'-(3-chloro-2-fluorophenyl)-N-(4-((2-(3-((2-(2,6-dioxopiperidin-3-yl)-1-oxoisoindolin-4-yl)amino)azetidin-1-yl)ethyl)carbamoyl)phenyl)-2''-oxodispiro[cyclohexane-1,2'-pyrrolidine-3',3''-indoline]-5'-carboxamide (LE-094)

LE-094 (22.7 mg, Yield: 86% from **MI-1061**) was obtained as white powder using the same synthetic strategy described for **LE-254**.

LC-MS(ESI) m/z $(M+H)^+$: 921.56; calcd for C48H48Cl2FN8O6 $(M+H)^+$ 921.31; >98% purity.

^{1}H NMR (400 MHz, MeOD) δ 7.86 (d, *J* = 8.1 Hz, 2H), 7.74 (t, *J* = 6.8 Hz, 1H), 7.67 (d, *J* = 8.3 Hz, 2H), 7.56 (dd, *J* = 8.2, 1.9 Hz, 1H), 7.37 (dd, *J* = 14.4, 7.2 Hz, 2H), 7.21 (t, *J* = 8.4 Hz, 2H), 7.13 (dd, *J* = 8.2, 1.7 Hz, 1H), 6.82 (d, *J* = 1.7 Hz, 1H), 6.77 – 6.56 (m, 1H), 5.38 (d, *J* = 10.9 Hz, 1H), 5.17 (dt, *J* = 17.6, 8.8 Hz, 1H), 4.99 (d, *J* = 11.0 Hz, 1H), 4.85 – 4.50 (m, 3H), 4.50 – 4.15 (m, 3H), 4.15 – 3.90

(m, 1H), 3.68 (s, 1H), 3.54 (s, 1H), 3.04 – 2.65 (m, 3H), 2.46 (dt, *J* = 13.5, 8.9 Hz, 1H), 2.29 – 2.13 (m, 2H), 2.06 – 1.87 (m, 3H), 1.80 (d, *J* = 11.8 Hz, 2H), 1.65 – 1.46 (m, 1H), 1.35 – 1.14 (m, 2H).

(3'R,4'S,5'R)-6''-chloro-4'-(3-chloro-2-fluorophenyl)-N-(4-((2-(4-(((2-(2,6-dioxopiperidin-3-yl)-1-oxoisoindolin-4-yl)amino)methyl)piperidin-1-yl)ethyl)carbamoyl)phenyl)-2''-oxodispiro[cyclohexane-1,2'-pyrrolidine-3',3''-indoline]-5'-carboxamide (LE-095)

LE-095 (13.7 mg, Yield: 49% from **MI-1061**) was obtained as white powder using the same synthetic strategy described for **LE-254**.

LC-MS(ESI) m/z $(M+H)^+$: 962.94; calcd for $C_{51}H_{54}Cl_2FN_8O_6$ $(M+H)^+$ 963.35; >98% purity.

^{1}H NMR (400 MHz, MeOD) δ 7.84 (d, *J* = 8.8 Hz, 2H), 7.72 (dd, *J* = 10.5, 4.0 Hz, 1H), 7.67 (d, *J* = 8.8 Hz, 2H), 7.52 (dd, *J* = 8.2, 2.4 Hz, 1H), 7.40 – 7.27 (m, 2H), 7.17 (t, *J* = 7.8 Hz, 1H), 7.14 – 7.05 (m, 2H), 6.86 (d, *J* = 8.1 Hz, 1H), 6.79 (d, *J* = 1.9 Hz, 1H), 5.29 (d, *J* = 10.7 Hz, 1H), 5.15 (dd, *J* = 13.3, 5.1 Hz, 1H), 4.95 (d, *J* = 10.8 Hz, 2H), 4.28 (q, *J* = 16.9 Hz, 2H), 3.85 – 3.64 (m, 4H), 3.53 – 3.33 (m, 2H), 3.22 – 3.19 (m, 1H), 3.06 – 2.71 (m, 5H), 2.45 (qd, *J* = 13.2, 4.7 Hz, 1H), 2.25 – 2.07 (m, 4H), 2.02 – 1.82 (m, 4H), 1.82 – 1.69 (m, 2H), 1.56 (dd, *J* = 24.8, 11.6 Hz, 3H), 1.41 – 1.05 (m, 3H).

(3'R,4'S,5'R)-6''-chloro-4'-(3-chloro-2-fluorophenyl)-N-(4-((2-(3-(((2-(2,6-dioxopiperidin-3-yl)-1-oxoisoindolin-4-yl)amino)methyl)azetidin-1-yl)ethyl)carbamoyl)phenyl)-2''-oxodispiro[cyclohexane-1,2'-pyrrolidine-3',3''-indoline]-5'-carboxamide (LE-096)

LE-096 (16.4 mg, Yield: 61% from **MI-1061**) was obtained as white powder using the same synthetic strategy described for **LE-254**.

LC-MS(ESI) m/z $(M+H)^+$: 934.92; calcd for $C_{49}H_{50}Cl_2FN_8O_6$ $(M+H)^+$ 935.32; >98% purity.

^{1}H NMR (400 MHz, MeOD) δ 7.69 (d, *J* = 8.0 Hz, 2H), 7.62 (t, *J* = 6.6 Hz, 1H), 7.58 – 7.50 (m, 2H), 7.43 (dd, *J* = 8.2, 2.4 Hz, 1H), 7.31 – 7.14 (m, 2H), 7.08 (t, *J* = 8.1 Hz, 1H), 7.00 (dt, *J* = 7.7, 3.9 Hz, 2H), 6.76 (dd, *J* = 29.7, 7.9 Hz, 1H), 6.69 (d, *J* = 1.9 Hz, 1H), 5.23 (d, *J* = 10.8 Hz, 1H), 5.04 (dd, *J* = 13.3, 4.9 Hz, 1H), 4.87 (d, *J* = 10.9 Hz, 1H), 4.45 – 3.94 (m, 5H), 3.85 (t, *J* = 9.2 Hz, 1H), 3.63 – 3.41 (m, 3H), 3.41 – 3.25 (m, 3H), 3.19 – 2.99 (m, 1H), 2.86 – 2.73 (m, 2H), 2.73 – 2.60 (m, 1H), 2.42 – 2.24 (m, 1H), 2.08 (d, *J* = 12.7 Hz, 2H), 1.93 – 1.76 (m, 3H), 1.67 (d, *J* = 11.5 Hz, 2H), 1.45 (dd, *J* = 27.2, 13.6 Hz, 1H), 1.21 – 1.04 (m, 2H).

(3'R,4'S,5'R)-6''-chloro-4'-(3-chloro-2-fluorophenyl)-N-(4-(4-((2-(2,6-dioxopiperidin-3-yl)-1-oxoisoindolin-4-yl)ethynyl)piperidine-1-carbonyl)phenyl)-2''-oxodispiro[cyclohexane-1,2'-pyrrolidine-3',3''-indoline]-5'-carboxamide (LE-102)

LE-102 (22.7 mg, Yield: 86% from **MI-1061**) was obtained as white powder using the same synthetic strategy described for **LE-004**.

LC-MS(ESI) m/z $(M+H)^+$: 915.39; calcd for $C_{50}H_{46}Cl_2FN_6O_6$ $(M+H)^+$ 915.28; >98% purity.

^{1}H NMR (400 MHz, MeOD) δ 7.77 (dd, *J* = 7.7, 0.8 Hz, 1H), 7.76 – 7.70 (m, 1H), 7.69 – 7.60 (m, 3H), 7.56 (dd, *J* = 8.3, 2.5 Hz, 1H), 7.52 (t, *J* = 7.7 Hz, 1H), 7.46 – 7.34 (m, 3H), 7.21 (t, *J* = 8.1 Hz, 1H), 7.13 (dd, *J* = 8.2, 1.9 Hz, 1H), 6.82 (d, *J* = 1.9 Hz, 1H), 5.38 (d, *J* = 11.0 Hz, 1H), 5.19 (dd, *J* = 13.3, 5.2 Hz, 1H), 4.99 (d, *J* = 11.0 Hz, 1H), 4.51 (q, *J* = 17.5 Hz, 2H), 4.11 (br s, 1H), 3.81 – 3.61 (m, 1H), 3.61 – 3.47 (m, 1H), 3.47 – 3.36 (m, 1H), 3.05 (dt, *J* = 12.2, 4.1 Hz, 1H), 3.01 – 2.85 (m, 2H), 2.80

(ddd, *J* = 17.5, 4.5, 2.4 Hz, 1H), 2.55 (qd, *J* = 13.2, 4.6 Hz, 1H), 2.29 – 2.14 (m, 2H), 2.10 – 1.88 (m, 5H), 1.87 – 1.66 (m, 4H), 1.55 (dd, *J* = 27.0, 13.4 Hz, 1H), 1.27 (td, *J* = 13.7, 3.7 Hz, 2H).

(3'R,4'S,5'R)-6''-chloro-4'-(3-chloro-2-fluorophenyl)-N-(4-(4-(2-(2-(2,6-dioxopiperidin-3-yl)-1-oxoisoindolin-4-yl)ethyl)piperidine-1-carbonyl)phenyl)-2''-oxodispiro[cyclohexane-1,2'-pyrrolidine-3',3''-indoline]-5'-carboxamide (LE-103)

LE-103 (16.7 mg, Yield: 63% from **MI-1061**) was obtained as white powder using the same synthetic strategy described for **LD-222**.

LC-MS(ESI) m/z $(M+H)^+$: 918.94; calcd for C50H50Cl2FN6O6 $(M+H)^+$ 919.32; >98% purity.

^{1}H NMR (400 MHz, MeOD) δ 7.73 (dd, *J* = 10.5, 3.9 Hz, 1H), 7.67 – 7.58 (m, 3H), 7.54 (dd, *J* = 8.2, 2.5 Hz, 1H), 7.49 – 7.42 (m, 2H), 7.41 – 7.32 (m, 3H), 7.19 (t, *J* = 8.1 Hz, 1H), 7.11 (dd, *J* = 8.2, 1.9 Hz, 1H), 6.79 (d, *J* = 1.9 Hz, 1H), 5.35 (d, *J* = 10.9 Hz, 1H), 5.17 (dd, *J* = 13.3, 5.1 Hz, 1H), 4.96 (d, *J* = 11.0 Hz, 1H), 4.68 – 4.55 (m, 1H), 4.48 (q, *J* = 17.0 Hz, 2H), 3.71 (d, *J* = 10.9 Hz, 1H), 3.11 – 2.68 (m, 7H), 2.53 (qd, *J* = 13.2, 4.6 Hz, 1H), 2.27 – 2.10 (m, 2H), 2.04 – 1.84 (m, 4H), 1.81 – 1.47 (m, 7H), 1.31 – 1.08 (m, 4H).

(3'R,4'S,5'R)-6''-chloro-4'-(3-chloro-2-fluorophenyl)-N-(4-(((1r,4R)-4-((2-(2,6-dioxopiperidin-3-yl)-1-oxoisoindolin-4-yl)ethynyl)cyclohexyl)carbamoyl)phenyl)-2''-oxodispiro[cyclohexane-1,2'-pyrrolidine-3',3''-indoline]-5'-carboxamide (LE-194)

LE-095 (18.1 mg, Yield: 68% from **MI-1061**) was obtained as white powder using the same synthetic strategy described for **LE-004**.

LC-MS(ESI) m/z $(M+H)^+$: 929.43; calcd for C51H48Cl2FN6O6 $(M+H)^+$ 929.30; >98% purity.

^{1}H NMR (400 MHz, MeOD) δ 7.85 – 7.69 (m, 4H), 7.69 – 7.58 (m, 3H), 7.57 – 7.44 (m, 2H), 7.37 (t, *J* = 7.0 Hz, 1H), 7.18 (t, *J* = 8.1 Hz, 1H), 7.11 (dd, *J* = 8.2, 1.9 Hz, 1H), 6.79 (d, *J* = 1.9 Hz, 1H), 5.31 (d, *J* = 10.7 Hz, 1H), 5.17 (dd, *J* = 13.3, 5.2 Hz, 1H), 4.96 (d, *J* = 10.9 Hz, 1H), 4.49 (q, *J* = 17.5 Hz, 2H), 3.96 – 3.75 (m, 1H), 2.99 – 2.70 (m, 3H), 2.63 – 2.44 (m, 2H), 2.28 – 2.08 (m, 4H), 2.07 – 1.84 (m, 5H), 1.78 (d, *J* = 11.4 Hz, 2H), 1.68 – 1.39 (m, 5H), 1.29 – 1.18 (m, 2H).

(3'R,4'S,5'R)-6''-chloro-4'-(3-chloro-2-fluorophenyl)-N-(4-(((1s,4R)-4-(2-(2-(2,6-dioxopiperidin-3-yl)-1-oxoisoindolin-4-yl)ethyl)cyclohexyl)carbamoyl)phenyl)-2''-oxodispiro[cyclohexane-1,2'-pyrrolidine-3',3''-indoline]-5'-carboxamide (LE-200)

LE-095 (21.5 mg, Yield: 80% from **MI-1061**) was obtained as white powder using the same synthetic strategy described for **LD-222**.

LC-MS(ESI) m/z $(M+H)^+$: 933.36; calcd for C51H52Cl2FN6O6 $(M+H)^+$ 933.33; >98% purity.

^{1}H NMR (400 MHz, MeOD) δ 7.82 – 7.75 (m, 2H), 7.74 – 7.68 (m, 1H), 7.68 – 7.60 (m, 3H), 7.51 (dd, *J* = 8.2, 2.4 Hz, 1H), 7.49 – 7.43 (m, 2H), 7.35 (dd, *J* = 11.0, 4.1 Hz, 1H), 7.16 (t, *J* = 8.1 Hz, 1H), 7.10 (dd, *J* = 8.2, 1.9 Hz, 1H), 6.78 (d, *J* = 1.9 Hz, 1H), 5.23 (d, *J* = 10.3 Hz, 1H), 5.17 (dd, *J* = 13.3, 5.1 Hz, 1H), 4.94 (d, *J* = 10.7 Hz, 1H), 4.49 (q, *J* = 16.9 Hz, 2H), 3.82 (ddd, *J* = 11.6, 8.0, 3.9 Hz, 1H),

2.99 – 2.68 (m, 5H), 2.54 (qd, *J* = 13.2, 4.6 Hz, 1H), 2.25 – 2.07 (m, 2H), 2.01 – 1.87 (m, 6H), 1.76 (t, *J* = 12.0 Hz, 2H), 1.66 – 1.49 (m, 3H), 1.42 – 1.25 (m, 4H), 1.25 – 1.08 (m, 4H).

(3'R,4'S,5'R)-6''-chloro-4'-(3-chloro-2-fluorophenyl)-N-(4-((3-(4-(((2-(2,6-dioxopiperidin-3-yl)-1-oxoisoindolin-4-yl)amino)methyl)-1H-imidazol-1-yl)propyl)carbamoyl)phenyl)-2''-oxodispiro[cyclohexane-1,2'-pyrrolidine-3',3''-indoline]-5'-carboxamide (LD-254)

LD-254 (30.6 mg, Yield: 90% from **MI-1061**) was obtained using the same synthetic strategy described for **LD-131**.

LC-MS(ESI) m/z $(M+H)^+$:960.28, 4.43 min; calcd for $C_{50}H_{49}Cl_2FN_9O_6$ $(M+H)^+$: 960.32; >98% purity.

^{1}H NMR (400 MHz, MeOD) δ 8.90 (s, 1H), 7.86 – 7.75 (m, 2H), 7.72 (t, *J* = 7.2 Hz, 1H), 7.67 – 7.56 (m, 3H), 7.52 (dd, *J* = 8.2, 2.4 Hz, 1H), 7.39 – 7.32 (m, 1H), 7.29 (t, *J* = 7.8 Hz, 1H), 7.21 – 7.12 (m, 2H), 7.11 (dd, *J* = 8.2, 1.9 Hz, 1H), 6.89 – 6.72 (m, 2H), 5.35 (d, *J* = 10.8 Hz, 1H), 5.15 (dt, *J* = 9.2, 4.9 Hz, 1H), 4.96 (dd, *J* = 10.9, 1.7 Hz, 1H), 4.53 (s, 2H), 4.41 – 4.29 (m, 2H), 4.25 (t, *J* = 6.7 Hz, 2H), 3.39 (t, *J* = 6.1 Hz, 2H), 2.97 – 2.71 (m, 3H), 2.46 (qd, *J* = 13.2, 4.7 Hz, 1H), 2.25 – 2.09 (m, 4H), 2.03 – 1.86 (m, 3H), 1.77 (d, *J* = 11.7 Hz, 2H), 1.66 – 1.47 (m, 1H), 1.27 – 1.12 (m, 2H).

(3'R,4'S,5'R)-6''-chloro-4'-(3-chloro-2-fluorophenyl)-N-(4-((3-(4-((2-(2,6-dioxopiperidin-3-yl)-1-oxoisoindolin-4-yl)ethynyl)-1H-pyrazol-1-yl)propyl)carbamoyl)phenyl)-2''-oxodispiro[cyclohexane-1,2'-pyrrolidine-3',3''-indoline]-5'-carboxamide (LE-243)

LE-243 (12.3 mg, Yield: 45% from **MI-1061**) was obtained using the same synthetic strategy described for **LE-004**.

LC-MS(ESI) m/z $(M+H)^+$:955.52; calcd for $C_{51}H_{46}Cl_2FN_8O_6$ $(M+H)^+$ 955.29; >98% purity.

^{1}H NMR (400 MHz, MeOD) δ 7.99 (d, *J* = 1.4 Hz, 1H), 7.83 – 7.74 (m, 3H), 7.74 – 7.66 (m, 3H), 7.63 (d, *J* = 8.6 Hz, 2H), 7.58 – 7.47 (m, 2H), 7.35 (t, *J* = 7.6 Hz, 1H), 7.17 (t, *J* = 8.0 Hz, 1H), 7.10 (dd, *J* = 8.2, 1.9 Hz, 1H), 6.78 (d, *J* = 1.9 Hz, 1H), 5.32 – 5.14 (m, 2H), 4.93 (d, *J* = 11.2 Hz, 1H), 4.55 (q, *J* = 17.6 Hz, 2H), 4.25 (t, *J* = 6.7 Hz, 2H), 3.39 (t, *J* = 6.6 Hz, 2H), 2.99 – 2.86 (m, 1H), 2.86 – 2.66 (m, 2H), 2.53 (qd, *J* = 13.2, 3.0 Hz, 1H), 2.24 – 2.10 (m, 4H), 2.02 – 1.82 (m, 3H), 1.82 – 1.67 (m, 2H), 1.55 (dd, *J* = 27.3, 13.7 Hz, 1H), 1.20 (t, *J* = 11.6 Hz, 2H).

(3'R,4'S,5'R)-6''-chloro-4'-(3-chloro-2-fluorophenyl)-N-(4-((3-(4-(2-(2-(2,6-dioxopiperidin-3-yl)-1-oxoisoindolin-4-yl)ethyl)-1H-pyrazol-1-yl)propyl)carbamoyl)phenyl)-2''-oxodispiro[cyclohexane-1,2'-pyrrolidine-3',3''-indoline]-5'-carboxamide (LE-244)

LE-244 (8.5 mg, Yield: 31% from **MI-1061**) was obtained using the same synthetic strategy described for **LD-222**.

LC-MS(ESI) m/z $(M+2H)^{2+}$:479.55; calcd for $C_{51}H_{51}Cl_2FN_8O_6$ $(M+2H)^{2+}$ 479.16; >98% purity.

^{1}H NMR (400 MHz, MeOD) δ 7.77 (dd, *J* = 8.9, 0.9 Hz, 2H), 7.74 – 7.67 (m, 1H), 7.66 – 7.58 (m, 3H), 7.54 (dd, *J* = 8.2, 2.5 Hz, 1H), 7.48 – 7.41 (m, 2H), 7.40 – 7.34 (m, 1H), 7.30 (s, 1H), 7.24 (s, 1H), 7.19 (dd, *J* = 8.5, 7.7 Hz, 1H), 7.12 (dd, *J* = 8.2, 2.0 Hz, 1H), 6.80 (d, *J* = 1.9 Hz, 1H), 5.35 (d, *J* = 10.9

Hz, 1H), 5.12 (ddd, *J* = 13.3, 5.1, 1.9 Hz, 1H), 4.97 (d, *J* = 11.0 Hz, 1H), 4.27 (q, *J* = 16.9 Hz, 2H), 4.12 (t, *J* = 6.7 Hz, 2H), 3.30 – 3.14 (m, 2H), 2.99 – 2.79 (m, 6H), 2.75 (ddd, *J* = 17.6, 4.5, 2.3 Hz, 1H), 2.46 (qd, *J* = 12.8, 4.0 Hz, 1H), 2.21 (d, *J* = 13.1 Hz, 1H), 2.16 – 2.08 (m, 1H), 2.08 – 1.89 (m, 5H), 1.78 (d, *J* = 11.9 Hz, 2H), 1.53 (q, *J* = 13.2 Hz, 1H), 1.24 (td, *J* = 14.2, 4.3 Hz, 2H).

(3'R,4'S,5'R)-6''-chloro-4'-(3-chloro-2-fluorophenyl)-N-(4-((2-(2-(2-((3-(2-(2,6-dioxopiperidin-3-yl)-1-oxoisoindolin-4-yl)prop-2-yn-1-yl)oxy)ethoxy)ethoxy)ethyl)carbamoyl)phenyl)-2''-oxodispiro[cyclohexane-1,2'-pyrrolidine-3',3''-indoline]-5'-carboxamide (LE-224)

LE-224 (17.2 mg, Yield: 60% from **MI-1061**) was obtained using the same synthetic strategy described for **LE-004**.

LC-MS(ESI) m/z $(M+2H)^{2+}$:496.68; calcd for C52H53Cl2FN6O9 $(M+2H)^{2+}$ 496.15; >98% purity.

^{1}H NMR (400 MHz, MeOD) δ 7.88 – 7.74 (m, 3H), 7.71 (t, *J* = 6.6 Hz, 1H), 7.67 – 7.55 (m, 3H), 7.55 – 7.43 (m, 2H), 7.40 – 7.30 (m, 1H), 7.18 (t, *J* = 8.1 Hz, 1H), 7.10 (dt, *J* = 8.2, 1.9 Hz, 1H), 6.79 (d, *J* = 1.9 Hz, 1H), 5.31 (d, *J* = 10.6 Hz, 1H), 5.16 (ddd, *J* = 13.2, 7.8, 5.2 Hz, 1H), 4.95 (dd, *J* = 10.9, 2.4 Hz, 1H), 4.48 (dd, *J* = 6.4, 3.9 Hz, 1H), 4.42 (d, *J* = 0.9 Hz, 2H), 3.90 – 3.38 (m, 12H), 3.03 – 2.70 (m, 3H), 2.57 – 2.38 (m, 1H), 2.17 (dd, *J* = 11.5, 6.5 Hz, 2H), 2.05 – 1.82 (m, 3H), 1.77 (d, *J* = 11.8 Hz, 2H), 1.61 – 1.46 (m, 1H), 1.41 – 1.01 (m, 3H).

(3'R,4'S,5'R)-6''-chloro-4'-(3-chloro-2-fluorophenyl)-N-(4-((5-(2-(2,6-dioxopiperidin-3-yl)-1-oxoisoindolin-5-yl)pent-4-yn-1-yl)carbamoyl)phenyl)-2''-oxodispiro[cyclohexane-1,2'-pyrrolidine-3',3''-indoline]-5'-carboxamide (LE-178)

LE-178 (18.1 mg, Yield: 71% from **MI-1061**) was obtained using the same synthetic strategy described for **LE-004**.

LC-MS(ESI) m/z $(M+H)^+$:889.38; calcd for $C_{48}H_{44}Cl_2FN_6O_6$ $(M+H)^+$ 889.27; >98% purity.

^{1}H NMR (400 MHz, MeOD) δ 7.82 – 7.74 (m, 2H), 7.71 (ddd, *J* = 6.4, 4.0, 1.5 Hz, 1H), 7.66 (dd, *J* = 7.9, 4.2 Hz, 1H), 7.61 – 7.46 (m, 4H), 7.38 (dt, *J* = 9.2, 8.4 Hz, 2H), 7.19 (t, *J* = 8.0 Hz, 1H), 7.15 – 7.06 (m, 1H), 6.80 (d, *J* = 1.9 Hz, 1H), 5.35 (dd, *J* = 10.8, 8.6 Hz, 1H), 5.24 – 5.08 (m, 1H), 4.96 (dd, *J* = 11.0, 3.8 Hz, 1H), 4.55 – 4.28 (m, 2H), 3.66 – 3.44 (m, 2H), 2.97 – 2.84 (m, 2H), 2.84 – 2.72 (m, 1H), 2.55 (t, *J* = 6.4 Hz, 2H), 2.53 – 2.40 (m, 1H), 2.27 – 2.10 (m, 2H), 2.04 – 1.87 (m, 5H), 1.78 (d, *J* = 12.3 Hz, 2H), 1.62 – 1.43 (m, 1H), 1.30 – 1.15 (m, 2H).

(3'R,4'S,5'R)-6''-chloro-4'-(3-chloro-2-fluorophenyl)-N-(4-((5-(2-(2,6-dioxopiperidin-3-yl)-3-oxoisoindolin-5-yl)pent-4-yn-1-yl)carbamoyl)phenyl)-2''-oxodispiro[cyclohexane-1,2'-pyrrolidine-3',3''-indoline]-5'-carboxamide (LE-179)

LE-179 (15.4 mg, Yield: 60% from **MI-1061**) was obtained using the same synthetic strategy described for **LE-004**.

LC-MS(ESI) m/z $(M+H)^+$:889.32; calcd for $C_{48}H_{44}Cl_2FN_6O_6$ $(M+H)^+$ 889.27; >98% purity.

^{1}H NMR (400 MHz, MeOD) δ 7.83 – 7.76 (m, 2H), 7.76 – 7.68 (m, 2H), 7.63 – 7.57 (m, 3H), 7.54 (dd, *J* = 8.3, 2.5 Hz, 1H), 7.49 (dd, *J* = 7.9, 1.0 Hz, 1H), 7.41 – 7.34 (m, 1H), 7.19 (t, *J* = 8.0 Hz, 1H), 7.12 (dd, *J* = 8.2, 1.9 Hz, 1H), 6.80 (d, *J* = 1.9 Hz, 1H), 5.36 (d, *J* = 10.9 Hz, 1H), 5.15 (ddd, *J* = 13.3, 5.1, 1.5 Hz, 1H), 4.97 (d, *J* = 11.0 Hz, 1H), 4.57 – 4.34 (m, 2H), 3.53 (t, *J* = 6.9 Hz, 2H), 2.90 (ddd, *J*

= 15.3, 10.3, 3.6 Hz, 2H), 2.78 (ddd, *J* = 17.6, 4.5, 2.3 Hz, 1H), 2.59 – 2.43 (m, 3H), 2.26 – 2.12 (m, 2H), 2.04 – 1.86 (m, 5H), 1.78 (d, *J* = 11.9 Hz, 2H), 1.53 (dd, *J* = 27.2, 13.4 Hz, 1H), 1.30 – 1.18 (m, 2H).

(3'R,4'S,5'R)-6''-chloro-4'-(3-chloro-2-fluorophenyl)-N-(4-((5-(2-(2,6-dioxopiperidin-3-yl)-1-oxoisoindolin-5-yl)pentyl)carbamoyl)phenyl)-2''-oxodispiro[cyclohexane-1,2'-pyrrolidine-3',3''-indoline]-5'-carboxamide (LE-180)

LE-180 (21.5 mg, Yield: 84% from **MI-1061**) was obtained using the same synthetic strategy described for **LD-222**.

LC-MS(ESI) m/z $(M+H)^+$:893.28; calcd for $C_{48}H_{48}Cl_2FN_6O_6$ $(M+H)^+$ 893.29964; >98% purity.

^{1}H NMR (400 MHz, MeOD) δ 7.76 – 7.69 (m, 3H), 7.66 – 7.63 (m, 1H), 7.63 – 7.58 (m, 2H), 7.54 (dd, *J* = 8.2, 2.5 Hz, 1H), 7.40 – 7.29 (m, 3H), 7.18 (t, *J* = 8.0 Hz, 1H), 7.11 (dd, *J* = 8.2, 1.9 Hz, 1H), 6.80 (d, *J* = 1.9 Hz, 1H), 5.35 (d, *J* = 10.8 Hz, 1H), 5.12 (dt, *J* = 13.3, 5.4 Hz, 1H), 4.98 (d, *J* = 10.9 Hz, 1H), 4.47 – 4.30 (m, 2H), 3.40 – 3.32 (m, 2H), 2.97 – 2.84 (m, 2H), 2.84 – 2.68 (m, 3H), 2.54 – 2.38 (m, 1H), 2.24 – 2.08 (m, 2H), 2.03 – 1.88 (m, 3H), 1.80 – 1.47 (m, 7H), 1.44 – 1.33 (m, 2H), 1.29 – 1.17 (m, 2H).

(3'R,4'S,5'R)-6''-chloro-4'-(3-chloro-2-fluorophenyl)-N-(4-((5-(2-(2,6-dioxopiperidin-3-yl)-3-oxoisoindolin-5-yl)pentyl)carbamoyl)phenyl)-2''-oxodispiro[cyclohexane-1,2'-pyrrolidine-3',3''-indoline]-5'-carboxamide (LE-181)

LE-181 (22.4 mg, Yield: 87% from **MI-1061**) was obtained using the same synthetic strategy described for **LD-222**.

LC-MS(ESI) m/z $(M+H)^+$:893.27; calcd for $C_{48}H_{48}Cl_2FN_6O_6$ $(M+H)^+$ 893.29964; >98% purity.

^{1}H NMR (400 MHz, MeOD) δ 7.78 – 7.68 (m, 3H), 7.65 – 7.57 (m, 3H), 7.53 (dd, *J* = 8.2, 2.5 Hz, 1H), 7.48 – 7.39 (m, 2H), 7.37 – 7.30 (m, 1H), 7.16 (t, *J* = 8.1 Hz, 1H), 7.10 (dd, *J* = 8.2, 1.9 Hz, 1H), 6.79 (d, *J* = 1.9 Hz, 1H), 5.34 (d, *J* = 10.8 Hz, 1H), 5.14 (ddd, *J* = 13.3, 5.1, 3.0 Hz, 1H), 4.96 (d, *J* = 10.9 Hz, 1H), 4.50 – 4.31 (m, 2H), 3.33 (t, *J* = 7.1 Hz, 2H), 2.97 – 2.65 (m, 5H), 2.48 (qd, *J* = 13.1, 4.5 Hz, 1H), 2.25 – 2.09 (m, 2H), 2.02 – 1.85 (m, 3H), 1.76 (d, *J* = 11.6 Hz, 2H), 1.72 – 1.48 (m, 5H), 1.43 – 1.32 (m, 2H), 1.27 – 1.14 (m, 2H).

(3'R,4'S,5'R)-6''-chloro-4'-(3-chloro-2-fluorophenyl)-N-(4-((5-(((S)-1-((2S,4R)-4-hydroxy-2-(((S)-1-(4-(4-methylthiazol-5-yl)phenyl)ethyl)carbamoyl)pyrrolidin-1-yl)-3,3-dimethyl-1-oxobutan-2-yl)amino)-5-oxopentyl)carbamoyl)phenyl)-2''-oxodispiro[cyclohexane-1,2'-pyrrolidine-3',3''-indoline]-5'-carboxamide (LE-175)

(2S,4R)-1-((S)-2-amino-3,3-dimethylbutanoyl)-4-hydroxy-N-((S)-1-(4-(4-methylthiazol-5-yl)phenyl)ethyl)pyrrolidine-2-carboxamide (**113**) was synthesized according to the publication from Crews Group. And then **LE-175** (21.3 mg, Yield: 67% from **MI-1061**) was synthesized with the same synthetic strategy described for **LD-186** from compound **113** instead of lenalidomide.

LC-MS(ESI) m/z $(M+H)^+$:1107.41, 5.765 min; calcd for $C_{58}H_{66}Cl_2FN_8O_7S$ $(M+H)^+$: 1107.41; >95% purity.

^{1}H NMR (400 MHz, MeOD) δ 9.01 (s, 1H), 7.88 – 7.74 (m, 2H), 7.72 (t, *J* = 6.5 Hz, 1H), 7.69 – 7.60 (m, 2H), 7.53 (dd, *J* = 8.4, 2.6 Hz, 1H), 7.47 – 7.30 (m, 5H), 7.19 (t, *J* = 8.1 Hz, 1H), 7.14 – 7.05 (m, 1H), 6.80 (d, *J* = 1.9 Hz, 1H), 5.38 (d, *J* = 11.0 Hz, 1H), 5.02 – 4.96 (m, 2H), 4.65 – 4.51 (m, 2H), 4.43 (s, 1H), 3.88 (d, *J* = 11.2 Hz, 1H), 3.74 (dd, *J* = 11.0, 3.9 Hz, 1H), 3.37 (t, *J* = 6.5 Hz, 2H), 2.95 (d, *J* = 8.1 Hz, 1H), 2.49 (s, 3H), 2.37 – 2.12 (m, 4H), 2.06 – 1.84 (m, 4H), 1.78 (d, *J* = 11.8 Hz, 2H), 1.72 – 1.59 (m, 4H), 1.55 – 1.42 (m, 4H), 1.36 – 1.14 (m, 2H), 1.03 (s, 9H).

(3'R,4'S,5'R)-6''-chloro-4'-(3-chloro-2-fluorophenyl)-N-(4-((2-(2-(3-(((S)-1-((2S,4R)-4-hydroxy-2-(((S)-1-(4-(4-methylthiazol-5-yl)phenyl)ethyl)carbamoyl)pyrrolidin-1-yl)-3,3-dimethyl-1-oxobutan-2-yl)amino)-3-oxopropoxy)ethoxy)ethyl)carbamoyl)phenyl)-2''-oxodispiro[cyclohexane-1,2'-pyrrolidine-3',3''-indoline]-5'-carboxamide (LE-176)

LE-176 (25.0 mg, Yield: 75% from **MI-1061**) was obtained using the same synthetic strategy described for **LE-175**.

LC-MS(ESI) m/z $(M+H)^+$:1167.64, 5.656 min; calcd for $C_{60}H_{70}Cl_2FN_8O_9S$ $(M+H)^+$: 1167.44; >95% purity.

^{1}H NMR (400 MHz, MeOD) δ 8.97 (s, 1H), 7.86 – 7.76 (m, 2H), 7.71 (dd, *J* = 10.4, 3.9 Hz, 1H), 7.66 – 7.58 (m, 2H), 7.53 (dd, *J* = 8.2, 2.5 Hz, 1H), 7.47 – 7.30 (m, 5H), 7.19 (t, *J* = 8.1 Hz, 1H), 7.10 (dd, *J* = 8.2, 1.9 Hz, 1H), 6.79 (d, *J* = 1.9 Hz, 1H), 5.38 (d, *J* = 10.9 Hz, 1H), 5.00 – 4.95 (m, 2H), 4.64 (s, 1H), 4.57 (dd, *J* = 11.9, 4.6 Hz, 1H), 4.42 (s, 1H), 3.86 (d, *J* = 11.2 Hz, 1H), 3.76 – 3.53 (m, 11H), 2.94 (d, *J* = 8.9 Hz, 1H), 2.62 – 2.40 (m, 5H), 2.26 – 2.09 (m, 2H), 2.04 – 1.86 (m, 4H), 1.78 (d, *J* = 11.9 Hz, 2H), 1.63 – 1.38 (m, 4H), 1.32 – 1.17 (m, 2H), 1.01 (s, 9H).

(3'R,4'S,5'R)-6''-chloro-4'-(3-chloro-2-fluorophenyl)-N-(4-(((S)-14-((2S,4R)-4-hydroxy-2-(((S)-1-(4-(4-methylthiazol-5-yl)phenyl)ethyl)carbamoyl)pyrrolidine-1-carbonyl)-15,15-dimethyl-12-oxo-3,6,9-trioxa-13-azahexadecyl)carbamoyl)phenyl)-2''-oxodispiro[cyclohexane-1,2'-pyrrolidine-3',3''-indoline]-5'-carboxamide (LE-177)

LE-177 (23.9 mg, Yield: 69% from **MI-1061**) was obtained using the same synthetic strategy described for **LE-175**.

LC-MS(ESI) m/z $(M+2H)^{2+}$:606.31, calcd for $C_{62}H_{75}Cl_2FN_8O_{10}S$ $(M+2H)^{2+}$: 606.23; >95% purity.

^{1}H NMR (400 MHz, MeOD) δ 8.94 (s, 1H), 7.87 – 7.76 (m, 2H), 7.76 – 7.66 (m, 1H), 7.66 – 7.57 (m, 2H), 7.54 (dd, *J* = 8.2, 2.5 Hz, 1H), 7.46 – 7.32 (m, 5H), 7.18 (t, *J* = 8.1 Hz, 1H), 7.11 (dd, *J* = 8.2, 2.0 Hz, 1H), 6.79 (d, *J* = 1.9 Hz, 1H), 5.36 (d, *J* = 10.9 Hz, 1H), 5.04 – 4.95 (m, 2H), 4.64 (s, 1H), 4.57 (dd, *J* = 9.9, 6.7 Hz, 1H), 4.43 (d, *J* = 1.8 Hz, 1H), 3.86 (d, *J* = 11.0 Hz, 1H), 3.76 – 3.53 (m, 15H), 2.94 (d, *J* = 8.7 Hz, 1H), 2.62 – 2.36 (m, 5H), 2.28 – 2.07 (m, 2H), 2.03 – 1.83 (m, 4H), 1.78 (d, *J* = 12.1 Hz, 2H), 1.61 – 1.44 (m, 4H), 1.29 – 1.18 (m, 2H), 1.02 (s, 9H).

(3'R,4'S,5'R)-6''-chloro-4'-(3-chloro-2-fluorophenyl)-N-(4-(((S)-17-((2S,4R)-4-hydroxy-2-(((S)-1-(4-(4-methylthiazol-5-yl)phenyl)ethyl)carbamoyl)pyrrolidine-1-carbonyl)-18,18-dimethyl-15-oxo-3,6,9,12-tetraoxa-16-azanonadecyl)carbamoyl)phenyl)-2''-oxodispiro[cyclohexane-1,2'-pyrrolidine-3',3''-indoline]-5'-carboxamide (LE-334)

LE-334 (19.5 mg, Yield: 54% from **MI-1061**) was obtained using the same synthetic strategy described for **LE-175**.

LC-MS(ESI) m/z $(M+2H)^{2+}$:628.18, calcd for $C_{64}H_{79}Cl_2FN_8O_{11}S$ $(M+2H)^{2+}$: 628.25; >95% purity.

^{1}H NMR (400 MHz, Methanol-d_4) δ 9.13 (s, 1H), 7.85 – 7.76 (m, 2H), 7.72 (ddd, *J* = 7.9, 6.3, 1.5 Hz, 1H), 7.68 – 7.58 (m, 2H), 7.54 (dd, *J* = 8.2, 2.5 Hz, 1H), 7.47 – 7.42 (m, 3H), 7.41 – 7.35 (m, 1H), 7.24 – 7.16 (m, 1H), 7.12 (dd, *J* = 8.2, 2.0 Hz, 1H), 6.80 (d, *J* = 1.9 Hz, 1H), 5.36 (d, *J* = 11.0 Hz, 1H), 5.03 – 4.96 (m, 2H), 4.72 – 4.59 (m, 1H), 4.57 (t, *J* = 8.4 Hz, 1H), 4.43 (s, 1H), 3.87 (d, *J* = 11.0 Hz, 1H), 3.76 – 3.54 (m, 19H), 2.97 (d, *J* = 9.8 Hz, 1H), 2.65 – 2.36 (m, 5H), 2.20 (t, *J* = 11.6 Hz, 2H), 2.07 – 1.89 (m, 4H), 1.79 (d, *J* = 12.9 Hz, 2H), 1.61 – 1.41 (m, 4H), 1.35 – 1.18 (m, 3H), 1.03 (s, 9H).

(3'R,4'S,5'R)-6''-chloro-4'-(3-chloro-2-fluorophenyl)-N-(4-((5-(2-(1-methyl-2,6-dioxopiperidin-3-yl)-1-oxoisoindolin-4-yl)pent-4-yn-1-yl)carbamoyl)phenyl)-2''-oxodispiro[cyclohexane-1,2'-pyrrolidine-3',3''-indoline]-5'-carboxamide (LE-157)

LE-157 (26 mg, Yield: 98% from **MI-1061**) was obtained as white powder using the same synthetic strategy described for **LE-004**.

LC-MS(ESI) m/z $(M+H)^+$: 903.35; calcd for $C_{49}H_{46}Cl_2FN_6O_6$ $(M+H)^+$: 903.28; >98% purity.

^{1}H NMR (400 MHz, Methanol-d_4) δ 7.76 – 7.68 (m, 3H), 7.68 – 7.62 (m, 1H), 7.56 (ddd, *J* = 8.3, 2.7, 1.3 Hz, 1H), 7.53 – 7.44 (m, 3H), 7.44 – 7.33 (m, 2H), 7.23 – 7.15 (m, 1H), 7.11 (dd, *J* = 8.2, 2.0 Hz, 1H), 6.79 (d, *J* = 1.9 Hz, 1H), 5.32 (d, *J* = 10.8 Hz, 1H), 5.15 (dt, *J* = 13.5, 4.7 Hz, 1H), 4.98 (d, *J* = 10.8 Hz, 1H), 4.41 – 4.27 (m, 2H), 3.57 (t, *J* = 6.7 Hz, 2H), 3.09 (d, *J* = 5.9 Hz, 3H), 2.96 – 2.89 (m, 2H), 2.58 (t, *J* = 6.5 Hz, 2H), 2.55 – 2.38 (m, 1H), 2.29 – 2.08 (m, 2H), 2.04 – 1.87 (m, 5H), 1.78 (d, *J* = 13.2 Hz, 2H), 1.62 – 1.49 (m, 1H), 1.33 – 1.14 (m, 3H).

(3'S,4'R,5'S)-6''-chloro-4'-(3-chloro-2-fluorophenyl)-N-(4-((5-(2-(2,6-dioxopiperidin-3-yl)-1-oxoisoindolin-4-yl)pent-4-yn-1-yl)carbamoyl)phenyl)-2''-oxodispiro[cyclohexane-1,2'-pyrrolidine-3',3''-indoline]-5'-carboxamide (LE-154)

LE-154 (27.9 mg, Yield: 87% from **4-((3'S,4'R,5'S)-6''-chloro-4'-(3-chloro-2-fluorophenyl)-2''-oxodispiro[cyclohexane-1,2'-pyrrolidine-3',3''-indoline]-5'-carboxamido)benzoic acid[11]**) was obtained as white powder using the same synthetic strategy described for **LE-004**.

LC-MS(ESI) m/z $(M+H)^+$: 903.35; calcd for $C_{49}H_{46}Cl_2FN_6O_6$ $(M+H)^+$: 903.28; >98% purity.

^{1}H NMR (400 MHz, Methanol-d_4) δ 7.75 – 7.68 (m, 3H), 7.64 (ddd, *J* = 12.7, 7.6, 1.1 Hz, 1H), 7.56 (dd, *J* = 8.2, 2.6 Hz, 1H), 7.52 – 7.46 (m, 2H), 7.46 – 7.42 (m, 1H), 7.41 – 7.31 (m, 2H), 7.19 (tdd, *J* = 8.2, 3.5, 1.1 Hz, 1H), 7.12 (dd, *J* = 8.2, 2.0 Hz, 1H), 6.80 (d, *J* = 2.0 Hz, 1H), 5.36 (dd, *J* = 10.8, 1.4 Hz, 1H), 5.13 (ddd, *J* = 13.1, 7.8, 5.1 Hz, 1H), 4.99 (dd, *J* = 10.9, 1.7 Hz, 1H), 4.41 – 4.31 (m, 2H), 3.57 (t, *J* = 6.6 Hz, 2H), 2.98 – 2.84 (m, 2H), 2.84 – 2.70 (m, 1H), 2.62 – 2.43 (m, 3H), 2.29 – 2.11 (m, 2H), 2.05 – 1.87 (m, 5H), 1.79 (d, *J* = 13.2 Hz, 2H), 1.62 – 1.48 (m, 1H), 1.25 (t, *J* = 13.5 Hz, 2H).

(3'R,4'S,5'R)-6''-chloro-4'-(3-chloro-2-fluorophenyl)-N-((1r,4R)-4-(methylcarbamoyl)cyclohexyl)-2''-oxodispiro[cyclohexane-1,2'-pyrrolidine-3',3''-indoline]-5'-carboxamide (HXA-110)

The synthetic strategy of the MDM2 inhibitors was previously reported.

Reaction 1:

In a roundbottom flask, (E)-6-chloro-3-(3-chloro-2-fluorobenzylidene)indolin-2-one (500 mg, 1.62 mmol), (5R,6S)-5,6-diphenyl-2-morpholinone (492 mg, 1.94 mmol), and cyclohexanone (0.51 mL, 4.9 mmol) were suspended in toluene (10 mL) and heated at reflux for 2 h at 140 °C. Then the reaction was cooled to room temperature and the solvent was removed under vacuum. The crude product was purified by column chromatography to give **108a** as a pale yellow solid.

Reaction 2:

Then crude product of **108a** was dissolved in 10 mL MeOH and 1 mL conc. sulfuric acid was slowly added to the reaction. After 2h, the solvent was slowly removed during 30 min by vacuum and the reaction was quenched by adding saturated sodium bicarbonate solution (30 mL) and product **109a** was extracted by DCM (30mL *3). The combined organic solution was washed by brine, dried by sodium sulfate and crude **109a** was obtained by removing solvent under vacuum.

Reaction 3:

Cerium ammonium nitrate (1.83 g, 3.3 mmol) was added to a solution of the resulting **109a** in MeCN (13 mL) and stirred for 5 min at room temperature, then H2O (13 mL) was added. After stirring the reaction for an additional 10 min, it was quenched with saturated sodium bicarbonate, brine was added, and the solution was extracted with EtOAc. The EtOAc solution was dried over sodium sulfate and concentrated under vacuum to obtain the diastereisomers of

products. The crude material was dissolved in a 3:1 mixture of MeOH/H2O that was acidified with trifluoroacetic acid and aged for 2 days. Then the product was purified by reverse phase C18 column to afford **110a**.

Reaction 4:

110a (450 mg, 0.89 mmol) was dissolved in THF (2.2 mL) and lithium hydroxide monohydrate (112 mg, 2.7 mmol) was added followed by water (2.2 mL) and methanol (0.3 mL). After 2 hours, water (3.5 mL) was added and the reaction was slowly neutralized with 2M hydrochloric acid and the suspension was stirred for 15 min in ice-bath. The resulting precipitate was filtered, washed with cold water and then with ether. The solid was then dried in desiccators under vacuum to produce the product **111a**.

Reaction 5:

HATU (100 mg, 0.26 eq.) and N,N-Diisopropylethylamine (0.12 mL, 0.66 mmol) were added to a solution of **111a** (100 mg, 0.22 mmol) in 3 mL DMF and stirred. After 10 minutes, trans-methyl 4-aminocyclohexanecarboxylate (52 mg, 0.33 mmol) was added to the reaction. After 30 minutes, the solvent was removed and the crude was dissolved in 3:1 methanol/water, acidified with trifluoroacetic acid and purified by reverse phase C18 column to afford to give **112a**.

Reaction 6:

112a (50 mg, 0.085 mmol) was dissolved in THF (1 mL) and lithium hydroxide monohydrate (14 mg, 0.27 mmol) was added followed by water (1 mL) and methanol (0.15 mL). After 2 hours, the

reaction was acidified by trifluoroacetic acid and purified by reverse phase C18 column to afford to give product. Then the product (20mg, 0.034 mmol was dissolved in 0.5 mL DMF. HATU (15 mg, 0.039) and N,N-Diisopropylethylamine (0.026 mL, 0.15 mmol) dissolved in DMF (0.5 mL) was added to the reaction After 10 minutes, methylamine hydrochloride (4.5 mL, 0.068 mmol) was added to the reaction. After 30 minutes, the solvent was removed and the crude was dissolved in 3:1 methanol/water, acidified with trifluoroacetic acid and purified by reverse-phase preparative HPLC. The purified fractions were combined, concentrated in vacuo, re-dissolved in H2O, frozen and lyophilized to give **HXA-110** (14.2 mg, Yield: 69%) as white powder.

LC-MS(ESI) /z $(M+H)^+$:600.98, calcd for C31H36Cl2FN4O3 $(M+H)^+$ 601.21; >95% purity.

^{1}H NMR (400 MHz, MeOD) δ 7.64 (t, *J* = 7.2 Hz, 1H), 7.48 (dd, *J* = 8.2, 2.0 Hz, 1H), 7.39 (dd, *J* = 11.0, 4.2 Hz, 1H), 7.16 (t, *J* = 8.1 Hz, 1H), 7.10 (dd, *J* = 8.2, 1.9 Hz, 1H), 6.79 (d, *J* = 1.8 Hz, 1H), 5.09 (d, *J* = 11.1 Hz, 1H), 4.78 (d, *J* = 11.2 Hz, 1H), 3.64 (dd, *J* = 13.6, 9.6 Hz, 1H), 2.85 (d, *J* = 9.5 Hz, 1H), 2.67 (s, 3H), 2.19 (d, *J* = 13.7 Hz, 1H), 2.10 – 1.59 (m, 10H), 1.59 – 1.41 (m, 3H), 1.32 – 1.13 (m, 3H), 0.87 (ddd, *J* = 25.4, 12.8, 3.4 Hz, 1H).

(3'R,4'R,5'R)-6''-chloro-4'-(3-chlorophenyl)-N-((1r,4R)-4-(methylcarbamoyl)cyclohexyl)-2''-oxodispiro[cyclohexane-1,2'-pyrrolidine-3',3''-indoline]-5'-carboxamide (LE-211)

LE-211 (15.3 mg, Yield: 74%) was obtained using the same synthetic strategy described for **HXA-109**.

LC-MS(ESI) m/z $(M+H)^+$:583.01, calcd for C31H37Cl2N4O3 $(M+H)^+$ 583.22; >95% purity.

^{1}H NMR (400 MHz, MeOD) δ 7.56 (d, *J* = 8.2 Hz, 1H), 7.34 (s, 1H), 7.25 (dt, *J* = 7.5, 1.9 Hz, 1H), 7.22 – 7.13 (m, 2H), 7.10 (dd, *J* = 8.2, 2.0 Hz, 1H), 6.76 (d, *J* = 1.9 Hz, 1H), 5.13 (d, *J* = 11.1 Hz, 1H), 4.35 (d, *J* = 11.1 Hz, 1H), 3.74 – 3.52 (m, 1H), 2.84 (d, *J* = 10.9 Hz, 1H), 2.67 (s, 3H), 2.19 (d, *J* = 12.9 Hz, 1H), 2.08 – 1.70 (m, 9H), 1.63 (dd, *J* = 9.1, 3.6 Hz, 1H), 1.58 – 1.39 (m, 3H), 1.29 – 1.12 (m, 3H), 0.96 – 0.83 (m, 1H).

(3'R,4'S,5'R)-6''-chloro-4'-(2-fluorophenyl)-N-((1r,4R)-4-(methylcarbamoyl)cyclohexyl)-2''-oxodispiro[cyclohexane-1,2'-pyrrolidine-3',3''-indoline]-5'-carboxamide (HXA-119)

HXA-119 (13.6 mg, Yield: 66%) was obtained using the same synthetic strategy described for **HXA-109**.

LC-MS(ESI) m/z $(M+H)^+$:567.05, calcd for $C_{31}H_{37}ClFN_4O_3$ $(M+H)^+$ 567.25; >95% purity.

^{1}H NMR (400 MHz, MeOD) δ 7.56 (d, *J* = 8.2 Hz, 1H), 7.20 (td, *J* = 8.0, 6.2 Hz, 1H), 7.14 – 7.05 (m, 2H), 7.04 – 6.90 (m, 2H), 6.75 (d, *J* = 1.9 Hz, 1H), 5.15 (d, *J* = 11.1 Hz, 1H), 4.37 (d, *J* = 11.1 Hz, 1H), 3.74 – 3.51 (m, 1H), 2.85 (d, *J* = 12.5 Hz, 1H), 2.67 (s, 3H), 2.19 (d, *J* = 13.0 Hz, 1H), 2.08 – 1.69 (m, 9H), 1.63 – 1.42 (m, 4H), 1.28 – 1.13 (m, 3H), 0.89 (ddd, *J* = 25.1, 12.8, 3.6 Hz, 1H).

(3'R,4'R,5'R)-6''-chloro-N-((1r,4R)-4-(methylcarbamoyl)cyclohexyl)-2''-oxo-4'-phenyldispiro[cyclohexane-1,2'-pyrrolidine-3',3''-indoline]-5'-carboxamide (LE-217)

LE-217 (13.2 mg, Yield: 64%) was obtained using the same synthetic strategy described for **HXA-109**.

LC-MS(ESI) m/z $(M+H)^+$:549.01, calcd for $C_{31}H_{38}ClN_4O_3$ $(M+H)^+$549.26; >95% purity.

^{1}H NMR (400 MHz, MeOD) δ 7.56 (d, *J* = 8.2 Hz, 1H), 7.31 – 7.14 (m, 5H), 7.09 (dd, *J* = 8.2, 1.9 Hz, 1H), 6.72 (d, *J* = 1.9 Hz, 1H), 5.20 (d, *J* = 11.2 Hz, 1H), 4.31 (d, *J* = 11.2 Hz, 1H), 3.61 (tt, *J* = 11.7, 3.8 Hz, 1H), 2.85 (d, *J* = 12.3 Hz, 1H), 2.66 (s, 3H), 2.20 (d, *J* = 12.3 Hz, 1H), 2.06 – 1.65 (m, 9H), 1.58 – 1.32 (m, 4H), 1.29 – 1.13 (m, 3H), 0.85 (ddd, *J* = 25.1, 12.9, 3.8 Hz, 1H).

(3R,4'R,5'R)-6-chloro-2',2'-dimethyl-N-((1r,4R)-4-(methylcarbamoyl)cyclohexyl)-2-oxo-4'-phenylspiro[indoline-3,3'-pyrrolidine]-5'-carboxamide (HXA-120)

HXA-120 (14.1 mg, Yield: 69%) was obtained using the same synthetic strategy described for **HXA-109**.

LC-MS(ESI) m/z $(M+H)^+$:509.03, calcd for $C_{28}H_{34}ClN_4O_3$ $(M+H)^+$ 509.23; >95% purity.

^{1}H NMR (400 MHz, MeOD) δ 7.58 (d, *J* = 7.6 Hz, 1H), 7.33 – 7.14 (m, 5H), 7.10 (t, *J* = 7.6 Hz, 1H), 6.71 (d, *J* = 7.8 Hz, 1H), 5.18 (dd, *J* = 11.2, 3.0 Hz, 1H), 4.37 (d, *J* = 11.2 Hz, 1H), 3.67 – 3.49 (m, 1H), 2.66 (s, 3H), 2.06 – 1.90 (m, 4H), 1.76 (dd, *J* = 40.9, 13.3 Hz, 2H), 1.64 – 1.25 (m, 7H), 1.18 (dd, *J* = 25.1, 13.0 Hz, 1H), 0.88 (dd, *J* = 24.9, 12.3 Hz, 1H).

(3'R,4'S,5'R)-6''-chloro-4'-(3-chloro-2-fluorophenyl)-N-((1r,4R)-4-((5-(2-(2,6-dioxopiperidin-3-yl)-1,3-dioxoisoindolin-4-yl)pent-4-yn-1-yl)carbamoyl)cyclohexyl)-2''-oxodispiro[cyclohexane-1,2'-pyrrolidine-3',3''-indoline]-5'-carboxamide (AA-231)

AA-231 (15.7 mg, Yield: 61%) was obtained using the same synthetic strategy described for **LE-004**.

LC-MS(ESI) m/z $(M+H)^+$:895.00, calcd for $C_{48}H_{50}Cl_2FN_6O_6$ $(M+H)^+$ 895.31; >95% purity.

^{1}H NMR (400 MHz, Methanol-d_4) δ 7.74 (dd, *J* = 7.6, 1.0 Hz, 1H), 7.70 – 7.55 (m, 2H), 7.55 – 7.44 (m, 2H), 7.39 (ddd, *J* = 8.5, 7.2, 1.6 Hz, 1H), 7.17 (td, *J* = 8.0, 1.1 Hz, 1H), 7.10 (ddd, *J* = 8.2, 2.0, 0.8 Hz, 1H), 6.79 (d, *J* = 1.9 Hz, 1H), 5.19 (dd, *J* = 13.4, 5.2 Hz, 1H), 5.15 – 5.03 (m, 1H), 4.79 (dd, *J* = 11.1, 1.6 Hz, 1H), 4.51 (q, *J* = 17.7 Hz, 2H), 3.69 – 3.54 (m, 1H), 3.42 – 3.32 (m, 2H), 3.01 – 2.74 (m, 3H), 2.67 – 2.45 (m, 3H), 2.25 – 2.13 (m, 2H), 2.07 – 1.73 (m, 10H), 1.67 – 1.59 (m, 1H), 1.58 – 1.41 (m, 3H), 1.37 (dd, *J* = 6.7, 3.6 Hz, 1H), 1.28 – 1.11 (m, 3H), 0.95 – 0.77 (m, 1H).

(3'R,4'R,5'R)-6''-chloro-4'-(3-chlorophenyl)-N-((1r,4R)-4-((5-(2-(2,6-dioxopiperidin-3-yl)-1,3-dioxoisoindolin-4-yl)pent-4-yn-1-yl)carbamoyl)cyclohexyl)-2''-oxodispiro[cyclohexane-1,2'-pyrrolidine-3',3''-indoline]-5'-carboxamide (LE-297)

LE-297 (11.4 mg, Yield: 45 %) was obtained using the same synthetic strategy described for **LE-004**.

LC-MS(ESI) m/z (M +H)$^+$:876.98, calcd for C48H51Cl2N6O6 (M +H)$^+$ 877.32; >95% purity.

^{1}H NMR (400 MHz, MeOD) δ 7.74 (dd, *J* = 7.6, 0.8 Hz, 1H), 7.65 – 7.52 (m, 2H), 7.49 (t, *J* = 7.6 Hz, 1H), 7.34 (d, *J* = 1.6 Hz, 1H), 7.26 (dt, *J* = 7.4, 1.6 Hz, 1H), 7.22 – 7.14 (m, 2H), 7.11 (dt, *J* = 8.2, 2.0 Hz, 1H), 6.76 (d, *J* = 1.9 Hz, 1H), 5.20 (ddd, *J* = 13.3, 5.1, 1.4 Hz, 1H), 5.12 (dd, *J* = 11.1, 1.4 Hz, 1H), 4.51 (q, *J* = 17.7 Hz, 2H), 4.37 (dd, *J* = 11.1, 6.0 Hz, 1H), 3.71 – 3.53 (m, 1H), 3.40 – 3.26 (m, 2H), 3.00 – 2.74 (m, 3H), 2.65 – 2.46 (m, 3H), 2.31 – 2.13 (m, 2H), 2.13 – 1.64 (m, 11H), 1.64 – 1.39 (m, 4H), 1.30 – 1.13 (m, 3H), 0.93 – 0.81 (m, 1H).

(3'R,4'S,5'R)-6''-chloro-N-((1r,4R)-4-((5-(2-(2,6-dioxopiperidin-3-yl)-1,3-dioxoisoindolin-4-yl)pent-4-yn-1-yl)carbamoyl)cyclohexyl)-4'-(2-fluorophenyl)-2''-oxodispiro[cyclohexane-1,2'-pyrrolidine-3',3''-indoline]-5'-carboxamide (LE-295)

LE-295 (13.7 mg, Yield: 55%) was obtained using the same synthetic strategy described for **LE-004**.

LC-MS(ESI) m/z $(M+H)^+$:861.05, calcd for C48H51ClFN6O6 $(M+H)^+$ 861.35; >95% purity.

^{1}H NMR (400 MHz, MeOD) δ 7.74 (d, *J* = 7.6 Hz, 1H), 7.70 – 7.52 (m, 2H), 7.48 (t, *J* = 7.6 Hz, 1H), 7.20 (dd, *J* = 14.1, 7.8 Hz, 1H), 7.10 (dd, *J* = 8.3, 1.8 Hz, 2H), 7.05 – 6.86 (m, 2H), 6.75 (d, *J* = 1.8 Hz, 1H), 5.20 (dd, *J* = 13.0, 4.8 Hz, 1H), 5.14 (dd, *J* = 11.1, 1.2 Hz, 1H), 4.51 (q, *J* = 17.7 Hz, 2H), 4.39 (dd, *J* = 11.1, 5.6 Hz, 1H), 3.60 (ddd, *J* = 15.4, 7.8, 3.9 Hz, 1H), 3.43 – 3.23 (m, 2H), 3.02 – 2.72 (m, 3H), 2.66 – 2.39 (m, 3H), 2.18 (dd, *J* = 11.2, 3.6 Hz, 2H), 2.09 – 1.65 (m, 11H), 1.63 – 1.36 (m, 4H), 1.31 – 1.11 (m, 3H), 0.94 – 0.78 (m, 1H).

(3'R,4'R,5'R)-6''-chloro-N-((1r,4R)-4-((5-(2-(2,6-dioxopiperidin-3-yl)-1,3-dioxoisoindolin-4-yl)pent-4-yn-1-yl)carbamoyl)cyclohexyl)-2''-oxo-4'-phenyldispiro[cyclohexane-1,2'-pyrrolidine-3',3''-indoline]-5'-carboxamide (LE-298)

LE-298 (18.3 mg, Yield: 75%) was obtained using the same synthetic strategy described for **LE-004**.

LC-MS(ESI) m/z $(M+H)^+$:843.03, calcd for C48H52ClN6O6 $(M+H)^+$ 843.36; >95% purity.

^{1}H NMR (400 MHz, MeOD) δ 7.73 (d, *J* = 7.6 Hz, 1H), 7.63 – 7.53 (m, 2H), 7.48 (t, *J* = 7.6 Hz, 1H), 7.30 – 7.15 (m, 5H), 7.09 (dt, *J* = 8.2, 1.6 Hz, 1H), 6.72 (d, *J* = 1.8 Hz, 1H), 5.27 – 5.08 (m, 2H), 4.50 (q, *J* = 17.8 Hz, 2H), 4.33 (dd, *J* = 11.2, 5.3 Hz, 1H), 3.59 (ddd, *J* = 11.8, 8.0, 4.0 Hz, 1H), 3.40 – 3.22 (m, 2H), 3.02 – 2.76 (m, 3H), 2.60 (ddt, *J* = 13.3, 10.0, 5.1 Hz, 1H), 2.50 (t, *J* = 6.7 Hz, 2H), 2.26 – 2.11 (m, 2H), 2.05 – 1.65 (m, 11H), 1.61 – 1.35 (m, 4H), 1.29 – 1.10 (m, 3H), 0.92 – 0.72 (m, 1H).

(3R,4'R,5'R)-6-chloro-N-((1r,4R)-4-((5-(2-(2,6-dioxopiperidin-3-yl)-1,3-dioxoisoindolin-4-yl)pent-4-yn-1-yl)carbamoyl)cyclohexyl)-2',2'-dimethyl-2-oxo-4'-phenylspiro[indoline-3,3'-pyrrolidine]-5'-carboxamide (LE-296)

LE-296 (10.0 mg, Yield: 43%) was obtained using the same synthetic strategy described for **LE-004**.

LC-MS(ESI) m/z $(M+H)^+$:803.03, calcd for $C_{45}H_{48}ClN_6O_6$ $(M+H)^+$ 803.33; >95% purity.

^{1}H NMR (400 MHz, MeOD) δ 7.74 (d, *J* = 7.5 Hz, 1H), 7.68 – 7.54 (m, 2H), 7.48 (t, *J* = 7.6 Hz, 1H), 7.37 – 7.14 (m, 5H), 7.14 – 6.98 (m, 1H), 6.73 (d, *J* = 1.9 Hz, 1H), 5.29 – 5.09 (m, 2H), 4.51 (q, *J* = 17.7 Hz, 2H), 4.38 (dd, *J* = 11.2, 5.3 Hz, 1H), 3.59 (ddd, *J* = 11.7, 7.5, 3.6 Hz, 1H), 3.39 – 3.25 (m, 2H), 3.02 – 2.74 (m, 2H), 2.66 – 2.41 (m, 3H), 2.25 – 2.11 (m, 1H), 2.09 – 1.86 (m, 5H), 1.86 – 1.66 (m, 4H), 1.58 – 1.28 (m, 6H), 1.16 (ddd, *J* = 25.2, 12.8, 3.5 Hz, 1H), 0.92 – 0.77 (m, 1H).

(3'R,4'S,5'R)-6''-chloro-4'-(3-chloro-2-fluorophenyl)-N-methyl-2''-oxodispiro[cyclohexane-1,2'-pyrrolidine-3',3''-indoline]-5'-carboxamide (LD-103)

LD-103 (15.1 mg, Yield: 74%) was obtained as white powder using the same synthetic strategy described for **LD-222**.

LC-MS(ESI) m/z $(M+H)^+$:476.32, calcd for $C_{24}H_{25}Cl_2FN_3O_2$ $(M+H)^+$ 476.13; >95% purity.

^{1}H NMR (400 MHz, Methanol-d_4) δ 7.63 (ddd, *J* = 8.0, 6.3, 1.6 Hz, 1H), 7.52 (dd, *J* = 8.2, 2.7 Hz, 1H), 7.38 (td, *J* = 7.7, 7.3, 1.6 Hz, 1H), 7.17 (td, *J* = 8.0, 1.2 Hz, 1H), 7.11 (dd, *J* = 8.2, 2.0 Hz, 1H), 6.77 (d, *J* = 2.0 Hz, 1H), 5.15 (d, *J* = 10.9 Hz, 1H), 4.83 (d, *J* = 11.0 Hz, 1H), 2.91 – 2.80 (m, 1H), 2.80 – 2.67 (m, 3H), 2.17 (dd, *J* = 14.4, 3.1 Hz, 1H), 2.04 – 1.82 (m, 3H), 1.81 – 1.68 (m, 2H), 1.62 – 1.41 (m, 1H), 1.28 – 1.14 (m, 2H).

(3'R,4'S,5'R)-6''-chloro-4'-(3-chloro-2-fluorophenyl)-N-(3-(2-(2,6-dioxopiperidin-3-yl)-1-oxoisoindolin-4-yl)propyl)-2''-oxodispiro[cyclohexane-1,2'-pyrrolidine-3',3''-indoline]-5'-carboxamide (LE-010)

LE-010 (7.8 mg, Yield: 48%) was obtained as white powder using the same synthetic strategy described for **LD-222**.

LC-MS(ESI) m/z $(M+H)^+$:746.45, calcd for $C_{39}H_{39}Cl_2FN_5O_5$ $(M+H)^+$ 746.23; >95% purity.

^{1}H NMR (400 MHz, Methanol-d_4) δ 7.73 – 7.58 (m, 2H), 7.50 (dd, *J* = 8.3, 2.5 Hz, 1H), 7.43 (td, *J* = 7.6, 2.1 Hz, 1H), 7.34 (dddd, *J* = 8.6, 7.3, 5.7, 1.6 Hz, 1H), 7.24 (ddd, *J* = 7.6, 5.4, 1.0 Hz, 1H), 7.18 (tt, *J* = 8.1, 1.2 Hz, 1H), 7.13 – 7.06 (m, 1H), 6.78 (d, *J* = 1.9 Hz, 1H), 5.26 – 5.11 (m, 2H), 4.82 (d, *J* = 11.2 Hz, 1H), 4.51 – 4.29 (m, 2H), 3.50 – 3.34 (m, 1H), 3.12 – 2.99 (m, 1H), 2.99 – 2.74 (m, 3H),

2.57 – 2.36 (m, 3H), 2.27 – 2.09 (m, 2H), 2.01 – 1.83 (m, 3H), 1.82 – 1.64 (m, 4H), 1.50 (dd, *J* = 15.3, 11.9 Hz, 1H), 1.21 (td, *J* = 13.8, 4.0 Hz, 2H).

(3'R,4'S,5'R)-6''-chloro-4'-(3-chloro-2-fluorophenyl)-N-(4-(2-(2,6-dioxopiperidin-3-yl)-1-oxoisoindolin-4-yl)butyl)-2''-oxodispiro[cyclohexane-1,2'-pyrrolidine-3',3''-indoline]-5'-carboxamide (LE-016)

LE-016 (10.4 mg, Yield: 63%) was obtained as white powder using the same synthetic strategy described for **LD-222**.

LC-MS(ESI) m/z $(M+H)^+$:760.51, calcd for $C_{40}H_{41}Cl_2FN_5O_5$ $(M+H)^+$ 760.25; >95% purity.

^{1}H NMR (400 MHz, Methanol-d_4) δ 7.67 – 7.61 (m, 2H), 7.48 (tt, *J* = 8.7, 5.4 Hz, 2H), 7.38 – 7.21 (m, 2H), 7.16 – 7.06 (m, 2H), 6.77 (d, *J* = 2.0 Hz, 1H), 5.24 – 5.10 (m, 2H), 4.77 (d, *J* = 11.1 Hz, 1H), 4.53 – 4.35 (m, 2H), 3.44 – 3.35 (m, 1H), 3.26 – 2.69 (m, 5H), 2.64 – 2.43 (m, 3H), 2.21 – 2.13 (m, 2H), 1.91 (dd, *J* = 21.1, 11.4 Hz, 3H), 1.76 (d, *J* = 13.4 Hz, 2H), 1.58 – 1.35 (m, 5H), 1.24 – 1.13 (m, 2H).

(3'R,4'S,5'R)-6''-chloro-4'-(3-chloro-2-fluorophenyl)-N-(5-(2-(2,6-dioxopiperidin-3-yl)-1-oxoisoindolin-4-yl)pentyl)-2''-oxodispiro[cyclohexane-1,2'-pyrrolidine-3',3''-indoline]-5'-carboxamide (LD-277)

LD-277 (7.8 mg, Yield: 48%) was obtained as white powder using the same synthetic strategy described for **LD-222**.

LC-MS(ESI) m/z $(M+H)^+$:746.45, calcd for $C_{39}H_{39}Cl_2FN_5O_5$ $(M+H)^+$ 746.23; >95% purity.

^{1}H NMR (400 MHz, Methanol-d_4) δ 7.65 (dd, *J* = 7.4, 3.9 Hz, 2H), 7.52 – 7.40 (m, 3H), 7.34 (ddd, *J* = 8.0, 6.1, 2.6 Hz, 1H), 7.15 (t, *J* = 8.0 Hz, 1H), 7.10 (dt, *J* = 8.2, 2.4 Hz, 1H), 6.77 (d, *J* = 2.0 Hz, 1H), 5.18 (dt, *J* = 13.3, 5.6 Hz, 1H), 5.07 (d, *J* = 10.8 Hz, 1H), 4.76 (d, *J* = 2.4 Hz, 1H), 4.53 – 4.40 (m, 2H), 3.37 (ddd, *J* = 13.5, 6.9, 2.5 Hz, 1H), 3.03 (dt, *J* = 10.1, 7.0 Hz, 2H), 2.91 (dd, *J* = 13.3, 5.0 Hz, 1H), 2.84 – 2.76 (m, 1H), 2.73 – 2.64 (m, 1H), 2.63 – 2.46 (m, 3H), 2.39 – 2.33 (m, 1H), 2.23 – 2.09 (m, 2H), 1.95 – 1.83 (m, 3H), 1.73 (t, *J* = 11.1 Hz, 2H), 1.56 – 1.29 (m, 5H), 1.17 – 1.09 (m, 2H).

(3'R,4'S,5'R)-6''-chloro-4'-(3-chloro-2-fluorophenyl)-N-(2-(3-(2-(2,6-dioxopiperidin-3-yl)-1-oxoisoindolin-4-yl)propoxy)ethyl)-2''-oxodispiro[cyclohexane-1,2'-pyrrolidine-3',3''-indoline]-5'-carboxamide (LE-344)

LE-344 (8.2 mg, Yield: 48%) was obtained as white powder using the same synthetic strategy described for **LD-222**.

LC-MS(ESI) m/z $(M+H)^+$:790.23, calcd for $C_{41}H_{43}Cl_2FN_5O_6$ $(M+H)^+$ 790.26; >95% purity.

^{1}H NMR (400 MHz, Methanol-d_4) δ 7.69 – 7.60 (m, 2H), 7.53 – 7.44 (m, 2H), 7.41 (dd, *J* = 7.6, 1.2 Hz, 1H), 7.27 (dddd, *J* = 23.7, 8.5, 7.1, 1.5 Hz, 1H), 7.17 – 7.06 (m, 2H), 6.76 (dd, *J* = 1.9, 0.8 Hz, 1H), 5.25 – 5.12 (m, 1H), 4.79 (d, *J* = 11.0 Hz, 1H), 4.55 – 4.35 (m, 2H), 3.58 (dtd, *J* = 13.9, 6.2, 4.1 Hz, 1H), 3.38 – 3.09 (m, 5H), 3.02 – 2.85 (m, 2H), 2.84 – 2.76 (m, 2H), 2.63 (td, *J* = 7.5, 2.3 Hz, 2H), 2.53 (qd, *J* = 13.2, 4.6 Hz, 1H), 2.24 – 2.12 (m, 2H), 2.00 – 1.87 (m, 3H), 1.81 – 1.68 (m, 4H), 1.51 (q, *J* = 13.8 Hz, 1H), 1.25 – 1.15 (m, 2H).

(3'R,4'S,5'R)-6''-chloro-4'-(3-chloro-2-fluorophenyl)-N-(2-(2-(3-(2-(2,6-dioxopiperidin-3-yl)-1-oxoisoindolin-4-yl)propoxy)ethoxy)ethyl)-2''-oxodispiro[cyclohexane-1,2'-pyrrolidine-3',3''-indoline]-5'-carboxamide (LD-257)

LD-257 (7.8 mg, Yield: 48%) was obtained as white powder using the same synthetic strategy described for **LD-222**.

LC-MS(ESI) m/z $(M+H)^+$:834.35, calcd for $C_{43}H_{47}Cl_2FN_5O_7$ $(M+H)^+$ 834.28; >95% purity.

^{1}H NMR (400 MHz, Methanol-d_4) δ 7.67 (dd, *J* = 6.4, 2.3 Hz, 1H), 7.65 – 7.58 (m, 1H), 7.57 – 7.41 (m, 3H), 7.29 (dd, *J* = 8.0 Hz, 1H), 7.19 – 7.01 (m, 2H), 6.75 (d, *J* = 2.0 Hz, 1H), 5.19 (dd, *J* = 13.3, 5.2 Hz, 1H), 4.75 (d, *J* = 10.4 Hz, 1H), 4.56 – 4.37 (m, 2H), 3.66 – 3.31 (m, 12H), 3.00 – 2.86 (m, 1H), 2.86 – 2.72 (m, 3H), 2.56 – 2.45 (m, 1H), 2.22 – 2.13 (m, 1H), 2.08 – 1.61 (m, 8H), 1.58 – 1.45 (m, 1H), 1.22 – 1.01 (m, 2H).

(3'R,4'S,5'R)-6''-chloro-4'-(3-chloro-2-fluorophenyl)-N-(2-(2-(2-(3-(2-(2,6-dioxopiperidin-3-yl)-1-oxoisoindolin-4-yl)propoxy)ethoxy)ethoxy)ethyl)-2''-oxodispiro[cyclohexane-1,2'-pyrrolidine-3',3''-indoline]-5'-carboxamide (LD-256)

LD-256 (6.5 mg, Yield: 34%) was obtained as white powder using the same synthetic strategy described for **LD-222**.

LC-MS(ESI) m/z $(M+H)^+$:878.65, calcd for $C_{45}H_{51}Cl_2FN_5O_8$ $(M+H)^+$ 878.31; >95% purity.

^{1}H NMR (400 MHz, Methanol-d_4) δ 7.73 – 7.61 (m, 2H), 7.55 – 7.45 (m, 3H), 7.35 (t, *J* = 7.5 Hz, 1H), 7.20 – 7.04 (m, 2H), 6.78 (d, *J* = 1.9 Hz, 1H), 5.21 (dt, *J* = 13.3, 4.8 Hz, 1H), 4.79 (d, *J* = 10.7

Hz, 1H), 4.60 – 4.40 (m, 2H), 3.74 – 3.38 (m, 13H), 3.33 – 3.18 (m, 2H), 2.95 (ddd, *J* = 17.6, 13.5, 5.4 Hz, 1H), 2.88 – 2.77 (m, 3H), 2.75 – 2.61 (m, 1H), 2.61 – 2.45 (m, 1H), 2.25 – 2.16 (m, 1H), 2.09 (d, *J* = 13.8 Hz, 1H), 2.02 – 1.67 (m, 7H), 1.55 (q, *J* = 13.9 Hz, 1H), 1.27 – 1.05 (m, 2H).

(3'R,4'S,5'R)-6''-chloro-4'-(3-chloro-2-fluorophenyl)-N-(5-(2-(1-methyl-2,6-dioxopiperidin-3-yl)-1-oxoisoindolin-4-yl)pentyl)-2''-oxodispiro[cyclohexane-1,2'-pyrrolidine-3',3''-indoline]-5'-carboxamide (LE-024)

LE-024 (7.1 mg, Yield: 42%) was obtained as white powder using the same synthetic strategy described for **LD-222**.

LC-MS(ESI) m/z $(M+H)^+$:788.31, calcd for $C_{42}H_{45}Cl_2FN_5O_5$ $(M+H)^+$ 788.28; >95% purity.

(S)-2-((S)-2-((R)-2-isobutyramdo-2-methylpent-4-enamido)-5-(3-((2,2,4,6,7-pentamethyl-2,3-dihydrobenzofuran-5-yl)sulfonyl)guanidino)pentanamido)butanoic acid (302).

Fmoc-2-Abu-OH (8.1 mmol, 2.6 g) was loaded on the 2.7 mmol 2-chlorotrityl chloride resin (ChemPep) (1.2 mmol/g) overnight in CH_2Cl_2 and in the presence of DIPEA (8.1 mmol, 1.4 mL). Then, the resin was washed with DMF, MeOH, CH_2Cl_2, respectively, mixed with DIPEA (0.29 mmol, 0.5 mL) in MeOH:CH_2Cl_2 (1:5) and was shaken for 30 min to endcap unreacted 2-chlorotrityl group on the resin. Next, classical chain elongation was carried out with Fmoc chemistry. The carboxylic acid intermediate (**26**) was cleaved from the resin by treatment with 4 ml of 1% trifluoroacetic acid in CH_2Cl_2 (3×10 min). The filtrate was evaporated and the remaining crude was purified with preparative HPLC using the C18 reverse phase column (Waters, Sunfire™ Prep C_{18} OBD™, 5µm, 50×100mm), yielding 0.9 g white powder (70 % yield).

MS (ESI): m/z calculated for $[M+H]^+$ 693.37, found 693.42.

^{1}H NMR (300 MHz, CD_3OD) δ: 5.79-5.63 (m, 1H), 5.12-5.03 (m, 2H), 4.45-4.36 (m, 1H), 4.24 (dd, *J* = 5.2, 8.4 Hz, 1H), 3.24-3.15 (m, 2H), 3.00 (s, 2H), 2.79-2.67 (m, 1H), 2.60-2.43 (m, 8H), 2.08 (s, 3H), 1.99-1.51 (m, 6H), 1.45 (s, 6H), 1.40 (s, 3H), 1.07 (d, *J* = 6.8 Hz, 6H), 0.97 (t, *J* = 7.4 Hz, 3H). ^{13}C NMR (75 MHz, CD_3OD) δ : 179.89, 176.19, 175.20, 174.09, 133.74, 126.49, 119.96, 118.86, 88.10, 60.30, 60.21, 55.49, 54.00, 44.04, 41.91, 36.07, 30.31, 28.89, 25.75, 23.06, 20.17, 19.91, 19.77, 18.48, 12.71, 11.03.

(9H-fluoren-9-yl)methyl (R)-2-((2-(allylamino)-2-oxo-1-phenylethyl)amino)-2-oxoacetate (303a).

2.7 mmol (1 g) Fmoc-R-phenylglycine was mixed with allylamine hydrochloride (4.1 mmol, 0.38 g), EDCI (4.1 mmol, 0.79 g), HOAt (4.1 mmol, 0.55 g), 3 equiv DIPEA (8.1 mmol, 1.4 mL) in 100 mL CH_2Cl_2 and stirred at room temperature for 3h. The reaction mixture was quenched with H_2O and extracted to CH_2Cl_2. The organic layer together with a white precipitate was collected and concentrated in vacuo. The remaining white solid was washed from CH_2Cl_2 yielding 0.96 g intermediate **(303a)** as white powder (86 % yield).

HRMS (ESI): m/z calc. for $C_{26}H_{25}N_2O_3$ $[M + H]^+$ 413.1860, found 413.1862.

^{1}H NMR (300 MHz, CD_3CN) δ : 7.85 (d, *J* = 7.5 Hz, 2H), 7.68 (d, *J* = 7.0 Hz, 2H), 7.47-7.29 (m, 9H), 6.83 (brs, 1H), 6.47 (brs, 1H), 5.85-5.71 (m, 1H), 5.16 (d, *J* = 6.6 Hz, 1H), 5.07-4.96 (m, 2H), 4.35 (d, *J* = 6.8 Hz, 2H), 4.24 (t, *J* = 6.9 Hz, 1H), 3.81-3.74 (m, 2H).

^{13}C NMR (75 MHz, CD_3CN): δ 170.75, 145.28, 145.18, 142.26, 135.61, 129.81, 129.24, 128.81, 128.42, 128.24, 126.30, 121.09, 115.87, 67.53, 59.96, 48.18, 42.31.

(R)-N-((6S,9S,12R)-9-ethyl-1-imino-7,10,13-trioxo-1-(2,2,4,6,7-pentamethyl-2,3-dihydrobenzofuran-5-sulfonamido)-12-phenyl-2,8,11,14-tetraazaheptadec-16-en-6-yl)-2-isobutyramido-2-methylpent-4-enamide (304a).

Intermediate **304a** was treated with diethylamine (20 equiv.) in CH_3CN for 2h at room temperature followed by removal of the solvent and diethylamine in vacuo. The resulting crude was further dried under vacuum, then taken into CH_2Cl_2 and mixed with the corresponding **303a** (1.5 equiv.), EDCI (1.5 equiv.), HOAt (1.5 equiv.) and diisopropylethylamine (1.5 equiv.). The reaction mixture was stirred at room temperature for 2 h, quenched with H_2O and extracted to CH_2Cl_2. The organic layers were collected and dried over anhydrous Na_2SO_4, filtered, evaporated and purified over flash chromatography using EtOAc:MeOH (30:1). White solid (72 % yield). **(304a)** as white solid (62 % yield).

HRMS (ESI): m/z calc. for $C_{44}H_{65}N_8O_8S$ $[M+H]^+$ 865.4641, found 865.4642.

^{1}H NMR (300 MHz, CD_3OD) δ : 7.45-7.28 (m, 5H), 5.84-5.64 (m, 2H), 5.42 (s, 1H), 5.14-4.99 (m, 4H), 4.26-4.19 (m, 2H), 3.89-3.69 (m, 2H), 3.15 (t, *J* = 6.7 Hz, 2H), 2.99 (s, 2H), 2.74-2.65 (m, 1H), 2.60-2.40 (m, 8H), 2.07 (s, 3H), 1.98-1.48 (m, 6H), 1.45 (s, 6H), 1.37 (s, 3H), 1.13-1.06 (m, 6H), 0.92 (t, *J* = 7.4 Hz, 3H).

^{13}C NMR (75 MHz, CD_3OD): δ 180.33, 176.96, 174.56, 174.22, 172.49, 160.08, 158.33, 139.58, 138.59, 135.36, 134.61, 134.16, 133.72, 129.93, 129.55, 129.21, 126.22, 119.95, 118.64, 116.31,

87.87, 59.99, 59.54, 56.93, 55.03, 44.19, 42.92, 41.24, 36.15, 30.01, 28.91, 25.96, 23.42, 20.43, 20.03, 19.84, 19.75, 18.57, 12.69, 11.25.

N-((3R,6S,9S,12R)-6-ethyl-9-(3-guanidinopropyl)-12-methyl-2,5,8,11-tetraoxo-3-phenyl-1,4,7,10-tetraazacyclohexadecan-12-yl)isobutyramide (MM-401).

To a solution of intermediate **304a** in CH_2Cl_2, Hoveyda-Grubbs 2nd Generation catalyst (0.5 equiv.) was added under N_2 atmosphere, and the reaction mixture stirred at 45 ^oC overnight under N_2 atmosphere. Another portion of the catalyst (0.5 equiv.) was added and stirred further overnight under the same conditions before filtering through celite and concentrating in vacuo. The remaining crude was purified over flash chromatography using CH_2Cl_2:MeOH. The cyclic product was taken up to MeOH and the double bond was reduced using 10% Pd/C under 1 atm of H_2. The reaction mixture was filtered through celite and concentrated. The remaining crude was refluxed in CH_2Cl_2: Trifluoroacetic acid:H_2O (20:10:0.5) for 2h in order to remove the Pbf group from arginine guanidine, and evaporated. The crude product was purified with preparative HPLC using the C18 reverse phase column (Waters, Sunfire™ Prep C_{18} OBD™, 5µm, 50×100mm). The final compound then dissolved in CH_3CN:H_2O (1:1) and lyophilized to obtain white solid (53% yield over 3 steps).

HRMS (ESI+): m/z calculated for $C_{29}H_{47}N_8O_5$ $[M+H]^+$ 587.3664, found 587.3664.

^{1}H NMR (300 MHz, MeOD): δ 7.42-7.30 (m, 5H), 5.25 (s, 1H), 4.30 (dd, *J* = 4.2, 9.8 Hz, 1H), 4.16 (dd, *J* = 6.2, 7.7 Hz, 1H), 3.51-3.42 (m, 1H), 3.19 (t, *J* = 6.9 Hz, 2H), 3.12-2.99 (m, 1H), 2.59-2.48 (m, 1H), 1.94-1.26 (m, 15H), 1.15-1.08 (m, 6H), 0.92 (t, *J* = 7.4 Hz, 3H).

^{13}C NMR (75 MHz, MeOD-d_4): δ 179.86, 176.83, 174.99, 173.64, 172.97, 158.86, 137.93, 130.06, 129.69, 129.32, 61.24, 60.70, 56.67, 55.27, 41.91, 40.34, 39.25, 36.12, 29.99, 26.39, 25.94, 22.81, 21.83, 20.06, 19.91, 10.84.

N-((3R,6S,9S,12R)-6-ethyl-9-(3-guanidinopropyl)-2,5,8,11-tetraoxo-3-phenyl-1,4,7,10-tetraazacyclohexadecan-12-yl)isobutyramide CF_3COOH salt (LC-058).

Fmoc-D-Phg-OH (0.5 mmol, 0.17 g) was loaded on the 0.1 mmol 2-chlorotrityl chloride resin (ChemPep) (1 mmol/g) overnight in CH_2Cl_2 and in the presence of 2,4,6-collidine (3 mmol, 0.4 mL). Then, the resin was washed with DMF, MeOH, CH_2Cl_2, respectively, mixed with DIPEA (0.29 mmol, 0.5 mL) in MeOH:CH_2Cl_2 (1:5) and was shaken for 30 min to endcap unreacted 2-chlorotrityl group on the resin. Next, classical chain elongation was carried out with Fmoc chemistry. The peptide intermediate (**306d**) was cleaved from the resin by treatment of **305d** with 4 ml of 1% trifluoroacetic acid in CH_2Cl_2 (3×10 min). The filtrate was evaporated and followed by treatment with 10% trifluoroacetic acid in CH_2Cl_2 for 30 min. Then the solvent was evaporated and the remaining crude was purified with preparative HPLC using the C18 reverse phase column (Waters, Sunfire™ Prep C_{18} OBD™, 5µm, 50×100mm) to yield **306d.** White powder,

MS (ESI): m/z calculated for $C_{41}H_{63}N_8O_9S$ $[M+H]^+$ 843.44, found 843.38.

Intermediate **306d** (50 mg, 0.05 mmol) dissolved in 5 mL DMF was slowly added to a solution of HATU (38 mg, 0.1 mmol) and DIPEA (0.05 mL, 0.25 mmol) in 5 mL DMF during 30 min. The reaction was stirred for another 30 min and then the solvent was evaporated. The remaining crude was

purified with preparative HPLC using the C18 reverse phase column (Waters, Sunfire™ Prep C_{18} OBD™, 5µm, 50×100mm) to yield **307d**. White powder,

MS (ESI): m/z calculated for $C_{41}H_{61}N_8O_8S$ $[M+H]^+$ 825.43, found 825.36.

The cyclic product **307d** was then dissolved in trifluoroacetic acid:H_2O (95:5) and stirred at room temperature for 2h in order to remove the Pbf group from arginine guanidine. Then the solvent was evaporated and the crude product was purified with preparative HPLC using the C18 reverse phase column (Waters, Sunfire™ Prep C_{18} OBD™, 5µm, 50×100mm). The final compound **LC-058** then dissolved in CH_3CN:H_2O (1:1) and lyophilized. White solid (12.7 % yield over 4 steps).

HRMS (ESI): m/z calculated for $C_{28}H_{45}N_8O_5$ $[M+H]^+$ 573.3513, found 573.3507.

^{1}H NMR (400 MHz, CD_3OD) δ 7.50-7.28 (m, 5H), 5.14 (s, 1H), 4.28 (t, *J* = 6.8 Hz, 1H), 4.13 (dd, *J* = 10.4, 5.2 Hz, 1H), 4.08-3.99 (m, 1H), 3.54-3.41 (m, 1H), 3.18 (td, *J* = 7.1, 2.5 Hz, 2H), 3.04-2.97 (m, 1H), 2.62-2.51 (m, 1H), 1.94-1.54 (m, 9H), 1.47-1.24 (m, 3H), 1.13 (dd, *J* = 6.9, 3.3 Hz, 6H), 0.90 (t, *J* = 7.5 Hz, 3H).

^{13}C NMR (101 MHz, CD_3OD) δ 180.51, 175.63, 174.34, 173.64, 172.92, 158.63, 137.30, 129.92, 129.67, 129.31, 61.54, 57.09, 56.08, 55.83, 41.61, 39.68, 35.72, 32.14, 29.95, 29.24, 26.68, 26.53, 23.37, 19.93, 19.74, 10.25.

N-((3R,6S,9S,12R)-6-ethyl-9-(3-guanidinopropyl)-2,5,8,11-tetraoxo-3-phenyl-1,4,7,10-tetraazacyclopentadecan-12-yl)isobutyramide CF_3COOH salt (LC-043-1).

A method applied for **LC-042-1** was used to make **LC-043-1** starting from resin. White solid (21.5 % yield over 4 steps).

HRMS (ESI): m/z calculated for $C_{27}H_{43}N_8O_5$ $[M+H]^+$ 559.3356, found 559.3351.

^{1}H NMR (400 MHz, CD_3OD) δ 7.47-7.25 (m, 5H), 5.27 (s, 1H), 4.31 (dd, *J* = 10.5, 5.0 Hz, 1H), 4.20 (dd, *J* = 7.9, 6.4 Hz, 1H), 3.96 (dd, *J* = 9.5, 3.7 Hz, 1H), 3.46-3.37 (m, 1H), 3.24-3.01 (m, 3H), 2.65-2.49 (m, 1H), 1.93-1.60 (m, 10H), 1.15 (dd, *J* = 6.9, 5.9 Hz, 6H), 0.93 (t, *J* = 7.5 Hz, 3H).

^{13}C NMR (101 MHz, CD_3OD) δ 180.68, 175.30, 174.76, 173.75, 172.98, 158.61, 137.32, 129.90, 129.58, 129.22, 60.94, 56.96, 56.23, 55.33, 41.56, 39.56, 35.76, 29.84, 28.93, 26.58, 26.15, 19.96, 19.63, 10.67.

N-((3R,6S,9S,12R)-6-ethyl-9-(3-guanidinopropyl)-2,5,8,11-tetraoxo-3-phenyl-1,4,7,10-tetraazacyclotetradecan-12-yl)isobutyramide CF_3COOH salt (LC-042-1).

A method applied for **LC-058** was used to make **LC-042-1** starting from resin. White solid (21.7 % yield over 4 steps).

HRMS (ESI): m/z calculated for $C_{26}H_{41}N_8O_5$ $[M+H]^+$ 545.3200, found 545.3197.

^{1}H NMR (400 MHz, CD_3OD) δ 7.44-7.36 (m, 2H), 7.36-7.26 (m, 3H), 5.44 (s, 1H), 4.33-4.21 (m, 2H), 4.18 (dd, *J* = 7.7, 6.2 Hz, 1H), 3.68 (dt, *J* = 14.4, 3.7 Hz, 1H), 3.26-3.10 (m, 2H), 2.88 (dd, *J* = 14.3, 11.8 Hz, 1H), 2.65 (hept, *J* = 6.6 Hz, 1H), 2.55-2.39 (m, 1H), 2.22-2.03 (m, 1H), 1.89-1.59 (m, 6H), 1.19 (dd, *J* = 13.8, 6.8 Hz, 6H), 0.94 (t, *J* = 7.4 Hz, 3H).

^{13}C NMR (101 MHz, CD_3OD) δ 181.84, 175.27, 175.05, 172.50, 172.27, 158.65, 139.13, 129.49, 129.39, 128.96, 58.55, 57.07, 55.76, 54.13, 41.74, 36.09, 35.68, 30.21, 28.78, 26.53, 24.52, 20.38, 19.42, 11.07.

(R)-2-((((9H-fluoren-9-yl)methoxy)carbonyl)amino)-4-(dibenzylamino)-2-methylbutanoic acid CF_3COOH salt (308).

(R)-2-Fmoc-NH-2-methylpent-4-enoic acid (1 mmol, 350 mg) was dissolved in THF/H_2O (2.6 mL/ 1 mL) in a flask. The hood lights were turned off and the flask was covered by aluminum foil. Osmium tetroxide (0.05 mmol in 0.32 mL H_2O) was added to the flask. After 5 min, $NaIO_4$ (2.5 mmol, 535 mg) was added in small portions over a 15 min period. The reaction was kept at room temperature for 4 h before it was filtrated and the THF was evaporated off. The residue was dissolved in EtOAc and saturated NH_4Cl aqueous solution was added. The aqueous phase was extracted with EtOAc (2 x 30 mL) and the organic phase was combined, washed with brine, and dried over anhydrous Na_2SO_4. The solution was concentrated in vacuo and the crude product was dissolved in 1,2-dichloroethane (3 mL) in a flask. Then dibenzylamine (1.5 mmol, 0.29 mL) and sodium triacetoxyborohydride (3 mmol, 636 mg) were added to the flask. The reaction was stirred at room temperature until the starting material disappeared on TLC. The solvent was evaporated and the remaining crude was purified with C-18 reverse phase flash column to yield **308**. White solid (75 % yield over 2 steps)

MS (ESI): m/z calculated for $C_{34}H_{35}N_2O_4$ $[M+H]^+$ 535.26, found 535.23.

^{1}H NMR (400 MHz, Methanol-d_4) δ 7.80 (d, *J* = 7.6 Hz, 2H), 7.62 (dd, *J* = 15.7, 7.5 Hz, 2H), 7.48-7.35 (m, 12H), 7.33-7.25 (m, 2H), 4.43-4.05 (m, 7H), 3.25-3.03 (m, 2H), 2.55 (q, *J* = 8.3, 6.5 Hz, 1H), 2.46-2.20 (m, 1H), 1.35 (s, 3H).

^{13}C NMR (101 MHz, MeOD) δ 176.68, 157.48, 145.26, 145.07, 142.58, 142.56, 132.20, 131.24, 130.45, 130.44, 128.86, 128.19, 126.29, 126.14, 120.98, 67.91, 58.81, 58.40, 48.28, 31.28, 24.16.

N-((3R,6S,9S,12R)-6-ethyl-9-(3-guanidinopropyl)-12-methyl-2,5,8,11-tetraoxo-3-phenyl-1,4,7,10-tetraazacyclotetradecan-12-yl)isobutyramide CF_3COOH salt (LC-081).

Fmoc-D-Phg-OH (0.5 mmol, 0.17 g) was loaded on the 0.1 mmol 2-chlorotrityl chloride resin (ChemPep) (1 mmol/g) overnight in CH_2Cl_2 and in the presence of 2,4,6-collidine (3 mmol, 0.4 mL). Then, the resin was washed with DMF, MeOH, CH_2Cl_2, respectively, mixed with DIPEA (0.29 mmol, 0.5 mL) in MeOH:CH_2Cl_2 (1:5) and was shaken for 30 min to endcap unreacted 2-chlorotrityl group on the resin. Next, classical chain elongation was carried out with Fmoc chemistry. The peptide intermediate was cleaved from the resin by treatment of **309a** with 4 ml of 1% trifluoroacetic acid in CH_2Cl_2 (3×10 min). The filtrate was evaporated and the residue was dissolved in anhydrous ethanol. Pd/C (20 mg) was added to the flask and the reaction was stirred at H_2 atmosphere for 12h at 50 ^{o}C. Then the reaction was filtered, the filtrate was evaporated and the remaining crude was purified with preparative HPLC using the C18 reverse phase column (Waters, Sunfire™ Prep C_{18} OBD™, 5µm, 50×100mm) to yield **310a. W**hite powder,

MS (ESI): m/z calculated for $C_{40}H_{61}N_8O_9S$ $[M+H]^+$ 829.43, found 829.25.

The method applied for **LC-058** was used to make **LC-081** starting from **310a**. White solid (8.7 % yield over 4 steps).

HRMS (ESI): m/z calculated for $C_{27}H_{43}N_8O_5$ $[M+H]^+$ 559.3352, found 559.3351.

^{1}H NMR (400 MHz, Methanol-d_4) δ 7.49-7.37 (m, 2H), 7.37-7.20 (m, 3H), 5.46 (d, *J* = 9.2 Hz, 1H), 4.38 (dd, *J* = 10.5, 3.8 Hz, 1H), 4.24-4.06 (m, 1H), 3.85-3.63 (m, 1H), 3.26-3.16 (m, 2H), 2.76-2.56 (m, 3H), 2.24-2.07 (m, 1H), 1.92-1.59 (m, 5H), 1.53 (s, 3H), 1.40-1.32 (m, 1H), 1.23 (d, *J* = 6.9 Hz, 3H), 1.16 (d, *J* = 6.7 Hz, 3H), 0.96 (t, *J* = 7.4 Hz, 3H).

^{13}C NMR (101 MHz, MeOD) δ 182.07, 177.62, 175.47, 172.28, 172.11, 158.66, 139.36, 129.48, 129.42, 128.86, 59.98, 58.21, 57.51, 55.53, 41.72, 38.63, 36.40, 35.98, 28.83, 26.67, 24.75, 21.17, 18.90, 11.06.

N-((3R,6S,9S,12R)-6-ethyl-9-(3-guanidinopropyl)-12-methyl-2,5,8,11-tetraoxo-3-phenyl-1,4,7,10-tetraazacyclopentadecan-12-yl)isobutyramide CF_3COOH salt (LC-044).

A method applied for **LC-058** was used to make **LC-044** starting from resin. White solid (19.4 % yield over 4 steps).

HRMS (ESI): m/z calculated for $C_{28}H_{45}N_8O_5$ $[M+H]^+$ 573.3513, found 573.3506.

^{1}H NMR (400 MHz, CD_3OD) δ 7.55-7.23 (m, 5H), 5.35 (s, 1H), 4.40 (dd, *J* = 10.0, 4.7 Hz, 1H), 4.16 (dd, *J* = 8.6, 6.3 Hz, 1H), 3.41-3.33 (m, 1H), 3.24-3.12 (m, 3H), 2.65-2.37 (m, 1H), 2.00-1.48 (m, 10H), 1.46 (s, 3H), 1.12 (dd, *J* = 6.8, 2.5 Hz, 6H), 0.94 (t, *J* = 7.4 Hz, 3H).

^{13}C NMR (101 MHz, CD_3OD) δ 179.91, 176.79, 174.82, 174.33, 172.75, 158.62, 138.00, 129.82, 129.37, 128.93, 60.47, 60.37, 56.91, 55.12, 41.74, 40.12, 37.57, 35.81, 28.76, 26.24, 25.14, 23.68, 21.04, 19.97, 19.36, 11.00.

N-((3R,6S,9S,12R)-6-ethyl-9-(3-guanidinopropyl)-12-methyl-2,5,8,11-tetraoxo-3-phenyl-1,4,7,10-tetraazacycloheptadecan-12-yl)isobutyramideCF_3COOH salt (HK-06-223C).

HK-06-223C was prepared as **MM-401**. White solid (28 % yield over 3 steps).

HRMS (ESI): m/z calc. for $C_{30}H_{49}N_8O_5$ $[M+H]^+$ 601.3820, found601.3827.

^{1}H NMR (300 MHz, CD_3OD) δ: 7.45-7.32 (m, 5H), 5.22 (s, 1H), 4.45-4.31 (m, 2H), 3.28-3.13 (m, 4H), 2.59-2.49 (m, 1H), 1.97-1.05 (m, 23H), 0.89 (t, *J* = 7.5 Hz, 3H).

^{13}C NMR (75 MHz, CD_3OD) δ: 179.80, 176.66, 174.54, 173.62, 173.32, 158.81, 137.54, 130.08, 129.79, 129.44, 61.04, 60.91, 55.74, 54.59, 41.83, 41.69, 39.95, 36.05, 30.64, 29.75, 27.18, 27.10, 26.14, 25.08, 21.12, 20.33, 19.48, 10.18.

N-((3R,6S,9S,12R)-6-ethyl-9-(3-guanidinopropyl)-12-methyl-2,5,8,11-tetraoxo-3-phenyl-1,4,7,10-tetraazacyclooctadecan-12-yl)isobutyramide CF_3COOH salt (HK-05-121C).

HK-05-121C prepared as **MM-401** White solid (46 % yield over 3 steps).

HRMS (ESI): m/z calc. for $C_{31}H_{51}N_8O_5$ $[M+H]^+$ 615.3977, found 615.3976.

^{1}H NMR (300 MHz, CD_3OD) δ: 7.45-7.29 (m, 5H), 5.40 (s, 1H), 4.29-4.19 (m, 2H), 3.59-3.47 (m, 1H), 3.19 (t, *J* = 6.7Hz, 2H), 3.09-2.96 (m, 1H), 2.63-2.52 (m, 1H), 2.02-1.59 (m, 8H), 1.58-1.27 (m, 11H), 1.14 (d, *J* = 6.5Hz, 3H), 1.12 (d, *J* = 6.5Hz, 3H), 0.89 (t, *J* = 7.4 Hz, 3H).

^{13}C NMR (75 MHz, CD_3OD) δ: 180.53, 177.59, 174.48, 173.99, 172.88, 158.86, 138.38, 129.97, 129.57, 60.67, 59.87, 56.51, 55.22, 42.04, 39.80, 37.53, 36.09, 29.98, 28.42, 28.38, 26.42, 25.37, 22.72, 22.47, 20.08, 19.94, 10.69.

N-((3R,6S,9S,12R)-6-ethyl-9-(3-guanidinopropyl)-12-methyl-2,5,8,11-tetraoxo-3-phenyl-1,4,7,10-tetraazacycloicosan-12-yl)isobutyramide CF_3COOH salt (HK-06-229C).

HK-06-229C was prepared as **MM-401.** White solid (27 % yield over 3 steps).

HRMS (ESI): m/z calc. for $C_{33}H_{55}N_8O_5$ $[M+H]^+$ 643.4290, found 643.4292.

^{1}H NMR (300 MHz, CD_3OD) δ: 7.41-7.30 (m, 5H), 5.40 (s, 1H), 4.34-4.28 (m, 1H), 4.18 (t, *J* = 7.1 Hz, 1H), 3.55-3.44 (m, 1H), 3.17 (t, *J* = 6.9 Hz, 2H), 3.07-2.95 (m, 1H), 2.61-2.50 (m, 1H), 2.00-1.28 (m, 23H), 1.16-1.07 (m, 6H), 0.92 (t, *J* = 7.4 Hz, 3H).

^{13}C NMR (75 MHz, CD_3OD) δ: 180.22, 176.92, 174.53, 174.30, 172.69, 158.81, 138.70, 130.03, 129.55, 129.39, 60.72, 59.51, 57.11, 54.55, 42.14, 40.03, 38.56, 36.13, 30.28, 29.31, 28.92, 28.63, 28.04, 26.56, 26.16, 26.10, 23.50, 22.76, 20.05, 10.81.

N-((3R,6S,9S,12R)-6-ethyl-12-methyl-9-(3-(3-methylguanidino)propyl)-2,5,8,11-tetraoxo-3-phenyl-1,4,7,10-tetraazacyclotetradecan-12-yl)isobutyramide CF_3COOH salt (LC-089).

A method applied for **LC-081** was used to make **LC-089** starting from resin. White solid (15.4 % yield over 4 steps).

HRMS (ESI): m/z calculated for $C_{28}H_{45}N_8O_5$ $[M+H]^+$ 573.3507, found 573.3511.

^{1}H NMR (400 MHz, Methanol-*d*$_4$) δ 7.44-7.37 (m, 2H), 7.37-7.26 (m, 3H), 5.48-5.44 (m, 1H), 4.38 (dd, *J* = 10.5, 3.7 Hz, 1H), 4.17 (td, *J* = 7.0, 3.2 Hz, 1H), 3.80-3.72 (m, 1H), 3.28-3.16 (m, 2H), 2.83 (s, 3H), 2.75-2.57 (m, 3H), 2.25-2.11 (m, 1H), 1.96-1.69 (m, 4H), 1.53 (s, 3H), 1.41-1.32 (m, 1H), 1.22 (d, *J* = 6.9 Hz, 3H), 1.16 (d, *J* = 6.7 Hz, 3H), 0.95 (t, *J* = 7.4 Hz, 3H).

^{13}C NMR (101 MHz, MeOD) δ 182.17, 177.63, 175.52, 172.28, 172.10, 158.21, 139.37, 129.49, 129.41, 128.86, 60.07, 58.20, 57.47, 55.52, 41.75, 38.63, 36.41, 36.02, 28.88, 28.31, 26.64, 24.75, 21.18, 18.90, 11.06.

N-((3S,6S,9S,12R)-6-ethyl-12-methyl-9-(3-(3-methylguanidino)propyl)-2,5,8,11-tetraoxo-3-phenyl-1,4,7,10-tetraazacyclotetradecan-12-yl)isobutyramide CF_3COOH salt (LC-088).

LC-088 was obtained in the synthesis of **LC-089** starting from reisn, as D-α-phenylglycine was isomerized to L-α-phenylglycine during the solid phase peptide synthesis. White solid (7 % yield over 4 steps).

HRMS (ESI): m/z calculated for $C_{28}H_{45}N_8O_5$ $[M+H]^+$ 573.3507, found 573.3504. ^{1}H NMR (300 MHz, Methanol-*d*$_4$) δ 7.36-7.19 (m, 5H), 5.21 (s, 1H), 4.27 (dd, *J* = 8.8, 6.3 Hz, 1H), 4.00 (dd, *J* = 8.5, 6.0 Hz, 1H), 3.38 (dt, *J* = 14.6, 3.9 Hz, 1H), 3.28-3.14 (m, 2H), 3.04 (t, *J* = 13.5 Hz, 1H), 2.84 (s, 3H),

2.70- 2.53 (m, 2H), 2.00-1.60 (m, 7H), 1.55 (s, 3H), 1.20 (d, J = 5.5 Hz, 3H), 1.18 (d, J = 5.3 Hz, 3H), 0.91 (t, *J* = 7.4 Hz, 3H).

^{13}C NMR (101 MHz, MeOD) δ 181.09, 177.37, 174.97, 173.54, 171.64, 158.20, 138.80, 129.24, 128.74, 128.60, 60.17, 59.82, 57.73, 57.65, 41.83, 37.48, 37.15, 36.12, 28.51, 28.30, 26.74, 26.11, 21.12, 19.18, 10.88.

N-((3R,6S,9S,12R)-9-(3-guanidinopropyl)-6-isopropyl-12-methyl-2,5,8,11-tetraoxo-3-phenyl-1,4,7,10-tetraazacyclotetradecan-12-yl)isobutyramide (LC-313)

LC-313 was synthesized using the procedure applied for **LC-081** to yield 11.7 mg, white powder, 20 % yield over 4 steps.

LC-MS(ESI) m/z $(M+H)^+$: 573.43; calcd for $C_{28}H_{45}N_8O_5$ $(M+H)^+$: 573.35; >98% purity.

^{1}H NMR (400 MHz, Methanol-d_4) δ 8.53 (s, 1H), 8.23 (d, *J* = 3.6 Hz, 1H), 7.98 (t, *J* = 9.7 Hz, 2H), 7.93 – 7.85 (m, 1H), 7.45 – 7.36 (m, 2H), 7.36 – 7.24 (m, 3H), 5.47 (d, *J* = 9.0 Hz, 1H), 4.59 (dd, *J* = 10.2, 3.9 Hz, 1H), 4.15 (ddd, *J* = 7.7, 6.3, 3.5 Hz, 1H), 3.75 (td, *J* = 13.1, 10.9, 3.2 Hz, 1H), 3.28 – 3.14 (m, 2H), 2.76 – 2.61 (m, 3H), 2.61 – 2.50 (m, 1H), 1.98 – 1.66 (m, 4H), 1.52 (s, 3H), 1.38 – 1.29 (m, 1H), 1.21 (d, *J* = 6.9 Hz, 3H), 1.18 (d, *J* = 6.7 Hz, 3H), 1.03 (d, *J* = 6.9 Hz, 3H), 0.92 (d, *J* = 6.9 Hz, 3H).

N-((3R,6S,9S,12R)-9-(3-guanidinopropyl)-12-methyl-2,5,8,11-tetraoxo-3-phenyl-6-propyl-1,4,7,10-tetraazacyclotetradecan-12-yl)isobutyramide (LC-300)

LC-300 was synthesized using the procedure applied for **LC-081** to yield 19.6 mg, white powder, 34 % yield over 4 steps.

LC-MS(ESI) m/z $(M+H)^+$: 573.33; calcd for $C_{28}H_{45}N_8O_5$ $(M+H)^+$: 573.35; >98% purity.

^{1}H NMR (400 MHz, Methanol-d_4) δ 8.64 (s, 1H), 8.38 (d, *J* = 4.0 Hz, 1H), 8.19 (d, *J* = 9.5 Hz, 1H), 8.03 (d, *J* = 9.2 Hz, 1H), 7.93 – 7.86 (m, 1H), 7.45 – 7.39 (m, 2H), 7.36 – 7.25 (m, 3H), 5.46 (d, *J* = 9.2 Hz, 1H), 4.47 (ddd, *J* = 11.0, 9.5, 3.6 Hz, 1H), 4.15 (ddd, *J* = 7.5, 6.3, 4.0 Hz, 1H), 3.83 – 3.68 (m, 1H), 3.30 – 3.15 (m, 2H), 2.75 – 2.57 (m, 3H), 2.18 – 2.05 (m, 1H), 1.91 – 1.65 (m, 5H), 1.53 (s, 3H), 1.47 – 1.26 (m, 4H), 1.23 (d, *J* = 6.9 Hz, 3H), 1.16 (d, *J* = 6.6 Hz, 3H), 0.93 (t, *J* = 7.3 Hz, 3H).

N-((3R,6S,9S,12R)-6-((R)-sec-butyl)-9-(3-guanidinopropyl)-12-methyl-2,5,8,11-tetraoxo-3-phenyl-1,4,7,10-tetraazacyclotetradecan-12-yl)isobutyramide (LC-314)

LC-314 was synthesized using the procedure applied for **LC-081** to yield 7.8 mg, white powder, 14 % yield over 4 steps.

LC-MS(ESI) m/z $(M+H)^+$: 587.44; calcd for $C_{29}H_{47}N_8O_5$ $(M+H)^+$: 587.37; >98% purity.

^{1}H NMR (400 MHz, Methanol-d_4) δ 8.53 (s, 1H), 8.22 (d, *J* = 3.6 Hz, 1H), 8.01 (d, *J* = 9.0 Hz, 1H), 7.92 (t, *J* = 9.7 Hz, 2H), 7.42 – 7.35 (m, 2H), 7.35 – 7.23 (m, 3H), 5.46 (d, *J* = 9.0 Hz, 1H), 4.61 (dd, *J* = 10.2, 3.7 Hz, 1H), 4.14 (ddd, *J* = 7.7, 6.3, 3.5 Hz, 1H), 3.75 (td, *J* = 9.6, 5.3 Hz, 1H), 3.28 – 3.13 (m, 2H), 2.77 – 2.57 (m, 3H), 2.36 – 2.23 (m, 1H), 1.94 – 1.58 (m, 5H), 1.52 (s, 3H), 1.36 – 1.25 (m, 2H), 1.22 (d, *J* = 6.9 Hz, 3H), 1.18 (d, *J* = 6.7 Hz, 3H), 0.97 – 0.89 (m, 6H).

N-((8S,11R,16R)-8-(3-guanidinopropyl)-11-methyl-7,10,15,18-tetraoxo-16-phenyl-6,9,14,17-tetraazaspiro[4.13]octadecan-11-yl)isobutyramide (LC-322)

LC-322 was synthesized using the procedure applied for **LC-081** to yield 4.2 mg, white powder, 7 % yield over 4 steps.

LC-MS(ESI) m/z $(M+H)^+$: 585.43; calcd for C29H45N8O5 $(M+H)^+$: 585.35; >98% purity.

***N*-((3*R*,6*S*,9*S*,12*R*)-6-ethyl-9-(3-guanidinopropyl)-3,12-dimethyl-2,5,8,11-tetraoxo-1,4,7,10-tetraazacyclotetradecan-12-yl)isobutyramide (AK-012)**

AK-012 was synthesized using the procedure applied for **LC-081**, white powder, 38 % yield over 4 steps.

MS (ESI): m/z calculated for C22H41N8O5 $[M+H]^+$ 497.32, found 497.20.

^{1}H NMR (400 MHz, Methanol-d_4) δ 8.50 (s, 1H), 8.24 (d, *J* = 4 Hz, 1H), 8.15 (d, *J* = 9.6 Hz, 1H), 7.62-7.58 (m, 1H), 7.52-7.45 (m, 1H), 4.51-4.38 (m, 2H), 4.12-4.05 (m, 1H), 3.78-3.68 (m, 1H), 3.28-3.18 (m, 3H), 2.76-2.68 (m, 1H), 2.65-2.50 (m, 2H), 2.22-2.12 (m, 1H), 1.92-1.83 (m, 2H), 1.80-1.65 (m, 4H), 1.50 (s, 3H), 1.36-1.28 (m, 6H), 1.19 (d, *J* = 6.8 Hz, 3H), 1.14 (d, *J* = 6.8 Hz, 3H), 0.94 (t, *J* = 7.6 Hz, 3H).

***N*-((3*R*,6*S*,9*S*,12*R*)-6-ethyl-9-(3-guanidinopropyl)-3-isobutyl-12-methyl-2,5,8,11-tetraoxo-1,4,7,10-tetraazacyclotetradecan-12-yl)isobutyramide (AK-010)**

AK-010 was synthesized using the procedure applied for **LC-081**, white powder, 35 % yield over 4 steps.

MS (ESI): m/z calculated for C25H47N8O5 $[M+H]^+$ 539.37, found 539.28.

^{1}H NMR (400 MHz, Methanol-d_4) δ 8.52 (s, 1H), 8.27-8.21 (m, *2*H), 7.61-7.57 (m, 1H), 7.27 (d, *J* = 9.2 Hz, 1H), 4.53-4.38 (m, 2H), 4.16-4.08 (m, 1H), 3.68-3.78 (m, 1H), 3.28-3.18 (m, 3H), 2.72-2.64 (m, 1H), 2.60-2.51 (m, 2H), 2.22-2.12 (m, 1H), 1.92-1.82 (m, 3H), 1.78-1.68 (m, 3H), 1.65-1.55 (m, 1H), 1.54-1.42 (m, 5H), 1.38-1.28 (m, 1H), 1.18 (d, *J* = 7.2 Hz, 3H), 1.16-1.08 (m, 5H), 0.97-0.90 (m, 9H).

***N*-((3*R*,6*S*,9*S*,12*R*)-3-cyclopentyl-6-ethyl-9-(3-guanidinopropyl)-12-methyl-2,5,8,11-tetraoxo-1,4,7,10-tetraazacyclotetradecan-12-yl)isobutyramide (AK-020)**

AK-020 was synthesized using the procedure applied for **LC-081**, white powder, 31 % yield over 4 steps.

MS (ESI): m/z calculated for C26H47N8O5 $[M+H]^+$ 551.37, found 551.46.

^{1}H NMR (400 MHz, Methanol-d_4) δ 8.48 (s, 1H), 8.23-8.17 (m, 2H), 7.62-7.59 (m, 1H), 7.35 (d, *J* = 10.0 Hz, 1H), 4.55-4.44 (m, 2H), 4.11-4.07 (m, 1H), 3.75-3.71 (m, 1H), 3.28-3.15 (m, 3H), 2.78-2.48 (m, 4H), 2.28-2.15 (m, 1H), 1.92-1.83 (m, 2H), 1.82-1.62 (m, 6H), 1.58-1.45 (m, 8H), 1.38-1.35 (m, 2H), 1.34-1.23 (m, 2H), 1.18 (d, *J* = 6.8 Hz, 3H), 1.13 (d, *J* = 6.8 Hz, 3H), 0.94 (t, *J* = 7.6 Hz, 3H).

***N*-((3*R*,6*S*,9*S*,12*R*)-3-cyclohexyl-6-ethyl-9-(3-guanidinopropyl)-12-methyl-2,5,8,11-tetraoxo-1,4,7,10-tetraazacyclotetradecan-12-yl)isobutyramide (AK-011)**

AK-011 was synthesized using the procedure applied for **LC-081**, white powder, 51 % yield over 4 steps.

MS (ESI): m/z calculated for $C_{27}H_{49}N_8O_5$ $[M+H]^+$ 565.38, found 565.39.

^{1}H NMR (400 MHz, Methanol-d_4) δ 8.54 (s, 1H), 8.25-8.17 (m, 2H), 7.64-7.58 (m, 1H), 7.28 (d, *J* = 9.6 Hz, 1H), 4.53-4.44 (m, 1H), 4.39-4.33 (m, 1H), 4.15-4.08 (m, 1H), 3.82-3.72 (m, 1H), 3.28-3.15 (m, 3H), 2.70-2.62 (m, 1H), 2.60-2.50 (m, 2H), 2.25-2.15 (m, 2H), 1.90-1.82 (m, 2H), 1.80-1.60 (m, 9H), 1.48 (s, 3H), 1.35-1.25 (m, 4H), 1.20-1.00 (m, 10H), 0.94 (t, *J* = 7.2 Hz, 3H).

***N*-((3*R*,6*S*,9*S*,12*R*)-3-(cyclohexylmethyl)-6-ethyl-9-(3-guanidinopropyl)-12-methyl-2,5,8,11-tetraoxo-1,4,7,10-tetraazacyclotetradecan-12-yl)isobutyramide (LC-261)**

LC-261 was synthesized using the procedure applied for **LC-081**, white powder, 34 % yield over 4 steps.

MS (ESI): m/z calculated for $C_{28}H_{51}N_8O_5$ $[M+H]^+$ 579.40, found 579.47.

^{1}H NMR (400 MHz, Methanol-d_4) δ 8.59 (s, 1H), 8.30-8.20 (m, 2H), 7.59 (d, *J* = 8.4 Hz, 1H), 7.28 (d, *J* = 9.6 Hz, 1H), 4.54-4.47 (m, 1H), 4.46-4.39 (m, 1H), 4.14-4.08 (m, 1H), 3.80-3.67 (m, 1H), 3.30-3.18 (m, 3H), 2.73-2.63 (m, 1H), 2.61-2.50 (m, 2H), 2.23-2.12 (m, 1H), 1.98-1.80 (m, 4H), 1.79-1.60 (m, 8H), 1.51-1.38 (m, 4H), 1.37-1.15 (m, 9H), 1.12 (d, *J* = 6.8 Hz, 3H), 1.15-0.85 (m, 6H).

***N*-((3*R*,6*S*,9*S*,12*R*)-3-benzyl-6-ethyl-9-(3-guanidinopropyl)-12-methyl-2,5,8,11-tetraoxo-1,4,7,10-tetraazacyclotetradecan-12-yl)isobutyramide (AK-005)**

AK-005 was synthesized using the procedure applied for **LC-081**, white powder, 56 % yield over 4 steps.

MS (ESI): m/z calculated for $C_{28}H_{45}N_8O_5$ $[M+H]^+$ 573.35, found 573.35.

^{1}H NMR (400 MHz, Methanol-d_4) δ 8.52 (s, 1H), 8.22 (d, *J* = 4.4 Hz, 1H), 8.15 (d, *J* = 9.6 Hz, 1H), 7.33 (d, *J* = 9.6 Hz, 1H), 7.25-7.14 (m, 5H), 4.66-4.59 (m, 1H), 4.24-4.14 (m, 1H), 4.13-4.09 (m, 1H), 3.82-3.72 (m, 1H), 3.48-3.42 (m, 1H), 3.30-3.15 (m, 1H), 2.75-2.55 (m, 4H), 2.07-1.97 (m, 1H), 1.90-1.82 (m, 1H), 1.80-1.60 (m, 4H), 1.50 (s, 3H), 1.38-1.28 (m, 1H), 1.18 (d, *J* = 6.8 Hz, 3H), 1.11 (d, *J* = 6.8 Hz, 3H), 0.86 (t, *J* = 7.6 Hz, 3H).

***N*-((3*R*,6*S*,9*S*,12*R*)-6-ethyl-3-(2-fluorobenzyl)-9-(3-guanidinopropyl)-12-methyl-2,5,8,11-tetraoxo-1,4,7,10-tetraazacyclotetradecan-12-yl)isobutyramide (AK-021)**

AK-021 was synthesized using the procedure applied for **LC-081**, white powder, 30 % yield over 4 steps.

MS (ESI): m/z calculated for $C_{28}H_{44}FN_8O_5$ $[M+H]^+$ 591.34, found 591.47.

^{1}H NMR (400 MHz, Methanol-d_4) δ 8.54 (s, 1H), 8.20 (d, *J* = 4.4 Hz, 1H), 8.13 (d, *J* = 9.6 Hz, 1H), 7.68-7.60 (m, 1H), 7.45-7.40 (m, 1H), 7.27-7.18 (m, 2H), 7.08-6.98 (m, 2H), 4.74-4.67 (m, 1H), 4.20-4.10 (m, 1H), 3.85-3.75 (m, 1H), 3.65-3.55 (m, 1H), 3.25-3.15 (m, 3H), 2.73-2.58 (m, 4H),

2.05-1.95 (m, 1H), 1.88-1.80 (m, 2H), 1.78-1.68 (m, 2H), 1.65-1.55 (m, 2H), 1.49 (s, 3H), 1.40-1.28 (m, 4H), 1.18 (d, *J* = 6.8 Hz, 3H), 1.11 (d, *J* = 6.8 Hz, 3H), 0.86 (t, *J* = 7.6 Hz, 3H).

_N_-((3_R_,6_S_,9_S_,12_R_)-6-ethyl-3-(3-fluorobenzyl)-9-(3-guanidinopropyl)-12-methyl-2,5,8,11-tetraoxo-1,4,7,10-tetraazacyclotetradecan-12-yl)isobutyramide (AK-022)

AK-022 was synthesized using the procedure applied for **LC-081**, white powder, 31 % yield over 4 steps.

MS (ESI): m/z calculated for $C_{28}H_{44}FN_8O_5$ $[M+H]^+$ 591.34, found 591.45.

^{1}H NMR (400 MHz, Methanol-d_4) δ 8.54 (s, 1H), 8.21 (d, *J* = 4.0 Hz, 1H), 8.11 (d, *J* = 9.6 Hz, 1H), 7.65-7.58 (m, 1H), 7.35 (d, *J* = 9.6 Hz, 1H), 7.30-7.20 (m, 1H), 7.03-6.95 (m, 2H), 6.94-6.86 (m, 1H), 4.69-4.62 (m, 1H), 4.28-4.20 (m, 1H), 4.13-4.07 (m, 1H), 3.82-3.72 (m, 1H), 3.47-3.40 (m, 1H), 3.30-3.20 (m, 2H), 2.80-2.72 (m, 1H), 2.70-2.50 (m, 3H), 2.10-2.00 (m, 1H), 1.95-1.80 (m, 3H), 1.79-1.60 (m, 4H), 1.48 (s, 3H), 1.40-1.28 (m, 3H), 1.18 (d, *J* = 6.8 Hz, 3H), 1.11 (d, *J* = 6.8 Hz, 3H), 0.88 (t, *J* = 7.6 Hz, 3H).

_N_-((3_R_,6_S_,9_S_,12_R_)-6-ethyl-3-(4-fluorobenzyl)-9-(3-guanidinopropyl)-12-methyl-2,5,8,11-tetraoxo-1,4,7,10-tetraazacyclotetradecan-12-yl)isobutyramide (AK-036)

AK-036 was synthesized using the procedure applied for **LC-081**, white powder, 27 % yield over 4 steps.

MS (ESI): m/z calculated for $C_{28}H_{44}FN_8O_5$ $[M+H]^+$ 591.34, found 591.43.

^{1}H NMR (400 MHz, Methanol-d_4) δ 8.55 (s, 1H), 8.23 (d, *J* = 4.4 Hz, 1H), 8.10 (d, *J* = 9.6 Hz, 1H), 7.65-7.60 (m, 1H), 7.34 (d, *J* = 9.6 Hz, 1H), 7.21-7.16 (m, 2H), 7.00-6.90 (m, 2H), 4.65-4.57 (m, 1H), 4.30-4.20 (m, 1H), 4.12-4.06 (m, 1H), 3.83-3.73 (m, 1H), 3.43-3.36 (m, 1H), 3.30-3.15 (m, 3H), 2.80-2.72 (m, 1H), 2.71-2.50 (m, 3H), 2.10-2.00 (m, 1H), 1.90-1.80 (m, 2H), 1.79-1.60 (m, 4H), 1.48 (s, 3H), 1.35-1.27 (m, 1H), 1.17 (d, *J* = 6.8 Hz, 3H), 1.11 (d, *J* = 6.8 Hz, 3H), 0.88 (t, *J* = 7.2 Hz, 3H).

_N_-((3_R_,6_S_,9_S_,12_R_)-6-ethyl-9-(3-guanidinopropyl)-12-methyl-3-(naphthalen-1-ylmethyl)-2,5,8,11-tetraoxo-1,4,7,10-tetraazacyclotetradecan-12-yl)isobutyramide (AK-033)

AK-033 was synthesized using the procedure applied for **LC-081**, white powder, 15 % yield over 4 steps.

MS (ESI): m/z calculated for $C_{32}H_{47}N_8O_5$ $[M+H]^+$ 623.37, found 623.48.

^{1}H NMR (400 MHz, Methanol-d_4) δ 8.54 (s, 1H), 8.23-8.18 (m, 1H), 8.12 (d, *J* = 10.0 Hz, 1H), 7.85-7.73 (m, 3H), 7.70-7.63 (m, 2H), 7.47-7.35 (m, 4H), 4.78-4.70 (m, 1H), 4.23-4.16 (m, 1H), 4.15-4.07 (m, 1H), 3.85-3.75 (m, 1H), 3.65-3.58 (m, 1H), 3.30-3.20 (m, 2H), 2.95-2.85 (m, 1H), 2.70-2.52 (m, 3H), 2.00-1.93 (m, 1H), 1.88-1.81 (m, 2H), 1.78-1.65 (m, 2H), 1.64-1.55 (m, 1H), 1.48 (s, 3H), 1.40-1.30 (m, 1H), 1.18 (d, *J* = 6.8 Hz, 3H), 1.11 (d, *J* = 6.8 Hz, 3H), 0.83 (t, *J* = 7.6 Hz, 3H).

N-((3R,6S,9S,12R)-6-ethyl-9-(3-guanidinopropyl)-3,12-dimethyl-2,5,8,11-tetraoxo-3-phenyl-1,4,7,10-tetraazacyclotetradecan-12-yl)isobutyramide (LC-294)

LC-294 was synthesized using the procedure applied for **LC-081** to yield 2.5 mg, white powder, 5 % yield over 4 steps.

LC-MS(ESI) m/z $(M+H)^+$: 573.32; calcd for $C_{28}H_{45}N_8O_5$ $(M+H)^+$: 573.35; >98% purity.

N-((3R,6S,9S,12R)-6-ethyl-3-(2-fluorophenyl)-9-(3-guanidinopropyl)-12-methyl-2,5,8,11-tetraoxo-1,4,7,10-tetraazacyclotetradecan-12-yl)isobutyramide (LC-334)

LC-334 was synthesized using the procedure applied for **LC-081** to yield 10.5 mg, white powder, 18 % yield over 4 steps.

LC-MS(ESI) m/z $(M+H)^+$: 577.39; calcd for $C_{27}H_{42}FN_8O_5$ $(M+H)^+$: 577.33; >98% purity.

^{1}H NMR (400 MHz, Methanol-d_4) δ 8.62 (s, 1H), 8.35 (d, *J* = 3.9 Hz, 1H), 8.18 (d, *J* = 9.5 Hz, 1H), 8.07 (d, *J* = 9.2 Hz, 1H), 7.89 – 7.73 (m, 1H), 7.43 (td, *J* = 7.5, 1.7 Hz, 1H), 7.36 – 7.26 (m, 1H), 7.14 (td, *J* = 7.6, 1.2 Hz, 1H), 7.08 (ddd, *J* = 9.6, 8.3, 1.2 Hz, 1H), 5.84 (d, *J* = 9.2 Hz, 1H), 4.41 (td, *J* = 10.1, 3.7 Hz, 1H), 4.15 (td, *J* = 7.5, 7.0, 3.9 Hz, 1H), 3.87 – 3.65 (m, 1H), 3.22 (ddt, *J* = 13.6, 11.4, 7.1 Hz, 2H), 2.79 – 2.50 (m, 3H), 2.19 (m, *J* = 14.8, 7.5, 3.8 Hz, 1H), 1.93 – 1.67 (m, 5H), 1.52 (s, 3H), 1.36 – 1.28 (m, 1H), 1.22 (d, *J* = 6.9 Hz, 3H), 1.16 (d, *J* = 6.6 Hz, 3H), 0.96 (t, *J* = 7.4 Hz, 3H).

N-((3R,6S,9S,12R)-6-ethyl-3-(3-fluorophenyl)-9-(3-guanidinopropyl)-12-methyl-2,5,8,11-tetraoxo-1,4,7,10-tetraazacyclotetradecan-12-yl)isobutyramide (LC-321)

LC-321 was synthesized using the procedure applied for **LC-081** to yield 8.0 mg, white powder, 14 % yield over 4 steps.

LC-MS(ESI) m/z $(M+H)^+$: 577.34; calcd for C27H42FN8O5 $(M+H)^+$: 577.33; >98% purity.

^{1}H NMR (400 MHz, Methanol-d_4) δ 8.64 (s, 1H), 8.38 (d, *J* = 3.9 Hz, 1H), 8.16 (d, *J* = 9.5 Hz, 1H), 8.06 (d, *J* = 9.2 Hz, 1H), 7.86 (dd, *J* = 9.9, 2.9 Hz, 1H), 7.34 (td, *J* = 8.0, 5.9 Hz, 1H), 7.21 (dt, *J* = 7.7, 1.2 Hz, 1H), 7.17 (dt, *J* = 9.8, 2.1 Hz, 1H), 7.11 – 6.91 (m, 1H), 5.49 (d, *J* = 9.2 Hz, 1H), 4.39 (td, *J* = 10.1, 3.6 Hz, 1H), 4.17 (td, *J* = 7.5, 7.0, 3.9 Hz, 1H), 3.85 – 3.64 (m, 1H), 3.28 – 3.15 (m, 2H), 2.76 – 2.55 (m, 3H), 2.19 (ddd, *J* = 14.2, 7.4, 3.7 Hz, 1H), 1.87 – 1.66 (m, 5H), 1.53 (s, 3H), 1.37 (dd, *J* = 6.7, 3.7 Hz, 1H), 1.22 (d, *J* = 6.9 Hz, 3H), 1.16 (d, *J* = 6.6 Hz, 3H), 0.96 (t, *J* = 7.4 Hz, 3H).

_N_-((3_R_,6_S_,9_S_,12_R_)-6-ethyl-3-(4-fluorophenyl)-9-(3-guanidinopropyl)-12-methyl-2,5,8,11-tetraoxo-1,4,7,10-tetraazacyclotetradecan-12-yl)isobutyramide (AK-035-2)

AK-035-2 was synthesized using the procedure applied for **LC-081** to yield 8.0 mg, white powder, 10 % yield over 4 steps.

MS (ESI): m/z calculated for $C_{27}H_{42}FN_8O_5$ $[M+H]^+$ 577.33, found 577.34.

^{1}H NMR (400 MHz, Methanol-d_4) δ 8.61 (s, 1H), 8.35-8.30 (m, 1H), 8.16 (d, *J* = 9.6 Hz, 1H), 8.02 (d, *J* = 9.2 Hz, 1H), 7.90-7.82 (m, 1H), 7.44-7.39 (m, 2H), 7.07-7.02 (m, 2H), 5.47 (d, *J* = 8.8 Hz, 1H), 4.44-4.35 (m, 1H), 4.20-4.10 (m, 1H), 3.80-3.72 (m, 1H), 3.30-3.17 (m, 3H), 2.80-2.60 (m, 3H), 2.24-2.12 (m, 1H), 1.92-1.68 (m, 6H), 1.53 (s, 3H), 1.38-1.32 (m, 1H), 1.22 (d, *J* = 6.8 Hz, 3H), 1.20-1.10 (m, 4H), 0.96 (t, *J* = 7.6 Hz, 3H).

***N*-((3*R*,6*S*,9*S*,12*R*)-3-(2-chlorophenyl)-6-ethyl-9-(3-guanidinopropyl)-12-methyl-2,5,8,11-tetraoxo-1,4,7,10-tetraazacyclotetradecan-12-yl)isobutyramide (AK-057)**

AK-057 was synthesized using the procedure applied for **LC-081** to yield 8.0 mg, white powder, 26 % yield over 4 steps.

MS (ESI): m/z calculated for C27H42ClN8O5 $[M+H]^+$ 593.30, found 593.29.

^{1}H NMR (400 MHz, Methanol-d_4) δ 8.40 (s, 2H), 8.24 (d, *J* = 5.2 Hz, 1H), 7.99 (d, *J* = 9.2 Hz, 1H), 7.90-7.85 (m, 1H), 7.55-7.45 (m, 1H), 7.35-7.25 (m, 3H), 7.20-7.24 (m, 1H), 5.25-5.23 (m, 1H), 4.35-4.25 (m, 1H), 4.10-3.99 (m, 1H), 3.40-3.05 (m, 3H), 2.70-2.55 (m, 3H), 2.05-1.60 (m, 8H), 1.25-1.15 (m, 6H), 0.86 (t, *J* = 7.6 Hz, 3H).

***N*-((6*S*,9*S*,12*R*)-3-(3-chlorophenyl)-6-ethyl-9-(3-guanidinopropyl)-12-methyl-2,5,8,11-tetraoxo-1,4,7,10-tetraazacyclotetradecan-12-yl)isobutyramide (AK-058)**

AK-058 was synthesized using the procedure applied for **LC-081** to yield 8.0 mg, white powder, 15 % yield over 4 steps.

MS (ESI): m/z calculated for C27H42ClN8O5 $[M+H]^+$ 593.30, found 593.29.

^{1}H NMR (400 MHz, Methanol-d_4) δ 8.60 (s, 1H), 8.31 (d, *J* = 4.0 Hz, 1H), 8.21 (d, *J* = 9.2 Hz, 1H), 8.10 (d, *J* = 8.8 Hz, 1H), 7.80-7.70 (m, 1H), 7.51-7.48 (m, 1H), 7.42-7.41 (m, 1H), 7.32-7.28 (m, 2H), 6.05(d, *J* = 9.2 Hz, 1H), 4.43-4.39 (m, 1H), 4.19-4.18 (m, 1H), 3.85-3.70 (m, 1H), 3.33-3.25 (m, 2H), 2.78-2.62 (m, 3H), 2.28-2.15 (m, 1H), 1.90-1.70 (m, 5H), 1.54 (s, 3H), 1.40-1.32 (m, 1H), 1.25 (d, *J* = 6.8 Hz, 3H), 1.20 (d, *J* = 6.8 Hz, 3H), 0.97 (t, *J* = 7.2 Hz, 3H).

***N*-((3*R*,6*S*,9*S*,12*R*)-3-(4-chlorophenyl)-6-ethyl-9-(3-guanidinopropyl)-12-methyl-2,5,8,11-tetraoxo-1,4,7,10-tetraazacyclotetradecan-12-yl)isobutyramide (AK-059)**

AK-059 was synthesized using the procedure applied for **LC-081** to yield 8.0 mg, white powder, 20 % yield over 4 steps.

MS (ESI): m/z calculated for $C_{27}H_{42}ClN_8O_5$ $[M+H]^+$ 593.30, found 593.29.

^{1}H NMR (400 MHz, Methanol-d_4) δ 8.40-8.39 (m, 2H), 8.23-8.21 (d, *J* = 6 Hz, 1H), 8.00 (d, *J* = 9.2 Hz, 1H), 7.87-7.85 (m, 1H), 7.51-7.49 (m, 1H), 7.33 (d, *J* = 8.4 Hz, 2H), 7.26 (d, *J* = 8.4 Hz, 2H), 5.24 (s, 1H), 4.32-4.27 (m, 1H), 4.04-4.03 (m, 1H), 3.35-3.20 (m, 2H), 3.18-3.08 (m, 1H), 2.70-2.55 (m, 1H), 2.00-1.60 (m, 8H), 1.56 (s, 3H), 1.25-1.15 (m, 6H), 1.05 (t, *J* = 7.2 Hz, 3H).

***N*-((3*R*,6*S*,9*S*,12*R*)-6-ethyl-9-(3-guanidinopropyl)-3-(2-methoxyphenyl)-12-methyl-2,5,8,11-tetraoxo-1,4,7,10-tetraazacyclotetradecan-12-yl)isobutyramide (AK-042)**

AK-042 was synthesized using the procedure applied for **LC-081** to yield 8.0 mg, white powder, 25% yield over 4 steps.

MS (ESI): m/z calculated for $C_{28}H_{45}N_8O_6$ $[M+H]^+$ 589.35, found 589.25.

^{1}H NMR (400 MHz, Methanol-d_4) δ 8.51 (s, 1H), 8.32 (d, *J* = 9.6 Hz, 1H), 8.19 (d, *J* = 4 Hz, 1H), 7.89 (d, *J* = 9.2 Hz), 7.32-7.22 (m, 2H), 7.00-6.89 (m, 2H), 5.76 (d, *J* = 9.2 Hz, 1H), 4.45-4.35 (m, 1H), 4.25-4.15 (m, 1H), 3.85 (s, 3H), 3.82-3.72 (m, 1H), 3.40-3.15 (m, 3H), 2.75-2.60 (m, 2H), 2.20-2.15 (m, 1H), 1.80-1.70 (m, 4H), 1.79-1.60 (m, 4H), 1.53 (s, 3H), 1.38-1.32 (m, 1H), 1.22 (d, *J* = 6.8 Hz, 3H), 1.20-1.10 (m, 4H), 0.96 (t, *J* = 7.6 Hz, 3H).

N-((3R,6S,9S,12R)-6-ethyl-9-(3-guanidinopropyl)-3-(3-methoxyphenyl)-12-methyl-2,5,8,11-tetraoxo-1,4,7,10-tetraazacyclotetradecan-12-yl)isobutyramide (LC-345)

LC-345 was synthesized using the procedure applied for **LC-202** from **LC-343** to yield 2.3 mg, white powder, 42 % yield.

LC-MS(ESI) m/z $(M+H)^+$: 589.36; calcd for $C_{28}H_{45}N_8O_6$ $(M+H)^+$: 589.35; >98% purity.

^{1}H NMR (400 MHz, Methanol-d_4) δ 8.59 (s, 1H), 8.32 (d, *J* = 4.1 Hz, 1H), 8.19 (d, *J* = 9.5 Hz, 1H), 7.96 (d, *J* = 9.2 Hz, 1H), 7.87 (d, *J* = 9.2 Hz, 1H), 7.22 (t, *J* = 7.9 Hz, 1H), 7.08 – 7.01 (m, 1H), 6.97 (dt, *J* = 7.6, 1.2 Hz, 1H), 6.89 – 6.77 (m, 1H), 5.42 (d, *J* = 9.1 Hz, 1H), 4.38 (td, *J* = 10.1, 3.8 Hz, 1H), 4.16 (td, *J* = 7.5, 7.1, 4.1 Hz, 1H), 3.91 – 3.65 (m, 4H), 3.29 – 3.15 (m, 2H), 2.78 – 2.54 (m, 3H), 2.18 (ddd, *J* = 14.1, 7.4, 3.9 Hz, 1H), 1.94 – 1.62 (m, 5H), 1.53 (s, 3H), 1.41 – 1.34 (m, 1H), 1.28 – 1.20 (m, 3H), 1.16 (d, *J* = 6.7 Hz, 3H), 0.95 (t, *J* = 7.4 Hz, 3H).

N-((3R,6S,9S,12R)-6-ethyl-9-(3-guanidinopropyl)-3-(4-methoxyphenyl)-12-methyl-2,5,8,11-tetraoxo-1,4,7,10-tetraazacyclotetradecan-12-yl)isobutyramide (LC-339)

LC-339 was synthesized using the procedure applied for **LC-081** to yield 6.0 mg, white powder, 10 % yield over 4 steps.

LC-MS(ESI) m/z $(M+H)^+$: 589.38; calcd for $C_{28}H_{45}N_8O_6$ $(M+H)^+$: 589.35; >98% purity.

^{1}H NMR (400 MHz, Methanol-d_4) δ 8.59 (s, 1H), 8.32 (d, *J* = 4.1 Hz, 1H), 8.20 (d, *J* = 9.5 Hz, 1H), 7.92 (d, *J* = 9.2 Hz, 1H), 7.85 (d, *J* = 9.2 Hz, 1H), 7.39 – 7.25 (m, 2H), 6.94 – 6.83 (m, 2H), 5.41 (d, *J* = 9.2 Hz, 1H), 4.37 (td, *J* = 10.1, 3.8 Hz, 1H), 4.15 (td, *J* = 7.5, 7.0, 4.0 Hz, 1H), 3.91 – 3.61 (m, 4H),

3.28 – 3.12 (m, 2H), 2.74 – 2.52 (m, 3H), 2.26 – 2.11 (m, 1H), 1.96 – 1.69 (m, 5H), 1.52 (s, 3H), 1.40 – 1.31 (m, 1H), 1.22 (d, *J* = 6.9 Hz, 3H), 1.16 (d, *J* = 6.6 Hz, 3H), 0.95 (t, *J* = 7.4 Hz, 3H).

N-((3R,6S,9S,12R)-6-ethyl-9-(3-guanidinopropyl)-12-methyl-3-(naphthalen-1-yl)-2,5,8,11-tetraoxo-1,4,7,10-tetraazacyclotetradecan-12-yl)isobutyramide (LC-324)

LC-324 was synthesized using the procedure applied for **LC-081** to yield 3.3 mg, white powder, 6 % yield over 4 steps.

LC-MS(ESI) m/z $(M+H)^+$: 609.35; calcd for C31H45N8O5 $(M+H)^+$: 609.35; >98% purity.

N-((3R,6S,9S,12R)-6-ethyl-9-(3-guanidinopropyl)-12-methyl-3-(naphthalen-2-yl)-2,5,8,11-tetraoxo-1,4,7,10-tetraazacyclotetradecan-12-yl)isobutyramide (LC-326)

LC-326 was synthesized using the procedure applied for **LC-081** to yield 9 mg, white powder, 15 % yield over 4 steps.

LC-MS(ESI) m/z $(M+H)^+$: 609.42; calcd for C31H45N8O5 $(M+H)^+$: 609.35; >98% purity.

^{1}H NMR (400 MHz, Methanol-d_4) δ 8.63 (s, 1H), 8.37 (d, *J* = 4.0 Hz, 1H), 8.22 (d, *J* = 9.5 Hz, 1H), 8.13 (d, *J* = 9.2 Hz, 1H), 7.94 (d, *J* = 8.5 Hz, 1H), 7.89 – 7.78 (m, 4H), 7.58 (dd, *J* = 8.5, 1.8 Hz, 1H), 7.52 – 7.38 (m, 2H), 5.66 (d, *J* = 9.1 Hz, 1H), 4.40 (td, *J* = 10.1, 3.7 Hz, 1H), 4.19 (td, *J* = 7.1, 4.0 Hz, 1H), 3.88 – 3.73 (m, 1H), 3.28 – 3.11 (m, 2H), 2.79 – 2.55 (m, 3H), 2.28 – 2.10 (m, 1H), 1.92 – 1.68 (m, 5H), 1.55 (s, 3H), 1.43 – 1.34 (m, 1H), 1.24 (d, *J* = 6.9 Hz, 3H), 1.18 (d, *J* = 6.7 Hz, 3H), 0.97 (t, *J* = 7.4 Hz, 3H).

N-((3R,6S,9S,12R)-6-ethyl-12-methyl-2,5,8,11-tetraoxo-9-phenethyl-3-phenyl-1,4,7,10-tetraazacyclotetradecan-12-yl)isobutyramide (LC-186-2)

LC-186-2 was synthesized using the procedure applied for **LC-081** to yield 3.9 mg, white powder, 7 % yield over 3 steps.

LC-MS(ESI) m/z $(M+H)^+$: 564.39; calcd for $C_{31}H_{42}N_5O_5$ $(M+H)^+$: 564.32; >98% purity.

^{1}H NMR (400 MHz, Methanol-d_4) δ 8.56 (s, 1H), 8.31 (d, *J* = 4.3 Hz, 1H), 8.21 (d, *J* = 9.5 Hz, 1H), 7.99 (d, *J* = 9.2 Hz, 1H), 7.88 (d, *J* = 9.2 Hz, 1H), 7.53 – 7.38 (m, 2H), 7.38 – 7.25 (m, 5H), 7.25 – 7.08 (m, 3H), 5.46 (d, *J* = 9.2 Hz, 1H), 4.39 (td, *J* = 10.1, 3.8 Hz, 1H), 4.10 (ddd, *J* = 8.1, 5.6, 4.2 Hz, 1H), 3.84 – 3.68 (m, 1H), 2.86 – 2.56 (m, 5H), 2.24 – 2.01 (m, 3H), 1.86 – 1.71 (m, 1H), 1.55 (s, 3H), 1.42 – 1.32 (m, 1H), 1.23 (d, *J* = 6.9 Hz, 3H), 1.17 (d, *J* = 6.6 Hz, 3H), 0.97 (t, *J* = 7.4 Hz, 3H).

N-((3R,6S,9S,12R)-6-ethyl-12-methyl-2,5,8,11-tetraoxo-3-phenyl-9-(3-phenylpropyl)-1,4,7,10-tetraazacyclotetradecan-12-yl)isobutyramide (LC-183-2)

LC-183-2 was synthesized using the procedure applied for **LC-081** to yield 3.9 mg, white powder, 7 % yield over 3 steps.

LC-MS(ESI) m/z $(M+H)^+$: 578.43; calcd for $C_{32}H_{44}N_5O_5$ $(M+H)^+$: 578.33; >98% purity.

^{1}H NMR (400 MHz, Methanol-d_4) δ 8.53 (s, 1H), 8.20 (d, *J* = 3.9 Hz, 1H), 8.11 (d, *J* = 9.5 Hz, 1H), 8.02 (d, *J* = 9.2 Hz, 1H), 7.87 (d, *J* = 9.4 Hz, 1H), 7.46 – 7.37 (m, 2H), 7.37 – 7.21 (m, 5H), 7.21 – 7.06 (m, 3H), 5.45 (d, *J* = 9.2 Hz, 1H), 4.36 (td, *J* = 10.1, 3.7 Hz, 1H), 4.19 – 4.05 (m, 1H), 3.84 – 3.68 (m, 1H), 2.76 – 2.49 (m, 5H), 2.16 (ddd, *J* = 14.2, 7.4, 3.8 Hz, 1H), 1.90 – 1.67 (m, 5H), 1.51

(s, 3H), 1.37 – 1.32 (m, 1H), 1.20 (d, *J* = 6.9 Hz, 3H), 1.12 (d, *J* = 6.7 Hz, 3H), 0.91 (t, *J* = 7.4 Hz, 3H).

N-((3R,6S,9S,12R)-6-ethyl-12-methyl-2,5,8,11-tetraoxo-3-phenyl-9-(3-ureidopropyl)-1,4,7,10-tetraazacyclotetradecan-12-yl)isobutyramide (LC-187-2)

LC-187-2 was synthesized using the procedure applied for **LC-081** to yield 3.2 mg, white powder, 6 % yield over 3 steps.

LC-MS(ESI) m/z $(M+H)^+$: 560.26; calcd for $C_{27}H_{42}N_7O_6$ $(M+H)^+$: 560.32; >98% purity.

^{1}H NMR (400 MHz, Methanol-d_4) δ 8.57 (s, 1H), 8.48 (s, 1H), 8.18 (d, *J* = 9.5 Hz, 1H), 8.04 (d, *J* = 9.2 Hz, 1H), 7.52 – 7.40 (m, 2H), 7.40 – 7.15 (m, 4H), 5.46 (d, *J* = 9.3 Hz, 1H), 4.39 (td, *J* = 10.1, 3.7 Hz, 1H), 4.14 (td, *J* = 6.5, 3.6 Hz, 1H), 3.83 – 3.71 (m, 1H), 3.17 (q, *J* = 6.6 Hz, 2H), 2.77 – 2.60 (m, 3H), 2.19 (ddt, *J* = 14.9, 11.3, 7.2 Hz, 1H), 1.93 – 1.77 (m, 3H), 1.67 – 1.59 (m, 2H), 1.54 (s, 3H), 1.39 – 1.33 (m, 1H), 1.22 (d, *J* = 6.9 Hz, 3H), 1.16 (d, *J* = 6.7 Hz, 3H), 0.96 (t, *J* = 7.4 Hz, 3H)

N-((3R,6S,9S,12R)-9-(4-(dimethylamino)butyl)-6-ethyl-12-methyl-2,5,8,11-tetraoxo-3-phenyl-1,4,7,10-tetraazacyclotetradecan-12-yl)isobutyramide (LC-169)

LC-169 was synthesized using the procedure applied for **LC-164** from **LC-167** to yield 3.9 mg, white powder, 32 % yield.

LC-MS(ESI) m/z $(M+H)^+$: 559.45; calcd for $C_{29}H_{47}N_6O_5$ $(M+H)^+$: 559.36; >98% purity.

^{1}H NMR (400 MHz, Methanol-d_4) δ 8.60 (s, 1H), 8.32 (d, *J* = 4.1 Hz, 1H), 8.18 (d, *J* = 9.5 Hz, 1H), 8.00 (d, *J* = 9.2 Hz, 1H), 7.87 (d, *J* = 9.3 Hz, 1H), 7.58 – 7.39 (m, 2H), 7.39 – 7.16 (m, 3H), 5.46 (d, *J* = 9.2 Hz, 1H), 4.37 (td, *J* = 10.1, 3.8 Hz, 1H), 4.14 (td, *J* = 7.5, 7.0, 4.0 Hz, 1H), 3.82 – 3.69 (m, 1H), 3.12 (dd, *J* = 9.2, 6.9 Hz, 2H), 2.88 (s, 6H), 2.75 – 2.57 (m, 3H), 2.17 (dtd, *J* = 14.8, 7.4, 3.9 Hz, 1H), 1.95 – 1.83 (m, 2H), 1.83 – 1.67 (m, 3H), 1.61 – 1.41 (m, 5H), 1.40 – 1.32 (m, 1H), 1.23 (d, *J* = 6.9 Hz, 3H), 1.16 (d, *J* = 6.7 Hz, 3H), 0.95 (t, *J* = 7.4 Hz, 3H).

N-((3R,6S,9S,12R)-6-ethyl-12-methyl-9-(2-((1-methylpiperidin-4-yl)amino)ethyl)-2,5,8,11-tetraoxo-3-phenyl-1,4,7,10-tetraazacyclotetradecan-12-yl)isobutyramide (LC-174)

LC-174 was synthesized using the procedure applied for **LC-164** from **LC-172** to yield 3.8 mg, white powder, 65 % yield.

LC-MS(ESI) m/z (M +2H)$^{2+}$: 300.93; calcd for C31H51N7O5 (M +2H)$^{2+}$: 300.70; >98% purity.

^{1}H NMR (400 MHz, Methanol-d_4) δ 8.64 (s, 1H), 7.96 (d, *J* = 9.2 Hz, 1H), 7.94 – 7.83 (m, 1H), 7.47 – 7.38 (m, 2H), 7.38 – 7.21 (m, 3H), 5.47 (d, *J* = 9.2 Hz, 1H), 4.40 (dd, *J* = 10.5, 3.9 Hz, 1H), 4.30 (t, *J* = 7.5 Hz, 1H), 3.77 (t, *J* = 10.1 Hz, 1H), 3.64 (d, *J* = 12.5 Hz, 2H), 3.53 – 3.40 (m, 1H), 3.39 – 3.30 (m, 1H), 3.29 – 3.21 (m, 1H), 3.20 – 3.00 (m, 2H), 2.89 (s, 3H), 2.77 – 2.56 (m, 3H), 2.49 – 2.32 (m, 2H), 2.32 – 2.08 (m, 3H), 2.08 – 1.87 (m, 2H), 1.81 (ddd, *J* = 14.2, 10.5, 7.3 Hz, 1H), 1.54 (s, 3H), 1.40 – 1.31 (m, 1H), 1.22 (d, *J* = 6.9 Hz, 3H), 1.15 (d, *J* = 6.6 Hz, 3H), 0.95 (t, *J* = 7.4 Hz, 3H).

N-((3R,6S,9S,12R)-6-ethyl-12-methyl-9-(3-((1-methylpiperidin-4-yl)amino)propyl)-2,5,8,11-tetraoxo-3-phenyl-1,4,7,10-tetraazacyclotetradecan-12-yl)isobutyramide (LC-164)

LC-162 (18 mg, 0.035 mmol) was dissolved in DCE (2 mL). N-methyl-4-piperidone (6.5 uL, 0.5mmol) and $NaBH(OAc)_3$ (30 mg, 0.14 mmol) were added to the reaction. The reaction was stirred at room temperature for 4 hr and then quenched with saturated ammonium chloride solution (10 mL). The product was extracted with ethyl acetate (3* 10mL) and the combined organic solution was dried and concentrated under vacuum. The residue was purified with preparative HPLC using the C18 reverse phase column (Waters, Sunfire™ Prep C_{18} OBD™, 5µm, 50×100mm), yielding **LC-164 (**10.7 mg, white powder, 50 % yield).

LC-MS(ESI) m/z $(M+H)^+$: 614.53; calcd for C32H52N7O5 $(M+H)^+$: 614.40; >98% purity.

^{1}H NMR (400 MHz, Methanol-d_4) δ 8.61 (s, 1H), 8.43 (d, *J* = 4.1 Hz, 1H), 8.21 (d, *J* = 9.5 Hz, 1H), 7.99 (d, *J* = 9.1 Hz, 1H), 7.89 (dd, *J* = 9.4, 2.6 Hz, 1H), 7.45 – 7.37 (m, 2H), 7.37 – 7.24 (m, 3H), 5.46 (d, *J* = 9.2 Hz, 1H), 4.38 (td, *J* = 10.1, 3.8 Hz, 1H), 4.15 (dd, *J* = 7.6, 4.1 Hz, 1H), 3.79 – 3.71 (m, 1H), 3.65 (d, *J* = 12.6 Hz, 2H), 3.48 – 3.38 (m, 1H), 3.17 – 3.08 (m, 3H), 2.88 (s, 3H), 2.74 – 2.61 (m, 3H), 2.38 (d, *J* = 13.5 Hz, 2H), 2.18 (ddd, *J* = 14.2, 7.4, 3.9 Hz, 1H), 1.95 – 1.75 (m, 6H), 1.53 (s, 3H), 1.43 – 1.24 (m, 2H), 1.22 (d, *J* = 6.9 Hz, 3H), 1.15 (d, *J* = 6.6 Hz, 3H), 0.95 (t, *J* = 7.4 Hz, 3H).

N-((3R,6S,9S,12R)-9-(3-((4,5-dihydro-1H-imidazol-2-yl)amino)propyl)-6-ethyl-12-methyl-2,5,8,11-tetraoxo-3-phenyl-1,4,7,10-tetraazacyclotetradecan-12-yl)isobutyramide (LC-210)

LC-210 was synthesized using the procedure applied for **LC-202** from **LC-162** to yield 1.4 mg, white powder, 24 % yield.

LC-MS(ESI) m/z $(M+H)^+$: 583.31; calcd for C29H43N8O5 $(M+H)^+$: 583.34; >98% purity.

^{1}H NMR (400 MHz, Methanol-d_4) δ 8.80 (d, *J* = 6.7 Hz, 1H), 8.63 (d, *J* = 10.6 Hz, 1H), 8.33 (d, *J* = 4.0 Hz, 1H), 8.19 (d, *J* = 9.4 Hz, 1H), 7.99 (d, *J* = 9.1 Hz, 1H), 7.86 (d, *J* = 9.1 Hz, 1H), 7.52 – 7.23 (m, 5H), 6.89 – 6.82 (m, 1H), 5.45 (s, 1H), 4.38 (td, *J* = 10.0, 3.9 Hz, 1H), 4.22 – 4.12 (m, 1H), 3.96 – 3.88 (m, 1H), 3.80 – 3.56 (m, 2H), 2.76 – 2.51 (m, 3H), 2.23 – 2.14 (m, 1H), 1.99 – 1.67 (m, 5H), 1.53 (s, 3H), 1.40 – 1.31 (m, 2H), 1.22 (d, *J* = 6.9 Hz, 3H), 1.15 (d, *J* = 6.6 Hz, 3H), 0.93 (t, *J* = 7.4 Hz, 3H).

N-((3R,6S,9S,12R)-6-ethyl-12-methyl-2,5,8,11-tetraoxo-3-phenyl-9-(3-(pyridin-2-ylamino)propyl)-1,4,7,10-tetraazacyclotetradecan-12-yl)isobutyramide (LC-182)

LC-162 (5mg, 0.01 mmol) was dissolved in 2-fluoropyridine (0.2 mL). The reaction was heated to 120 ^{o}C for 4 hr under microwave. Then the reaction was cooled to room temperature and the residue was purified with preparative HPLC using the C18 reverse phase column (Waters, Sunfire™ Prep C_{18} OBD™, 5µm, 50×100mm), yielding **LC-182** (2.6 mg, , white powder, 45 % yield).

LC-MS(ESI) m/z (M +H)$^+$: 594.34; calcd for C31H44N7O5 (M +H)$^+$: 594.34; >98% purity.

^{1}H NMR (400 MHz, Methanol-d_4) δ 8.61 (s, 1H), 8.37 (d, *J* = 4.0 Hz, 1H), 8.23 (d, *J* = 9.5 Hz, 1H), 7.99 (d, *J* = 9.2 Hz, 1H), 7.95 – 7.78 (m, 3H), 7.47 – 7.38 (m, 2H), 7.37 – 7.23 (m, 3H), 7.05 (d, *J* = 9.1 Hz, 1H), 6.89 (t, *J* = 6.7 Hz, 1H), 5.47 (d, *J* = 9.2 Hz, 1H), 4.39 (td, *J* = 10.0, 3.7 Hz, 1H), 4.27 – 4.15 (m, 1H), 3.76 (t, *J* = 11.2 Hz, 1H), 3.52 – 3.38 (m, 2H), 2.78 – 2.57 (m, 3H), 2.18 (ddd, *J* = 14.2, 7.5, 4.0 Hz, 1H), 1.99 – 1.72 (m, 5H), 1.53 (s, 3H), 1.40 – 1.29 (m, 2H), 1.22 (d, *J* = 6.8 Hz, 3H), 1.16 (d, *J* = 6.5 Hz, 3H), 0.93 (t, *J* = 7.4 Hz, 3H).

N-((3R,6S,9S,12R)-6-ethyl-12-methyl-2,5,8,11-tetraoxo-3-phenyl-9-(3-(pyrimidin-2-ylamino)propyl)-1,4,7,10-tetraazacyclotetradecan-12-yl)isobutyramide (LC-227)

LC-227 was synthesized using the procedure applied for **LC-202** from **LC-162** to yield 2.3 mg, white powder, 69 % yield.

LC-MS(ESI) m/z $(M+H)^+$: 595.43; calcd for $C_{30}H_{43}N_8O_5$ $(M+H)^+$: 595.34; >98% purity.

^{1}H NMR (400 MHz, Methanol-d_4) δ 8.60 (s, 1H), 8.42 (d, *J* = 5.1 Hz, 2H), 8.31 (d, *J* = 4.0 Hz, 1H), 8.17 (d, *J* = 9.6 Hz, 1H), 8.02 (d, *J* = 9.2 Hz, 1H), 7.87 (d, *J* = 9.3 Hz, 1H), 7.50 – 7.22 (m, 5H), 6.79 (t, *J* = 5.1 Hz, 1H), 5.46 (d, *J* = 9.2 Hz, 1H), 4.38 (td, *J* = 10.1, 3.7 Hz, 1H), 4.23 – 4.13 (m, 1H), 3.82 – 3.71 (m, 1H), 3.48 (td, *J* = 7.0, 2.7 Hz, 2H), 2.75 – 2.56 (m, 3H), 2.22 – 2.11 (m, 1H), 1.96 – 1.86 (m, 2H), 1.86 – 1.71 (m, 3H), 1.53 (s, 3H), 1.36 – 1.28 (m, 2H), 1.21 (d, *J* = 6.9 Hz, 3H), 1.12 (d, *J* = 6.7 Hz, 3H), 0.93 (t, *J* = 7.4 Hz, 3H).

N-((3R,6S,9S,12R)-9-(3-((4,5-dihydro-1H-imidazol-2-yl)amino)propyl)-6-ethyl-12-methyl-2,5,8,11-tetraoxo-3-phenyl-1,4,7,10-tetraazacyclotetradecan-12-yl)isobutyramide (LC-202)

LC-162 (5mg, 0.01 mmol) was dissolved in Ethanol (0.2 mL) and DIEA (0.05 mL). 2-Methylthio-2-imidazoline hydroiodide (25mg, 0.1 mmol) was added to the reaction. The reaction was heated to 120 ^oC for 4 hr under microwave under there is no starting materials left checked by UPLC. Then the reaction was cooled to room temperature and the residue was purified with preparative HPLC using the C18 reverse phase column (Waters, Sunfire™ Prep C_{18} OBD™, 5µm, 50×100mm), yielding **LC-202** (3.1 mg, , white powder, 53 % yield).

LC-MS(ESI) m/z $(M+H)^+$: 585.47; calcd for $C_{29}H_{45}N_8O_5$ $(M+H)^+$: 585.35; >98% purity.

^{1}H NMR (400 MHz, Methanol-d_4) δ 8.60 (s, 1H), 8.33 (d, *J* = 4.1 Hz, 1H), 8.20 (d, *J* = 9.6 Hz, 1H), 7.99 (d, *J* = 9.2 Hz, 1H), 7.87 (d, *J* = 9.3 Hz, 1H), 7.44 – 7.38 (m, 2H), 7.36 – 7.25 (m, 3H), 5.46 (d, *J* = 9.2 Hz, 1H), 4.38 (td, *J* = 10.1, 3.8 Hz, 1H), 4.15 (td, *J* = 7.0, 4.1 Hz, 1H), 3.81 – 3.73 (m, 1H), 3.70 (s, 4H), 3.29 – 3.22 (m, 2H), 2.76 – 2.62 (m, 3H), 2.18 (ddt, *J* = 15.0, 7.5, 3.7 Hz, 1H), 1.92 – 1.71 (m, 5H), 1.53 (s, 3H), 1.40 – 1.30 (m, 2H), 1.23 (d, *J* = 6.9 Hz, 3H), 1.16 (d, *J* = 6.6 Hz, 3H), 0.95 (t, *J* = 7.4 Hz, 3H).

N-((3R,6S,9S,12R)-6-ethyl-12-methyl-2,5,8,11-tetraoxo-3-phenyl-9-(3-((1,4,5,6-tetrahydropyrimidin-2-yl)amino)propyl)-1,4,7,10-tetraazacyclotetradecan-12-yl)isobutyramide (LC-337)

LC-337 was synthesized using the procedure applied for **LC-202** from **LC-162** to yield 7.2 mg, white powder, 65 % yield.

LC-MS(ESI) m/z $(M+H)^+$: 599.46; calcd for $C_{30}H_{47}N_8O_5$ $(M+H)^+$: 599.37; >98% purity.

^{1}H NMR (400 MHz, Methanol-d_4) δ 8.60 (s, 1H), 8.33 (d, *J* = 4.1 Hz, 1H), 8.20 (d, *J* = 9.5 Hz, 1H), 7.99 (d, *J* = 9.2 Hz, 1H), 7.93 – 7.82 (m, 1H), 7.48 – 7.37 (m, 2H), 7.37 – 7.23 (m, 3H), 5.46 (d, *J* = 9.1 Hz, 1H), 4.38 (td, *J* = 10.1, 3.8 Hz, 1H), 4.15 (td, *J* = 7.1, 4.0 Hz, 1H), 3.81 – 3.71 (m, 1H), 3.38 – 3.32 (m, 4H), 3.26 – 3.08 (m, 2H), 2.76 – 2.57 (m, 3H), 2.26 – 2.10 (m, 1H), 1.98 – 1.90 (m, 2H), 1.90 – 1.65 (m, 5H), 1.53 (s, 3H), 1.42 – 1.32 (m, 1H), 1.22 (d, *J* = 6.9 Hz, 3H), 1.16 (d, *J* = 6.6 Hz, 3H), 0.95 (t, *J* = 7.4 Hz, 3H).

N-((3R,6S,9S,12R)-9-(3-(3-acetylguanidino)propyl)-6-ethyl-12-methyl-2,5,8,11-tetraoxo-3-phenyl-1,4,7,10-tetraazacyclotetradecan-12-yl)isobutyramide (LC-315)

LC-315 was synthesized using the procedure applied for **LC-202** from **LC-162** to yield 3.4 mg, white powder, 61 % yield.

LC-MS(ESI) m/z $(M+H)^+$: 601.44; calcd for $C_{29}H_{44}N_8O_6$ $(M+H)^+$: 600.34; >98% purity.

^{1}H NMR (400 MHz, Methanol-d_4) δ 8.60 (s, 1H), 8.33 (d, *J* = 4.0 Hz, 1H), 8.21 (d, *J* = 9.5 Hz, 1H), 7.99 (d, *J* = 9.2 Hz, 1H), 7.87 (d, *J* = 9.2 Hz, 1H), 7.49 – 7.37 (m, 2H), 7.37 – 7.20 (m, 3H), 5.46 (d, *J* = 9.2 Hz, 1H), 4.39 (td, *J* = 10.1, 3.8 Hz, 1H), 4.22 – 4.14 (m, 1H), 3.82 – 3.71 (m, 1H), 3.46 – 3.34 (m, 2H), 2.75 – 2.58 (m, 3H), 2.25 – 2.08 (m, 4H), 1.97 – 1.73 (m, 5H), 1.53 (s, 3H), 1.40 – 1.33 (m, 1H), 1.22 (d, *J* = 6.9 Hz, 3H), 1.16 (d, *J* = 6.7 Hz, 3H), 0.95 (t, *J* = 7.4 Hz, 3H).

N-((3R,6S,9S,12R)-6-ethyl-12-methyl-3-(naphthalen-2-yl)-2,5,8,11-tetraoxo-9-(3-((1,4,5,6-tetrahydropyrimidin-2-yl)amino)propyl)-1,4,7,10-tetraazacyclotetradecan-12-yl)isobutyramide (LC-395)

LC-395 was synthesized using the procedure applied for **LC-202** from **LC-162** to yield 3.9 mg, white powder, 68 % yield.

LC-MS(ESI) m/z $(M+H)^+$: 649.45; calcd for $C_{34}H_{49}N_8O_5$ $(M+H)^+$: 649.38; >98% purity.

^{1}H NMR (400 MHz, Methanol-d_4) δ 8.64 (s, 1H), 8.38 (d, *J* = 4.1 Hz, 1H), 8.22 (d, *J* = 9.5 Hz, 1H), 8.12 (d, *J* = 9.1 Hz, 1H), 7.93 (d, *J* = 8.8 Hz, 1H), 7.89 – 7.77 (m, 4H), 7.58 (dd, *J* = 8.5, 1.7 Hz, 1H), 7.51 – 7.44 (m, 2H), 5.65 (d, *J* = 9.1 Hz, 1H), 4.40 (td, *J* = 10.1, 3.7 Hz, 1H), 4.19 (td, *J* = 7.0, 3.9

Hz, 1H), 3.80 (t, *J* = 11.2 Hz, 1H), 3.37 – 3.32 (m, 4H), 3.26 – 3.10 (m, 2H), 2.78 – 2.59 (m, 3H), 2.27 – 2.17 (m, 1H), 1.97 – 1.65 (m, 7H), 1.55 (s, 3H), 1.40 – 1.34 (m, 1H), 1.24 (d, *J* = 6.9 Hz, 3H), 1.17 (d, *J* = 6.6 Hz, 3H), 0.96 (t, *J* = 7.5 Hz, 3H).

Cell Growth Inhibition, Apoptosis Analysis, and Western Blotting Assay

The human acute leukemia RS4;11 cell line (CRL-1873) was purchased from the American Type Culture Collection. In all experiments, RS4;11 human leukemia cells were used within three months of thawing fresh vials. RS4;11 cells were cultured in RPMI 1640 media supplemented with 10% FBS and 1% penicillin–streptomycin at 37 °C in a humidified atmosphere containing 5% CO2 in air.

In cell growth experiments, cells were seeded in 96-well cell culture plates at a density of 10000−20000 cells/well in 100 μL of culture medium. Each compound tested was serially diluted in the appropriate medium, and 100 μL of the diluted solution containing the tested compound was added to the appropriate wells of the cell plate. After addition of the tested compound, the cells were incubated for 4 days at 37 °C in an atmosphere of 5% CO2. Cell growth was evaluated by a lactate dehydrogenase-based WST-8 assay (Dojindo Molecular Technologies) using a Tecan Infinite M1000 multimode microplate reader (Tecan, Morrisville, NC). The WST-8 reagent was added to the plate, incubated for at least 1 h, and read at 450 nm. The readings were normalized to the DMSO-treated cells, and the IC50 was calculated by nonlinear regression analysis using GraphPad Prism 6 software.

To assess the effect of long-term treatment of compound **LC-089** on leukemia cells, MOLM-13 and MV4;11 cell lines were plated at a density of $5x10^4$cell/ml (2 ml total) in 24-well plates, and treated with the relevant concentrations On day 4, cell viability for each treatment was measured using the WST-8 cell count kit. Then 10% of viable cells from each well were transferred to freshly prepared medium containing corresponding concentrations of compound **LC-089** and cultured for additional 3 days. On day 7, cell viability for each treatment was determined.

For Western blot analysis, 2 × 106 cells/well were treated with compounds at the indicated concentrations for various times. Cells were collected and lysed in RIPA buffer containing protease inhibitors. An amount of 20 μg of lysate was run in each lane of a PAGE–SDS and blotted into PVDF membranes. Antibodies for immunoblotting were MDM2 (SMP14) and p53 (DO-1) purchased from Santa Cruz.

Efficacy and Pharmacodynamics Studies in the RS4;11 Xenograft Model in Mice

All animal experiments were done under the guidelines of the University of Michigan Committee for Use and Care of Animals and using an approved animal protocol (PRO00005315, PI, Shaomeng Wang).

To develop xenograft tumors, 5 × 106 RS4;11 cells with 50% Matrigel were injected subcutaneously on the dorsal side of severe combined immunodeficient (SCID) mice, obtained from Charles River, one tumor per mouse. When tumors reached ∼100 mm3, mice were randomly assigned to treatment and vehicle control groups. Animals were monitored daily for

any signs of toxicity and weighed 2–3 times per week during the treatment and weighed at least weekly after the treatment ended. Tumor size was measured 2–3 times per week by electronic calipers during the treatment period and at least weekly after the treatment was ended. Tumor volume was calculated as V = LW2/2, where L is the length and W is the width of the tumor.

For pharmacodynamic analysis, resected RS4;11 xenograft tumor tissues were ground into powder in liquid nitrogen and lysed in lysis buffer (1% CHAPS, 150 mM NaCl, 20 mM Tris-HCl, 1 mM. EDTA, 1 mM EGTA, and COMPLETE proteinase inhibitor (Roche)). Whole tumor lysates were separated on 4–20% Novex gels. The separated proteins were transferred to a polyvinylidene difluoride membrane for immunoblotting. The following antibodies were used: antibodies for MDM2(SMP14), p53 (DO-1), GAPDH (FL-335) from Santa Cruz Biotechnology; p21 (12D1), PARP (46D11), and caspase-3 (8G10) from Cell Signaling Technology. The secondary antibody used was horseradish peroxidase conjugated goat anti-rabbit (Thermo Scientific). The BIO-RAD Clarity Western Enhanced Chemiluminescence Substrates and HyBlot Chemiluminescence film were used for signal development and detection using a SRX-101A tabletop processor (Konica Minolta).

Determination of Drug Concentrations in Plasma and RS4;11 Tumor Tissue

Pharmacokinetics of compound 23 was determined in female SCID C.B-17 mice bearing RS4;11 tumors following a single intravenous dose of 5 mg/kg. **LE-102** was dissolved in the vehicle containing 20% (v/v) polyethylene glycol 400, 6% (v/v) Cremophor EL and 74% (v/v) PBS (20% PCP). Mice were sacrificed at 1, 2, 4, 8, 24 and 48 h after drug treatment and at 6 h after vehicle treatment, followed by collection of blood samples (300 µL) and tumor samples. Blood samples

were centrifuged at 15 000 rpm for 10 min, then the supernatant plasma was saved for analysis. Isolated tumor samples were immediately frozen and ground with a mortar and pestle in liquid nitrogen. All plasma and tumor samples were stored at −80 °C prior to analysis.

Plasma and tumor concentrations of **LE-102** were determined by a LC–MS/MS method developed and validated for this study. The LC–MS/MS method, consisting of a Shimadzu HPLC system and chromatographic separation of tested compound, was achieved using a Waters XBridge-C18 column (5 cm × 2.1 mm, 3.5 µm). An AB Sciex QTrap 5500 mass spectrometer equipped with an electrospray ionization source (Applied Biosystems, Toronto, Canada) in the positive-ion multiple reaction monitoring (MRM) mode was used for detection. The mobile phases were 0.1% formic acid in purified water (A) and 0.1% formic acid in acetonitrile (B). The gradient (B) was held at 10% (0–0.3 min), increased to 95% at 0.7 min, then held at isocratic 95% B for 2.3 min and then immediately stepped back down to 10% for 2 min re-equilibration. The flow rate was set at 0.4 mL/min.

Competitive Binding Experiments to WDR5 Protein

The binding affinities of these synthesized compounds were tested using a fluorescence polarization (FP) based competitive binding assay described earlier.[111] Briefly, to a 5 µl solution of the tested compound in DMSO, 120 µl of pre-incubated complex solution (N-terminal His-tagged WDR5 protein (residues 24-334), named WDR5Δ23, and 5-FAM labeled tracer) in assay buffer (0.1M Phosphate, 25mM KCl, 0.01% Triton, pH 6.5) was added, giving final concentrations of WDR5Δ23 and the tracer to be 4 nM and 0.6 nM, respectively. The plates were incubated at room temperature on a shaker for 3h, and then the mP values were measured using the Tecan

Infinite M-1000 plate reader (Tecan U.S., Research Triangle Park, NC). K_i values were calculated using the equation described previously.[111, 137]

***In vitro* cell-free MLL HMT functional assay**

The recombinant MLL complex containing human MLL (MLL1) protein (3735 - 3973) with N-terminal GST tag and MW= 53.7 kDa; full length human WDR5 with N-terminal 6×His tag and MW= 35 kDa; full length human ASH2L with N-terminal 6×His tag and MW= 61 kDa; full length human RbBP5 with N-terminal 6×His-tag and MW= 60 kDa, and full length human DPY30 with N-terminal 6×His-tag and MW=12 kDa, and recombinant nucleosomes were obtained from Activmotif (Carlsbad, CA). Anti-Histone H3 Lysine 4 (H3K4me1-2) AlphaLISA acceptor beads, AlphaScreen Streptavidin donor beads and biotinylated anti-H3 (C-terminus) antibody were obtained from PerkinElmer Life Sciences (Waltham, MA). 2.5 µl of compound serial dilutions in assay buffer with 4% DMSO and 5 µl of the pentameric MLL complex solution were added into a white low volume 384 well microtiter plate which was incubated for 30 minutes with gentle shaking at room temperature, followed by adding 2.5 µL of SAM/Nucleosome mixture. The methylation reaction was performed in 50 mM Tris, pH 8.5 with 1 mM DTT and 0.01% Tween-20 added right before the assay. Final concentrations of MLL complex, SAM, and nucleosomes were 5 nM, 200 nM, and 3 nM, respectively. Final DMSO in the reaction mixture was 1%. The reaction was allowed to perform for 120 minutes in dark with gentle shaking at room temperature. Concentrations of reaction components and times were adjusted accordingly for assay development experiments. 5 µL of high salt stopping solution (50 mM Tris, pH 7.4 with 1 M NaCl, 0.1% Tween-20, and 0.3% poly-L-Lysine) was added to stop the methylation reactions for 15

minutes. 5 µl of 5x acceptor beads/biotinylated anti-H3 antibody mixture in detection buffer (50 mM Tris, pH 7.4 with 0.3 M NaCl, 0.1% Tween-20, and 0.001% poly-L-Lysine) was added, followed by 1 hour incubation at room temperature to allow full interaction between antibodies and methylated nucleosomes. Add 5 µl of 5x streptavidin donor beads in detection and incubate 30 minutes.

Plates were read on a BMG CLARIOstar microplate reader with an excitation wavelength of 680 nm and emission wavelength of 615 nm. IC_{50} values of compounds were obtained by fitting the fluorescence intensities detected at 615 nm *vs* compound concentrations in a sigmoidal dose-response curve (variable slope) with a non-linear regression, using Graphpad Prism 6.0 software (Graphpad Software, San Diego, CA).

Computational Docking

Docking studies were performed using our previously reported structure of WDR5 in complex with **MM-101** (PDB ID: 4GM3) with the GOLD[26-27] program (version 5.2) with the Arg moiety of compound **MM-101** serving as a scaffold for constrained docking. For each genetic algorithm (GA) run, a maximum number of 200,000 operations were performed on a population of five islands of 100 individuals. Operator weights for cross-over, mutation, and migration were set to 95, 95, and 10, respectively. The docking simulations were terminated after 10 runs for each ligand, using the Goldscore fitness function to evaluate the docked conformations. The top 10 conformations were saved for analysis of the predicted docking modes.

NONMEM code for population PK study

```
$PROBLEM 5-COMPARTMENT ORAL MPA;

$DATA ../MPA_MPAG_AcMPAG_Feng.csv IGNORE=C

$INPUT C ID TIME AMT ADDL II CONC XDV DV=LNDV MDV CMT NDOS AGE WT SEX ALT AST
CREA TBIL HB

$SUBROUTINES ADVAN5 TRANS1

$MODEL

   NCOMPARTMENTS=5

   COMP=(1)    ;DOSE

   COMP=(2)    ;CENTRAL COMPARTMENT FOR Parent

   COMP=(3)    ;CENTRAL COMPARTMENT FOR MPAG

   COMP=(4)    ;CENTRAL COMPARTMENT FOR AcMPAG

   COMP=(5)    ;PERIPH COMPARTMENT FOR Parent



$PK

MU_1 = THETA(1)
```

```
MU_2 = THETA(2)

MU_3 = THETA(3)

MU_4 = THETA(4)

MU_5 = THETA(5)

MU_6 = THETA(6)

MU_7 = THETA(7)

MU_8 = THETA(8)

MU_9 = THETA(9)

MU_10 = THETA(10)

MU_11 = THETA(11)



CLM1  = EXP(MU_1+ETA(1))    ;CLM=CL_MPAG, LN(CLM)=MU_1+ETA(1)

V3   = EXP(MU_2+ETA(2))    ;V3 for MPAG

CL1  = EXP(MU_3+ETA(3))    ;CL1 for MPA

V2   = EXP(MU_4+ETA(4))    ;V2 for CENTRAL Parent
```

```
V5   = EXP(MU_5+ETA(5))     ;V5 for PERIPH Parent

Q    = EXP(MU_6+ETA(6))

K12  = EXP(MU_7+ETA(7))     ;MPA absorption RATE CONSTANT

K31  = EXP(MU_8+ETA(8))     ;EHR

CLM2  = EXP(MU_9+ETA(9))     ;CLM2=CL_AcMPAG,

V4   = EXP(MU_10+ETA(10))     ;V4 for AcMPAG

K41  = EXP(MU_11+ETA(11))     ;EHR of AcMPAG

FM1   = 0.9

FM2   = 0.1



K20=CL1*(1-FM1-FM2)/V2

K23=CL1*FM1/V2

K24=CL1*FM2/V2

K30=CLM1/V3

K40=CLM2/V4
```

```
K25=Q/V2

K52=Q/V5



S2 = V2/1000 ;Scaling factor

S3 = V3/1000 ;Scaling factor

S4 = V4/1000 ;Scaling factor



$ERROR (OBSERVATION ONLY)

;OBSERVATION ONLY: do not estimate EPSs for missing DVs

IPRED=LOG(F)

QSF=0

QK=0

IF (CMT.EQ.4) QK=1

IF (CMT.EQ.3) QSF=1

Y=LOG(F)+((1-QSF)*(1-QK)*ERR(1)+QSF*(1-QK)*ERR(2)+QK*(1-QSF)*ERR(3))
```

```
$THETA

(0,0.19)       ;1 CLM1 of MPAG

$THETA  (0,2.97)       ;2 V3 for MPAG CENTRAL COMP

$THETA  (0,2.93)       ;3 CL1

$THETA  (0,4.23)       ;4 V2 for MPA CENTRAL COMP

$THETA  (0,7.68)       ;5 V4 for MPA Periph COMP

$THETA  (0,3.35)       ;6 Q

$THETA  (-5,-0.095)    ;7 KA

$THETA  (-20,-10.7)    ;8 K31

$THETA  (0,1.69)       ;9 CLM2 of AcMPAG

$THETA  (0,4.46)       ;10 V5 for AcMPAG

$THETA  (-30,-3.74)    ;11 K41


$OMEGA
```

0.5 ;1.CLM1_MPAG

2.27 ;2.V3

0.25 ;3.CL1

0.76 ;4.V2

3.38 ;5.V4

0.79 ;6.Q

0.00001 FIX ;7.KA(K12)

0.00001 FIX ;8.K31

0.39 ;9.CLM2_AcMPAG

0.79 ;10.V5

0.00001 FIX ;11.K41

$SIGMA

0.5

0.2

```
0.4

;$EST METHOD=ITS INTER NITER=100 PRINT=10 NOABORT NOPRIOR=1 MCETA=10 NOCOV=0

$EST METHOD=SAEM EONLY=0 INTER CTYPE=3 NBURN=15000 NITER=1000 PRINT=500 DF=0
IACCEPT=0.4 NOCOV=0

$EST METHOD=IMP EONLY=1 NITER=5 ISAMPLE=1000 PRINT=1 DF=4 IACCEPT=1.0 MAPITER=0
NOCOV=0

$COVARIANCE MATRIX=R PRINT=E COMPRESS UNCONDITIONAL

$TABLE ID TIME AMT DV IPRED K12 CL1 CLM1 CLM2 V2 V3 V4 V5 K31 K41 WT CWRES CMT
CIWRES

NOPRINT ONEHEADER FILE=run8.fit

$TABLE ID ETAS(1:LAST)

NOPRINT ONEHEADER FILE=run8.eta
```

References

1. Wade, M.; Li, Y. C.; Wahl, G. M., MDM2, MDMX and p53 in oncogenesis and cancer therapy. *Nat Rev Cancer* **2013,** *13* (2), 83-96.

2. Brown, C. J.; Lain, S.; Verma, C. S.; Fersht, A. R.; Lane, D. P., Awakening guardian angels: drugging the p53 pathway. *Nat Rev Cancer* **2009,** *9* (12), 862-73.

3. Stiewe, T., The p53 family in differentiation and tumorigenesis. *Nat Rev Cancer* **2007,** *7* (3), 165-8.

4. Hainaut, P.; Hollstein, M., p53 and human cancer: the first ten thousand mutations. *Adv Cancer Res* **2000,** *77*, 81-137.

5. Momand, J.; Zambetti, G. P.; Olson, D. C.; George, D.; Levine, A. J., The mdm-2 oncogene product forms a complex with the p53 protein and inhibits p53-mediated transactivation. *Cell* **1992,** *69* (7), 1237-45.

6. Freedman, D. A.; Wu, L.; Levine, A. J., Functions of the MDM2 oncoprotein. *Cell Mol Life Sci* **1999,** *55* (1), 96-107.

7. Wu, X.; Bayle, J. H.; Olson, D.; Levine, A. J., The p53-mdm-2 autoregulatory feedback loop. *Genes Dev* **1993,** *7* (7A), 1126-32.

8. Juven-Gershon, T.; Oren, M., Mdm2: the ups and downs. *Mol Med* **1999,** *5* (2), 71-83.

9. Ding, Q.; Zhang, Z.; Liu, J. J.; Jiang, N.; Zhang, J.; Ross, T. M.; Chu, X. J.; Bartkovitz, D.; Podlaski, F.; Janson, C.; Tovar, C.; Filipovic, Z. M.; Higgins, B.; Glenn, K.; Packman, K.; Vassilev, L.

T.; Graves, B., Discovery of RG7388, a potent and selective p53-MDM2 inhibitor in clinical development. *J Med Chem* **2013,** *56* (14), 5979-83.

10. Holzer, P.; Masuya, K.; Furet, P.; Kallen, J.; Valat-Stachyra, T.; Ferretti, S.; Berghausen, J.; Bouisset-Leonard, M.; Buschmann, N.; Pissot-Soldermann, C.; Rynn, C.; Ruetz, S.; Stutz, S.; Chene, P.; Jeay, S.; Gessier, F., Discovery of a Dihydroisoquinolinone Derivative (NVP-CGM097): A Highly Potent and Selective MDM2 Inhibitor Undergoing Phase 1 Clinical Trials in p53wt Tumors. *J Med Chem* **2015,** *58* (16), 6348-58.

11. Aguilar, A.; Lu, J.; Liu, L.; Du, D.; Bernard, D.; McEachern, D.; Przybranowski, S.; Li, X.; Luo, R.; Wen, B.; Sun, D.; Wang, H.; Wen, J.; Wang, G.; Zhai, Y.; Guo, M.; Yang, D.; Wang, S., Discovery of 4-((3'R,4'S,5'R)-6''-Chloro-4'-(3-chloro-2-fluorophenyl)-1'-ethyl-2''-oxodispiro[cyclohexane-1,2'-pyrrolidine-3',3''-indoline]-5'-carboxamido)bicyclo[2.2.2]octane -1-carboxylic Acid (AA-115/APG-115): A Potent and Orally Active Murine Double Minute 2 (MDM2) Inhibitor in Clinical Development. *J Med Chem* **2017,** *60* (7), 2819-2839.

12. Li, Z. H., Discovery of AMG 232, an inhibitor of the MDM2-p53 interaction: From lead to a clinical candidate. *Cancer Research* **2014,** *74* (19).

13. Vu, B.; Wovkulich, P.; Pizzolato, G.; Lovey, A.; Ding, Q.; Jiang, N.; Liu, J. J.; Zhao, C.; Glenn, K.; Wen, Y.; Tovar, C.; Packman, K.; Vassilev, L.; Graves, B., Discovery of RG7112: A Small-Molecule MDM2 Inhibitor in Clinical Development. *Acs Med Chem Lett* **2013,** *4* (5), 466-9.

14. Wang, S.; Sun, W.; Zhao, Y.; McEachern, D.; Meaux, I.; Barriere, C.; Stuckey, J. A.; Meagher, J. L.; Bai, L.; Liu, L.; Hoffman-Luca, C. G.; Lu, J.; Shangary, S.; Yu, S.; Bernard, D.; Aguilar, A.; Dos-Santos, O.; Besret, L.; Guerif, S.; Pannier, P.; Gorge-Bernat, D.; Debussche, L.,

SAR405838: an optimized inhibitor of MDM2-p53 interaction that induces complete and durable tumor regression. *Cancer Res* **2014,** *74* (20), 5855-65.

15. Lai, A. C.; Crews, C. M., Induced protein degradation: an emerging drug discovery paradigm. *Nat Rev Drug Discov* **2017,** *16* (2), 101-114.

16. Crews, C. M.; Georg, G.; Wang, S., Inducing Protein Degradation as a Therapeutic Strategy. *J Med Chem* **2016,** *59* (11), 5129-30.

17. Neklesa, T. K.; Winkler, J. D.; Crews, C. M., Targeted protein degradation by PROTACs. *Pharmacol Ther* **2017,** *174*, 138-144.

18. Lu, J.; Qian, Y.; Altieri, M.; Dong, H.; Wang, J.; Raina, K.; Hines, J.; Winkler, J. D.; Crew, A. P.; Coleman, K.; Crews, C. M., Hijacking the E3 Ubiquitin Ligase Cereblon to Efficiently Target BRD4. *Chem Biol* **2015,** *22* (6), 755-63.

19. Winter, G. E.; Buckley, D. L.; Paulk, J.; Roberts, J. M.; Souza, A.; Dhe-Paganon, S.; Bradner, J. E., DRUG DEVELOPMENT. Phthalimide conjugation as a strategy for in vivo target protein degradation. *Science* **2015,** *348* (6241), 1376-81.

20. Raina, K.; Lu, J.; Qian, Y.; Altieri, M.; Gordon, D.; Rossi, A. M.; Wang, J.; Chen, X.; Dong, H.; Siu, K.; Winkler, J. D.; Crew, A. P.; Crews, C. M.; Coleman, K. G., PROTAC-induced BET protein degradation as a therapy for castration-resistant prostate cancer. *Proc Natl Acad Sci U S A* **2016,** *113* (26), 7124-9.

21. Neklesa, T. K.; Jin, M. Z.; Crew, A. P.; Rossi, A. K.; Willard, R. R.; Dong, H. Q.; Siu, K.; Wang, J.; Gordon, D. A.; Chen, X.; Ferraro, C.; Crews, C. M.; Coleman, K.; Winkler, J. D., ARV-330: Androgen receptor PROTAC degrader for prostate cancer. *J Clin Oncol* **2016,** *34* (2).

22. Lai, A. C.; Toure, M.; Hellerschmied, D.; Salami, J.; Jaime-Figueroa, S.; Ko, E.; Hines, J.; Crews, C. M., Modular PROTAC Design for the Degradation of Oncogenic BCR-ABL. *Angew Chem Int Ed Engl* **2016,** *55* (2), 807-10.

23. Demizu, Y.; Shibata, N.; Hattori, T.; Ohoka, N.; Motoi, H.; Misawa, T.; Shoda, T.; Naito, M.; Kurihara, M., Development of BCR-ABL degradation inducers via the conjugation of an imatinib derivative and a cIAP1 ligand. *Bioorg Med Chem Lett* **2016,** *26* (20), 4865-4869.

24. Bondeson, D. P.; Mares, A.; Smith, I. E.; Ko, E.; Campos, S.; Miah, A. H.; Mulholland, K. E.; Routly, N.; Buckley, D. L.; Gustafson, J. L.; Zinn, N.; Grandi, P.; Shimamura, S.; Bergamini, G.; Faelth-Savitski, M.; Bantscheff, M.; Cox, C.; Gordon, D. A.; Willard, R. R.; Flanagan, J. J.; Casillas, L. N.; Votta, B. J.; den Besten, W.; Famm, K.; Kruidenier, L.; Carter, P. S.; Harling, J. D.; Churcher, I.; Crews, C. M., Catalytic in vivo protein knockdown by small-molecule PROTACs. *Nat Chem Biol* **2015,** *11* (8), 611-7.

25. Aguilar, A.; Sun, W.; Liu, L.; Lu, J.; McEachern, D.; Bernard, D.; Deschamps, J. R.; Wang, S., Design of chemically stable, potent, and efficacious MDM2 inhibitors that exploit the retro-mannich ring-opening-cyclization reaction mechanism in spiro-oxindoles. *J Med Chem* **2014,** *57* (24), 10486-98.

26. Toledo, F.; Wahl, G. M., Regulating the p53 pathway: in vitro hypotheses, in vivo veritas. *Nat Rev Cancer* **2006,** *6* (12), 909-23.

27. Vousden, K. H.; Lu, X., Live or let die: the cell's response to p53. *Nat Rev Cancer* **2002,** *2* (8), 594-604.

28. Feki, A.; Irminger-Finger, I., Mutational spectrum of p53 mutations in primary breast and ovarian tumors. *Crit Rev Oncol Hematol* **2004,** *52* (2), 103-16.

29. Oliner, J. D.; Saiki, A. Y.; Caenepeel, S., The Role of MDM2 Amplification and Overexpression in Tumorigenesis. *Cold Spring Harb Perspect Med* **2016,** *6* (6).

30. Momand, J.; Jung, D.; Wilczynski, S.; Niland, J., The MDM2 gene amplification database. *Nucleic Acids Res* **1998,** *26* (15), 3453-9.

31. Wang, S.; Zhao, Y.; Aguilar, A.; Bernard, D.; Yang, C. Y., Targeting the MDM2-p53 Protein-Protein Interaction for New Cancer Therapy: Progress and Challenges. *Cold Spring Harb Perspect Med* **2017,** *7* (5).

32. Momand, J.; Wu, H. H.; Dasgupta, G., MDM2--master regulator of the p53 tumor suppressor protein. *Gene* **2000,** *242* (1-2), 15-29.

33. Kussie, P. H.; Gorina, S.; Marechal, V.; Elenbaas, B.; Moreau, J.; Levine, A. J.; Pavletich, N. P., Structure of the MDM2 oncoprotein bound to the p53 tumor suppressor transactivation domain. *Science* **1996,** *274* (5289), 948-53.

34. Vassilev, L. T.; Vu, B. T.; Graves, B.; Carvajal, D.; Podlaski, F.; Filipovic, Z.; Kong, N.; Kammlott, U.; Lukacs, C.; Klein, C.; Fotouhi, N.; Liu, E. A., In vivo activation of the p53 pathway by small-molecule antagonists of MDM2. *Science* **2004,** *303* (5659), 844-8.

35. Zhao, Y. J.; Liu, L.; Sun, W.; Lu, J. F.; McEachern, D.; Li, X. Q.; Yu, S. H.; Bernard, D.; Ochsenbein, P.; Ferey, V.; Carry, J. C.; Deschamps, J. R.; Sun, D. X.; Wang, S. M., Diastereomeric Spirooxindoles as Highly Potent and Efficacious MDM2 Inhibitors. *Journal of the American Chemical Society* **2013,** *135* (19), 7223-7234.

36. Arnhold, V.; Schmelz, K.; Proba, J.; Winkler, A.; Wunschel, J.; Toedling, J.; Deubzer, H. E.; Kunkele, A.; Eggert, A.; Schulte, J. H.; Hundsdoerfer, P., Reactivating TP53 signaling by the novel

MDM2 inhibitor DS-3032b as a therapeutic option for high-risk neuroblastoma. *Oncotarget* **2018,** *9* (2), 2304-2319.

37. Salami, J.; Crews, C. M., Waste disposal-An attractive strategy for cancer therapy. *Science* **2017,** *355* (6330), 1163-1167.

38. Wells, J. A.; McClendon, C. L., Reaching for high-hanging fruit in drug discovery at protein-protein interfaces. *Nature* **2007,** *450* (7172), 1001-9.

39. Sakamoto, K. M.; Kim, K. B.; Kumagai, A.; Mercurio, F.; Crews, C. M.; Deshaies, R. J., Protacs: chimeric molecules that target proteins to the Skp1-Cullin-F box complex for ubiquitination and degradation. *Proc Natl Acad Sci U S A* **2001,** *98* (15), 8554-9.

40. Sakamoto, K. M.; Kim, K. B.; Verma, R.; Ransick, A.; Stein, B.; Crews, C. M.; Deshaies, R. J., Development of Protacs to target cancer-promoting proteins for ubiquitination and degradation. *Mol Cell Proteomics* **2003,** *2* (12), 1350-8.

41. Schneekloth, J. S., Jr.; Fonseca, F. N.; Koldobskiy, M.; Mandal, A.; Deshaies, R.; Sakamoto, K.; Crews, C. M., Chemical genetic control of protein levels: selective in vivo targeted degradation. *J Am Chem Soc* **2004,** *126* (12), 3748-54.

42. Hines, J.; Gough, J. D.; Corson, T. W.; Crews, C. M., Posttranslational protein knockdown coupled to receptor tyrosine kinase activation with phosphoPROTACs. *Proc Natl Acad Sci U S A* **2013,** *110* (22), 8942-7.

43. Raina, K.; Crews, C. M., Targeted protein knockdown using small molecule degraders. *Curr Opin Chem Biol* **2017,** *39*, 46-53.

44. Schneekloth, A. R.; Pucheault, M.; Tae, H. S.; Crews, C. M., Targeted intracellular protein degradation induced by a small molecule: En route to chemical proteomics. *Bioorg Med Chem Lett* **2008,** *18* (22), 5904-8.

45. Naito, M.; Ohoka, N.; Shibata, N.; Hattori, T., Degradation of oncogenic proteins by SNIPER compounds. *Cancer Sci* **2018,** *109*, 562-562.

46. Itoh, Y.; Ishikawa, M.; Naito, M.; Hashimoto, Y., Protein knockdown using methyl bestatin-ligand hybrid molecules: design and synthesis of inducers of ubiquitination-mediated degradation of cellular retinoic acid-binding proteins. *J Am Chem Soc* **2010,** *132* (16), 5820-6.

47. Itoh, Y.; Ishikawa, M.; Kitaguchi, R.; Okuhira, K.; Naito, M.; Hashimoto, Y., Double protein knockdown of cIAP1 and CRABP-II using a hybrid molecule consisting of ATRA and IAPs antagonist. *Bioorg Med Chem Lett* **2012,** *22* (13), 4453-7.

48. Okuhira, K.; Demizu, Y.; Hattori, T.; Ohoka, N.; Shibata, N.; Nishimaki-Mogami, T.; Okuda, H.; Kurihara, M.; Naito, M., Development of hybrid small molecules that induce degradation of estrogen receptor-alpha and necrotic cell death in breast cancer cells. *Cancer Sci* **2013,** *104* (11), 1492-8.

49. Ito, T.; Ando, H.; Suzuki, T.; Ogura, T.; Hotta, K.; Imamura, Y.; Yamaguchi, Y.; Handa, H., Identification of a primary target of thalidomide teratogenicity. *Science* **2010,** *327* (5971), 1345-50.

50. Zhou, B.; Hu, J.; Xu, F.; Chen, Z.; Bai, L.; Fernandez-Salas, E.; Lin, M.; Liu, L.; Yang, C. Y.; Zhao, Y.; McEachern, D.; Przybranowski, S.; Wen, B.; Sun, D.; Wang, S., Discovery of a Small-Molecule Degrader of Bromodomain and Extra-Terminal (BET) Proteins with Picomolar Cellular Potencies and Capable of Achieving Tumor Regression. *J Med Chem* **2018,** *61* (2), 462-481.

51. Remillard, D.; Buckley, D. L.; Paulk, J.; Brien, G. L.; Sonnett, M.; Seo, H. S.; Dastjerdi, S.; Wuhr, M.; Dhe-Paganon, S.; Armstrong, S. A.; Bradner, J. E., Degradation of the BAF Complex Factor BRD9 by Heterobifunctional Ligands. *Angew Chem Int Ed Engl* **2017,** *56* (21), 5738-5743.

52. Martin, L. J.; Koegl, M.; Bader, G.; Cockcroft, X. L.; Fedorov, O.; Fiegen, D.; Gerstberger, T.; Hofmann, M. H.; Hohmann, A. F.; Kessler, D.; Knapp, S.; Knesl, P.; Kornigg, S.; Muller, S.; Nar, H.; Rogers, C.; Rumpel, K.; Schaaf, O.; Steurer, S.; Tallant, C.; Vakoc, C. R.; Zeeb, M.; Zoephel, A.; Pearson, M.; Boehmelt, G.; McConnell, D., Structure-Based Design of an in Vivo Active Selective BRD9 Inhibitor. *J Med Chem* **2016,** *59* (10), 4462-75.

53. Robb, C. M.; Contreras, J. I.; Kour, S.; Taylor, M. A.; Abid, M.; Sonawane, Y. A.; Zahid, M.; Murry, D. J.; Natarajan, A.; Rana, S., Chemically induced degradation of CDK9 by a proteolysis targeting chimera (PROTAC). *Chem Commun (Camb)* **2017,** *53* (54), 7577-7580.

54. Buckley, D. L.; Van Molle, I.; Gareiss, P. C.; Tae, H. S.; Michel, J.; Noblin, D. J.; Jorgensen, W. L.; Ciulli, A.; Crews, C. M., Targeting the von Hippel-Lindau E3 ubiquitin ligase using small molecules to disrupt the VHL/HIF-1alpha interaction. *J Am Chem Soc* **2012,** *134* (10), 4465-8.

55. Frost, J.; Galdeano, C.; Soares, P.; Gadd, M. S.; Grzes, K. M.; Ellis, L.; Epemolu, O.; Shimamura, S.; Bantscheff, M.; Grandi, P.; Read, K. D.; Cantrell, D. A.; Rocha, S.; Ciulli, A., Potent and selective chemical probe of hypoxic signalling downstream of HIF-alpha hydroxylation via VHL inhibition. *Nat Commun* **2016,** *7*, 13312.

56. Buckley, D. L.; Gustafson, J. L.; Van Molle, I.; Roth, A. G.; Tae, H. S.; Gareiss, P. C.; Jorgensen, W. L.; Ciulli, A.; Crews, C. M., Small-molecule inhibitors of the interaction between the E3 ligase VHL and HIF1alpha. *Angew Chem Int Ed Engl* **2012,** *51* (46), 11463-7.

57. Zengerle, M.; Chan, K. H.; Ciulli, A., Selective Small Molecule Induced Degradation of the BET Bromodomain Protein BRD4. *Acs Chem Biol* **2015,** *10* (8), 1770-7.

58. Zhang, Z.; Ding, Q.; Liu, J. J.; Zhang, J.; Jiang, N.; Chu, X. J.; Bartkovitz, D.; Luk, K. C.; Janson, C.; Tovar, C.; Filipovic, Z. M.; Higgins, B.; Glenn, K.; Packman, K.; Vassilev, L. T.; Graves, B., Discovery of potent and selective spiroindolinone MDM2 inhibitor, RO8994, for cancer therapy. *Bioorgan Med Chem* **2014,** *22* (15), 4001-9.

59. Huggins, D. J.; Sherman, W.; Tidor, B., Rational approaches to improving selectivity in drug design. *J Med Chem* **2012,** *55* (4), 1424-44.

60. Fischer, E. S.; Bohm, K.; Lydeard, J. R.; Yang, H.; Stadler, M. B.; Cavadini, S.; Nagel, J.; Serluca, F.; Acker, V.; Lingaraju, G. M.; Tichkule, R. B.; Schebesta, M.; Forrester, W. C.; Schirle, M.; Hassiepen, U.; Ottl, J.; Hild, M.; Beckwith, R. E.; Harper, J. W.; Jenkins, J. L.; Thoma, N. H., Structure of the DDB1-CRBN E3 ubiquitin ligase in complex with thalidomide. *Nature* **2014,** *512* (7512), 49-53.

61. Mori, T.; Ito, T.; Liu, S.; Ando, H.; Sakamoto, S.; Yamaguchi, Y.; Tokunaga, E.; Shibata, N.; Handa, H.; Hakoshima, T., Structural basis of thalidomide enantiomer binding to cereblon. *Sci Rep* **2018,** *8* (1), 1294.

62. Ottis, P.; Crews, C. M., Proteolysis-Targeting Chimeras: Induced Protein Degradation as a Therapeutic Strategy. *Acs Chem Biol* **2017,** *12* (4), 892-898.

63. Lu, G.; Middleton, R. E.; Sun, H.; Naniong, M.; Ott, C. J.; Mitsiades, C. S.; Wong, K. K.; Bradner, J. E.; Kaelin, W. G., Jr., The myeloma drug lenalidomide promotes the cereblon-dependent destruction of Ikaros proteins. *Science* **2014,** *343* (6168), 305-9.

64. Richardson, P. G.; Xie, W.; Jagannath, S.; Jakubowiak, A.; Lonial, S.; Raje, N. S.; Alsina, M.; Ghobrial, I. M.; Schlossman, R. L.; Munshi, N. C.; Mazumder, A.; Vesole, D. H.; Kaufman, J. L.; Colson, K.; McKenney, M.; Lunde, L. E.; Feather, J.; Maglio, M. E.; Warren, D.; Francis, D.; Hideshima, T.; Knight, R.; Esseltine, D. L.; Mitsiades, C. S.; Weller, E.; Anderson, K. C., A phase 2 trial of lenalidomide, bortezomib, and dexamethasone in patients with relapsed and relapsed/refractory myeloma. *Blood* **2014,** *123* (10), 1461-9.

65. Walczak, M. J.; Petzold, G.; Thoma, N. H., Targeted protein degradation: You can glue it too! *Nat Chem Biol* **2017,** *13* (5), 452-453.

66. Huang, X.; Dixit, V. M., Drugging the undruggables: exploring the ubiquitin system for drug development. *Cell Res* **2016,** *26* (4), 484-98.

67. Kronke, J.; Udeshi, N. D.; Narla, A.; Grauman, P.; Hurst, S. N.; McConkey, M.; Svinkina, T.; Heckl, D.; Comer, E.; Li, X.; Ciarlo, C.; Hartman, E.; Munshi, N.; Schenone, M.; Schreiber, S. L.; Carr, S. A.; Ebert, B. L., Lenalidomide causes selective degradation of IKZF1 and IKZF3 in multiple myeloma cells. *Science* **2014,** *343* (6168), 301-5.

68. Matyskiela, M. E.; Lu, G.; Ito, T.; Pagarigan, B.; Lu, C. C.; Miller, K.; Fang, W.; Wang, N. Y.; Nguyen, D.; Houston, J.; Carmel, G.; Tran, T.; Riley, M.; Nosaka, L.; Lander, G. C.; Gaidarova, S.; Xu, S.; Ruchelman, A. L.; Handa, H.; Carmichael, J.; Daniel, T. O.; Cathers, B. E.; Lopez-Girona, A.; Chamberlain, P. P., A novel cereblon modulator recruits GSPT1 to the CRL4(CRBN) ubiquitin ligase. *Nature* **2016,** *535* (7611), 252-7.

69. Cesa, L. C.; Mapp, A. K.; Gestwicki, J. E., Direct and Propagated Effects of Small Molecules on Protein-Protein Interaction Networks. *Front Bioeng Biotechnol* **2015,** *3*, 119.

70. Choi, J.; Chen, J.; Schreiber, S. L.; Clardy, J., Structure of the FKBP12-rapamycin complex interacting with the binding domain of human FRAP. *Science* **1996,** *273* (5272), 239-42.

71. Griffith, J. P.; Kim, J. L.; Kim, E. E.; Sintchak, M. D.; Thomson, J. A.; Fitzgibbon, M. J.; Fleming, M. A.; Caron, P. R.; Hsiao, K.; Navia, M. A., X-ray structure of calcineurin inhibited by the immunophilin-immunosuppressant FKBP12-FK506 complex. *Cell* **1995,** *82* (3), 507-22.

72. Ribrag, V.; Damien, S.; Gharibo, M.; Gironella, M.; Santoro, A.; Rasco, D. W.; Edenfield, W.; Wei, X.; James, A.; Hagner, P.; Gandhi, A. K.; Chopra, R.; DiMartino, J. F.; Pourdehnad, M.; Stoppa, A. M., CC-122 Degrades the Lymphoid Transcription Factor Aiolos (IKZF3) By Modulating Cereblon and Shows Clinical Activity in a Phase Ib Study of Subjects with Relapsed or Refractory Non-Hodgkin's Lymphoma and Multiple Myeloma. *Blood* **2014,** *124* (21).

73. Matyskiela, M. E.; Zhang, W.; Man, H. W.; Muller, G.; Khambatta, G.; Baculi, F.; Hickman, M.; LeBrun, L.; Pagarigan, B.; Carmel, G.; Lu, C. C.; Lu, G.; Riley, M.; Satoh, Y.; Schafer, P.; Daniel, T. O.; Carmichael, J.; Cathers, B. E.; Chamberlain, P. P., A Cereblon Modulator (CC-220) with Improved Degradation of Ikaros and Aiolos. *J Med Chem* **2018,** *61* (2), 535-542.

74. Hansen, J. D.; Condroski, K.; Correa, M.; Muller, G.; Man, H. W.; Ruchelman, A.; Zhang, W.; Vocanson, F.; Crea, T.; Liu, W.; Lu, G.; Baculi, F.; LeBrun, L.; Mahmoudi, A.; Carmel, G.; Hickman, M.; Lu, C. C., Protein Degradation via CRL4(CRBN) Ubiquitin Ligase: Discovery and Structure-Activity Relationships of Novel Glutarimide Analogs That Promote Degradation of Aiolos and/or GSPT1. *J Med Chem* **2018,** *61* (2), 492-503.

75. Ishoey, M.; Chorn, S.; Singh, N.; Jaeger, M. G.; Brand, M.; Paulk, J.; Bauer, S.; Erb, M. A.; Parapatics, K.; Muller, A. C.; Bennett, K. L.; Ecker, G. F.; Bradner, J. E.; Winter, G. E., Translation

Termination Factor GSPT1 Is a Phenotypically Relevant Off-Target of Heterobifunctional Phthalimide Degraders. *Acs Chemical Biology* **2018,** *13* (3), 553-560.

76. Han, T.; Goralski, M.; Gaskill, N.; Capota, E.; Kim, J.; Ting, T. C.; Xie, Y.; Williams, N. S.; Nijhawan, D., Anticancer sulfonamides target splicing by inducing RBM39 degradation via recruitment to DCAF15. *Science* **2017,** *356* (6336).

77. Uehara, T.; Minoshima, Y.; Sagane, K.; Sugi, N. H.; Mitsuhashi, K. O.; Yamamoto, N.; Kamiyama, H.; Takahashi, K.; Kotake, Y.; Uesugi, M.; Yokoi, A.; Inoue, A.; Yoshida, T.; Mabuchi, M.; Tanaka, A.; Owa, T., Selective degradation of splicing factor CAPERalpha by anticancer sulfonamides. *Nat Chem Biol* **2017,** *13* (6), 675-680.

78. Delker, C.; Raschke, A.; Quint, M., Auxin dynamics: the dazzling complexity of a small molecule's message. *Planta* **2008,** *227* (5), 929-41.

79. Sheard, L. B.; Tan, X.; Mao, H.; Withers, J.; Ben-Nissan, G.; Hinds, T. R.; Kobayashi, Y.; Hsu, F. F.; Sharon, M.; Browse, J.; He, S. Y.; Rizo, J.; Howe, G. A.; Zheng, N., Jasmonate perception by inositol-phosphate-potentiated COI1-JAZ co-receptor. *Nature* **2010,** *468* (7322), 400-5.

80. Che, Y. G., A. M.; Shanmugasundaram, V. Noe, M. C., Inducing Protein-Protein interactions with Molecular Glues. *Bioorg Med Chem Lett* **2018**.

81. Inder, K. L. L., D.; Zheng, Y. Z.; Parton, R. G.; Foster, L. J.; Hill, M. M., Normalization of protein at diJerent stages in SILAC subcellular proteomics affects functional analysis. *J. Integr. Omics* **2012,** *2* (2), 114-122.

82. Chen, D.; Shah, A.; Nguyen, H.; Loo, D.; Inder, K. L.; Hill, M. M., Online quantitative proteomics p-value calculator for permutation-based statistical testing of peptide ratios. *J Proteome Res* **2014,** *13* (9), 4184-91.

83. Hess, J. L., MLL: a histone methyltransferase disrupted in leukemia. *Trends Mol Med* **2004,** *10* (10), 500-7.

84. Jude, C. D.; Climer, L.; Xu, D.; Artinger, E.; Fisher, J. K.; Ernst, P., Unique and independent roles for MLL in adult hematopoietic stem cells and progenitors. *Cell Stem Cell* **2007,** *1* (3), 324-37.

85. Meyer, C.; Hofmann, J.; Burmeister, T.; Groger, D.; Park, T. S.; Emerenciano, M.; Pombo de Oliveira, M.; Renneville, A.; Villarese, P.; Macintyre, E.; Cave, H.; Clappier, E.; Mass-Malo, K.; Zuna, J.; Trka, J.; De Braekeleer, E.; De Braekeleer, M.; Oh, S. H.; Tsaur, G.; Fechina, L.; van der Velden, V. H.; van Dongen, J. J.; Delabesse, E.; Binato, R.; Silva, M. L.; Kustanovich, A.; Aleinikova, O.; Harris, M. H.; Lund-Aho, T.; Juvonen, V.; Heidenreich, O.; Vormoor, J.; Choi, W. W.; Jarosova, M.; Kolenova, A.; Bueno, C.; Menendez, P.; Wehner, S.; Eckert, C.; Talmant, P.; Tondeur, S.; Lippert, E.; Launay, E.; Henry, C.; Ballerini, P.; Lapillone, H.; Callanan, M. B.; Cayuela, J. M.; Herbaux, C.; Cazzaniga, G.; Kakadiya, P. M.; Bohlander, S.; Ahlmann, M.; Choi, J. R.; Gameiro, P.; Lee, D. S.; Krauter, J.; Cornillet-Lefebvre, P.; Te Kronnie, G.; Schafer, B. W.; Kubetzko, S.; Alonso, C. N.; zur Stadt, U.; Sutton, R.; Venn, N. C.; Izraeli, S.; Trakhtenbrot, L.; Madsen, H. O.; Archer, P.; Hancock, J.; Cerveira, N.; Teixeira, M. R.; Lo Nigro, L.; Moricke, A.; Stanulla, M.; Schrappe, M.; Sedek, L.; Szczepanski, T.; Zwaan, C. M.; Coenen, E. A.; van den Heuvel-Eibrink, M. M.; Strehl, S.; Dworzak, M.; Panzer-Grumayer, R.; Dingermann, T.; Klingebiel,

T.; Marschalek, R., The MLL recombinome of acute leukemias in 2013. *Leukemia* **2013,** *27* (11), 2165-76.

86. Borkhardt, A.; Wuchter, C.; Viehmann, S.; Pils, S.; Teigler-Schlegel, A.; Stanulla, M.; Zimmermann, M.; Ludwig, W. D.; Janka-Schaub, G.; Schrappe, M.; Harbott, J., Infant acute lymphoblastic leukemia - combined cytogenetic, immunophenotypical and molecular analysis of 77 cases. *Leukemia* **2002,** *16* (9), 1685-90.

87. Felix, C. A.; Lange, B. J.; Chessells, J. M., Pediatric Acute Lymphoblastic Leukemia: Challenges and Controversies in 2000. *Hematology Am Soc Hematol Educ Program* **2000**, 285-302.

88. Krivtsov, A. V.; Armstrong, S. A., MLL translocations, histone modifications and leukaemia stem-cell development. *Nat Rev Cancer* **2007,** *7* (11), 823-33.

89. Thiel, A. T.; Blessington, P.; Zou, T.; Feather, D.; Wu, X.; Yan, J.; Zhang, H.; Liu, Z.; Ernst, P.; Koretzky, G. A.; Hua, X., MLL-AF9-induced leukemogenesis requires coexpression of the wild-type Mll allele. *Cancer Cell* **2010,** *17* (2), 148-59.

90. Milne, T. A.; Kim, J.; Wang, G. G.; Stadler, S. C.; Basrur, V.; Whitcomb, S. J.; Wang, Z.; Ruthenburg, A. J.; Elenitoba-Johnson, K. S.; Roeder, R. G.; Allis, C. D., Multiple interactions recruit MLL1 and MLL1 fusion proteins to the HOXA9 locus in leukemogenesis. *Mol Cell* **2010,** *38* (6), 853-63.

91. Grebien, F.; Vedadi, M.; Getlik, M.; Giambruno, R.; Grover, A.; Avellino, R.; Skucha, A.; Vittori, S.; Kuznetsova, E.; Smil, D.; Barsyte-Lovejoy, D.; Li, F.; Poda, G.; Schapira, M.; Wu, H.; Dong, A.; Senisterra, G.; Stukalov, A.; Huber, K. V. M.; Schonegger, A.; Marcellus, R.; Bilban, M.; Bock, C.; Brown, P. J.; Zuber, J.; Bennett, K. L.; Al-Awar, R.; Delwel, R.; Nerlov, C.; Arrowsmith, C.

H.; Superti-Furga, G., Pharmacological targeting of the Wdr5-MLL interaction in C/EBPalpha N-terminal leukemia. *Nat Chem Biol* **2015,** *11* (8), 571-578.

92. Karatas, H.; Townsend, E. C.; Cao, F.; Chen, Y.; Bernard, D.; Liu, L.; Lei, M.; Dou, Y.; Wang, S., High-affinity, small-molecule peptidomimetic inhibitors of MLL1/WDR5 protein-protein interaction. *J Am Chem Soc* **2013,** *135* (2), 669-82.

93. Dou, Y.; Milne, T. A.; Ruthenburg, A. J.; Lee, S.; Lee, J. W.; Verdine, G. L.; Allis, C. D.; Roeder, R. G., Regulation of MLL1 H3K4 methyltransferase activity by its core components. *Nat Struct Mol Biol* **2006,** *13* (8), 713-9.

94. Tkachuk, D. C.; Kohler, S.; Cleary, M. L., Involvement of a homolog of Drosophila trithorax by 11q23 chromosomal translocations in acute leukemias. *Cell* **1992,** *71* (4), 691-700.

95. Zieminvanderpoel, S.; Mccabe, N. R.; Gill, H. J.; Espinosa, R.; Patel, Y.; Harden, A.; Rubinelli, P.; Smith, S. D.; Lebeau, M. M.; Rowley, J. D.; Diaz, M. O., Identification of a Gene, Mll, That Spans the Breakpoint in 11q23 Translocations Associated with Human Leukemias. *P Natl Acad Sci USA* **1991,** *88* (23), 10735-10739.

96. Slany, R. K.; Zeisig, B. B.; Milne, T.; Martin, M. E.; Borkhardt, A.; Chanda, S.; Hess, J. L.; Garcia, M., Hoxa9 and Meis1 are key targets for MLL-ENL mediated cellular immortalization. *Blood* **2003,** *102* (11), 170a-170a.

97. Krivtsov, A. V.; Twomey, D.; Feng, Z.; Stubbs, M. C.; Wang, Y.; Faber, J.; Levine, J. E.; Wang, J.; Hahn, W. C.; Gilliland, D. G.; Golub, T. R.; Armstrong, S. A., Transformation from committed progenitor to leukaemia stem cell initiated by MLL-AF9. *Nature* **2006,** *442* (7104), 818-22.

98. Ballabio, E.; Milne, T. A., Molecular and Epigenetic Mechanisms of MLL in Human Leukemogenesis. *Cancers (Basel)* **2012,** *4* (3), 904-44.

99. Chen, C. W.; Armstrong, S. A., Targeting DOT1L and HOX gene expression in MLL-rearranged leukemia and beyond. *Exp Hematol* **2015,** *43* (8), 673-84.

100. Lim, D. A.; Huang, Y. C.; Swigut, T.; Mirick, A. L.; Garcia-Verdugo, J. M.; Wysocka, J.; Ernst, P.; Alvarez-Buylla, A., Chromatin remodelling factor Mll1 is essential for neurogenesis from postnatal neural stem cells. *Nature* **2009,** *458* (7237), 529-33.

101. Gan, T.; Jude, C. D.; Zaffuto, K.; Ernst, P., Developmentally induced Mll1 loss reveals defects in postnatal haematopoiesis. *Leukemia* **2010,** *24* (10), 1732-41.

102. Marschalek, R., Mixed lineage leukemia: roles in human malignancies and potential therapy. *Febs J* **2010,** *277* (8), 1822-31.

103. Milne, T. A.; Hughes, C. M.; Lloyd, R.; Yang, Z.; Rozenblatt-Rosen, O.; Dou, Y.; Schnepp, R. W.; Krankel, C.; Livolsi, V. A.; Gibbs, D.; Hua, X.; Roeder, R. G.; Meyerson, M.; Hess, J. L., Menin and MLL cooperatively regulate expression of cyclin-dependent kinase inhibitors. *Proc Natl Acad Sci U S A* **2005,** *102* (3), 749-54.

104. Xia, Z. B.; Popovic, R.; Chen, J.; Theisler, C.; Stuart, T.; Santillan, D. A.; Erfurth, F.; Diaz, M. O.; Zeleznik-Le, N. J., The MLL fusion gene, MLL-AF4, regulates cyclin-dependent kinase inhibitor CDKN1B (p27kip1) expression. *Proc Natl Acad Sci U S A* **2005,** *102* (39), 14028-33.

105. Yokoyama, A.; Somervaille, T. C.; Smith, K. S.; Rozenblatt-Rosen, O.; Meyerson, M.; Cleary, M. L., The menin tumor suppressor protein is an essential oncogenic cofactor for MLL-associated leukemogenesis. *Cell* **2005,** *123* (2), 207-18.

106. Caslini, C.; Yang, Z.; El-Osta, M.; Milne, T. A.; Slany, R. K.; Hess, J. L., Interaction of MLL amino terminal sequences with menin is required for transformation. *Cancer Res* **2007,** *67* (15), 7275-83.

107. Southall, S. M.; Wong, P. S.; Odho, Z.; Roe, S. M.; Wilson, J. R., Structural basis for the requirement of additional factors for MLL1 SET domain activity and recognition of epigenetic marks. *Mol Cell* **2009,** *33* (2), 181-91.

108. Wysocka, J.; Swigut, T.; Milne, T. A.; Dou, Y.; Zhang, X.; Burlingame, A. L.; Roeder, R. G.; Brivanlou, A. H.; Allis, C. D., WDR5 associates with histone H3 methylated at K4 and is essential for H3 K4 methylation and vertebrate development. *Cell* **2005,** *121* (6), 859-72.

109. Dharmarajan, V.; Lee, J. H.; Patel, A.; Skalnik, D. G.; Cosgrove, M. S., Structural basis for WDR5 interaction (Win) motif recognition in human SET1 family histone methyltransferases. *J Biol Chem* **2012,** *287* (33), 27275-89.

110. Alicea-Velazquez, N. L.; Shinsky, S. A.; Loh, D. M.; Lee, J. H.; Skalnik, D. G.; Cosgrove, M. S., Targeted Disruption of the Interaction between WD-40 Repeat Protein 5 (WDR5) and Mixed Lineage Leukemia (MLL)/SET1 Family Proteins Specifically Inhibits MLL1 and SETd1A Methyltransferase Complexes. *J Biol Chem* **2016,** *291* (43), 22357-22372.

111. Karatas, H.; Townsend, E. C.; Bernard, D.; Dou, Y.; Wang, S., Analysis of the binding of mixed lineage leukemia 1 (MLL1) and histone 3 peptides to WD repeat domain 5 (WDR5) for the design of inhibitors of the MLL1-WDR5 interaction. *J Med Chem* **2010,** *53* (14), 5179-85.

112. Cao, F.; Townsend, E. C.; Karatas, H.; Xu, J.; Li, L.; Lee, S.; Liu, L.; Chen, Y.; Ouillette, P.; Zhu, J.; Hess, J. L.; Atadja, P.; Lei, M.; Qin, Z. S.; Malek, S.; Wang, S.; Dou, Y., Targeting MLL1 H3K4 methyltransferase activity in mixed-lineage leukemia. *Mol Cell* **2014,** *53* (2), 247-61.

113. Karatas, H.; Li, Y.; Liu, L.; Ji, J.; Lee, S.; Chen, Y.; Yang, J.; Huang, L.; Bernard, D.; Xu, J.; Townsend, E. C.; Cao, F.; Ran, X.; Li, X.; Wen, B.; Sun, D.; Stuckey, J. A.; Lei, M.; Dou, Y.; Wang, S., Discovery of a Highly Potent, Cell-Permeable Macrocyclic Peptidomimetic (MM-589) Targeting the WD Repeat Domain 5 Protein (WDR5)-Mixed Lineage Leukemia (MLL) Protein-Protein Interaction. *J Med Chem* **2017,** *60* (12), 4818-4839.

114. Senisterra, G.; Wu, H.; Allali-Hassani, A.; Wasney, G. A.; Barsyte-Lovejoy, D.; Dombrovski, L.; Dong, A.; Nguyen, K. T.; Smil, D.; Bolshan, Y.; Hajian, T.; He, H.; Seitova, A.; Chau, I.; Li, F.; Poda, G.; Couture, J. F.; Brown, P. J.; Al-Awar, R.; Schapira, M.; Arrowsmith, C. H.; Vedadi, M., Small-molecule inhibition of MLL activity by disruption of its interaction with WDR5. *The Biochemical journal* **2013,** *449* (1), 151-9.

115. Bolshan, Y.; Getlik, M.; Kuznetsova, E.; Wasney, G. A.; Hajian, T.; Poda, G.; Nguyen, K. T.; Wu, H.; Dombrovski, L.; Dong, A.; Senisterra, G.; Schapira, M.; Arrowsmith, C. H.; Brown, P. J.; Al-Awar, R.; Vedadi, M.; Smil, D., Synthesis, Optimization, and Evaluation of Novel Small Molecules as Antagonists of WDR5-MLL Interaction. *Acs Med Chem Lett* **2013,** *4* (3), 353-7.

116. Getlik, M.; Smil, D.; Zepeda-Velazquez, C.; Bolshan, Y.; Poda, G.; Wu, H.; Dong, A.; Kuznetsova, E.; Marcellus, R.; Senisterra, G.; Dombrovski, L.; Hajian, T.; Kiyota, T.; Schapira, M.; Arrowsmith, C. H.; Brown, P. J.; Vedadi, M.; Al-Awar, R., Structure-Based Optimization of a Small Molecule Antagonist of the Interaction Between WD Repeat-Containing Protein 5 (WDR5) and Mixed-Lineage Leukemia 1 (MLL1). *J Med Chem* **2016,** *59* (6), 2478-96.

117. Li, D. D.; Wang, Z. H.; Chen, W. L.; Xie, Y. Y.; You, Q. D.; Guo, X. K., Structure-based design of ester compounds to inhibit MLL complex catalytic activity by targeting mixed lineage leukemia 1 (MLL1)-WDR5 interaction. *Bioorgan Med Chem* **2016,** *24* (22), 6109-6118.

118. Li, D. D.; Chen, W. L.; Xu, X. L.; Jiang, F.; Wang, L.; Xie, Y. Y.; Zhang, X. J.; Guo, X. K.; You, Q. D.; Sun, H. P., Structure-based design and synthesis of small molecular inhibitors disturbing the interaction of MLL1-WDR5. *Eur J Med Chem* **2016,** *118*, 1-8.

119. Li, D. D.; Chen, W. L.; Wang, Z. H.; Xie, Y. Y.; Xu, X. L.; Jiang, Z. Y.; Zhang, X. J.; You, Q. D.; Guo, X. K., High-affinity small molecular blockers of mixed lineage leukemia 1 (MLL1)-WDR5 interaction inhibit MLL1 complex H3K4 methyltransferase activity. *Eur J Med Chem* **2016,** *124*, 480-489.

120. Song, J. J.; Kingston, R. E., WDR5 interacts with mixed lineage leukemia (MLL) protein via the histone H3-binding pocket. *J Biol Chem* **2008,** *283* (50), 35258-64.

121. Staatz, C. E.; Tett, S. E., Clinical pharmacokinetics and pharmacodynamics of mycophenolate in solid organ transplant recipients. *Clin Pharmacokinet* **2007,** *46* (1), 13-58.

122. Staatz, C. E.; Tett, S. E., Pharmacology and toxicology of mycophenolate in organ transplant recipients: an update. *Arch Toxicol* **2014,** *88* (7), 1351-89.

123. Sherwin, C. M.; Fukuda, T.; Brunner, H. I.; Goebel, J.; Vinks, A. A., The evolution of population pharmacokinetic models to describe the enterohepatic recycling of mycophenolic acid in solid organ transplantation and autoimmune disease. *Clin Pharmacokinet* **2011,** *50* (1), 1-24.

124. Kiang, T. K. L.; Ensom, M. H. H., Population Pharmacokinetics of Mycophenolic Acid: An Update. *Clin Pharmacokinet* **2018,** *57* (5), 547-558.

125. Allison, A. C.; Kowalski, W. J.; Muller, C. D.; Eugui, E. M., Mechanisms of action of mycophenolic acid. *Ann N Y Acad Sci* **1993,** *696*, 63-87.

126. Allison, A. C.; Eugui, E. M., Mechanisms of action of mycophenolate mofetil in preventing acute and chronic allograft rejection. *Transplantation* **2005,** *80* (2 Suppl), S181-90.

127. Placebo-controlled study of mycophenolate mofetil combined with cyclosporin and corticosteroids for prevention of acute rejection. European Mycophenolate Mofetil Cooperative Study Group. *Lancet* **1995,** *345* (8961), 1321-5.

128. Zegarska, J.; Hryniewiecka, E.; Zochowska, D.; Tszyrsznic, W.; Jazwiec, R.; Borowiec, A.; Pawlowska, E.; Dadlez, M.; Paczek, L., Mycophenolic Acid Metabolites Acyl-Glucuronide and Glucoside Affect the Occurrence of Infectious Complications and Bone Marrow Dysfunction in Liver Transplant Recipients. *Ann Transplant* **2015,** *20*, 483-92.

129. Langers, P.; Press, R. R.; Inderson, A.; Cremers, S. C.; den Hartigh, J.; Baranski, A. G.; van Hoek, B., Limited sampling model for advanced mycophenolic acid therapeutic drug monitoring after liver transplantation. *Ther Drug Monit* **2014,** *36* (2), 141-7.

130. Barau, C.; Furlan, V.; Debray, D.; Taburet, A. M.; Barrail-Tran, A., Population pharmacokinetics of mycophenolic acid and dose optimization with limited sampling strategy in liver transplant children. *Br J Clin Pharmacol* **2012,** *74* (3), 515-24.

131. Wang, X. X.; Liu, W.; Zheng, T.; Park, J. M.; Smith, D. E.; Feng, M. R., Population pharmacokinetics of mycophenolic acid and its glucuronide metabolite in lung transplant recipients with and without cystic fibrosis. *Xenobiotica* **2017,** *47* (8), 697-704.

132. Wang, X. X.; Feng, M. R.; Nguyen, H.; Smith, D. E.; Cibrik, D. M.; Park, J. M., Population pharmacokinetics of mycophenolic acid in lung transplant recipients with and without cystic fibrosis. *Eur J Clin Pharmacol* **2015,** *71* (6), 673-679.

133. Yoshimura, K.; Yano, I.; Yamamoto, T.; Kawanishi, M.; Isomoto, Y.; Yonezawa, A.; Kondo, T.; Takaori-Kondo, A.; Matsubara, K., Population pharmacokinetics and pharmacodynamics of mycophenolic acid using the prospective data in patients undergoing hematopoietic stem cell transplantation. *Bone Marrow Transplant* **2018,** *53* (1), 44-51.

134. Hwang, S.; Song, G. W.; Jung, D. H.; Park, G. C.; Ahn, C. S.; Moon, D. B.; Ha, T. Y.; Kim, K. H.; Lee, S. G., Intra-individual variability of mycophenolic acid concentration according to renal function in liver transplant recipients receiving mycophenolate monotherapy. *Ann Hepatobiliary Pancreat Surg* **2017,** *21* (1), 11-16.

135. Lecker, S. H.; Goldberg, A. L.; Mitch, W. E., Protein degradation by the ubiquitin-proteasome pathway in normal and disease states. *J Am Soc Nephrol* **2006,** *17* (7), 1807-19.

136. Stockwell, B., Outsmarting Cancer. A biologist talks about what makes disease-causing proteins so difficult to target with drugs. *Sci Am* **2011,** *305* (4), 20.

137. Nikolovska-Coleska, Z.; Wang, R.; Fang, X.; Pan, H.; Tomita, Y.; Li, P.; Roller, P. P.; Krajewski, K.; Saito, N. G.; Stuckey, J. A.; Wang, S., Development and optimization of a binding assay for the XIAP BIR3 domain using fluorescence polarization. *Anal Biochem* **2004,** *332* (2), 261-73.